DEVELOPMENT OF VALID MODELS FOR STRUCTURAL DYNAMIC ANALYSIS

A thesis submitted for the degree of

Doctor of Philosophy

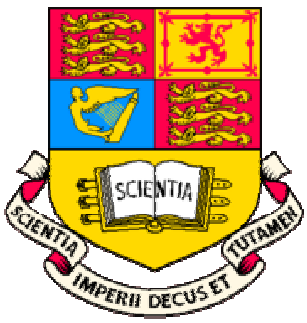

By

Jose Vicente García

Department of Mechanical Engineering

Imperial College London – University of London

October 2008

I declare that this thesis is my own work and that where any material could be construed as the work of others, it is fully cited and referenced.

Jose Vicente García

2nd October 2008

To Laura

Abstract

In the aeroengine industry, simulation models have become the driving force behind the optimisation of any new engine design. This approach delivers significant time and cost benefits to engine manufacturers but it is not risk-free. Increasing reliance on simulation means that inaccurate predictions can have a greater impact than ever before. That is why the final design models should be fully validated prior to full-scale production.

In the field of structural dynamic analysis, predictions from a Finite Element Model (FEM) of the whole engine are used to optimise the engine's design. Traditionally the validation of such FEM could only take place once the first engine prototypes were available for testing. This occurs late in the design cycle when any redesign would inevitably incur serious cost and time penalties.

This thesis presents a novel methodology to validate a complex assembly model by validating only a few of its constituent components using supermodels as the reference. The virtual nature of this approach means that the assembly models are validated early in the design cycle, well ahead of manufacture. Moreover, the cost of model validation in a virtual environment is a fraction of that required when using physical testing as the reference. This methodology is successfully applied to a series of industrial Case Studies. Practical application of this approach also highlights the need to include the effects of component joints when validating assembly models.

Finally, supermodels are central to the assembly model validation strategy proposed. The development of supermodelling techniques invariably requires physical testing and appropriate methods to discriminate between valid and invalid supermodels. The traditional deterministic approach to model validation is not suitable for supermodels. For this reason, a robust probabilistic approach for the validation of supermodels is described in this thesis and demonstrated using an industrial Case Study.

Acknowledgements

I would like to express my sincere gratitude to my supervisor, Prof. David J. Ewins, for his valuable advice, support, encouragement and guidance throughout the course of this work. I would also like to thank Dr. Paul N. Bennett (Rolls-Royce) for his relentless support during all these years and his most valuable input into this project.

I would like to thank Rolls-Royce and the European Union for funding this work under the VIVACE project (Framework VI, AIP3-CT-2003-502917). If not for the continued support and advice from Dr. Graham Harlin (Rolls-Royce) this work would have not been possible. Thanks are extended to the partners involved in VIVACE, particularly Mr. Steve T. Knight (Rolls-Royce), Mr. Michael J. Annear (Rolls-Royce), Mr. Karl-Heinz Dufour (Rolls-Royce), Dr. Bernard C. Staples (Rolls-Royce), Dr. Christoph W. Schwingshackl (Imperial College London), Dr. Gan Chen (Imperial College London), Dr. Chaoping Zang (Imperial College London), Dr. Bart Peeters (LMS International), Mr. Philip Baker (Assystem) and Mr. Markus Andersson (Volvo Aero).

I would like to thank Mr. David A. Hogan, Mr. Edward Green, Mr. Stuart Yeo and Dr. Mark Walters (Rolls-Royce) for encouraging me to embark on this project and also to Miss Nina Hancock (Imperial College London) for all her administrative support.

To my fiancée, Laura, for her love and care during these years and also to my parents for their support and encouragement when I needed it the most.

Contents

Nomenclature

Basic Terms, Dimensions and Subscripts

N	total number of degrees of freedom
n	total number of finite elements
j,k	integers
r	current mode number
m	mode multiplicity
p	parameter
E	Young's modulus
ρ	material density
V	volume
C_k	contribution of the k-th component model to the accuracy of the assembly predictions
K_r, K_θ, K_z	translational stiffness of the joint model in the radial, circumferential and axial directions
R_r, R_θ, R_z	rotational stiffness of the joint model in the radial, circumferential and axial directions
i	$\sqrt{-1}$
σ	standard deviation
σ^2	variance
cov	covariance

Matrices, Vectors and Scalars

$[\ ]$	matrix
$\{\ \}$	column vector
$[\ ]^T$	transpose of a matrix
$\overline{[\ ]}$	truncated matrix
$[\ ]^{-1}$	inverse of a matrix
$\{\ \}^T$	transpose of a column vector
$[I]$	identity matrix
δ	Kronecker's delta
$[H]$	transformation matrix
$[S]$	sensitivity matrix
$[W_Z]$	response weighting matrix
$[W_P]$	parameter weighting matrix

Spatial Modal Properties

$[M]$	mass matrix
$[K]$	stiffness matrix
$[m]_j$	mass matrix of the j-th finite element
$[k]_j$	stiffness matrix of the j-th finite element
$\{F\}$	force vector
$\{X\}$	response vector

Modal and Response Properties

ω	frequency (rad/s)
ω_r	natural frequency of the r-th mode
$[\omega]$	natural frequency matrix
$\{\phi\}_r$	mass-normalised modeshape of the r-th mode
$[\phi]$	mass-normalised modeshape matrix
η_r	structural damping loss factor of the r-th mode
$[\omega_0]$	original natural frequency predictions
$[\phi_0]$	original modeshape predictions
$[\omega_X]$	reference natural frequencies for model validation
$[\phi_X]$	reference modeshapes for model validation
$\{Z_0\}$	original response vector
$\{Z_X\}$	reference response vector
$\{Z_U\}$	updated response vector
$\{f_t\}_r$	internal force vector of the r-th mode in the t-th test configuration

Standard Abbreviations

CAD	Computed Aided Design
COC	Combustor Outer Casing
CT	Computed Tomography
DOF	Degree of Freedom
DoE	Design of Experiment
FBH	Front Bearing Housing
FEM	Finite Element Model
FOGV	Fan Outlet Guided Vanes
FRF	Frequency Response Function
HPC	High Performance Computing
HPTIPTC	High Pressure Turbine – Intermediate Pressure Turbine Casing
LPTC	Low Pressure Turbine Casing
MAC	Modal Assurance Criterion
MR	Mount Ring
PCA	Principal Component Analysis
PDF	Probability Density Function
RBF	Radial Basis Function
RSM	Response Surface Model
SEREP	System Equivalent Reduction and Expansion Process
SIMO	Single Input Multiple Output
SISO	Single Input Single Output
WEM	Whole Engine Model

List of Figures

List of Tables

Chapter 1 - Introduction

1.1 Preamble

Engine failure caused by excessive vibration is an expensive reality for the aviation industry. Even when the levels of vibration are not safety-critical they can still have a detrimental effect on important aspects such as noise emissions or passenger comfort. As a result, achieving an acceptable vibration response is a primary concern for any new engine design.

The traditional design-test-redesign loop is not viable in the current market. The increasing pressures to deploy new products in short periods of time at a much reduced cost means that designs must be “right first time” and that the amount of testing must be kept to an absolute minimum. It is no surprise, then, that simulation tools have become the major driving force in the design of new engines. In the field of structural dynamics, the Finite Element Modelling technique has established itself as the industry standard for the prediction of the dynamic response of aeroengines.

The increasing reliance on Finite Element Models (FEM) during the engine design phase means that inaccurate predictions can lead to severe design flaws. That is why engine manufactures need to validate the models used during the design phase before the final design is released into full-scale production. Moreover, it is common for the aviation authorities to demand convincing evidence of the validity of those models before any new engine design is cleared for flight.

The traditional approach to validating the structural model of an engine is to compare its predictions against measurements from a set of physical tests. However, engine prototypes are only available at very late stages in the development programme. This means that the validation of the engine’s structural model typically has to wait until the final engine design is practically frozen. If the structural model is found to be inaccurate at this stage, it is possible that the engine design is flawed and a redesign might be

required. Any change to the design at this point will escalate the cost of the project and will seriously compromise the deadline for entry into service.

In an ideal scenario the engine's structural model would be validated early in the design cycle, at a stage where design changes are still feasible and affordable. Nonetheless, the early stages of the design cycle are characterised by a total lack of manufactured prototypes. This rules out the possibility of using physical testing as the source of reference data for model validation.

This thesis presents a novel methodology to validate the structural models of complex assemblies, such as aeroengines, during the early stages of the design cycle. The reference data for validation is now provided by highly refined models, referred to as "supermodels", which serve as virtual substitutes for the manufactured parts and are readily available early in the design cycle.

It is important to point out that the use of supermodels as the reference data for the validation of complex assembly models does not rule out the need for physical testing. Supermodelling techniques are still under development and certain phenomena, such as the effects of assembly joints, remain very difficult to model accurately. The development of supermodelling techniques will inevitably require comprehensive research programmes for which physical testing will still be the cornerstone. However, this research can be carried out independently of any engine development programme, thereby removing physical testing from the critical path.

The focus of this work is on the validation of structural models used to predict the dynamic behaviour of jet engines. Nonetheless, the methodologies presented can be easily applicable to other industries where the structural dynamic response of their products is critical and the expected time-to-market is short.

1.2 Traditional Model Validation Approach

The design of a new engine always starts with a clear set of technical requirements. These are usually agreed between the engine manufacturer, the airframe manufacturer and the final customers (e.g. airlines, air forces, etc.). These requirements will no doubt include: fuel consumption, engine weight, thrust, vibration levels, etc. It must not be

forgotten that the final engine design must also comply with the latest safety and environmental legislation before it can cleared for flight.

In order to gain a competitive advantage, engine manufacturers strive to come up with designs that meet or exceed the technical requirements while keeping the engine costs to a minimum. It is also important to consider the benefit of a reduced time-to-market to secure early sales.

The optimisation of an engine design following a design-test-redesign loop is simply too expensive and time consuming in today's market. These days the engine design follows a process similar to that described in Figure 1.1.

The engine design typically starts with a coarse preliminary concept and evolves through iteration towards a detailed and highly optimised solution with the bare use of simulation models. From the structural dynamics point of view, a simplified finite element model of the engine, usually referred to as Whole Engine Model (WEM), is used to predict the overall dynamic behaviour of the engine at each design iteration. Figure 1.2 shows an example of a WEM. The predictions from the WEM are used to drive the detailed design of the engine's components. For instance, the WEM is typically used to predict the dynamic loads acting on the different components in the engine under normal (e.g. take off, cruise, landing) and abnormal (e.g. fan blade off) operating conditions. For a given component, these loads are input into the corresponding highly detailed stress model. If the predicted stress levels are too high, the component's design is strengthened. On the contrary, if the stress levels are well below the specified limits, the design is lightened to save weight.

A close look at the WEM in Figure 1.2 reveals that this model only captures the most basic characteristics of the engine. The detailed design features (e.g. holes, bosses) are completely ignored. This simplification is required to ensure that the model can be analysed in a timely manner with the available computing power. Nonetheless, the lack of detail in the WEM can have a detrimental effect on the accuracy of its predictions.

Obviously, if the models used to drive the design of the engine are flawed, the "virtually" optimised design might not be so optimum after all. That is why the design optimisation loop is typically followed by a test programme whose objective is to validate the engine design (i.e. Certification) before its release into production.

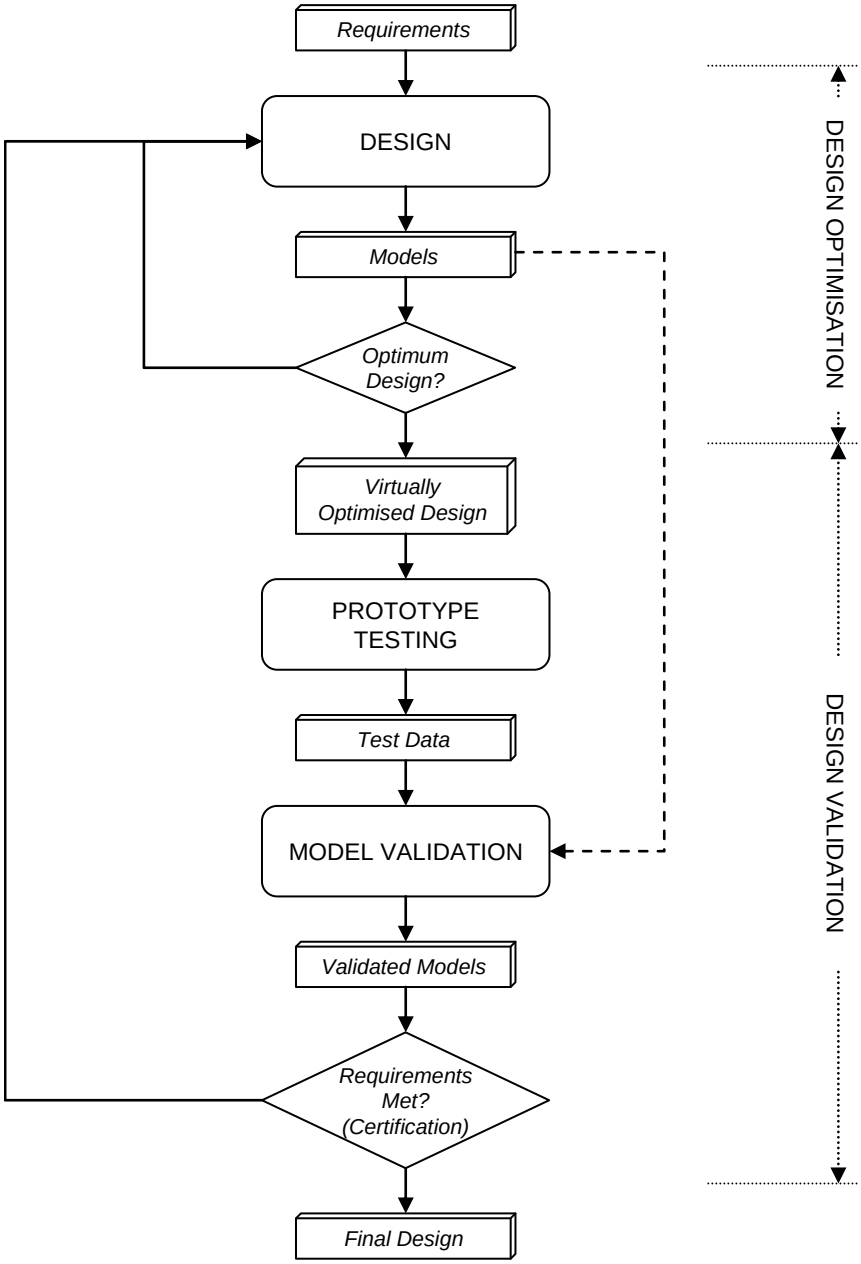

Figure 1.1. Current engine design cycle.

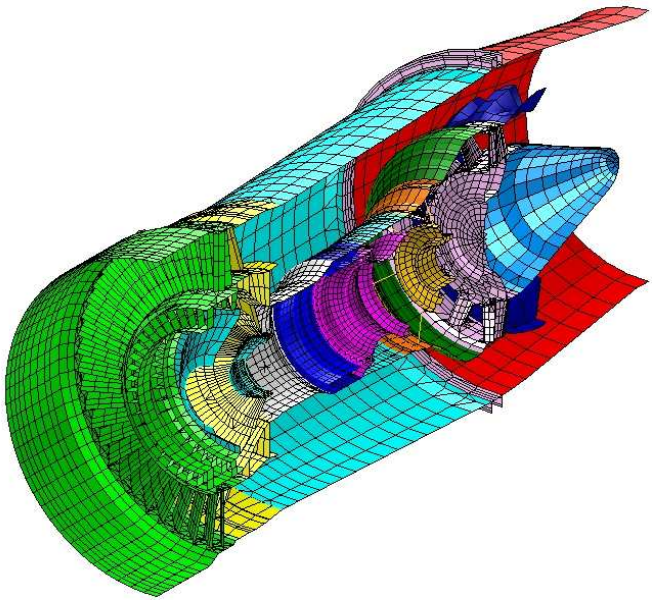

Figure 1.2. Whole Engine Model cross-section.

Testing an engine design over all potential normal and abnormal operating conditions would be prohibitive from a cost and time point of view. Imagine the potential cost of a test designed to measure the engine's dynamic response after an in-flight fan blade off event where the engine is still mounted on the wing and subject to the windmill effect. That is why it is common practice to take a more indirect approach. Typically, the predictions from the final models used during the design cycle are compared against the measurements from a limited number of carefully chosen tests. If the predictions and the measurements agree well for these tests it is assumed that the models will also provide accurate predictions under other engine operating conditions. Since these models were used to drive the design, the "virtually" optimised design is considered to be valid and full-scale production can start.

If the predictions and the measurements do not agree well, invalid design decisions might have been taken during the design cycle. The normal course of action in this case is first to correct the models to better match the measurements. The validated models are then used to evaluate the actual performance of the previously thought-to-be optimum design under the different engine operating conditions. Typically two different scenarios will emerge from this evaluation (i) the engine design is not optimum but still

fulfils the minimum technical requirements and (ii) the engine design does not fulfil the minimum technical requirements. In the former case, the engine manufacturer will decide whether it makes financial sense to incur the inevitable cost and time penalties associated with a redesign so that the engine design can be truly optimised. In the case where the technical requirements are not met there will be no other option but to redesign.

The number and type of tests used to validate the models are usually agreed between the engine manufacturer, the airframe manufacturer, the customers and the aviation authorities. When an engine manufacturer consistently demonstrates that its models accurately match the test data project after project, it will normally put a request forward to reduce the number of tests required in future programmes and hence reduce the development costs. There are already a few examples where the aviation authorities have cleared a design for flight based purely on model predictions without the need for physical testing. These examples are still few and far between and they are typically restricted to redesigns of small parts of the engine which original designs were previously cleared through testing. Nevertheless, these examples show that the aviation industry is increasingly open-minded about reducing the test programmes when an engine manufacturer consistently shows that the models used to drive the design are valid.

1.3 Virtual Model Validation

Let us imagine that we could use fully validated models during the design optimisation loop according to the process illustrated in Figure 1.3. On one hand, the “virtually” optimised design would be in fact optimum in the real world, hence avoiding costly redesigns. On the other hand, the predictions and the measurement would line up once the test data becomes available, hence giving strong arguments to the engine manufacturer to reduce the amount of testing required in future programmes.

The implementation of this approach poses a problem though. Where do we get the reference data from in order to validate the models? The design optimisation loop is typically characterised by the lack of manufactured prototypes. This discards physical testing as the reference data for model validation during the design loop.

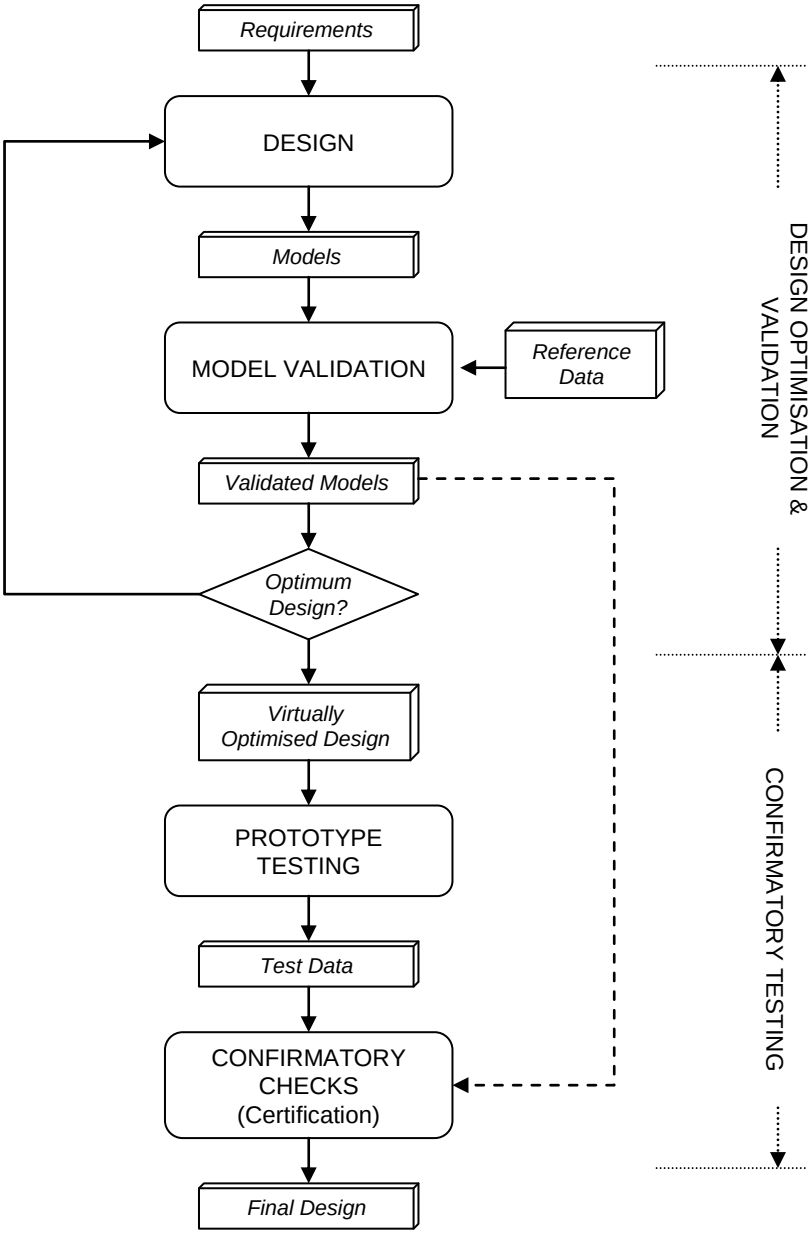

Figure 1.3. Ideal engine design cycle.

In the field of structural dynamic analysis, Fotsch [1] recently demonstrated that with the right modelling techniques and using the appropriate computing power it is possible to create Finite Element Models (FEM) whose predictions can rival the accuracy of the

measurements from a physical test. Fotsch named these highly refined models as “supermodels”. Figure 1.4 shows an example of a supermodel, in this case, the yellow component (i.e. Intermediate Casing) in the WEM in Figure 1.2. A closer look at some of the regions in this model reveals the high level of mesh refinement so characteristic of supermodels. The geometry of the component is captured in great detail. In fact, most supermodels will not make any simplification to the geometry of the manufactured component.

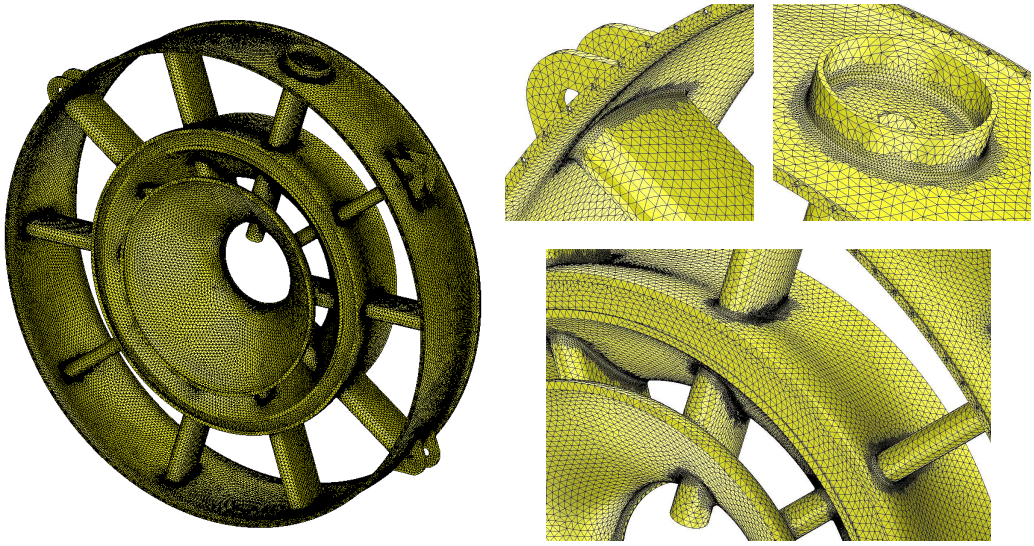

Figure 1.4. Supermodel details.

It is perhaps useful to reflect on these developments and to project forward from where we are today to anticipate whether and how far they may extend in the future. Can we use the predictions from a supermodel of the whole engine as the reference to validate the much simplified WEM during the design loop? The answer is: not yet. In the late 1990s, engineers in the aeroengine industry would be capable of routinely handling models of sizes up to a few hundreds of thousands of degrees of freedom (DOF). A decade later, this number has increased to a few million DOFs, this is, an order of magnitude improvement. Models of this size may be sufficient for first-generation supermodels of individual components, however, a supermodel of a whole engine containing all of its constituent parts (e.g. casings, blades, vanes, accessories, pipes, etc.) will probably require several billion DOFs. Even if future improvements in

computing power continue to allow an increase in model size of an order of magnitude every ten years, it will still take a few decades until a supermodel of a whole engine becomes viable. In the foreseeable future, therefore, the practice of using the maximum computing capacity for each component individually may well prove the optimum use of resources.

Can we use supermodels at a component level to validate the WEM? Potentially yes. A WEM is constructed by joining together the simplified models of the different components in the engine, see Figure 1.2. The individual component models in the WEM are typically referred to as component design models. One might expect that if all the individual component design models were valid, the WEM would also be valid. This means that we could validate the WEM by individually validating each of its constituent component design models using their corresponding supermodels as the reference.

This virtual validation approach could potentially facilitate the validation of the WEM during the design cycle as proposed in the process illustrated in Figure 1.3. However, a few issues need to be resolved before this approach can be efficiently and reliably implemented in practice.

First of all, a WEM is made up of many component design models. If one wanted to validate every single one of the components in the WEM, many supermodels would need to be created and analysed. Supermodels usually run on the very limits of current computing power. This means that the validation of all individual components could result in serious time penalties, hence slowing down the design cycle. A solution to this problem would be to focus the validation effort only on those components that have most influence on the accuracy of the WEM. Even though this is a very attractive solution, it requires the development of methods that allow the identification of such components.

Also, the validation of an individual component design model against its corresponding supermodel is not as straight-forward as one might initially think. For instance, a component design model could perfectly match the first 20 natural frequencies predicted by the corresponding supermodel in a free-free configuration and the model could still perform very badly when it is part of the WEM. The reason being that the boundary conditions applied to the component design model as part of the WEM are completely

different to those in a free-free configuration. New methods must be developed to validate individual component design models against supermodels so that they perform well when they are part of the WEM.

Finally, the interfaces between components (i.e. joints) might play an important role in the dynamic behaviour of the assembly. The effect of joints must therefore be assessed and, if necessary, incorporated into the overall validation process.

1.4 Research Objectives

The overall objective of this thesis is to develop methods so that complex assembly models used in structural dynamic analysis can be validated early in the design cycle, even before manufactured prototypes are available for testing. The virtual nature of the proposed validation strategy should be capable of reducing by an order of magnitude the cost and timescales currently associated with the validation of complex assembly models used in the aeroengine industry (e.g. WEM), which historically have required extensive test programmes.

The specific objectives of this thesis are:

- To develop methods that reduce the task of validating a simplified assembly model (i.e. assembly design model) to the simpler task of validating a much reduced number of its constituent components, typically less than one tenth of the total number of components in an aeroengine assembly. This reduction will facilitate the use of supermodels as the reference for validation.
- To develop methods that allow the validation of individual component design models against supermodels so that that the validated models perform well when they are part of the assembly and not just when they are considered in isolation. The accuracy of the validated component design models should be comparable to the variability expected from the manufactured components.
- To assess the effects of joints in the dynamic behaviour of assemblies and, if necessary, incorporate their effect into the overall validation strategy.
- To demonstrate the suitability of the virtual validation approach using a complex industrial Case Study.

- To support the development of supermodelling techniques by proposing appropriate techniques for the validation of supermodels against physical test data.

1.5 Scope of Model Validation

The work presented in this thesis will focus on the validation of complex assembly models so that they are capable of accurately predicting the natural frequencies and modeshapes of assembled structures made up of many components joined together. For lightly damped structures, most common in industry, the natural frequencies and modeshapes predicted by a FEM are the result of solving the following eigen problem:

$$\left([K] - \omega_r^2 [M]\right)\{\phi\}_r = 0 \tag{1.1}$$

where [K] is the model's stiffness matrix, [M] is the mass matrix while ω_r and $\{\phi\}_r$ are the natural frequency and modeshape predictions for the r-th mode, respectively.

The accurate prediction of the natural frequencies and modeshapes of a structure is essential for the accurate prediction of the more general forced response:

$$\{X(\omega)\} = \sum_{r=1}^{N} \frac{\{\phi\}_r^T \{F(\omega)\}\{\phi\}_r}{\omega_r^2 - \omega^2 + i\eta_r \omega_r^2} \tag{1.2}$$

where $\{X(\omega)\}$ is the predicted dynamic response of the structure (in the frequency domain) under a set of loads represented by the force vector $\{F(\omega)\}$, η_r is the structural damping loss factor of the r-th mode and ω is the frequency of excitation. The number N is equal to the total number of degrees of freedom (DOFs) in the model.

A close look at equation (1.2) reveals that those modes which natural frequencies are distant from the frequency of excitation barely contribute to the total response. Also, those modes which natural frequency is close to the excitation frequency but which modeshape is orthogonal or almost orthogonal to the force vector:

$$\{\phi\}_r^T \{F(\omega)\} \cong 0 \tag{1.3}$$

will have little influence in the total response.

As a result, the assembly model is typically only required to accurately predict the few modes that significantly contribute to the forced response to be considered valid.

1.6 Thesis Overview

Chapter 2 presents a novel methodology that facilitates the validation of an assembly design model by validating a reduced number of its constituent components. Sensitivity analysis is the backbone of this methodology and that is why this chapter begins with a comprehensive review of the most common sensitivity analysis methods in the field of structural dynamics. The chapter then describes how sensitivity analysis can be used to identify which are the components whose potential modelling errors have the biggest effect in the accuracy of the assembly predictions and which should therefore be given the highest priority for validation. A simple industrial Case Study is used to illustrate the proposed methodology.

Chapter 3 presents a new methodology to validate component design models so that they perform well when they are part of a bigger assembly. The problem of a component design model which accurately predicts the component's behaviour when it is considered in isolation but fails to perform properly when the model is part of a bigger assembly has already been reported in the literature. The chapter begins with a review of the existing solutions to overcome this problem. This is followed by the proposal of a novel method to validate a component design model making use of a so-called "hybrid assembly model" (i.e. model of the assembly where the original component design model is replaced by the corresponding supermodel) as the reference for validation. Finally, this chapter reviews the effect of ignoring the interfaces between components (i.e. joints) when validating assembly models. A method to incorporate the influence of joints in the validation process is also presented. The same Case Study used in the previous chapter is used again in this chapter to illustrate the proposed methodologies.

Chapter 4 describes the validation from start to end of a complex assembly model using the methods proposed in the previous chapters. This validation was carried out as part of a real engine certification program and hence represents the ideal scenario to review the strengths and weaknesses of the proposed methodology in a high-pressure industrial environment.

Supermodelling techniques are still in their early days and their development requires validating supermodels against the measurements from physical tests. **Chapter 5** highlights the shortcomings of the traditional deterministic approach to model validation when validating a supermodel using physical test data as the reference. This chapter then reviews a probabilistic model validation method which is better suited for the validation of supermodels. The suitability of this method is demonstrated using an industrial Case Study.

Chapter 6 begins with a summary of the overall conclusions of this thesis. This is then followed by summing up the most important contributions of this research work. The chapter concludes with suggestions for future work and some closing remarks from the author.

Chapter 2 - Prioritisation of Individual Components for Validation

2.1 Introduction

Typically, the validation of an assembly model (i.e. design model) used to drive the design of a complex structure has to wait until there are physical prototypes available for testing. This usually occurs at the very late stages in the design cycle when the final design is almost frozen. If the models are found to be inaccurate at this stage, the design will be based on inaccurate predictions and a redesign might be required. A redesign at this late stage will inevitably escalate the cost of the project and will incur serious delays.

Ideally, one would like to validate the assembly design model well within the design cycle. This would ensure that the design decisions are based on reliable predictions, hence ensuring truly optimised design solutions. Fotsch [1] demonstrated that highly refined models, usually referred to as supermodels, are capable of predictions that can rival the accuracy of the measurements from physical tests. The virtual nature of supermodels makes them the ideal reference for the validation, well within the design cycle, of the less refined design models.

However, the current computing technology limits the use of supermodels to individual components modelled in isolation. The creation and analysis of supermodels corresponding to complex assemblies (e.g. aeroengine) is not a reality yet. In fact, it might be many years until supermodels of complex assemblies become a reality. This compels us to find a solution where an assembly design model can be validated using the predictions from the supermodels of the individual components in the assembly.

It is important to keep in mind that complex assemblies can be made up of hundreds of components. In such cases, the creation and analysis of hundreds of component

supermodels would soon become an overwhelming task. Nevertheless, it is most likely that only a few of the constituent components in the assembly will actually play a significant role in its overall behaviour. It is those components that must be targeted for individual validation, hence reducing the complex task of validating an assembly model to the simpler job of validating only a few of its components.

This chapter will review some of the existing methods for component prioritisation and will introduce a novel approach to tackle the problem. As sensitivity analysis is an important element of the new method, a review of the most common sensitivity analysis methods used in structural dynamics will be presented first. An industrial Case Study will also be introduced to better illustrate the application of the proposed methodology.

2.2 Validation Strategy

An assembly (e.g. aeroengine) can be considered as the combination of its individual components and the interfaces (joints) between them:

$$\text{Assembly} = \sum \text{Components} + \sum \text{Joints} \tag{2.1}$$

For the time being we will assume that the effect of the joints in the behaviour of an assembly is negligible and that it is correct to model the connections between components as if the assembly was a continuous solid (i.e. rigid links between the coincident nodes of adjacent components). It shall be demonstrated in the next chapter that this is indeed not a valid assumption. However, it is easier to remove the influence of joints at this stage to better illustrate the validation strategy. Moreover, we shall see in the next chapter that the proposed validation strategy can easily be expanded to accommodate the presence of joints. If the influence of joints is ignored, equation (2.1) can be rewritten as:

$$\text{Assembly} \cong \sum \text{Components} \tag{2.2}$$

From (2.2) we can assume that if the models of all components in the assembly (i.e. component design models) are valid the assembly model will also be valid. Since it has been established that the creation of supermodels is feasible at a component level, each of the component design models in the assembly could be validated against its

corresponding supermodel. Figure 2.1 illustrates this principle where one the component design models in a WEM is validated against its corresponding supermodel.

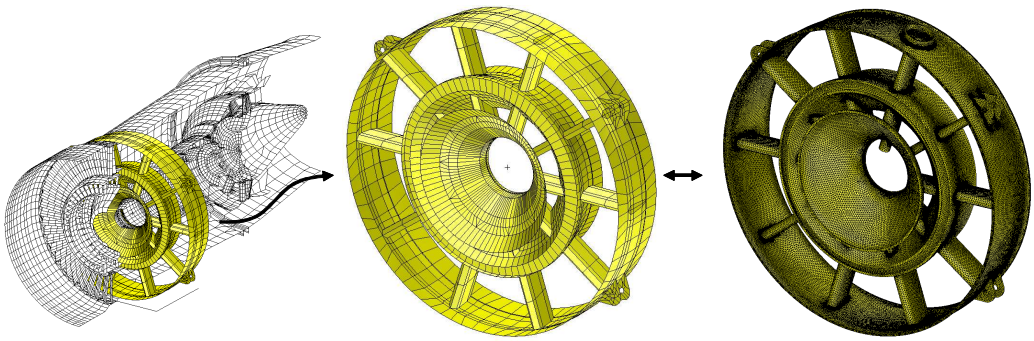

Figure 2.1. WEM validation component by component.

It is important to consider that a complex assembly model such as a WEM can be made up many component design models. The creation of supermodels is still not a straight-forward task. As a result, the validation of all component design models in a complex assembly, even though possible in theory, could become a daunting task.

It is most likely that the presence of modelling errors in some of the component design models will have a greater effect on the accuracy of the assembly model predictions. For instance, it is hard to imagine that the accurate modelling in a WEM of a pipe bracket would have the same effect as the appropriate definition of the front bearing support structure. If one could prioritise the components in the assembly according to their importance to the overall behaviour, the focus of the validation work could concentrate on those which are most relevant. This could massively reduce the task of validating complex assembly models to the validation of only a few of its constituent components.

A novel method for component prioritisation will be proposed in this chapter so that the most important component design models in an assembly model can be identified for individual validation.

2.3 Sensitivity Analysis

Sensitivity analysis is the cornerstone of the methodology developed in this work for component prioritisation. For this reason the next few pages are dedicated to review the basic concepts of sensitivity analysis in the context of structural dynamics.

If z(p) is a function dependant on the independent variable (or parameter) p, the value of z for values of p close to p_0 can be expressed using the Taylor series as:

$$z(p) = z(p_0) + \frac{1}{1!}\left.\frac{dz(p)}{dp}\right|_{p=p_0}(p - p_0) + \frac{1}{2!}\left.\frac{d^2z(p)}{dp^2}\right|_{p=p_0}(p - p_0)^2 + \frac{1}{3!}\left.\frac{d^3z(p)}{dp^3}\right|_{p=p_0}(p - p_0)^3 + \ldots \tag{2.3}$$

The values of the first two terms on the right hand side of equation (2.3) are typically the biggest contributors to the value of z(p). As a result:

$$z(p) \cong z(p_0) + \left.\frac{dz(p)}{dp}\right|_{p=p_0}(p - p_0) \tag{2.4}$$

is usually a good approximation of equation (2.3)

The term $\left.\frac{dz(p)}{dp}\right|_{p=p_0}$ in (2.4) represents the first-order sensitivity of function z(p) with respect to parameter p when evaluated at p_0. A high value of this derivative indicates that a small variation in the parameter p will lead to a big change in the value of z(p). Conversely, a low sensitivity means that even big changes in the parameter p will not have a significant effect on the value of z(p).

When the function z is dependant on more than one parameter, i.e. $z(p_1,p_2,p_3,\ldots)$ equation (2.4) is transformed into:

$$z(p_1,p_2,p_3,...) \cong z(p_{1_0},p_{2_0},p_{3_0},...) + \left.\frac{\partial z(p_1)}{\partial p_1}\right|_{\substack{p_1=p_{1_0}\\p_2=p_{2_0}\\p_3=p_{3_0}}} (p_1 - p_{1_0}) + \left.\frac{\partial z(p_2)}{\partial p_2}\right|_{\substack{p_1=p_{1_0}\\p_2=p_{2_0}\\p_3=p_{3_0}}} (p_2 - p_{2_0}) + \left.\frac{\partial z(p_3)}{\partial p_3}\right|_{\substack{p_1=p_{1_0}\\p_2=p_{2_0}\\p_3=p_{3_0}}} (p_3 - p_{3_0}) + ... \tag{2.5}$$

where the first-order sensitivity for each parameter is represented by the partial derivative of the function instead of the total derivative as in equation (2.4). Again, big changes to a parameter with low sensitivity will have little effect on the value of the function z while small changes to a parameter with high sensitivity will have a major effect on the value of z.

Let us now consider that the stiffness and mass matrices in a FEM depend on the values of the parameters $p_1,p_2,p_3,\ldots$:

$$[K] = [K(p_1,p_2,p_3,...)] \tag{2.6}$$

$$[M] = [M(p_1,p_2,p_3,...)] \tag{2.7}$$

The natural frequencies and modeshapes predicted by the FEM depend on the stiffness and mass matrices according to equation (1.1) which we recall here:

$$\left([K] - \omega_r^2 [M]\right)\{\phi\}_r = 0 \tag{2.8}$$

Hence:

$$\omega_r = \omega_r(p_1,p_2,p_3,...) \tag{2.9}$$

$$\{\phi\}_r = \{\phi\}_r(p_1,p_2,p_3,...) \tag{2.10}$$

If we wanted to make sure that the natural frequencies and the modeshapes predicted by the FEM are accurate, we should concentrate our effort in making sure that the parameters that affect the most the predictions are accurately described in the model. Mathematically these are the parameters that result in the highest sensitivities:

$$\frac{\partial \omega_r}{\partial p_j} \quad , \quad \frac{\partial \{\phi\}_r}{\partial p_j} \tag{2.11}$$

The following sections describe how to calculate these sensitivities. The simpler case where all the modes predicted by the FEM have distinct natural frequencies (i.e. non-degenerate problem) will be presented first. Later, the methods to calculate the natural frequency and modeshape sensitivities will be extended to cover the case where the model predicts more than one mode at the same frequency. This case is particularly relevant in the aeroengine industry where structures have a quasi axis-symmetric nature and most modes appear in orthogonal pairs.

The topic of sensitivity analysis in structural dynamic analysis is very broad. The following pages are only intended to give the reader a primer on the subject so that the rest of document can be well understood. Nonetheless, an extensive set of bibliography which covers the more complicated aspects of sensitivity analysis will be referenced for the interested reader.

2.3.1 Natural Frequency Sensitivity

The differentiation of (2.8) with respect to a general parameter p results in:

$$\left(\frac{\partial[K]}{\partial p} - \frac{\partial \omega_r^2}{\partial p}[M] - \omega_r^2 \frac{\partial[M]}{\partial p}\right)\{\phi\}_r + \left([K] - \omega_r^2[M]\right)\frac{\partial\{\phi\}_r}{\partial p} = \{0\} \tag{2.12}$$

where $\frac{\partial \omega_r^2}{\partial p}$ represents the sensitivity of the squared of the natural frequency with respect to changes in the parameter p. For practical reasons we show the sensitivity of the squared of the natural frequency instead of the sensitivity of the natural frequency as described in (2.11). The relationship between the two is straight-forward:

$$\frac{\partial \omega_r^2}{\partial p} = 2\omega_r \frac{\partial \omega_r}{\partial p} \tag{2.13}$$

If (2.12) is pre-multiplied by $\{\phi\}_r^T$, the resultant is:

$$\{\phi\}_r^T\left(\frac{\partial[K]}{\partial p} - \frac{\partial \omega_r^2}{\partial p}[M] - \omega_r^2 \frac{\partial[M]}{\partial p}\right)\{\phi\}_r + \{\phi\}_r^T\left([K] - \omega_r^2[M]\right)\frac{\partial\{\phi\}_r}{\partial p} = \{0\} \tag{2.14}$$

The term $\{\phi\}_r^T \left([K] - \omega_r^2 [M]\right)$ in equation (2.14) is invariably equal to 0 according to equation (2.8) as [K] and [M] are both symmetric. Furthermore, if $\{\phi\}_r$ is mass-normalised:

$$\{\phi\}_r^T [M] \{\phi\}_s = \delta_{rs} \tag{2.15}$$

$$\{\phi\}_r^T [K] \{\phi\}_s = \omega_r^2 \delta_{rs} \tag{2.16}$$

equation (2.14) can be re-written as:

$$\{\phi\}_r^T \frac{\partial [K]}{\partial p} \{\phi\}_r - \frac{\partial \omega_r^2}{\partial p} - \omega_r^2 \{\phi\}_{ri}^T \frac{\partial [M]}{\partial p} \{\phi\}_r = \{0\} \tag{2.17}$$

where the sensitivity of the natural frequency to changes in a parameter p can be expressed as:

$$\frac{\partial \omega_r^2}{\partial p} = \{\phi\}_r^T \frac{\partial [K]}{\partial p} \{\phi\}_r - \omega_r^2 \{\phi\}_r^T \frac{\partial [M]}{\partial p} \{\phi\}_r \tag{2.18}$$

According to equation (2.18), the natural frequency sensitivity can be explicitly calculated as long as the corresponding modeshape and the sensitivities of the stiffness and mass matrices are known.

The modeshape is usually calculated as part of the general eigenvalue solution to equation (2.8), hence it is readily available. However the sensitivities of the stiffness and mass matrices, $\frac{\partial [K]}{\partial p}$ and $\frac{\partial [M]}{\partial p}$ respectively, must be computed before the natural frequency sensitivity can be calculated.

In a general case, it can be difficult to explicitly calculate $\frac{\partial [K]}{\partial p}$ and $\frac{\partial [M]}{\partial p}$. Therefore it is common practice to calculate those terms using the finite difference approximations:

$$\frac{\partial [K]}{\partial p} \cong \frac{[K(p + \Delta p)] - [K(p)]}{\Delta p} \tag{2.19}$$

$$\frac{\partial [M]}{\partial p} \cong \frac{[M(p + \Delta p)] - [M(p)]}{\Delta p} \tag{2.20}$$

which requires a minimum computational effort.

As a result, all the terms required for the calculation of the eigenvalue sensitivity are either readily available or easy to compute, making the solving of the explicit equation (2.18) straight-forward.

In the 1960s, Rosenbrock [2], Morgan [3] and Reddy [4] formulated explicit equations to calculate the natural frequency sensitivity which do not require the use of the corresponding modeshape. Even though these are ingenious methods they are not widely used since, in general, the modeshapes are readily available as part of the general solution to the eigen problem (2.8).

2.3.2 Modeshape Sensitivity

Equation (2.12) can be reorganised to reflect the modeshape sensitivity problem:

$$\left([K] - \omega_r^2 [M]\right)\frac{\partial\{\phi\}_r}{\partial p} = \left(-\frac{\partial[K]}{\partial p} + \frac{\partial\omega_r^2}{\partial p}[M] + \omega_r^2\frac{\partial[M]}{\partial p}\right)\{\phi\}_r \tag{2.21}$$

In this equation the matrix $\left([K] - \omega_r^2 [M]\right)$ on the left hand side of the equation is invariably singular as ω_r^2 represents one of the matrix's eigenvalues. Since $\left([K] - \omega_r^2 [M]\right)^{-1}$ cannot be computed (it is singular), $\frac{\partial\{\phi\}_r}{\partial p}$ cannot be explicitly resolved.

Here we will review in detail two of the most common methods proposed to solve equation (2.21), one by Nelson [5] and the other by Fox and Kapoor [6].

Starting with Nelson's method, from the linear algebra it is known that the solution to (2.21) will take the general form of:

$$\frac{\partial\{\phi\}_r}{\partial p} = \{\psi\} - \alpha\{\phi\}_r \tag{2.22}$$

where $\{\psi\}$ is an arbitrary particular solution of:

$$\left([K] - \omega_r^2 [M]\right)\{\psi\} = \left(-\frac{\partial[K]}{\partial p} + \frac{\partial\omega_r^2}{\partial p}[M] + \omega_r^2\frac{\partial[M]}{\partial p}\right)\{\phi\}_r \tag{2.23}$$

Nelson proposed that one of the components in $\{\psi\}$ is set to zero. This particular solution will be valid as long as the corresponding component in $\{\phi\}_r$ is non-zero. Since most components in $\{\phi\}_r$ will be typically non-zero, this choice is straight-forward. As one of the components in $\{\psi\}$ is zero, the corresponding row and column in the equation (2.23) can be eliminated leading to:

$$\overline{\left([K]-\omega_r^2[M]\right)}\,\overline{\{\psi\}}=\overline{\left(-\frac{\partial[K]}{\partial p}+\frac{\partial\omega_r^2}{\partial p}[M]+\omega_r^2\frac{\partial[M]}{\partial p}\right)\{\phi\}_r} \tag{2.24}$$

The reduced matrix $\overline{\left([K]-\omega_r^2[M]\right)}$ is now non-singular (ω_r^2 is not he eigenvalue of this matrix but the full one) which means that the vector $\{\psi\}$ can be calculated using the following equation:

$$\overline{\{\psi\}}=\overline{\left([K]-\omega_r^2[M]\right)}^{-1}\overline{\left(-\frac{\partial[K]}{\partial p}+\frac{\partial\omega_r^2}{\partial p}[M]+\omega_r^2\frac{\partial[M]}{\partial p}\right)\{\phi\}_r} \tag{2.25}$$

The other factor in (2.23) which must be calculated to compute the modeshape sensitivity is α. In order to calculate this value, the mass-normalised condition in equation (2.15) is differentiated with respect to the parameter p:

$$\{\phi\}_r^T[M]\frac{\partial\{\phi\}_r}{\partial p}=-\frac{1}{2}\{\phi\}_r^T\frac{\partial[M]}{\partial p}\{\phi\}_r \tag{2.26}$$

Substituting (2.22) into (2.26) and reorganising the equation terms results in:

$$\alpha=\{\phi\}_r^T[M]\{\psi\}+\frac{1}{2}\{\phi\}_r^T\frac{\partial[M]}{\partial p}\{\phi\}_r \tag{2.27}$$

The major advantage of Nelson's method is the fact that the solution of the modeshape sensitivity is exact. However, the calculation of $\overline{\left([K]-\omega_r^2[M]\right)}^{-1}$ in equation (2.25) can be computationally expensive. This problem will be exacerbated if there is a requirement to calculate the sensitivity of many modeshapes, something very common in practice.

The prohibitive cost of the Nelson's method can be overcome by using the method proposed by Fox and Kapoor [6]. The basics of the Fox and Kapoor method are reviewed in the next lines.

The whole set of modeshapes $[\phi]$ calculated using equation (2.8) form a subspace of linearly independent vectors. As a result, the vector $\frac{\partial\{\phi\}_r}{\partial p}$ can be represented as:

$$\frac{\partial\{\phi\}_r}{\partial p} = \sum_{j=1}^{N} a_j \{\phi\}_j \tag{2.28}$$

where the coefficients a_j of the linear combination need to be calculated.

If (2.28) is substituted in (2.21) the resultant equation is:

$$\left([K] - \omega_r^2 [M]\right)\sum_{j=1}^{N} a_j \{\phi\}_j = \left(-\frac{\partial[K]}{\partial p} + \frac{\partial\omega_r^2}{\partial p}[M] + \omega_r^2 \frac{\partial[M]}{\partial p}\right)\{\phi\}_r \tag{2.29}$$

If equation (2.29) is pre-multiplied by any $\{\phi\}_j$ other than $\{\phi\}_r$ and considering the equations (2.15), (2.16) and (2.18), the coefficients a_j for any j other than r can be calculated according to:

$$a_j = \frac{\{\phi\}_j^T \frac{\partial[K]}{\partial p}\{\phi\}_r - \omega_r^2 \{\phi\}_j^T \frac{\partial[M]}{\partial p}\{\phi\}_r}{\omega_r^2 - \omega_j^2} \qquad \forall j \neq r \tag{2.30}$$

In order to resolve the term a_r the mass orthogonality condition (2.15) will be considered, similarly to Nelson's method. Substituting (2.28) into (2.26) and considering the orthogonality condition in equation (2.15), a_r can be calculated according to:

$$a_r = -\frac{1}{2}\{\phi\}_r^T \frac{\partial[M]}{\partial p}\{\phi\}_r \tag{2.31}$$

Considering the equations (2.28), (2.30) and (2.31), the Fox and Kapoor method to calculate the modeshape sensitivity can be written as:

$$\frac{\partial\{\phi\}_r}{\partial p} = \left(-\frac{1}{2}\{\phi\}_r^T \frac{\partial[M]}{\partial p}\{\phi\}_r \right)\{\phi\}_r + \sum_{\substack{j=1 \\ j\neq r}}^{N} \left(\frac{\{\phi\}_j^T \frac{\partial[K]}{\partial p}\{\phi\}_r - \omega_r^2 \{\phi\}_j^T \frac{\partial[M]}{\partial p}\{\phi\}_r}{\omega_r^2 - \omega_j^2} \right)\{\phi\}_j \tag{2.32}$$

According to the equation (2.32), all the modes that can be predicted by the FEM need to be calculated to compute the modeshape sensitivity of the r-th mode. Unfortunately, the calculation of all the modes that can be predicted by a FEM is computationally prohibitive. Just consider that the total number of modes that can be predicted by a FEM is equal to the total number of DOFs in the model, typically thousands or even millions. This does not mean that the method proposed by Fox and Kapoor cannot be used in practice. A close look at equation (2.32) reveals that the contribution of a mode j to the sensitivity $\frac{\partial\{\phi\}_r}{\partial p}$ is modulated by the factor $\frac{1}{\omega_r^2 - \omega_j^2}$. The addition of modes in (2.32) which are distant (in terms of natural frequency) from the mode of interest $\{\phi\}_r$ will have little effect on the accuracy of the calculations. In practice, only a few modes (L) whose natural frequencies ω_j are close of the natural frequency of the mode of interest ω_r need to be included to ensure a good approximation of the modeshape sensitivity:

$$\frac{\partial\{\phi\}_r}{\partial p} \cong \left(-\frac{1}{2}\{\phi\}_r^T \frac{\partial[M]}{\partial p}\{\phi\}_r \right)\{\phi\}_r + \sum_{\substack{j=1 \\ j\neq r}}^{L<N} \left(\frac{\{\phi\}_j^T \frac{\partial[K]}{\partial p}\{\phi\}_r - \omega_r^2 \{\phi\}_j^T \frac{\partial[M]}{\partial p}\{\phi\}_r}{\omega_r^2 - \omega_j^2} \right)\{\phi\}_j \tag{2.33}$$

According to equation (2.33) the modeshape sensitivity of the r-th mode can be calculated explicitly using the natural frequencies and modeshapes of only a few modes. The computational efficiency of this method typically makes it the preferred choice for the calculation of the modeshape sensitivities.

For the interested reader, there are other methods that have been proposed in recent years for the calculation of modeshape sensitivities. The works by Ojalvo and Zhang [7], Wang [8], Liu and Zhao [9], Géradin and Rixen [10] and Balmés [11] in the 1990s are amongst some of the most relevant contributions.

MAC Sensitivity

The sensitivity $\frac{\partial\{\phi\}_r}{\partial p}$ is a vector with as many components as DOFs in the model. It is difficult to infer from that vector the overall sensitivity of the modeshape to parameter changes.

One method to correlate two different modeshapes at an overall level is the Modal Assurance Criterion MAC [12]:

$$MAC\left(\{\phi\}_r, \{\phi\}_s\right) = \frac{\left|\{\phi\}_r^T \{\phi\}_s\right|^2}{\left(\{\phi\}_r^T \{\phi\}_r\right)\left(\{\phi\}_s^T \{\phi\}_s\right)} \tag{2.34}$$

The MAC is a scalar value that provides an overall estimation of the difference between two modeshapes. A MAC of 0 means that the two modeshapes are completely different in shape. A MAC of 1 indicates that the two modeshapes have the same shape.

According to equation (2.4), for small changes in the parameter p the following approximation is valid:

$$\{\tilde{\phi}\}_r(p_0 + \Delta p) \cong \{\phi\}_r(p_0) + \left.\frac{\partial\{\phi\}_r}{\partial p}\right|_{p=p0} \Delta p \tag{2.35}$$

The MAC correlation between the original modeshape $\{\phi\}_r$ and that subject to a parameter perturbation $\{\tilde{\phi}\}_r$ is:

$$MAC\left(\{\phi\}_r, \{\tilde{\phi}\}_r\right) = \frac{\left|\{\phi\}_r^T \{\tilde{\phi}\}_r\right|^2}{\left(\{\phi\}_r^T \{\phi\}_r\right)\left(\{\tilde{\phi}\}_r^T \{\tilde{\phi}\}_r\right)} \tag{2.36}$$

Obviously, the higher the eigenvector sensitivity $\frac{\partial\{\phi\}_r}{\partial p}$ the more different $\{\phi\}_r$ and $\{\tilde{\phi}\}_r$ will look like, hence reducing the value of the MAC. One can take advantage of this feature to evaluate the modeshape sensitivity at an overall level. Equation (2.37) represents the MAC sensitivity of the modeshape $\{\phi\}_r$ to changes in the parameter p.

$$\frac{\partial \mathrm{MAC}\left(\{\phi\}_r\right)}{\partial p} \cong -\left|\frac{\mathrm{MAC}\left(\{\phi\}_r, \{\tilde{\phi}\}_r\right) - \mathrm{MAC}\left(\{\phi\}_r, \{\phi\}_r\right)}{\Delta p}\right| = -\left|\frac{1}{\Delta p}\left(\frac{\left|\{\phi\}_r^T \{\tilde{\phi}\}_r\right|^2}{\left(\{\phi\}_r^T \{\phi\}_r\right)\left(\{\tilde{\phi}\}_r^T \{\tilde{\phi}\}_r\right)} - 1\right)\right| \tag{2.37}$$

The overall modeshape sensitivity can now be evaluated using a scalar rather than a vector. Please notice the use of the absolute values in equation (2.37). This is due to the fact that any change in the original modeshape $\{\phi\}_r$ will invariably reduce the value of the MAC. Subsequently the MAC sensitivity is always negative.

2.3.3 Repeated Natural Frequencies

The calculation of the natural frequency and modeshape sensitivities of a given mode using the equations described above is only valid when the natural frequency of the mode is distinct, this is, there is not any other mode with the same natural frequency. Most non-rotating machines are characterised for having all their modes at distinct natural frequencies and hence this is not an issue. However, most structures in the aeroengine industry have a quasi axis-symmetric or cyclic symmetric shape which means that most of the modes occur in orthogonal pairs.

We will now illustrate with a simple example why the methods described above are not suitable for calculating the natural frequency and modeshape sensitivities of a mode with a non-distinct natural frequency. Let us consider the simple axis-symmetric disk in Figure 2.2 (a) made of standard steel with a radius of 10 mm and a thickness of 0.25 mm. Figure 2.2 (b) shows the corresponding FEM made of shell elements while Figure 2.3 shows the predicted out-of-plane displacement for the first 2 non-rigid body modes of the disk in free-free configuration. These two modes occur at exactly the same frequency and have the same 2D shape. The only difference is that they are rotated $\frac{90^\circ}{2}$ with respect to each other to ensure orthogonality.

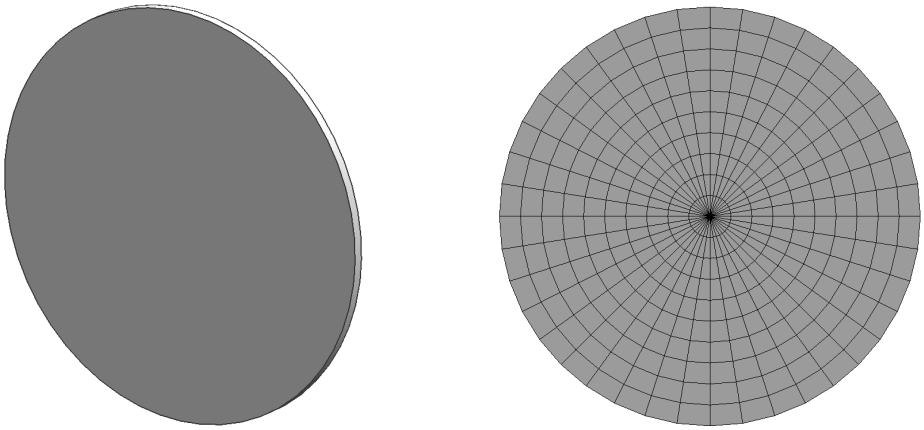

(a) (b)

Figure 2.2. Simple disk. (a) Geometry and (b) corresponding FEM.

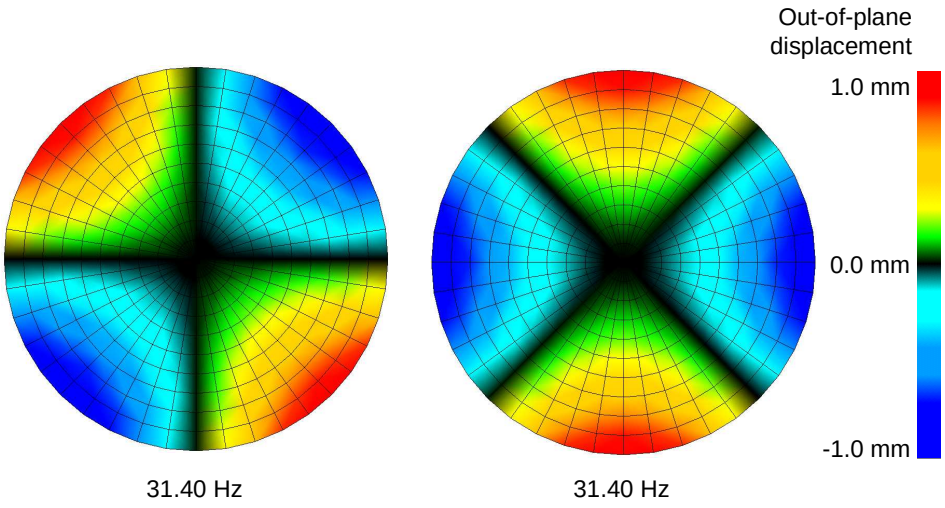

Figure 2.3. Simple disk. Modal predictions, first 2 non-rigid body modes.

If we rotated the nodal lines of both modes by the same arbitrary angle, the resultant two modes would also be a perfectly valid solution to the eigen problem in equation (2.8) and the modeshapes would fulfil the orthogonality conditions in equations (2.15) and (2.16). This means that the position of the nodal lines of the orthogonally paired modes is totally arbitrary.

What happens if the mass in the small area represented in Figure 2.4 is slightly decreased by 1%? The disk is no longer axis-symmetric. Now modes 1 and 2 have slightly different frequencies (i.e. frequency split) and the position of the nodal lines is not arbitrary anymore, see Figure 2.5. One of the nodal lines in mode 1 now lies exactly at the position where the mass was reduced. In the case of mode 2 the position where the mass was reduced coincides with an anti-node.

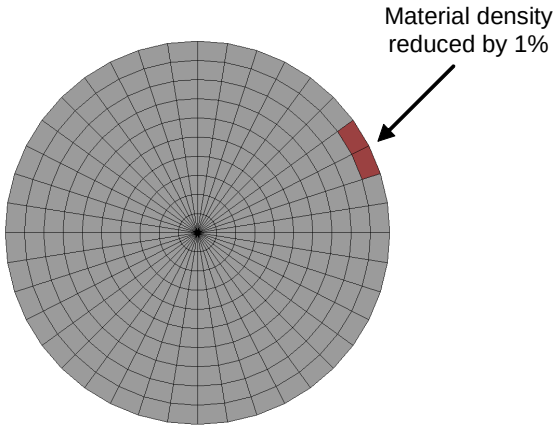

Figure 2.4. Simple disk. Parameter perturbation.

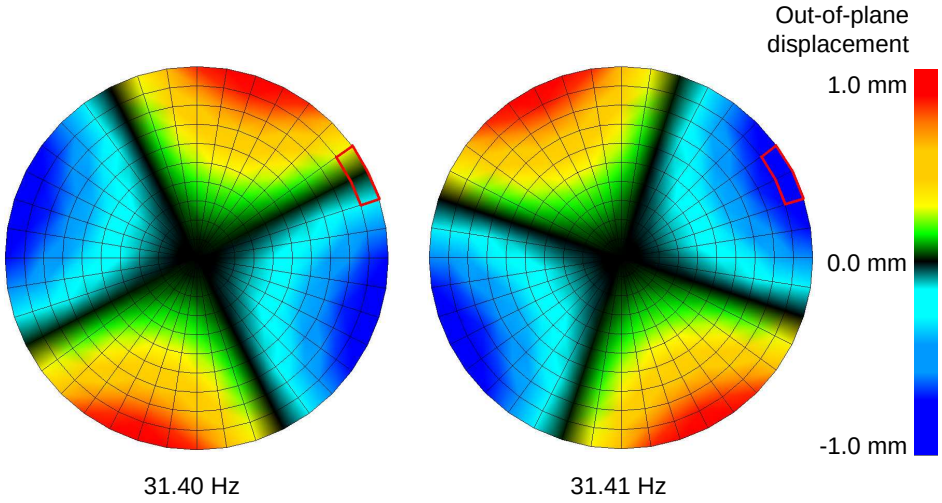

Figure 2.5. Simple disk. Predicted modes 1 and 2 after parameter perturbation.

Imagine that we wanted to assess the change in the modeshape of mode 1 due to the small mass change, or in other words, the modeshape sensitivity of mode 1 with respect to a parameter change. A look at Figures 2.3 and 2.5 reveals that the modeshape corresponding to mode 1 is practically the same before and after the parameter change. The only difference is that the modeshapes are rotated with respect to each other. As the nodal lines before the parameter change are positioned randomly, one would expect a low value of the modeshape sensitivity to the parameter change. However, if we performed a MAC correlation between the modeshape of mode 1 as illustrated in Figure 2.3 and the modeshape after the parameter change illustrated in Figure 2.5, the MAC value would be low, hence implying that that modeshape change is significant. In other words, the calculated modeshape sensitivity would be high. Moreover, as the nodal lines before the parameter change are positioned randomly the value of the MAC is also random. Obviously, this solution cannot be correct.

In the early 1980s Adelman and Haftka [13] proposed a solution to calculate the natural frequency sensitivities of all modes that share the same natural frequency. This solution is described next.

Let us consider a rectangular matrix $\overline{[\phi]}$ containing a set of m orthogonal modeshapes which share the same natural frequency. The value of m is equal to the total number of modes which share the same frequency (m is typically equal to 2 for axis-symmetric structures):

$$\overline{[\phi]} = [\phi_1 \phi_2 .....\phi_m] \tag{2.38}$$

This selection of modes is not unique. As explained above with a simple disc, there are an infinite number of mode combinations $\overline{[\phi]}$ that fulfil the equation (2.8) and the orthogonality properties in equations (2.15) and (2.16). One of those subsets, $[\Pi]$, will anticipate the modeshapes that result from introducing a parameter change in the model:

$$[\Pi] = \overline{[\phi]}[H] \tag{2.39}$$

where H is a transformation matrix. In general the transformation matrix will be different for every parameter since it is unlikely that two parameters will cause the modes to split in the same way. Just consider the case of the disc, if the mass change had occurred at a different position, the nodal lines would have rearranged in a different way.

By definition, the r-th mode in the equation (2.39):

$$\{\Pi\}_r = \overline{[\phi]}\{h\}_r \tag{2.40}$$

must fulfil the general equation (2.8):

$$\left([K] - \omega_r^2 [M]\right)\{\Pi\}_r = \{0\} \tag{2.41}$$

Substituting equation (2.40) into equation (2.41) results in:

$$\left([K] - \omega_r^2 [M]\right)\overline{[\phi]}\{h\}_r = \{0\} \tag{2.42}$$

Differentiating equation (2.42) with respect to a parameter p:

$$\left(\frac{\partial[K]}{\partial p} - \frac{\partial\omega_r^2}{\partial p}[M] - \omega_r^2\frac{\partial[M]}{\partial p}\right)\overline{[\phi]}\{h\}_r + \left([K] - \omega_r^2 [M]\right)\frac{\partial\overline{[\phi]}\{h\}_r}{\partial p} = \{0\} \tag{2.43}$$

Pre-multiplying (2.43) by $\overline{[\phi]}^T$ and using the orthogonality equations (2.15) and (2.16) results in:

$$\overline{[\phi]}^T\left(\frac{\partial[K]}{\partial p} - \omega_r^2\frac{\partial[M]}{\partial p}\right)\overline{[\phi]}\{h\}_r = \frac{\partial\omega_r^2}{\partial p}\{h\}_r \tag{2.44}$$

Equation (2.44) is an eigen problem where the only unknowns $\frac{\partial\omega_r^2}{\partial p}$ and $\{h\}_r$ are the eigenvalue and eigenvector respectively.

The term $\frac{\partial\omega_r^2}{\partial p}$ represents the natural frequency sensitivity of a mode $\{\Pi\}_r$ defined by (2.40). There are as many solutions to (2.44) as the multiplicity of the original modeshapes. Each of the solutions corresponds to one of the new split modes.

There is an interesting case where the solution to equation (2.44) is degenerate (repeated roots) and the eigenvector $\{h\}_r$ is not unequivocal. In practical terms this means that the parameter change does not provoke a split of the modes. This can be easily explained using the example of the simple disk above. Imagine now that the mass perturbation is uniformly distributed around the region defined in Figure 2.6. Since the change is also axis-symmetric the resultant modes from the change will have the same frequency. As it will be explained in subsequent sections of this chapter, this will never be the case in the methodology presented here for component prioritisation, and consequently no further attention will be paid here to this particular issue. The interested reader is referred to Friswell [14] for further information on how to deal with this problem.

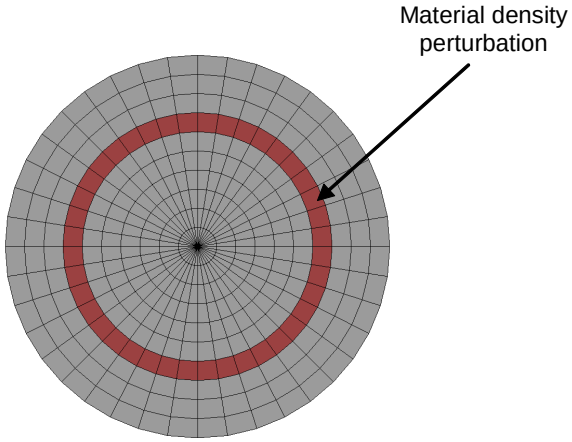

Figure 2.6. Simple disk. Axis-symmetric parameter perturbation.

In the case of the calculation of the modeshape sensitivity, a few authors have proposed different methods over the years. For instance, in the late 1980s and early 1990s, Zhang and Wei [15], Ojalvo [16], Mills-Curran [17] [18] and Dailey [19] extended the traditional Nelson's method described above while Lallement and Kosaneck [20], Juang *et al* [21], Bernard and Bronowicki [22] and Akgün [23] adapted the Fox and Kapoor's technique.

The interested reader is directed to these authors for further information. Here we will only show the final formulation of the extended version of the traditional Fox and Kapoor's method as it will be used in future sections of this work.

The modeshape sensitivity, $\frac{\partial\{\Pi\}_r}{\partial p}$, of a mode of multiplicity m which forms part of the subset $[\Pi]$ containing all m "re-aligned" modes can be calculated using the extended Fox and Kapoor method as:

$$\frac{\partial\{\Pi\}_r}{\partial p} = \{\upsilon\}_r + [\Pi]a_{rk} \tag{2.45}$$

where

$$\{\upsilon\}_r = \sum_{j=m+1}^{N} \frac{\{\phi\}_j^T \frac{\partial[K]}{\partial p}\{\Pi\}_r - \omega_r^2\{\phi\}_j^T \frac{\partial[M]}{\partial p}\{\Pi\}_r}{\omega_r^2 - \omega_j^2}\{\phi\}_j \tag{2.46}$$

$$a_{rk} = \frac{\{\Pi\}_k^T\left(\frac{\partial[K]}{\partial p} - \omega_r^2\frac{\partial[M]}{\partial p}\right)\{\upsilon\}_r}{\frac{\partial\omega_r^2}{\partial p} - \frac{\partial\omega_k^2}{\partial p}} + \frac{\{\Pi\}_k^T\left(\frac{\partial^2[K]}{\partial p^2} - \omega_r^2\frac{\partial^2[M]}{\partial p^2} - 2\frac{\partial\omega_r^2}{\partial p}\frac{\partial[M]}{\partial p}\right)\{\Pi\}_r}{2\left(\frac{\partial\omega_r^2}{\partial p} - \frac{\partial\omega_k^2}{\partial p}\right)}$$

$$\forall k = 1, m \qquad k \neq r \tag{2.47}$$

$$a_{rr} = -\frac{1}{2}\{\Pi\}_r^T \frac{\partial[M]}{\partial p}\{\Pi\}_r \tag{2.48}$$

2.4 Case Study

In order to ease the understanding of the model validation approach proposed in this work, the methodology will be illustrated using a real industry Case Study where the design model of an assembly of components will be validated from start to end.

Figure 2.7 shows the assembly design model in need of validation. The assembly is comprised of three aeroengine casings bolted together:

- Combustor Outer Casing, COC (red component);

- High Pressure Turbine – Intermediate Pressure Turbine Casing, HPTIPTC (yellow component) and;
- Low Pressure Turbine Casing, LPTC (blue component).

All the dimensions and material properties of the assembly model are nominal. Table 2.1 illustrates some of the characteristics of the assembly model.

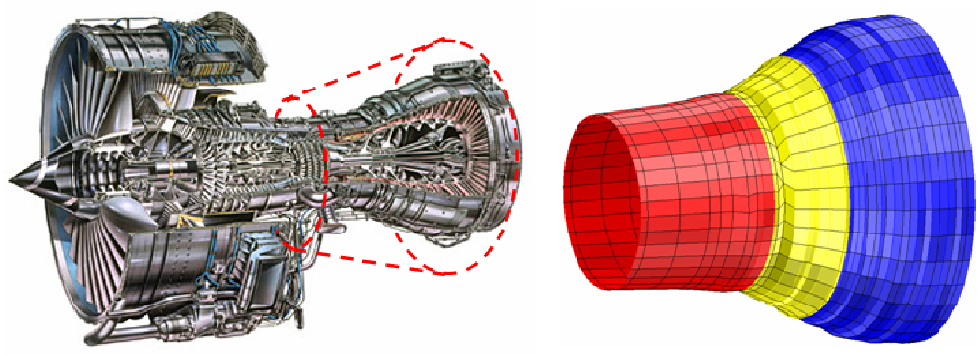

(a) (b)

Figure 2.7. Case Study assembly. (a) Location in the aeroengine and (b) design model.

As described at the beginning of this chapter, the assembly model will be validated by individually validating the most relevant of its constituent components using supermodels as the reference. Figure 2.8 describes this process. All the validation work is carried out in a virtual environment and well ahead of manufacture. Physical testing is only used at the end of the validation process as a confirmatory check (i.e. Certification).

	COC	HPTIPTC	LPTC	TOTAL
Total Number of DOFs	2,532	2,724	4,680	9,936
Total Number of Elements	434	684	1,044	2,162
Element Types	SHELL & BEAM	SHELL & BEAM	SHELL & BEAM	SHELL & BEAM

Table 2.1. Case Study assembly model.

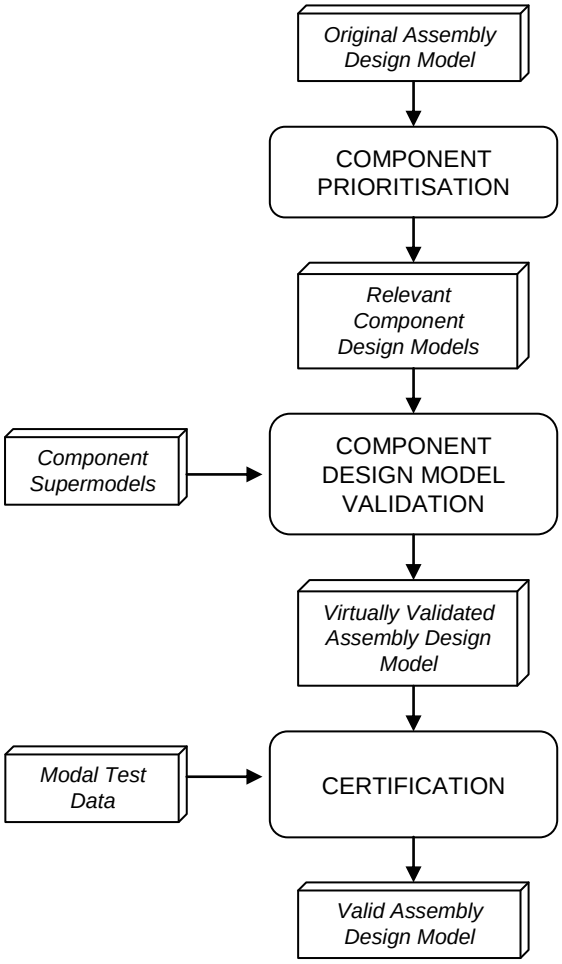

Figure 2.8. Assembly design model validation process.

Finally, it is important to point out that the methodology presented in this thesis can be applied to any assembly regardless of its number of constituent components.

2.4.1 Case Study Model Requirements

In the context of this work an assembly model is considered to be valid when it is capable of accurately predicting a specific set of modes (i.e. natural frequencies and modeshapes). These modes are typically the ones that contribute the most to the forced response calculations.

The assembly model validation strategy proposed here is independent of the modes chosen. For simplicity, the Case Study assembly model will be considered to be valid if it is capable of accurately predicting the first 20 non-rigid body modes of the structure when it is in free-free configuration. Figures 2.9 and 2.10 show the predicted modeshapes and the distribution of the natural frequencies* respectively. As expected, since the assembly design model is axis-symmetric the modes appear in orthogonal pairs.

These particular modes are selected for the following reasons.

- physical testing is used as a final confirmatory check of the validity of the "virtually" validated model. Free-free is an easy and relatively cheap configuration to achieve in practice. A more complex test configuration would increase the cost of the test and would not add any benefit for the demonstration of the technology proposed here. Also;
- 20 non-rigid body modes represent a sufficiently high number of modes to ensure that a successful model validation can be unequivocally attributed to the method being suitable and not simply by chance.

During the final check against the test data, the "virtually" validated assembly model will be considered valid if:

- all the natural frequency predictions fall within a ±5% error band when compared against the test results. And;
- the MAC correlation between the predicted and measured modeshapes is higher than 80% for all modes.

These error allowances should account for the fact that all the models used during the "virtual" validation (i.e. design models and supermodels) are nominal while the tested hardware is subject to manufacturing variability. Also, it is important to keep in mind that all physical tests are inevitably subject to measurement errors.

* The actual natural frequencies cannot be shown for commercial reasons.

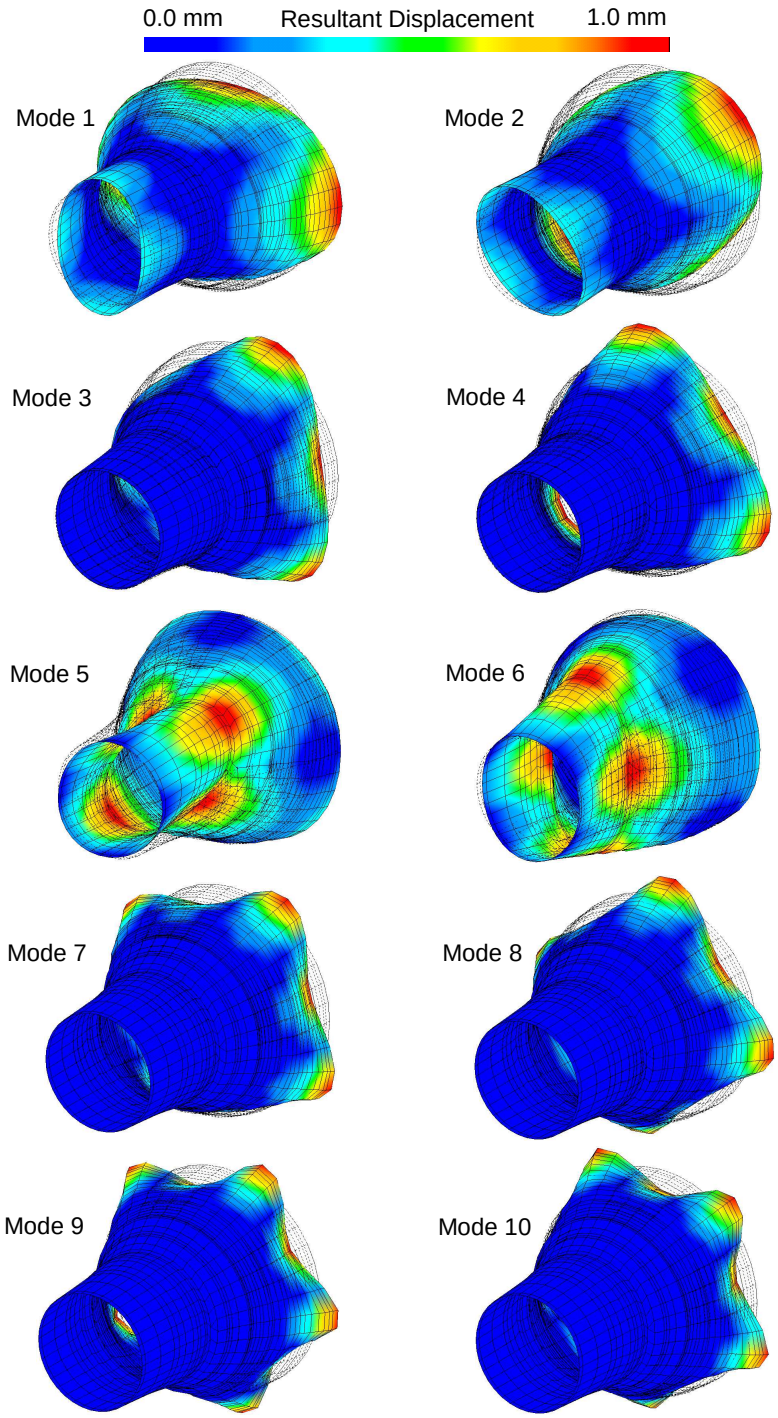
0.0 mm
Resultant Displacement
1.0 mm
Mode 1
Mode 2
Mode 3
Mode 4
Mode 5
Mode 6
Mode 7
Mode 8
Mode 9
Mode 10

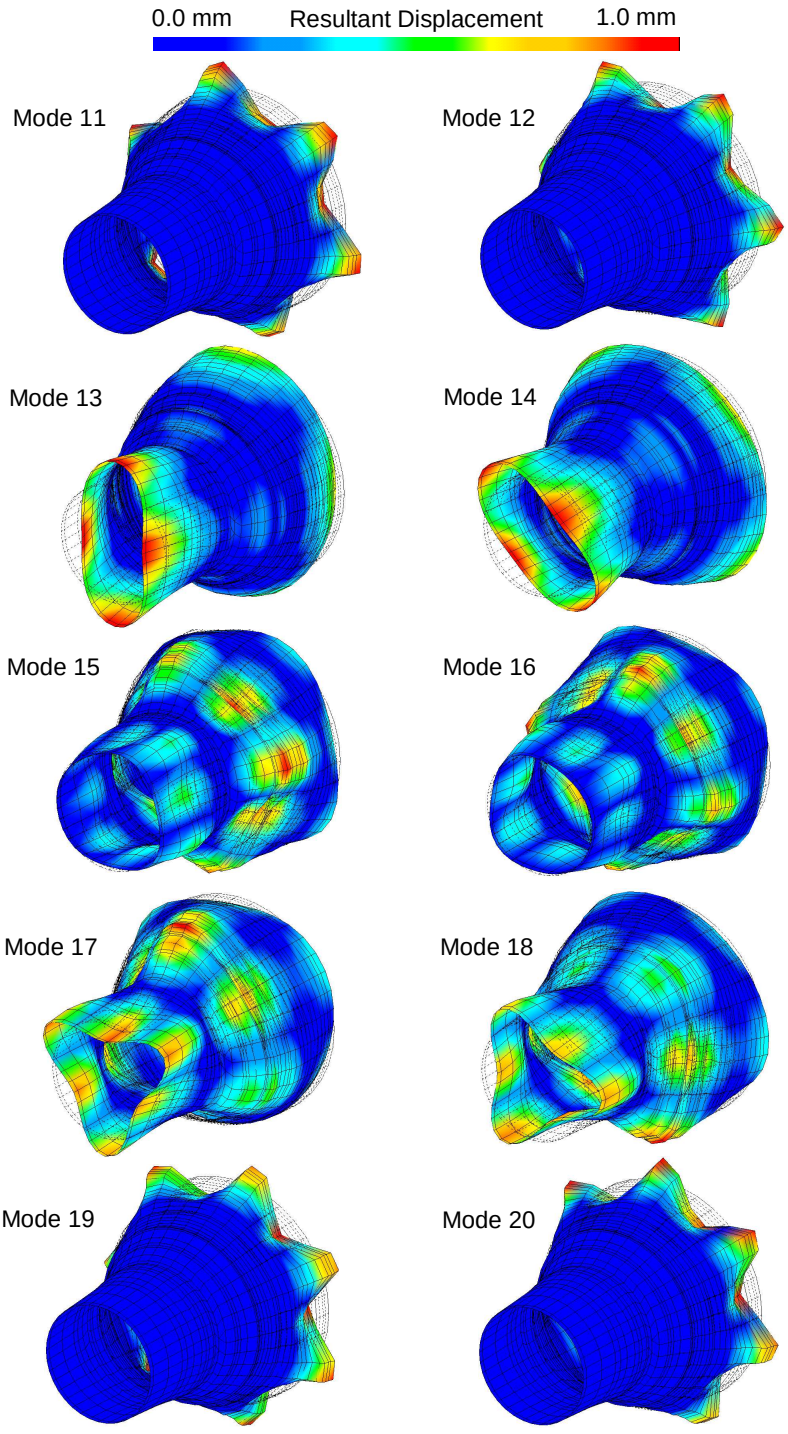

Figure 2.9. Case Study assembly model. Predicted first 20 non-rigid body modeshapes.

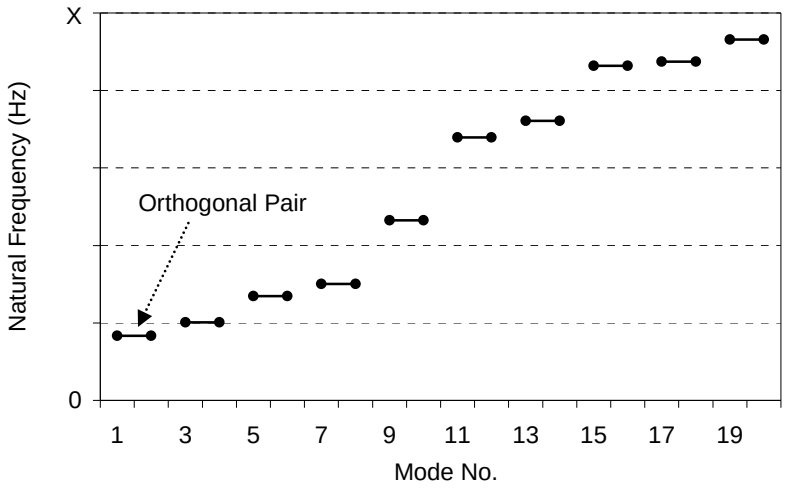

Figure 2.10. Case Study assembly model. Predicted natural frequency distribution.

In Chapter 5 a method is proposed that helps specifying acceptable limits for validation based, amongst others, on the expected manufacturing variability and the uncertainties associated with the physical test (e.g. instrument calibration). Nonetheless, for the moment the more traditional approach of setting limits based on intuition and experience will be followed. Furthermore, the limits described above are very tight and if anything, it is most likely that we are being conservative with the accuracy required.

2.5 Existing Methods for Component Prioritisation

The idea of validating an assembly model by validating only a few of its most relevant components is not new. At the beginning of the decade this concept was extensively studied during the CERES project [24] where Lenoir and Cogan [25] presented an analytical method to prioritise those components in most urgent need of validation. Before describing their approach it is important to understand how the design model of a component is created.

The design models of the components that make up an assembly must be simplified so that the final assembly model can be handled with the available computing power. For instance, Figure 2.11 shows the manufacturing CAD model of the Case Study COC

front flange and the corresponding design model. It is clear that most of the geometrical features in the flange such as holes, chamfers, fillet radii, etc. have been ignored in the design model and replaced by a simple 1D beam running along the edge of the component. The modeller will try to compensate for the geometry simplifications by "tuning" the parameters that define the beam (e.g. cross-section area, moments of inertia, etc.). This process is usually based on previous experiences with similar components. However the accurate definition of those parameters might be very difficult at times, especially when (i) a very coarse simplification is required, (ii) there is no previous experience with similar components or (iii) the geometry is very complex (e.g. hollow aerofoils). As a result, the confidence of the modeller on some of the parameters will be low.

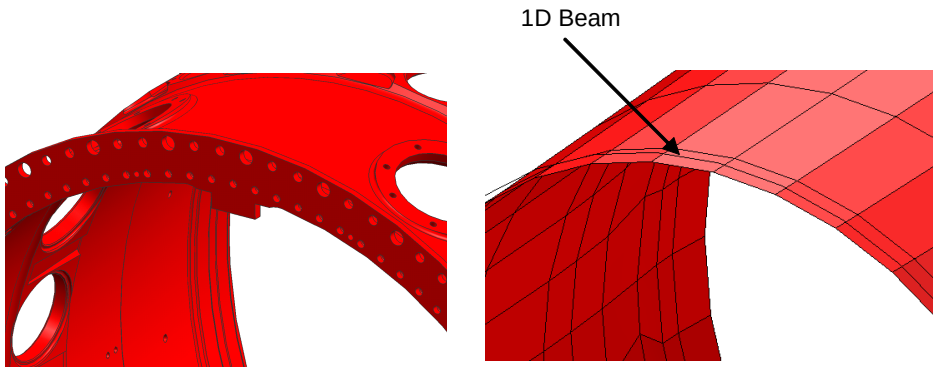

(a) (b)

Figure 2.11. COC front flange. (a) Manufacturing CAD model and (b) corresponding design model.

According to Lenoir and Cogan the most relevant component design models in an assembly can be identified following the next process:

- all the parameters in all the component design models which definition is "uncertain" must be identified first. Then;
- for each of the uncertain parameters, one must estimate the limits over which the "true" parameter value lies. Obviously, the more uncertainty over the definition of a parameter the bigger the range over which the parameter value might vary.

- For each of the component design models, a number of Craig-Bampton [26] reduced models are created. Each of the reduced models corresponds to a particular combination of the possible values of the uncertain parameters. Lenoir and Cogan proposed a method to best select the different combinations. Then;
- the different Craig-Bampton models corresponding to the different components are combined together to generate the full-assembly predictions. When there are not many models corresponding to each of the components, all possible combinations might be considered. Otherwise, a reduced number of combinations are used.
- The components which Craig-Bampton reduced models cause the biggest changes to the assembly predictions are prioritised for validation. Lenoir and Cogan use the so-called “Principal Component Analysis (PCA)” [27] [28] to quantitatively prioritise the importance of the different components.

The method proposed by Lenoir and Cogan is mathematically sound. However there is a fundamental issue that has hindered its application in industry. For the method to give reliable answers, all the uncertain parameters in all the component design models in the assembly must be identified upfront. Moreover, the user must accurately estimate for each parameter the limits over which the true parameter value lies.

Let us consider the Case Study of the three aeroengine casings. Figure 2.12 shows the actual geometry of a few regions in the assembly design model which are modelled using continuous shells and beams. All three component design models are simplified pretty much everywhere. This makes the identification of all the uncertain parameters in the component models very difficult. Moreover, the accurate estimation of the limits over which the true parameter values lie is almost impossible. This assembly is compromised of only three components, just imagine having to identify all the uncertain parameters in a model of a more complex assembly (e.g. whole aeroengine).

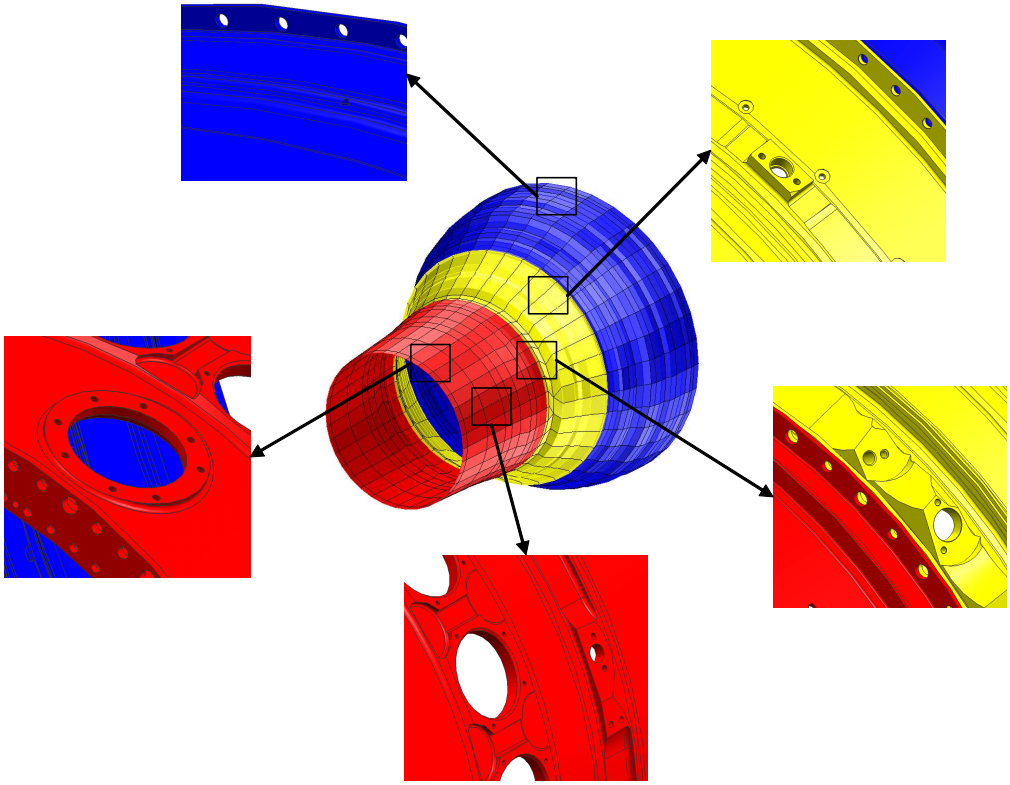

Figure 2.12. Case Study geometry simplifications.

2.6 Proposed Method for Component Prioritisation

According to equation (2.8), the accuracy of the modal properties predicted by a FEM depends on the right definition of the stiffness and mass matrices. The stiffness and mass matrices are in turn the result of the summation of the stiffness and mass matrices of all the individual finite elements in the model.

$$[K] = \sum_{j=1}^{n} [k]_j \tag{2.49}$$

$$[M] = \sum_{j=1}^{n} [m]_j \tag{2.50}$$

Small changes to the mass and stiffness matrices of some finite elements will have a bigger effect on the accuracy of the FEM predictions than others. The effect that

changes in a given finite element will have on the model predictions (i.e. natural frequencies and modeshapes) can be calculated using the following sensitivities:

$$\frac{\partial \text{Model Prediction}}{\partial [k]_j} \tag{2.51}$$

$$\frac{\partial \text{Model Prediction}}{\partial [m]_j} \tag{2.52}$$

A high sensitivity from (2.51) and/or (2.52) indicates that small changes to the modelling of a given finite element will have a big effect on the accuracy of the model predictions. Conversely, a finite element with a very low sensitivity indicates that even significant changes to its modelling will have little effect on the predictions from the model.

The denominators in (2.51) and (2.52) are matrices. This makes it very difficult, if not impossible, to calculate these sensitivities. This problem can be solved if a scalar could be representative of the matrix $[k]_j$ and another one for $[m]_j$. The Young's modulus and material density of the finite element can fill that role. An increase in the Young's modulus of the finite element will result in a stiffer element. Similarly an increase in material density of a finite element model will make the corresponding element heavier. Hence the sensitivities in (2.51) and (2.52) can be approximated as:

$$\frac{\partial \text{Model Prediction}}{\partial [k]_j} \cong \frac{\partial \text{Model Prediction}}{\partial E_j} \tag{2.53}$$

$$\frac{\partial \text{Model Prediction}}{\partial [m]_j} \cong \frac{\partial \text{Model Prediction}}{\partial \rho_j} \tag{2.54}$$

where E_j and ρ_j represent the Young's modulus and material density of the j-th finite element.

The sensitivities in (2.53) and (2.54) can be rewritten non-dimensionally as:

$$\frac{\partial \text{Model Prediction}}{\partial E_j} \frac{E_j}{\text{Model Prediction}} \tag{2.55}$$

$$\frac{\partial \text{Model Prediction}}{\partial \rho_j} \frac{\rho_j}{\text{Model Prediction}} \tag{2.56}$$

Imagine now that we calculated the sensitivity of the model predictions to changes in every single finite element in the model using (2.55) and (2.56). This would allow us to identify which are the finite elements in the model with the highest sensitivity. These finite elements should be modelled with greater care as any error in their definition will have a bigger impact on the accuracy of the model predictions.

There is also a big benefit of calculating the sensitivities for all finite elements in the model. When we calculate the sensitivity of the model predictions for all finite elements in the model we can plot the sensitivities back onto the model to identify the regions in the structure where a more careful modelling is required. For instance, let us consider the simple plate in Figure 2.13 (a) with dimensions 300x100x1 mm, a hole in the middle of 50 mm diameter and made of standard steel. Figure 2.13 (b) shows the corresponding FEM made of 6 noded triangular shells. Figure 2.13 (c) shows the modeshape prediction for the first non-rigid body mode in free-free configuration.

The colour of each of the finite elements in Figure 2.14 represents the sensitivity of the first mode's natural frequency to a change in the stiffness of the finite element using the ratio in (2.55). This plot allows us to easily identify the regions in the model where modelling errors will have the greatest effect on the accuracy of the predictions. Considering the modeshape for this mode it is no surprise that the regions that should be modelled with greater care are those on each side of the hole.

There is a problem though. The modeshape of the first mode of the plate is symmetric with respect to the vertical axis. As a result, one would expect that the accurate modelling of both sides of the hole would be equally important. However, the sensitivity plot is not symmetric with respect to the vertical axis. The reason lies in the characteristics of the mesh. In order to illustrate this point, let us consider a new a model of the plate, see Figure 2.15 (a), where the mesh density has been increased only on the left hand side. Figure 2.15 (b) shows the sensitivity results to changes in the stiffness (Young's modulus) of all finite elements.

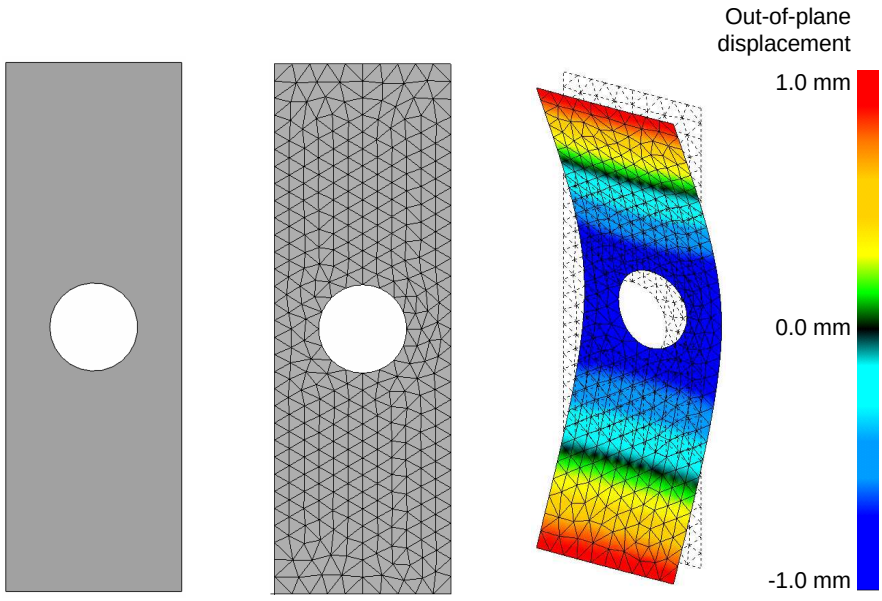

Figure 2.13. Simple plate. (a) Geometry, (b) FEM and (c) first non-rigid body mode.

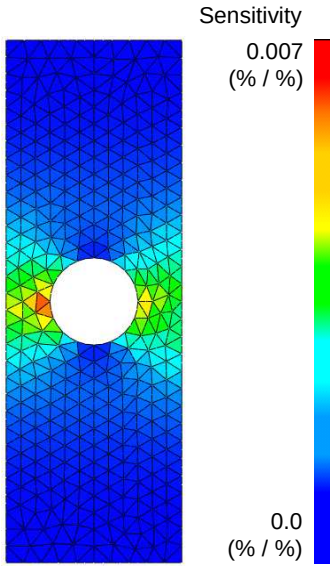

Figure 2.14. Simple plate sensitivity of the first natural frequency to stiffness changes.

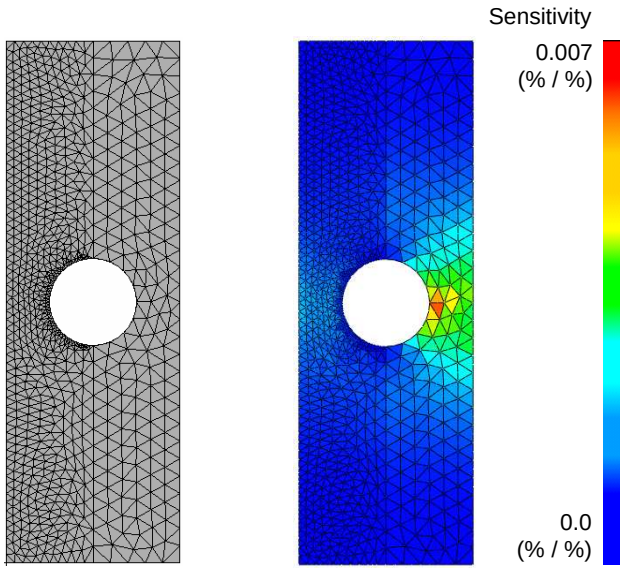

Figure 2.15. Plate model with high mesh density on the left hand side. (a) Mesh and (b) natural frequency sensitivity to stiffness changes.

The sensitivity on the left hand side has now vanished. This is because the ratios in (2.55) and (2.56) always favour big elements. They represent a bigger physical area, hence, changes to their stiffness and mass characteristics are likely to have a greater effect on the predictions. This is an important issue since, in practice, the most difficult regions to model are usually those with smaller elements. The use of (2.55) and (2.56) can incorrectly bias the focus towards regions having larger elements. This problem can be easily solved by weighting the sensitivity values according to the volume of the elements:

$$\frac{\partial \text{Model Prediction}}{\partial E_j} \frac{E_j}{\text{Model Prediction}} \frac{V_T}{V_j} \tag{2.57}$$

$$\frac{\partial \text{Model Prediction}}{\partial \rho_j} \frac{\rho_j}{\text{Model Prediction}} \frac{V_T}{V_j} \tag{2.58}$$

where V_j is the volume of the j-th finite element and V_T is the total volume of the model.

The ratios (2.57) and (2.58) will be referred to as sensitivity density. Figure 2.16 shows the sensitivity density for the simple plate with dissimilar mesh density on each side. The sensitivity is now symmetric and focussed on the right locations.

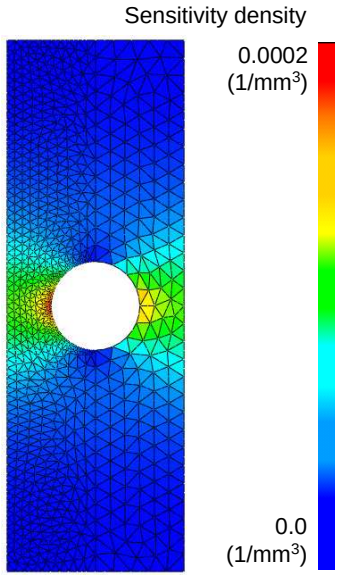

Figure 2.16. Plate with high mesh density on the left hand side. Sensitivity density of the natural frequency to stiffness changes.

Let us now consider the Case Study of the three casing assembly. The assembly model must accurately predict the first 20 free-free modes (natural frequencies and modeshapes) to be considered valid. Figures 2.17 and 2.18 show the natural frequency and modeshape sensitivity densities to changes in the stiffness (Young's modulus) and mass (material density) properties respectively. The sensitivities are calculated using (2.44), (2.45), (2.57) and (2.58). In order to ease the interpretation, each of the sensitivity contours is plotted on a model deformed according to the corresponding modeshape.

Please remember that this assembly model is axis-symmetric and that the first 20 modes appear as 10 orthogonal pairs. As already explained in Section 2.3.3 using a simple disc, the modification of a small region in a structure with orthogonal pairs will result in the reorientation of the modes. One of the modes in each pair will be more severely affected by the change than the other. It is only the highest change which is of

interest since it will have a bigger effect on the accuracy of the predictions. That is why only one sensitivity plot is presented for each mode pair.

Moreover, all the sensitivities have been normalised from 0 to 1 to facilitate the comparison between plots. The reader is reminded that:

- the natural frequency sensitivities are always positive for stiffness changes. An increase in stiffness will invariably increase the natural frequency, see equation (2.18);
- the natural frequency sensitivities are always negative for mass changes. An increase in mass will invariably decrease the natural frequency, see equation (2.18) and ;
- the MAC sensitivities are always negative for both stiffness and mass changes. Any change in either mass or stiffness will invariably result in a modification of the original modeshape and therefore a reduction in the MAC value, see equation (2.37).

The sensitivity contour plots can be used to prioritise the component design models in the assembly which are in most urgent need of validation. For instance, all the sensitivity plots corresponding to the mode pair 7-8 indicate that the accuracy in the predictions for this mode pair is mainly influenced by the quality of the LPT design model. The presence of modelling errors in the other two components will have a much lower effect in the predictions. As a result, if one only wanted to validate the assembly predictions for this mode pair, the validation of the LPT design model should be given the highest priority.

Some other interesting conclusions can be drawn from the analysis of Figures 2.17 and 2.18:

- for any given mode, the natural frequency and modeshape sensitivity might not look similar. This is particularly noticeable in the sensitivities to stiffness changes of the mode pair 5-6. Also;
- it is sometimes very difficult to anticipate where the sensitive areas will lie without the help of the sensitivity plots. See for instance the modeshape sensitivity to stiffness changes for the mode pair 19-20 in Figure 2.17. It would

be very difficult for anyone to foresee that the accurate modelling of the COC is important for the correct prediction of a mode which is totally dominated by the activity at the rear end of the LPTC. Finally;

- all the sensitivity plots are axis-symmetric. By definition, the sensitivity contour plot of an axis-symmetric model must also be axis-symmetric.

Finally, the calculation of the sensitivities for the thousands or even millions of finite elements in an assembly model might look computationally expensive. Nonetheless, it is not. When describing the methods for sensitivity analysis, particular attention was paid to those which are explicit. These methods facilitate the calculation of sensitivities at a much reduced computational cost. In fact, the calculation of the sensitivities does not take much longer than any standard FEM post processing operation (e.g. stress calculation from the nodal displacements).

2.6.1 Relative Importance of the Sensitivity to Mass Changes

Typically a component design model must match the mass properties (e.g. total mass, position of the centre of gravity, etc.) predicted by a detailed manufacturing CAD drawing of the component before it is ever used as part of a bigger assembly model. This is usually achieved by adjusting local material densities or adding concentrated masses in certain regions of the component design model. The end result being that the mass distribution of a component design model is usually very accurate.

There is however a much greater deal of uncertainty associated with the modelling of the stiffness. Not only because the modeller usually has not got any reference to compare against, as in the case of the mass properties, but also because the accurate modelling of the stiffness is usually much more complex than that of the mass.

For the reasons above, in most cases, when it comes to prioritise component design models for individual validation the focus should be on those that contain the regions of higher sensitivity to stiffness variations. The sensitivity to the mass distribution takes a secondary role since it is most likely that the mass properties of all the component design models are already accurately modelled.

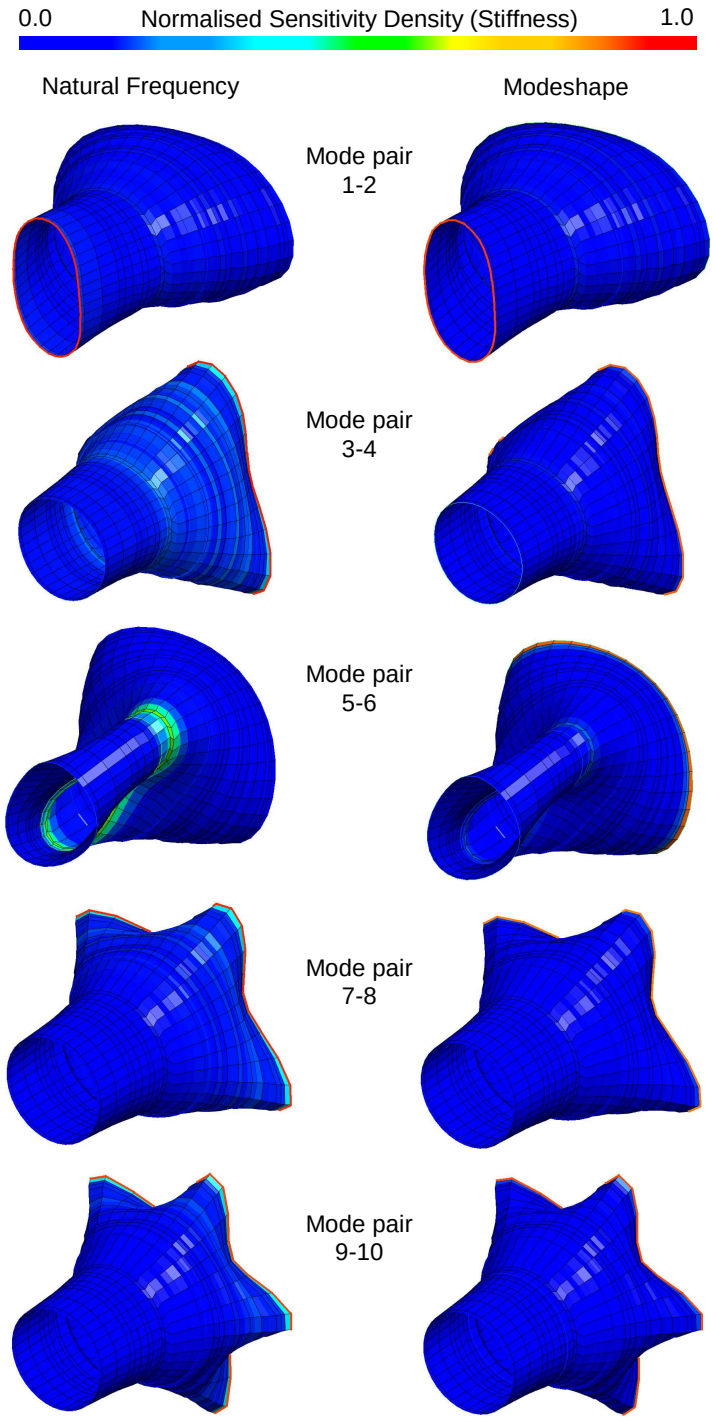
0.0
Normalised Sensitivity Density (Stiffness)
1.0
Natural Frequency
Modeshape
Mode pair 1-2
Mode pair 3-4
Mode pair 5-6
Mode pair 7-8
Mode pair 9-10

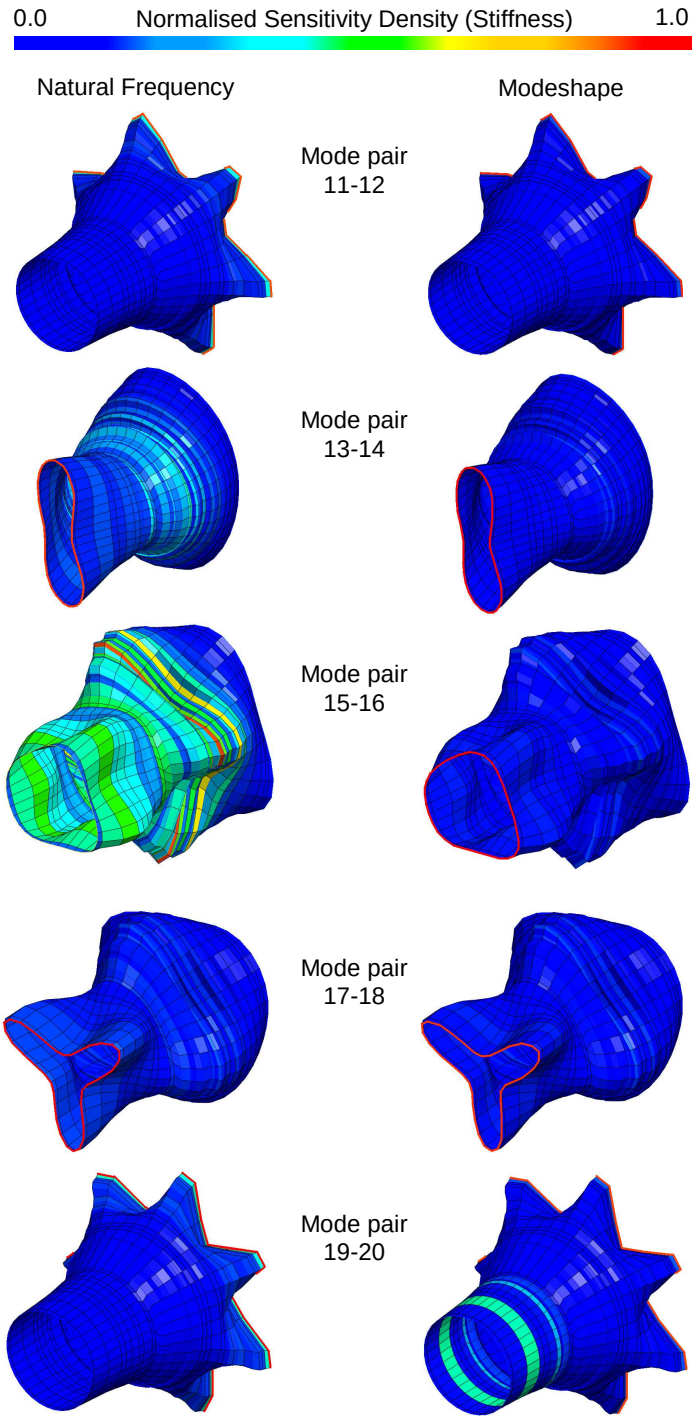

Figure 2.17. Case Study sensitivity density to changes in stiffness.

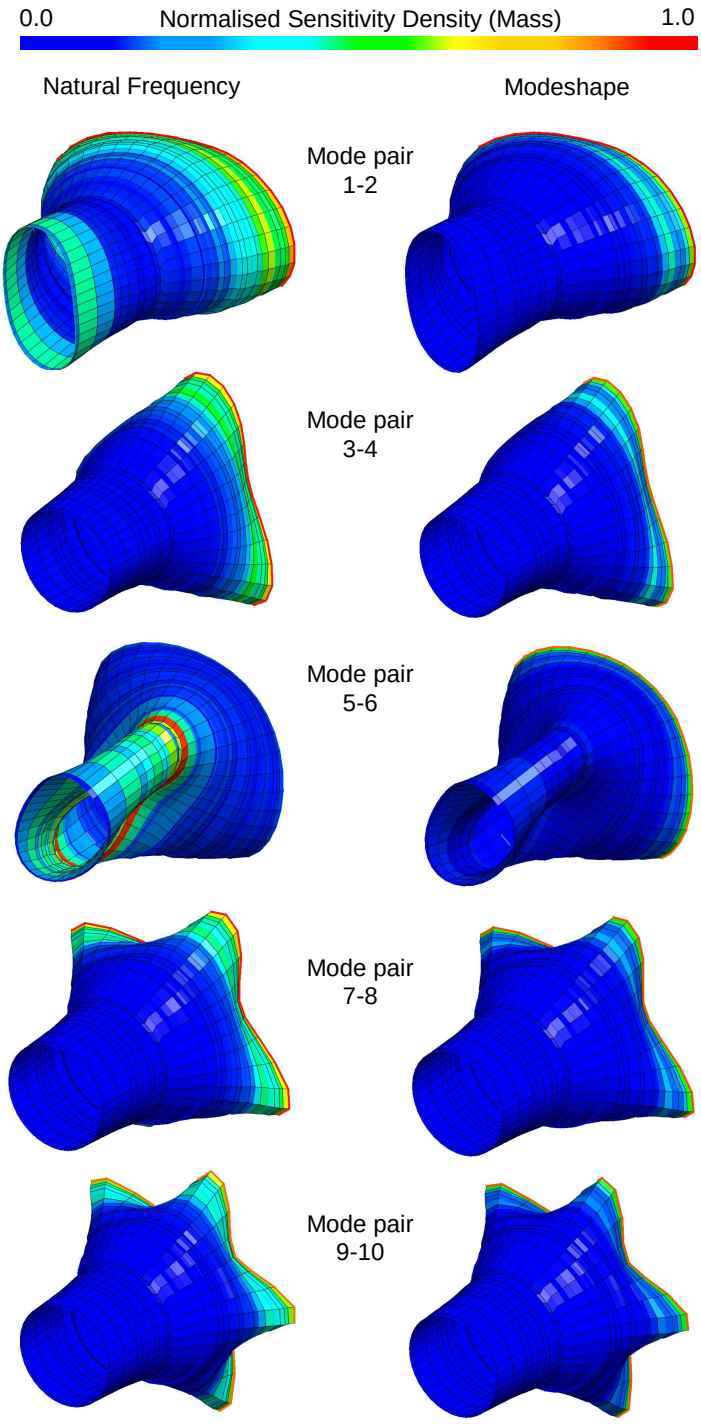
0.0
Normalised Sensitivity Density (Mass)
1.0
Natural Frequency
Modeshape
Mode pair 1-2
Mode pair 3-4
Mode pair 5-6
Mode pair 7-8
Mode pair 9-10

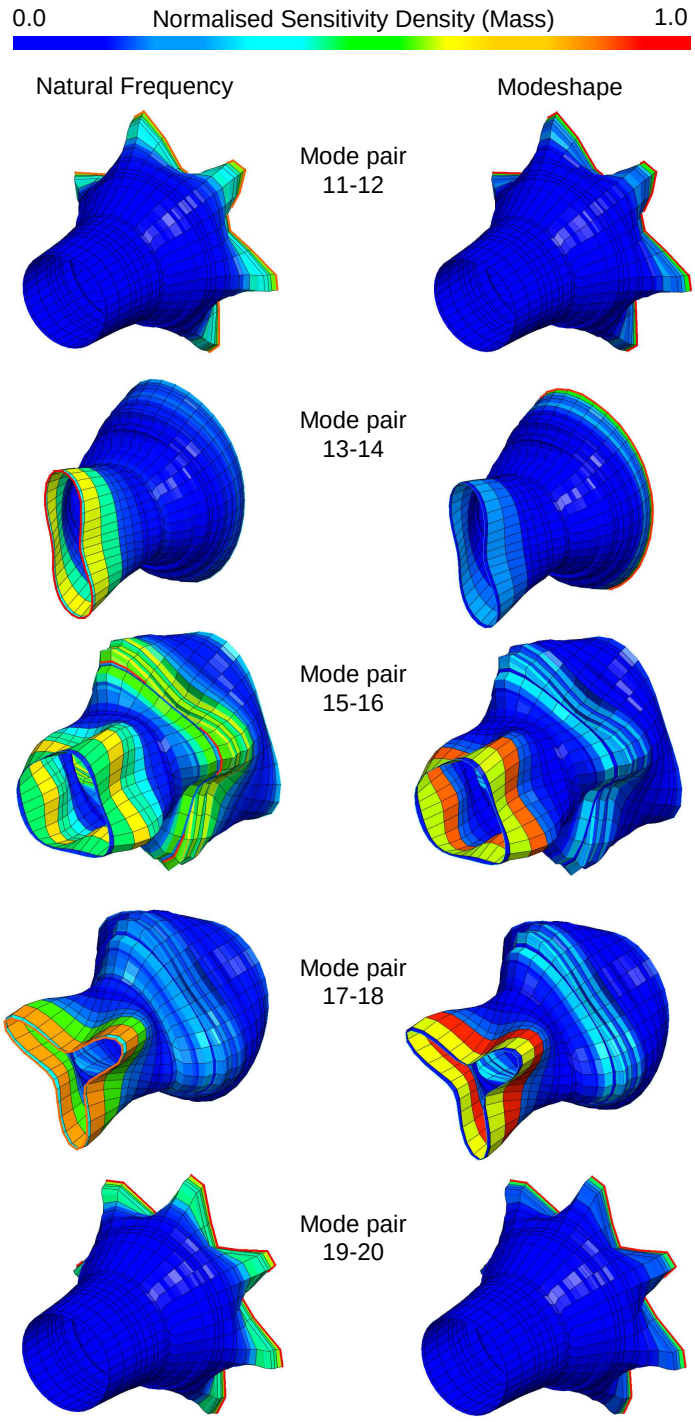

Figure 2.18. Case Study sensitivity density to changes in mass.

2.6.2 Component Prioritisation - Quantitative Assessment

The sensitivity density plot in Figure 2.17 (stiffness), and to a smaller extent that in Figure 2.18 (mass), can help identifying those components in the assembly in most urgent need of validation. In some cases, such as in mode pair 7-8, a look at the plot containing the sensitivity to stiffness changes is enough to reveal that only one of the components (i.e. LPT) requires validation. Nonetheless this decision gets more complicated for mode pair 15-16 where the sensitivity is more widely spread. In order to get rid of some of this subjective judgement and to make the method more robust for deployment in industry a quantitative approach for component prioritisation is proposed next.

The total sensitivity to variations in the stiffness of the k-th component design model in an assembly can be calculated by integrating the sensitivity density in (2.57) across the volume of the component:

$$\int_{V_{kj}} \left(\frac{\partial \text{Model Prediction}}{\partial E_j} \frac{E_j}{\text{Model Prediction}} \frac{V_T}{V_j} \right) dV \tag{2.59}$$

Considering that a FEM is a discrete system, the previous integral is equivalent to:

$$\sum_{j=1}^{n_k} \left(\frac{\partial \text{Model Prediction}}{\partial E_j} \frac{E_j}{\text{Model Prediction}} \frac{V_T}{V_j} \right) V_j \tag{2.60}$$

where and n_k is the total number of elements in the k-th component model. The ratio of a component's sensitivity with respect to the total in the assembly is given by:

$$C_k = \frac{\sum_{j=1}^{n_k} \left(\frac{\partial \text{Model Prediction}}{\partial E_j} \frac{E_j}{\text{Model Prediction}} \frac{V_T}{V_j} \right) V_j}{\sum_{j=1}^{n} \left(\frac{\partial \text{Model Prediction}}{\partial E_j} \frac{E_j}{\text{Model Prediction}} \frac{V_T}{V_j} \right) V_j} \tag{2.61}$$

where n is the total number of elements in the assembly model. Equation (2.61) can be simplified as:

$$C_k = \frac{\sum_{j=1}^{n_k}\left(\frac{\partial \text{Model Prediction}}{\partial E_j}\frac{E_j}{\text{Model Prediction}}\right)}{\sum_{j=1}^{n}\left(\frac{\partial \text{Model Prediction}}{\partial E_j}\frac{E_j}{\text{Model Prediction}}\right)} \tag{2.62}$$

This ratio can be used as an indicator of a component's relevance to the assembly predictions. Note that only the sensitivity to stiffness changes has been included in the calculations. In the unlikely event where there is a great deal of uncertainty associated with the modelling of the mass distribution, the same methodology could be followed using the sensitivities to mass changes.

The ratios in Figure 2.19 show the relative importance of each component design model in the Case Study to the accurate prediction of the first 20 assembly modes (natural frequencies and modeshapes). Again, only the sensitivities to stiffness changes are considered since there is typically little uncertainty about the mass distribution in the component design models.

As expected, those ratios confirm some of the initial conclusions drawn from looking at the sensitivity plots in Figure 2.17. However, now the information is easier to handle and a great deal of subjective judgement is replaced by numerical figures. Still the modeller has to decide the threshold over which the contribution of a component is considered relevant and hence needs individual validation. This decision is normally based on engineering judgement but will usually take into account:

- the accuracy required for the predictions. A higher accuracy will demand an accurate modelling of not only the most important regions but also of those of medium relevance. In such case, the threshold will be low. Also;
- the number of components in the assembly. In assemblies where there are many components it is unlikely that the sensitive regions will only be concentrated around one or two components. It is likely that they will be more widely spread. In this case, accurate predictions will demand a lower threshold to include more components.

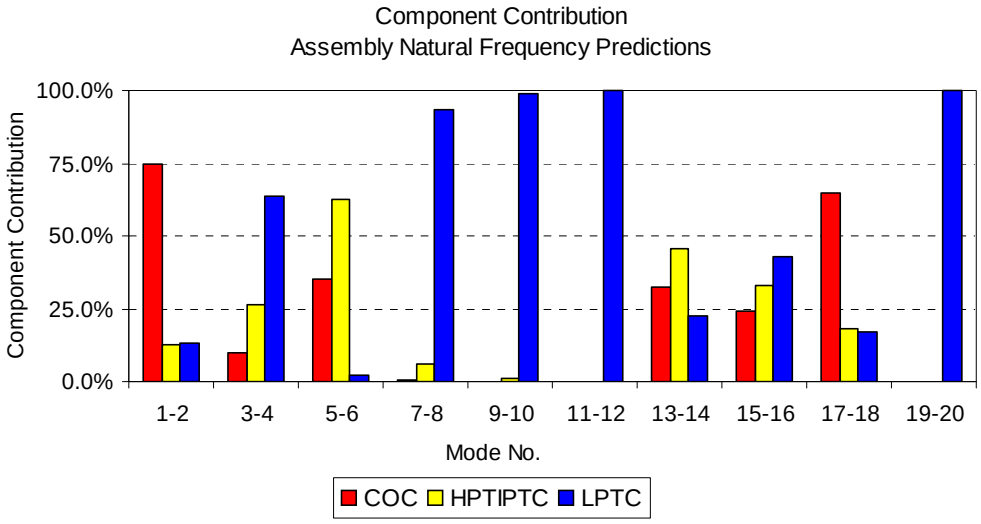

(a)

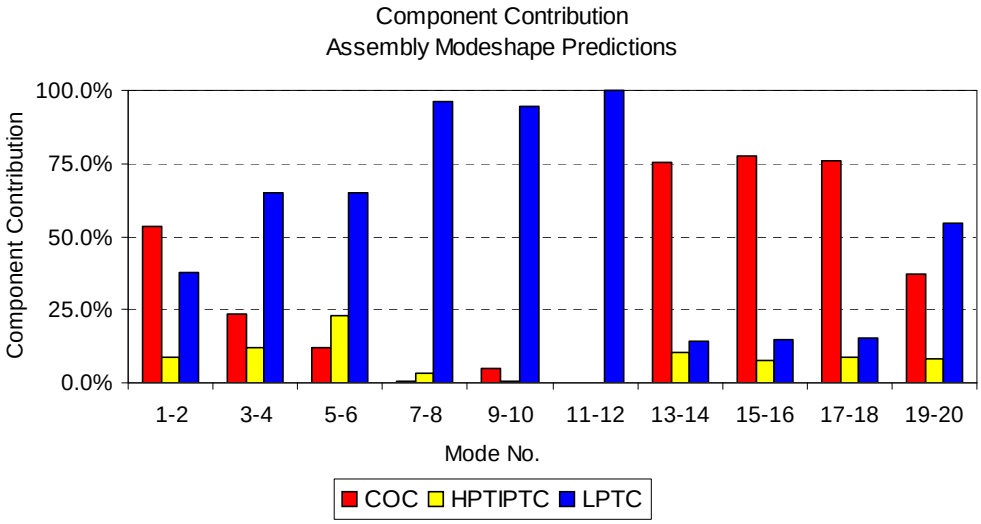

(b)

Figure 2.19. Case Study component prioritisation. Individual contribution to (a) natural frequency and (b) modeshape.

For the assembly Case Study here, a threshold of 25% is selected. According to this threshold, if the requirement for the assembly model was to accurately predict only mode pairs 7-8, 9-10 and 11-12, the ratios in Figure 2.19 would suggest that only the validation of the LPTC design model would be required.

If only the mode pair 1-2 was required, both the COC and the LPTC would need validation. The COC is the main contributor to the natural frequency and modeshape (around 75% and 50% respectively) while the LPTC still has a significant importance in the modeshape (around 40%).

The requirements for the Case Study assembly model are the accurate predictions of the first 20 modes (10 mode pairs). The contribution ratio of all three components is beyond the specified threshold (25%) for at least one of the mode pairs. This means that all three component design models will require individual validation.

2.6.3 Validation of the Component Prioritisation Method

In order to validate the component prioritisation method above, a small exercise is devised. Let us assume that the Young's modulus of the COC design model in the original Case Study assembly model has been incorrectly modelled and is 10% higher than it should. If the prioritisation method is correct, this modelling error should have a bigger effect on the assembly modes where the COC contributes the most. Figure 2.20 (a) shows the COC contribution to the accurate prediction of the assembly natural frequencies. Figure 2.20 (b) shows the error introduced by the incorrect modelling of the COC. Clearly the biggest errors occur in those modes where the COC contribution is higher. Conversely, those modes where the contribution is low do not seem to be affected by the modelling error.

Similarly to the case above, let us consider now that the modelling error (10% increase in the Young's modulus) has taken place in the HPTIPTC alone. Figure 2.21 show the same conclusions as above.

Figure 2.22 shows the same effects when the modelling errors only occur in the LPTC.

Finally, all three cases above are put together in Figure 2.23. It is clear that the higher the contribution of a component the more emphasis should be put into its validation as modelling errors will have a greater effect on the assembly predictions.

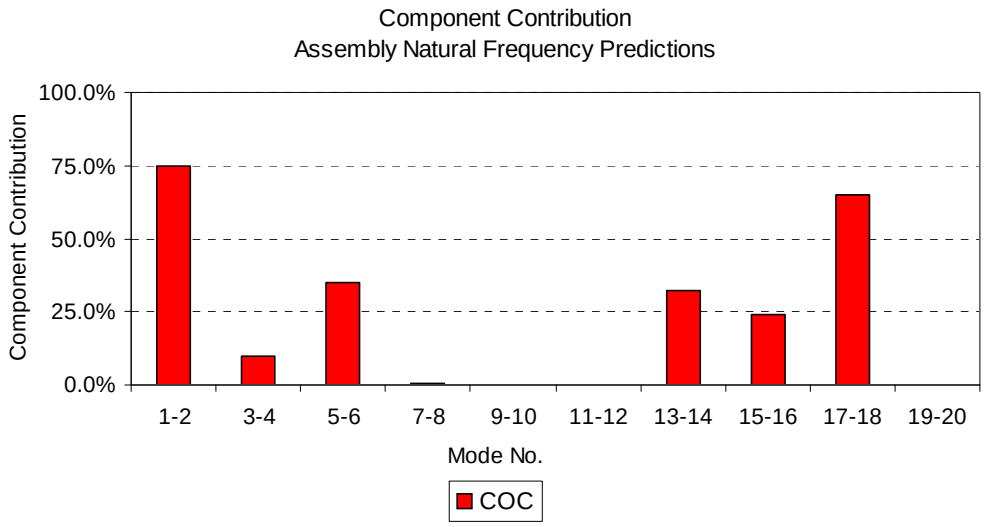

(a)

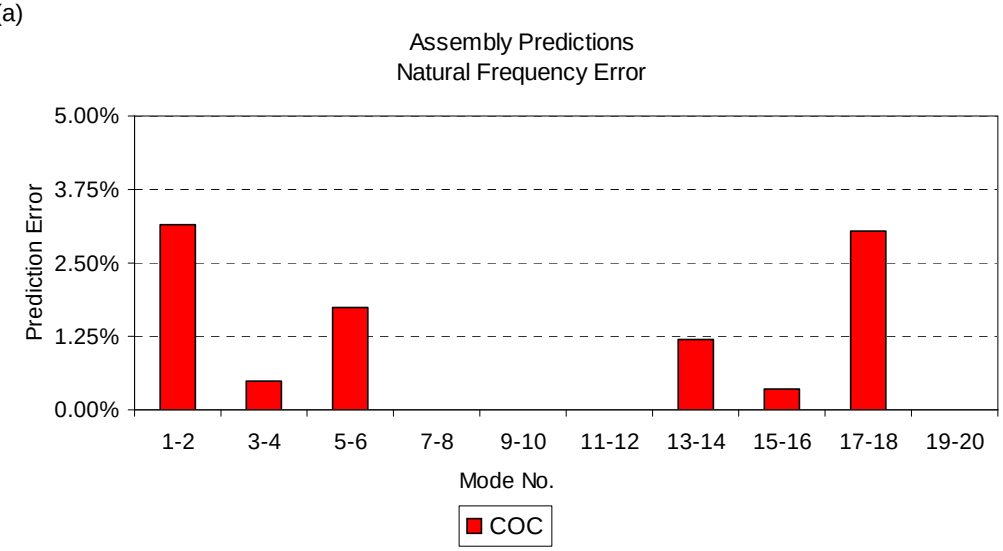

(b)

Figure 2.20. Validation of the component prioritisation method. (a) COC contribution to the assembly natural frequency predictions and (b) natural frequency error when the COC Young's modulus is incorrectly modelled (+10% with respect to nominal).

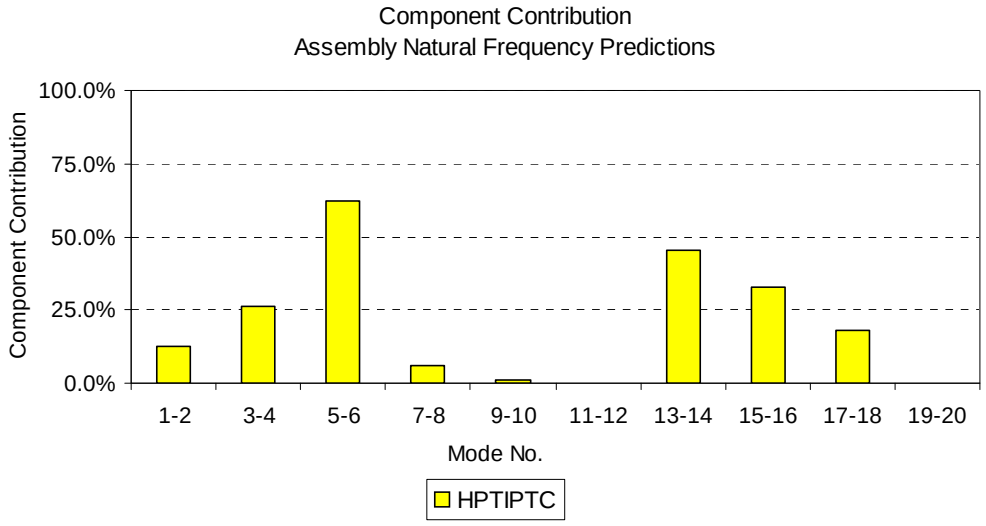

(a)

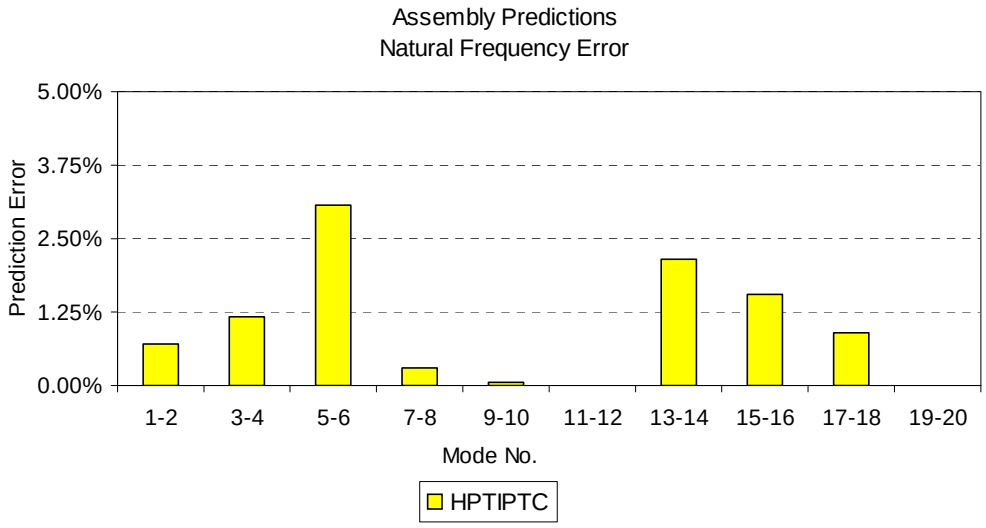

(b)

Figure 2.21. Validation of the component prioritisation method. (a) HPTIPTC contribution to the assembly natural frequency predictions and (b) natural frequency error when the HPTIPTC Young's modulus is incorrectly modelled (+10% with respect to nominal).

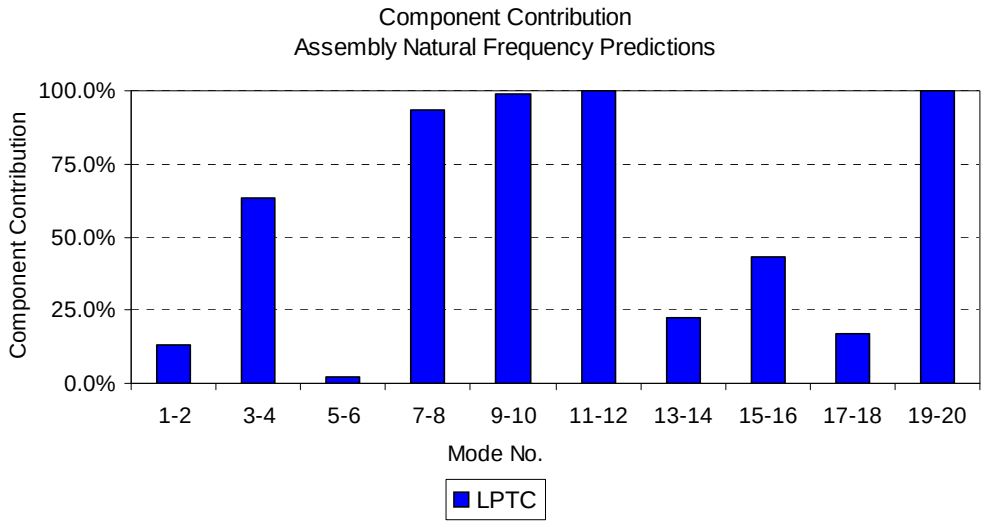

(a)

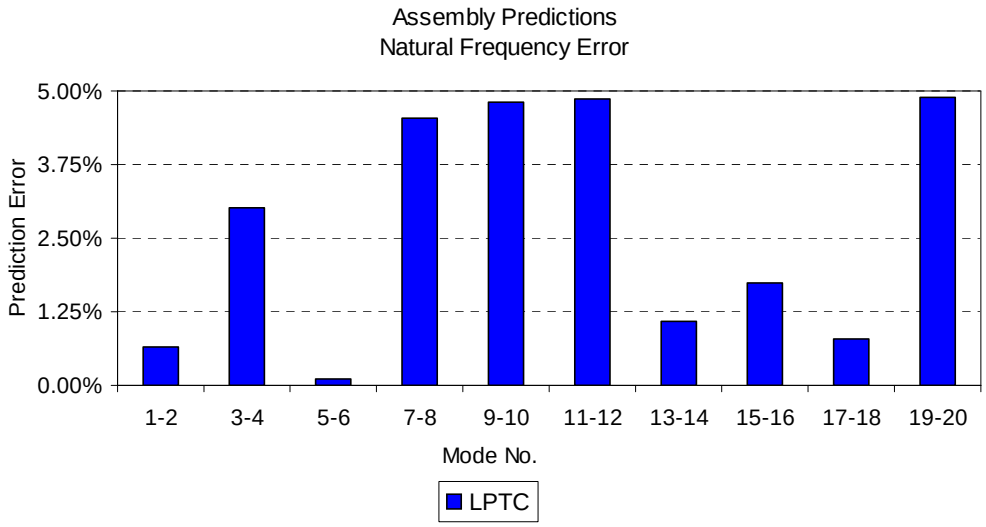

(b)

Figure 2.22. Validation of the component prioritisation method. (a) LPTC contribution to the assembly natural frequency predictions and (b) natural frequency error when the LPTC Young's modulus is incorrectly modelled (+10% with respect to nominal).

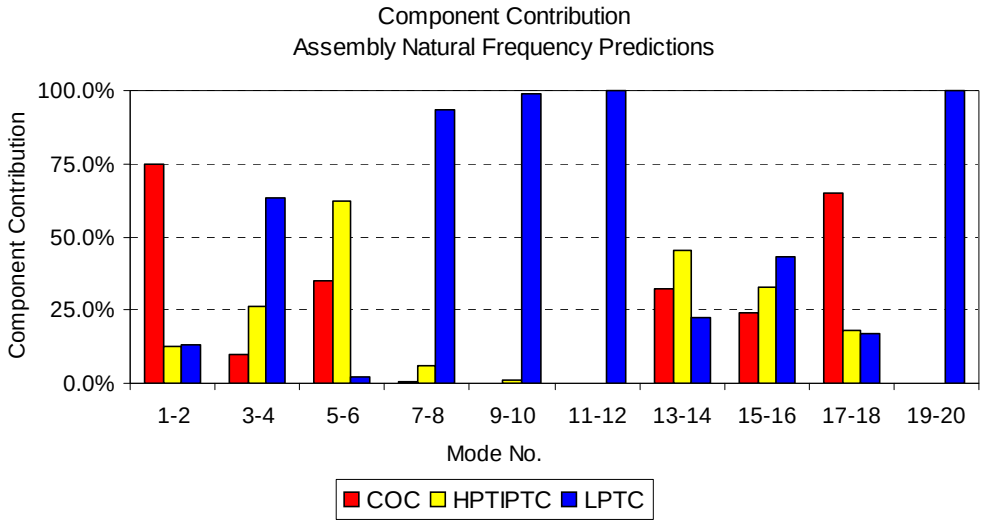

(a)

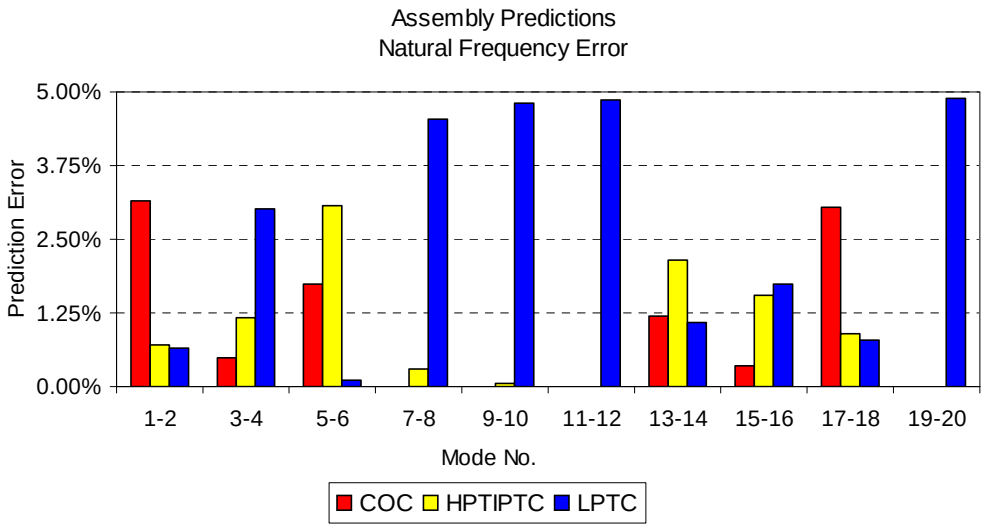

(b)

Figure 2.23. Validation of the component prioritisation method. (a) Component contribution to the assembly natural frequency predictions and (b) natural frequency error when the Young's modulus is incorrectly modelled (+10% with respect to nominal) in each component.

2.6.4 Limitations of the Proposed Method

The methodology presented above has certain limitations which must be understood by the user when prioritising components for individual validation:

- only first order sensitivities are considered in this work, hence ignoring the effects that second or higher order terms might have when predicting the consequences of parameter changes. The results from first-order analyses are usually accurate for small parameter changes only, or in other words, when the assembly model is reasonably accurate in the first place. First order sensitivities might not be accurate when the original assembly model is too coarse. Also;
- the sensitivities computed here only consider one parameter change at a time. The potential interdependence between parameters is not taken into account. This could be an issue if two regions in the model with low sensitivities when considered independently had a strong effect when combined together in a certain manner. This problem could be tackled by computing high-order cross-sensitivities. Finally;
- the definition of the threshold over which a component contribution ratio is considered relevant might not be easy at times. As explained above, the threshold level will be selected considering the accuracy requirements and the number of components. However this decision is still rather subjective. Clearer guidelines should be implemented to ensure consistency between users.

2.6.5 Other Applications of the Proposed Method

The sensitivity plots and component prioritisation methods presented here were developed with assembly model validation in mind. However their application could span across other fields, some of which are discussed below.

The sensitivity density plots such as those in Figures 2.17 and 2.18 indicate those regions in the model where an accurate modelling of the stiffness and mass is most important. This information can be used during the modelling stage to identify the areas in a model where a higher refinement may be appropriate.

Also, the sensitivity contour plots can be used to identify the regions in a structure where manufacturing tolerances should be more tightly controlled or where they can be relaxed. In those regions of high sensitivity, a big tolerance can result in a very dissimilar behaviour from one part to the next. As a result, the manufacturing tolerances should be tightened where the sensitivity is high and relaxed in places where the sensitivity is low.

2.7 Conclusions

A new methodology has been presented in this chapter to validate complex assembly models by validating a reduced number of its constituent components. The concept of validating an assembly by virtue of validating only a few of its components is not new though. However, existing methods for component prioritisation lack the robustness required for implementation in industry.

The new approach consists of identifying those regions in the assembly model where an inappropriate definition will have a significant impact on the accuracy of its predictions. It is the component models describing those regions that are given the highest priority for validation. The new approach is capable of quantifying the relative importance of each of the components in the assembly, hence removing a great deal of the subjective judgement traditionally associated with the prioritisation of components. The robustness of this method makes it highly suitable for deployment into industry.

Since sensitivity analysis is the backbone of the new technique, a thorough review of the most widespread sensitivity methods applicable to structural dynamic analysis has been carried out in this chapter. It has been shown why some of these methods are not well-suited to deal with cyclic-symmetric structures, so common in the aeroengine industry, due to the presence of more than one mode at the same frequency (i.e. orthogonal mode pairs). Appropriate methods capable of resolving this issue have also been reviewed. In all cases, particular emphasis has been paid to those methods that allow the explicit calculation of sensitivities as the new approach for component prioritisation requires a great deal of sensitivity analyses and explicit methods facilitate the calculations at a much reduced computational cost.

A representative Case Study has been presented to demonstrate the suitability of the proposed methods. The Case Study consisted of three aeroengine casings bolted

together for which the assembly design model needed validation. It has been shown how the components in the assembly could be successfully prioritised in a quantitative manner using the sensitivity-based methods presented in this chapter.

Chapter 3 - Validation of Individual Components

3.1 Introduction

When validating a component design model it is important to consider that the model must perform well when it is part of the assembly and not just when it is considered in isolation. A component design model which accurately predicts the modal properties of a component when it is in isolation, but fails to yield appropriate predictions when it is part of the assembly is not a valid model.

When the available computing power was still not sufficient to handle supermodels, physical testing on manufactured prototypes was the only source of reference data for the validation of component design models. However, the boundary conditions that can be applied to a component in a laboratory environment are typically very different from those that the component will experience when it is connected to the other parts in the assembly. Consequently, it is usually difficult to justify why a component design model which accurately resembles the dynamic behaviour of a component under laboratory conditions will also yield appropriate predictions when it is part of the assembly. Over the years, a few techniques have been proposed to bridge this important gap. In fact, this field of study has been given its own name, Test Strategy [24].

Test Strategy methods carefully select test configurations, and specific modes in each configuration, for which to validate a component design model. Theoretically, a component design model capable of accurately predicting the target modes in those configurations should yield appropriate predictions when it is part of the bigger assembly.

The appearance of supermodels has transformed the approach to model validation. Supermodels provide a virtual environment where not only is there no need for

manufacturing of prototypes but also the constraints of physical testing are not present anymore. In an ideal scenario, the same boundary conditions that the component design model is subject to when it is part of the assembly would be applied to the corresponding supermodel. The supermodel predictions would then provide an accurate estimation of the component's dynamic behaviour when it is part of the assembly. This would in turn represent the ideal reference data to validate the corresponding component design model. However, the correct application of the assembly boundary conditions to a component supermodel is not straight-forward and requires specialised techniques.

This chapter will first review some of the most relevant Test Strategy methods for the validation of component design models. Even though these methods were conceived with physical testing in mind, their analysis will highlight the main challenges faced when using supermodels as the reference for validation. Following this review, a novel technique to validate a component design model using the virtual reference provided by a supermodel will be presented. The Case Study introduced in the previous chapter will again be used here to illustrate some of the methods presented.

Finally, this chapter will explore the consequences of ignoring the effects of joints in the dynamic behaviour of assemblies. The industrial nature of the proposed Case Study will serve as an ideal vehicle to investigate this issue. A solution to incorporate the effects of joints into the overall validation strategy will be subsequently presented.

3.2 Model Updating

When validating any model (e.g. component design model), its predictions are typically compared against a reference. This reference will typically be the measurements from a physical test or the predictions from a supermodel. When the predictions from the original model correlate well with the reference, the model is considered to be valid and no further action is required. However there are occasions where the original model needs to be modified to better match the reference data. This process is usually referred to as Model Updating.

In order to illustrate the methods presented in this thesis, some of the Case Study component design models will need to be updated. As a result, it is worth reviewing here

some of the most common Model Updating techniques. Extensive literature is available on the subject with comprehensive reviews by Friswell and Mottershead [29], Berman and Nagy [30] and Ewins [31].

Very often the concept of Model Updating is interpreted differently in Academia and Industry. The description by Ewins [31] is widely accepted in Academia, *"Model Updating is the process of correcting the numerical values of individual parameters in a mathematical model using data obtained from an associated experimental model such that the updated model more correctly describes the dynamic properties of the subject structure"*. According to this definition, Model Updating is restricted to the correction of certain components of the stiffness and mass matrices of the original model to better match the reference data. Nonetheless, the basic characteristics of the matrices, such as the total number of DOFs, remain the same. This in turn means that not all models are capable of being updated. A model which is too coarse or which does not contain the appropriate DOFs might never be capable of accurately matching the reference data. There is a process called Verification which objective is to ensure that a model is susceptible of being updated. Chen [32] developed analytical techniques to verify models ahead of Model Updating.

On the other hand, the concept of Model Updating in industry is much broader. Any change to a model to better match the reference data is typically considered as a Model Update. Changes may include: modifications to the original mesh to better represent certain geometry features, use of different element types, etc.

In the context of this work Model Updating will only refer to the modification of existing parameters in the original model according to the academic description above.

Let us consider that the matrices:

$$[\omega_0] \quad , \quad [\phi_0] \tag{3.1}$$

contain the original model predictions for all the q modes that need to be predicted accurately. These modal properties must fulfil the general equation (1.1):

$$\left([K] - [M][\omega_0^2]\right)[\phi_0] = [0] \tag{3.2}$$

Let us also consider that the actual modal properties of the structure are:

$$[\omega_X] \quad , \quad [\phi_X] \tag{3.3}$$

This data will come from either a physical test or a supermodel and it is typically referred to as the reference data. When the differences between the predicted modal properties and the reference data are unacceptable, the original model will need to be updated according to:

$$\left(([K]+[\Delta K])-([M]+[\Delta M])\left[\omega_X^2\right]\right)[\phi_X]=[0] \tag{3.4}$$

where $[\Delta K]$ and $[\Delta M]$ are the modifications to the original stiffness and mass matrices respectively.

In the case where the reference data comes from physical testing, $[\omega_X]$ and $[\phi_X]$will be rectangular. The reason being that it is almost impossible to measure as many modes as DOFs in the original model. Furthermore, each of the measured modeshapes $\{\phi_X\}_j$ will only contain data for a limited number of DOFs. In many Model Updating methods the measured modeshapes $\{\phi_X\}_j$ need to be expanded to bring the vectors to their full dimension. The most common expansion methods are called SEREP (System Equivalent Reduction and Expansion Process) which are described in reference [33].

In the case where the reference data comes from a supermodel, as many modes as DOFs in the design model could be calculated (the supermodel has a bigger size than the original design model). However this can be computationally prohibitive. Hence $[\omega_X]$ and $[\phi_X]$ will usually be rectangular. In this case $[\phi_X]$ will not require expansion as it is most likely that all DOFs in the design model will have a matching pair in the supermodel.

Model Updating techniques are usually grouped into two types depending on their approach to calculating $[\Delta K]$ and $[\Delta M]$:

- Direct Methods, where any component in the stiffness and mass matrices is susceptible of being directly corrected to better match the reference data. The corrections might not have any physical meaning though. And;

- Indirect Methods, where physical parameters in the model are corrected to alleviate the initial discrepancies. Those changes are then translated into changes of the stiffness and mass matrices, hence the adjective of indirect.

The following sections describe the basics of the most relevant methods in each group.

3.2.1 Direct Methods

The Direct Matrix Updating and the Error Matrix Method are the most common direct techniques to calculate the stiffness and mass matrix corrections in equation (3.4).

According to the Direct Matrix Method:

$$\begin{aligned}[\Delta K] = {} & [M][\phi_X][\phi_X]^T[K][\phi_X][\phi_X]^T[M] + [M][\phi_X]\left[\omega_X^2\right][\phi_X]^T[M] \\ & -[K][\phi_X][\phi_X]^T[M] - [M][\phi_X][\phi_X]^T[K]\end{aligned} \tag{3.5}$$

and

$$[\Delta M] = [M][\phi_X][m]^{-1}([I] - [m])[m]^{-1}[\phi_X]^T[M] \tag{3.6}$$

where

$$[m] = [\phi_X]^T[M][\phi_X] \tag{3.7}$$

According to the Error Matrix Method:

$$[\Delta K] = [K]\left([\phi_0]\left[\omega_0^2\right]^{-1}[\phi_0]^T - [\phi_X]\left[\omega_X^2\right]^{-1}[\phi_X]^T\right)[K] \tag{3.8}$$

and

$$[\Delta M] = [M]\left([\phi_0][\phi_0]^T - [\phi_X][\phi_X]^T\right)[M] \tag{3.9}$$

The main advantage of the Direct Methods is their computational efficiency. Very little resources are required to calculate equations (3.5) to (3.9).

However, there are significant drawbacks to the use of Direct Methods:

- the correction matrices $[\Delta K]$ and $[\Delta M]$ may contain components which are not physically possible. For instance, $[\Delta K]$ could introduce an off-diagonal component in the original stiffness matrix $[K]$ which corresponds to two DOFs

which are not physically connected. This means that the resultant model might become a purely mathematical model with very little physical meaning. Moreover;

- the reference data typically contains information for a number of modes which is smaller than the number of DOFs in the model. The updating equations (3.5) to (3.9) only impose the restriction to accurately match the modal properties of the reference modes $[\omega_X]$ and $[\phi_X]$. The rest of the modal properties in the model can take up any value. This in turn means that there are many possible solutions, $[\Delta K]$ and $[\Delta M]$, to the updating problem. Again, this is indicative of the lack of physical meaning of the changes introduced to the original model. Also,
- equations (3.5) to (3.9) require a full dimension $[\phi_X]$ matrix. If the reference data comes from a physical test, the number of measured DOFs will be much lower than that of the model. As a result, the measured modeshapes will need to be expanded. Expansion methods usually make use of the stiffness and mass matrices of the original model. The fact that this model needs updating is an indication that these matrices are not very accurate in the first place. This can compromise the accuracy of the expanded modeshapes and subsequently of the method as a whole.

References [34] and [35] provide more information on the Direct Matrix Updating and Error Matrix Method techniques respectively.

3.2.2 Indirect Methods

Indirect Methods work by tuning a selected set of physical parameters in the original model to better match the reference data. These parameters might include, Young's modulus of certain elements or groups of elements, material densities, shell thicknesses, etc. This in turn ensures that the changes introduced to the model will have a physical meaning. This is a much more robust approach to Model Updating than the Direct Methods where the changes introduced to the original model might not have any physical meaning.

These methods are referred to as indirect because of the sequence followed by the updating process. Physical parameters are updated first. Then, these parameter changes are translated into the correction matrices $[\Delta K]$ and $[\Delta M]$. This is the opposite to the Direct Methods where the correction matrices $[\Delta K]$ and $[\Delta M]$ are calculated directly.

The most popular Indirect Methods are those based on parameter sensitivity. Let us consider the response vector:

$$\{Z_X\} = \begin{Bmatrix} \omega_{X\,1}^2 \\ \omega_{X\,2}^2 \\ \dots \\ \omega_{X\,q}^2 \\ \\ \{\phi_X\}_1 \\ \{\phi_X\}_2 \\ \dots \\ \{\phi_X\}_q \end{Bmatrix} \tag{3.10}$$

containing the reference natural frequencies and modeshapes from either a supermodel or a physical test. The corresponding vector containing the original predictions from the model is:

$$\{Z_0\} = \begin{Bmatrix} \omega_{0\,1}^2 \\ \omega_{0\,2}^2 \\ \dots \\ \omega_{0\,q}^2 \\ \\ \{\phi_0\}_1 \\ \{\phi_0\}_2 \\ \dots \\ \{\phi_0\}_q \end{Bmatrix} \tag{3.11}$$

The relationship between $\{Z_X\}$ and $\{Z_0\}$ can be approximated using the first-order Taylor approximation in equation (2.4):

$$\{Z_X\} \cong \{Z_0\} + [S](\{P_U\} - \{P_0\}) \tag{3.12}$$

where the components in vector $\{P_0\}$ correspond to the original values of the parameters selected for updating. Vector $\{P_U\}$ contains the updated values for those parameters.

The components of the sensitivity matrix [S] in equation (3.12) correspond to the first-order sensitivity of the modal properties with respect to changes in the parameters. The methods to calculate those sensitivities have been discussed in detail in the previous chapter.

If:

$$\{\Delta Z\} = \{Z_X\} - \{Z_0\} \tag{3.13}$$

$$\{\Delta P\} = \{P_U\} - \{P_0\} \tag{3.14}$$

then equation (3.12) can be rewritten as:

$$\{\Delta Z\} \cong [S]\{\Delta P\} \tag{3.15}$$

Equation (3.15) neglects the contribution of high order terms in the Taylor series. The resultant parameter values $\{P_U\}$ are an approximation and so equation (3.15) needs to be iterated a number of times to arrive at the correct values of the updated parameters.

The iterative nature of the Indirect Methods is their major drawback since their application can be computationally expensive at times. On the other hand, the results from the Model Update are physically meaningful. Furthermore there is no need to expand the eigenvectors in equation (3.10) when the reference data is provided by physical tests as only a reduced set of DOFs might be selected as responses.

Equation (3.15) can only be solved using

$$\{\Delta P\} = [S]^{-1}\{\Delta Z\} \tag{3.16}$$

when there are the same number of responses as parameters for updating. This is rather unusual and in most cases there will be either more responses than parameters (over-determined system) or more parameters than responses (under-determined system).

The various Indirect Methods for Model Updating differ in the way that equation (3.15) is solved.

Least-Squares Method

According to this method, the solution to equation (3.15) is given by:

$$\{\Delta P\} = \left([S]^T [S]\right)^{-1} [S]^T \{\Delta Z\} \tag{3.17}$$

for over-determined systems. In the case of under-determined systems, the solution is:

$$\{\Delta P\} = [S]^T \left([S]^T [S]\right)^{-1} \{\Delta Z\} \tag{3.18}$$

These equations represent the least-square solution for the updated parameters. In mathematical terms, equations (3.17) and (3.18) minimise the penalty function:

$$J = [S]\{\Delta P\} - \{\Delta Z\} \tag{3.19}$$

Weighted Method

The Weighted methods provide a solution to equation (3.15) which minimises the following penalty function:

$$J = \{\Delta Z\}[W_Z]\{\Delta Z\} + \{\Delta P\}[W_P]\{\Delta P\} \tag{3.20}$$

where $[W_Z]$ and $[W_P]$ are the response and parameter weighting matrices respectively. Both matrices are diagonal.

The solution to the updating problem is given by:

$$\{\Delta P\} = \left([W_P] + [S]^T [W_Z][S]\right)^{-1} [S]^T [W_R]\{\Delta Z\} \tag{3.21}$$

for over-determined systems. In the case of under-determined systems, the solution is:

$$\{\Delta P\} = [W_P]^{-1}[S]^T \left([W_Z]^{-1} + [S][W_P]^{-1}[S]^T\right)^{-1} \{\Delta Z\} \tag{3.22}$$

The major benefit of this approach with respect to the Least-Squares method is that the individual parameters and responses can be given different weights. The bigger the weighting assigned to a given response the more emphasis that the updating process will place on accurately matching the reference data from the supermodel or the

physical test. Conversely, a big weighting associated with a parameter will reduce the associated changes during the updating process. This can be particularly useful in certain cases. For instance, let us imagine that the accurate prediction of a particular natural frequency is more important than the rest. In this case this response would be given a bigger weighting. This will ensure that the correctness of the most relevant response is not compromised by the attempt to accurately predict other less important responses. Now let us consider that the uncertainty over the definition of one parameter in the model is high, this means that the range over which the parameter might vary is big. In this case a small parameter weighting will promote a bigger change when compared to other parameters that might have a smaller uncertainty associated.

Different weighting matrices have been proposed by many authors such as Link and Zhang [36], Link *et al* [37], Mottershead and Foster [38], Natke [39] and Collins *et al* [40].

3.3 Test Strategy

Before computers were sufficiently powerful to handle supermodels, component design models could only be validated using physical test data as the reference. Because of the cost limitations, the free-free configuration would typically be used to test the manufactured prototypes. A component design model would be considered to be valid if it was capable of accurately predicting the modal properties of the first few modes in free-free configuration.

Time after time it was discovered that the thought-to-be-valid component design models would not yield accurate predictions when they were part of a bigger assembly model. It is not difficult to see why since the dynamic properties of a component do not only depend on its stiffness and mass distribution but also on the boundary conditions that the component is subject to. The boundary conditions (or lack of) applied to a component in free-free configuration are very different from the boundary conditions that the component is subject to when it is part of a bigger assembly. As a result, accurate predictions of the first few free-free modes from a component design model does not ensure that the model will perform well when it is part of a bigger assembly.

Test Strategy is a concept first introduced at the beginning of this decade during the CERES project [24] and further developed for robust industrial application during VIVACE [41]. The objective of Test Strategy is to design an appropriate test configuration(s) to validate a component design model. The accurate prediction from the component design model of a carefully selected number of modes in that test configuration(s) should ensure a valid model when this is part of a bigger assembly.

The following lines describe the most important Test Strategy methods in chronological order. They differ from each other in their criteria for the selection of the most appropriate test configurations and the modal properties that should be targeted for validation.

3.3.1 Loaded Boundary Method

The Loaded Boundary method is one of the earliest Test Strategy methodologies and, not surprisingly, it is the most intuitive. It consists of designing special test fixtures that once attached to the component simulate the boundary conditions that the component is subject to when it is part of the assembly. As a result the modal properties of the component in the test configuration will resemble those when the component is mounted in the assembly.

The initial versions of this approach were also referred to as Mass-Loading Methods. The reason being that only the inertial properties of the rest of the components in the assembly would be mimicked using the test fixtures. For instance, if we were to validate the HPTIPTC design model corresponding to the Case Study, the manufactured component would be bolted to two fixtures, one on each end. The fixture at the front would have a similar weight and inertia properties as the COC. Likewise, the fixture at the back would have similar weight and inertia properties as the LPTC. Figure 3.1 schematically represents this method. Different variations of this method have been presented by Neibal [42] in the 1980s and Admire *et al* [43] and Karpel and Ricci [44] in the 1990s.

There are a few drawbacks to the Mass-Loading Methods:

- the stiffness of adjacent parts in the assembly also influence the dynamic behaviour of the component. This effect is not considered by these methods. In

practice this might mean that the addition of these fixtures is not sufficient to replicate the behaviour of the component when mounted in the assembly. Furthermore;

- the fixtures will invariably have a stiffness associated with them. For the case where the stiffness of the fixtures is very different from that of the adjacent components, this effect could further deviate the dynamic behaviour of the component in the test configuration when compared to that when mounted in the assembly. In the late 1980s Gwinn *et al* [45] proposed the use of many non-interconnected small masses attached to the bolt holes of the component flanges to reduce the effect of fixture stiffness. However this still does not solve the previous problem where the influence of the stiffness of the adjacent parts is ignored.

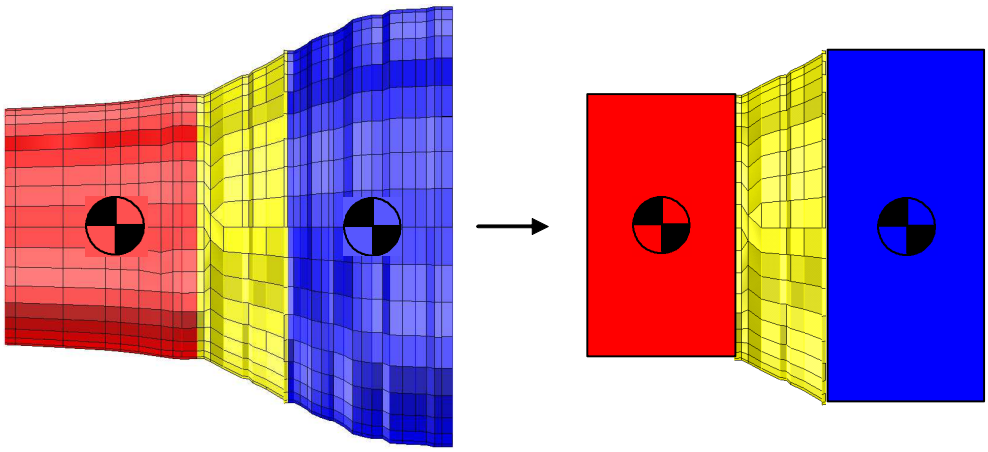

Figure 3.1. Case Study HPTIPTC. Test Strategy, Mass-Loading Method.

The more general Loaded-Boundary methods try to overcome the drawbacks of the Mass-Loading methods. Now, the design of the test fixtures does not only try to replicate the inertia properties of the adjacent components, but also their stiffness distribution. McGowan *et al* [46] demonstrated in the early 1990s the suitability of the Loaded-Boundary method for the validation of certain components in an experimental space station. Ghosh *et al* [47] performed a similar exercise at the end of that decade for the model validation of a cargo module in the International Space Station.

The application of the Loaded-Boundary methods in industry is hindered by a few factors though:

- the design of testing fixtures for a component that replicate the mass and stiffness distribution of the adjacent parts can be very difficult in practice. Also;
- the manufacturing of test fixtures is expensive and time consuming. The long lead times and high costs associated are prohibitive in most modern industries. Moreover;
- the use of test fixtures usually adds to the uncertainties of testing. It is important to consider that the fixtures will usually be bolted to the component. These joints will have an effect on the measured modal properties which is very difficult to control and account for during the model validation process. The end result is that many times these kinds of tests add as many problems as they solve.

3.3.2 CERES Method

Early this decade and as part of the CERES project [24] Perinpanayagam [48] proposed a Test Strategy method which would not require such complex test fixtures as in the Loaded-Boundary approach. The basics of this method are explained below.

Let us consider that the vector $\{\phi\}_r$ represents the r-th modeshape predicted by an assembly model and that $\{\varphi\}_r$ contains the components corresponding to one of component design models.

If the vector $\{\phi_f\}_j$ represents the j-th modeshape predicted by the component design model in a free-free configuration then,

$$\{\varphi\}_r = \sum_{j=1}^{N} a_j \{\phi_f\}_j \tag{3.23}$$

will be exact if N is equal to the total number of DOFs in the component design model.

Similarly, if $[f_f]$ contains the predicted internal forces corresponding to all free-free modeshapes then:

$$\{f\}_r \cong \sum_{j=1}^{N} b_j \{f_f\}_j \tag{3.24}$$

is usually a good approximation. Note that equation (3.24) is not necessarily exact as the internal forces $[f_f]$ do not necessarily form a linearly-independent subspace of vectors.

During a physical test it is impossible to measure as many free-free modes as DOFs in the component design model, usually thousands. In practice, only a small subset of modes M in the low frequency range will be measured. According to Perinpanayagam, if the following equations:

$$\{\varphi\}_r \cong \sum_{j=1}^{M} a_j \{\phi_f\}_j \tag{3.25}$$

$$\{f\}_r \cong \sum_{j=1}^{M} b_j \{f_f\}_j \tag{3.26}$$

are good approximations and the component design model is capable of accurately predicting all the M modes in free-free configuration then the model can be considered to be valid.

The validation effort could be further reduced if only those modes L with high coefficients in the linear combinations in (3.25) and (3.26) are targeted for validation:

$$\{\varphi\}_r \cong \sum_{j=1}^{L} a_j \{\phi_f\}_j \tag{3.27}$$

$$\{f\}_r \cong \sum_{j=1}^{L} b_j \{f_f\}_j \tag{3.28}$$

In physical terms, equations (3.27) and (3.28) mean that if the component design model is capable of accurately predicting a set of L modes in free-free configuration whose linear combination resembles the deformed shape and internal forces of the component when it is part of a bigger assembly then the model is valid.

The free-free configuration is the cheapest to achieve in a laboratory environment. Furthermore the uncertainty over any fixture joint is minimal. That is why free-free testing should always be the first option for model validation. However, at times, there

might not be any set of free-free modes in the measurable frequency range which linear combination accurately resembles the deflected shape and internal forces of the component when part of the assembly according to equations (3.27) and (3.28). In this case a different set of test configuration must be sought.

Perinpanayagam proposed selecting a number t of test configurations which would provide a number of L_t modes each, all within the measurement frequency range, so that:

$$\{\varphi\}_r \cong \sum_{j=1}^{L_1} a_{1j}\{\phi_1\}_j + \sum_{j=1}^{L_2} a_{2j}\{\phi_2\}_j + \ldots + \sum_{j=1}^{L_t} a_{tj}\{\phi_t\}_j \tag{3.29}$$

$$\{f\}_r \cong \sum_{j=1}^{L_1} b_{1j}\{f_1\}_j + \sum_{j=1}^{L_2} b_{2j}\{f_2\}_j + \ldots + \sum_{j=1}^{L_t} b_{tj}\{f_t\}_j \tag{3.30}$$

are accurate approximations.

The test configurations (other than free-free) that Perinpanayagam suggested would rank from perfectly rigid boundary conditions to more complex test fixtures.

There are a few drawbacks to this method:

- the methodology is useful to evaluate whether a set of test configurations is suitable for component model validation. However it does not guide the modeller in the selection of an appropriate set. The user must follow a trial and error process until a suitable solution is found. Also;
- similarly to the Loaded-Boundary method, test fixtures are still required. This usually comes with the penalties explained in the previous method. Nonetheless the design of the fixtures is less restrictive in this case. Now, none of the test modes need to resemble individually the assembly properties. Only the linear combination of different modes must mimic the component deflected shape and internal forces of the component when mounted in the assembly. Finally;
- it is difficult to demonstrate mathematically why a component design model which accurately predicts the modes selected by this method will yield accurate predictions when it is part of a bigger assembly.

3.3.3 VIVACE Method

Garcia and Ewins [49] recently proposed a method capable of demonstrating mathematically why the accurate prediction from the component design model of certain modes in different test configurations would ensure a valid model when this model is used as part of a bigger assembly. This method was developed as part of the VIVACE [41] programme and represents an extension of the method proposed by Perinpanayagam [48].

In order to illustrate the basic principles of this method, let us consider the validation of the Case Study assembly model. We will also consider that only the mode pair 17-18 needs to be accurately predicted for the assembly model to be considered valid. The sensitivity density contour to changes in stiffness is plotted in Figure 2.17. According to this plot, the correct definition of the stiffness characteristics of the COC front flange should be given the highest priority to ensure accurate predictions from the assembly model. Figure 3.2 shows the same sensitivity density as in Figure 2.17 but restricted to the COC design model.

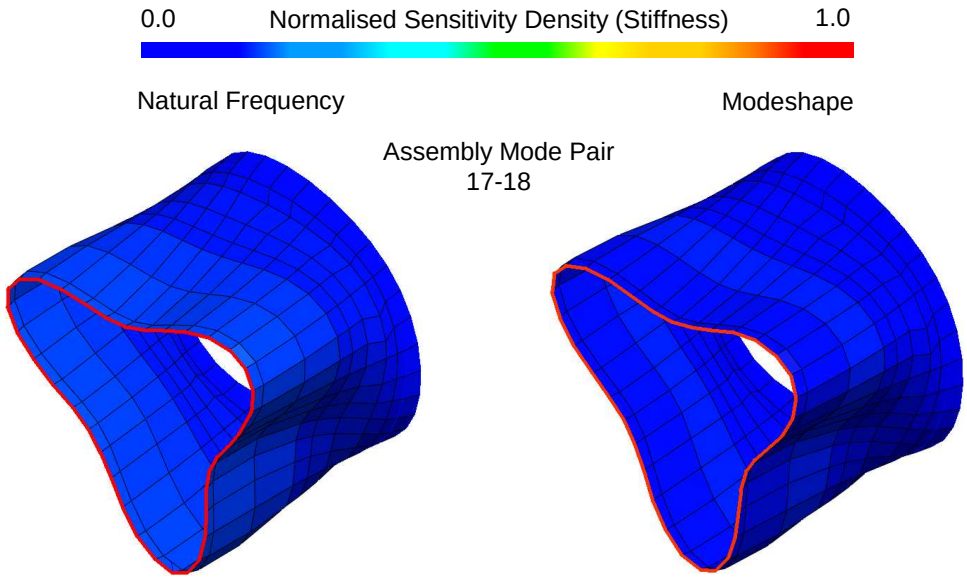

Figure 3.2. Case Study COC sensitivity density to changes in stiffness.

Let us consider now the COC in isolation and free-free configuration. Figure 3.3 shows the natural frequency sensitivity densities to stiffness changes of the first 8 free-free modes. Please note that the COC model is axis-symmetric and the modes appear as orthogonal pairs.

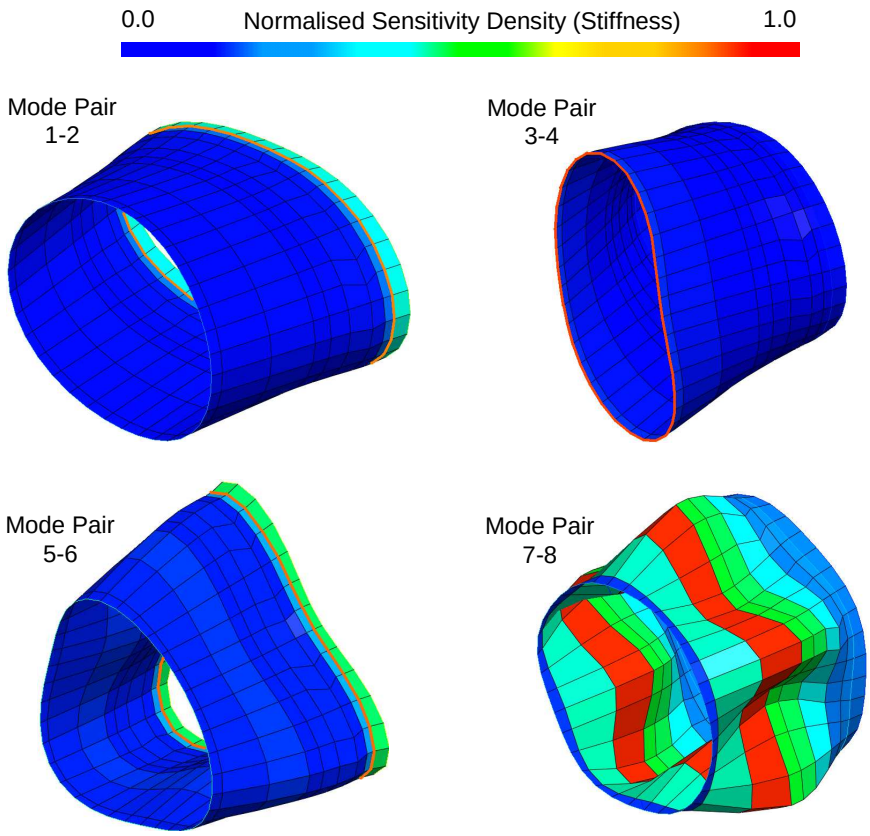

Figure 3.3. Case Study COC natural frequency sensitivity density to changes in stiffness. First 8 modes in free-free configuration.

A look at these sensitivity plots reveals that the natural frequency of mode pair 3-4 is also highly dependant on the stiffness distribution of the COC front flange. As a result one would expect that if the COC design model is capable of accurately predicting the natural frequency of this free-free mode it will also yield accurate predictions when the model is part of the assembly. On the contrary, the accurate prediction of the other 3 mode pairs does not add any value since they do not exercise the front flange. In this

case all validation effort could be reduced to the accurate prediction of a single mode in free-free configuration.

Interestingly, the CERES method would have not selected this free-free mode for validation. The shape of the free-free mode is 2D while the deformed shape when the COC is part of the assembly has a 3D shape. In fact, it is most likely that the CERES method would have selected the free-free mode pair 5-6 as the target for validation. This mode has a 3D shape similar to that of the component when it is part of the assembly. Nonetheless, the sensitivity plots in Figure 3.3 show that the free-free mode pair 5-6 barely exercises the front flange. As a result, the accurate prediction from the COC design model of this mode will not ensure accurate predictions when the component model is a part of the assembly.

The mathematical basis of the VIVACE method is as follows: if the vector $\{s\}_r$ contains the sensitivity data (natural frequency and modeshape) corresponding to a component design model when it is part of the assembly for the r-th mode and there are a set of L modes when the component is in a free-free configuration so that:

$$\{s\}_r \cong \sum_{j=1}^{L} a_j \{s_f\}_j \tag{3.31}$$

where the vector $\{s_f\}_j$ contains the sensitivity data corresponding to the j-th mode of the component in a free-free configuration, then, all the sensitive regions of the component model when it is part of the assembly are also exercised by the L modes of the component in the free-free configuration. As a result, the accurate prediction of the component design model of the L free-free modes should ensure a valid component model when it is part of the assembly.

Nonetheless, in a general case, all the free-free modes in the measurement frequency range might not be enough to ensure a good approximation. In this case, a set of test configurations t which provides a number of L_t modes each so that:

$$\{s\}_r \cong \sum_{j=1}^{L_1} a_{1j} \{s_1\}_j + \sum_{j=1}^{L_2} a_{2j} \{s_2\}_j + \ldots + \sum_{j=1}^{L_t} a_{tj} \{s_t\}_j \tag{3.32}$$

must be sought.

As with the CERES method the main drawbacks of this method are:

- the methodology is useful to evaluate whether a set of test configurations is suitable for component model validation. However it does not guide the modeller in the selection of an appropriate set. The user must follow a trial and error process until a suitable solution is found. Also;
- test fixtures are still required. Nonetheless the design of the fixtures is unlikely to be as complex as in the Loaded-Boundary method. It is likely that reasonably simple configurations will provide sufficient modal properties to exercise all the regions of interest in the component.

3.4 Validation Using Supermodels as the Reference

As a reminder, Figure 3.4 highlights this step in the validation process.

A component design model is only considered to be valid when it is capable of accurately predicting the dynamic properties of the component when part of the assembly. In order to satisfy this requirement, Test Strategy methods had to overcome the practical difficulties of replicating in a laboratory the interaction of the component with other parts of the assembly (i.e. boundary conditions).

Supermodels provide a virtual platform for the validation of component design models which are not subject to the shortcomings of physical testing. The application of boundary conditions to a supermodel is simply a mathematical exercise which is not constrained by the manufacturing costs or the uncertainties associated with the use of test fixtures.

Let us imagine that the same boundary conditions that the component design model is subject to when it is part of the assembly can be applied to the corresponding supermodel. The predictions from the supermodel would then accurately describe the dynamic properties of the component when it is mounted in the assembly. This is the ideal reference data for validation and the component design model will be considered to be valid when it is capable of predicting this behaviour accurately.

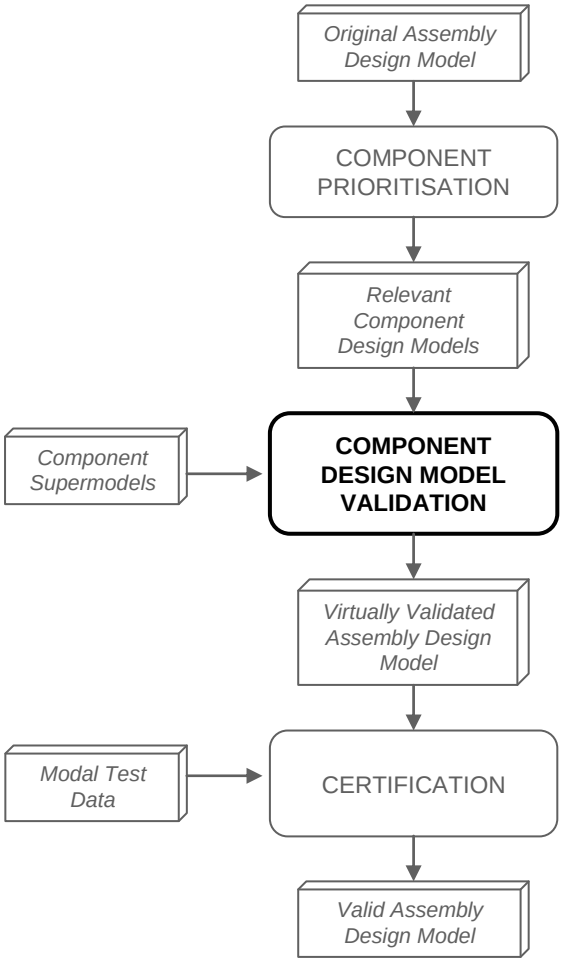

Figure 3.4. Validation using supermodels.

But, how do we apply the appropriate boundary conditions to a supermodel? A possible solution is to substitute the component design model in the assembly by the corresponding supermodel. In order to illustrate this method, let us consider that the HPTIPTC design model highlighted in Figure 3.5 (a) requires validation. The component design model can now be replaced by the corresponding supermodel and connected to the rest of the components in the assembly, see Figure 3.5 (b).

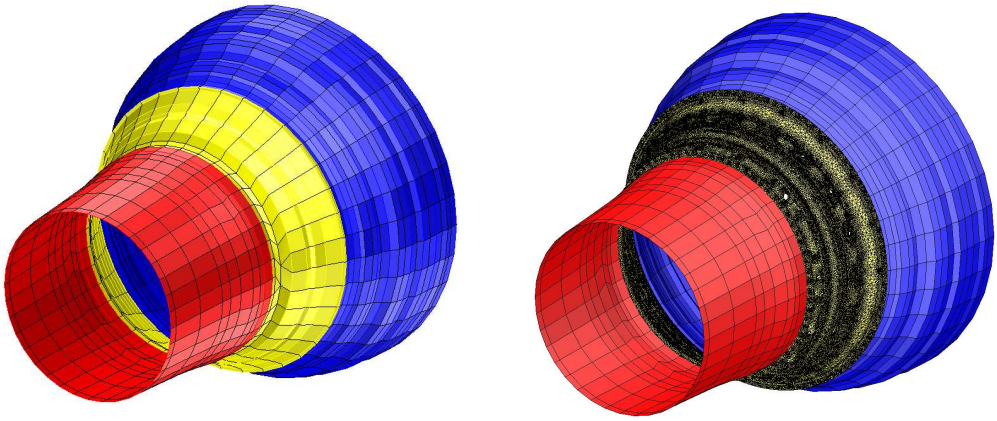

Figure 3.5. Component model validation using a supermodel as the reference. (a) Original Case Study design model and (b) HPTIPTC design model replaced by a supermodel.

The dynamic properties predicted by the supermodel in Figure 3.5 (b) will accurately describe the dynamic behaviour of the HPTIPTC when it is mounted in the assembly. These predictions are the ideal reference for the validation of the less refined component design model.

In both assemblies in Figure 3.5 the component design models corresponding to the adjacent parts (COC and LPTC) are the same. Subsequently, any differences in the predictions between both assembly models can only be attributed to the discrepancies in the dynamic properties predicted by the HPTIPTC design model and the corresponding supermodel. The validation process is then reduced to the updating of the parameter values in the original HPTIPTC design model (i.e. Model Updating) until the differences are reduced to a satisfactory level.

The assembly model with the component supermodel embedded in it is usually referred to as a “hybrid assembly model”. Such models have been used in the past for highly complex dynamic simulations (e.g. Fan Blade Off). However, as far as the author is aware this is the first time that hybrid assembly models have been used as the reference for model validation.

It is important to point out that the size of a supermodel is usually a few orders of magnitude bigger than that of the design models. Therefore the computational effort required to analyse a hybrid assembly model are not much different to those required when analysing the supermodel in isolation.

This method opens a completely new avenue in the field of model validation. Not only the associated costs are reduced by an order of magnitude (no manufactured parts, no physical testing, etc.) but also the quality of the validation process is dramatically increased. Apart from the most obvious quality benefits (e.g. wealth of noise-free data) the many doubts over the suitability of the boundary conditions used during a physical test will now vanish. Furthermore, the dynamic properties of a component can be validated under conditions, such as operating temperature gradients, which could never be matched in a laboratory but which are easy to reproduce in a virtual environment.

The successful application of this method is based on two main assumptions:

- the original assembly design model is representative of the structure. The predicted dynamic behaviour of the supermodel when it is mounted on the assembly depends on its boundary conditions. These are in turn determined by the interaction with the design models of the rest of the components in the assembly. If those models are not sufficiently accurate, the boundary conditions might not be representative of the real structure and so compromise the validity of the supermodel predictions.

  However, in practice, even when the design models of the adjacent components are not sufficiently accurate to be considered fully validated they will usually still be representative, ensuring that their effect on the component supermodel is properly predicted. Also;

- the supermodel can be seamlessly connected to the rest of the assembly design models. Usually the mesh density of a supermodel is much higher than that of the adjacent design model and the connection between them can be challenging.

3.4.1 Hybrid Assembly Models

One of the most essential requirements to create hybrid assembly models is the ability to connect supermodels to industry standard design models. In practice, the very different modelling approaches for these two types of models can make joining them very challenging. The refinement of supermodels usually requires the use of high density meshes. Moreover, supermodels are made of solid elements which will normally

make use of high-order interpolation functions. This is in clear contrast with the standard component design models where the mesh density is much reduced and the element types might not even be solid (1-D beam elements and 2-D shells are not uncommon). Figure 3.6 shows the region where the COC design model rear flange meets the HPTIPTC supermodel front flange.

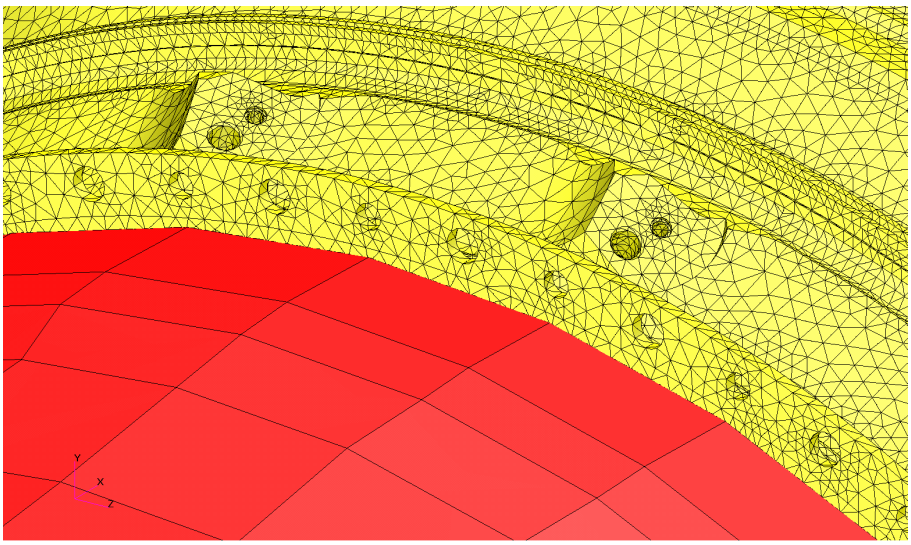

Figure 3.6. Case Study COC design model to HPTIPTC supermodel connection detail.

The problem of connecting two dissimilar meshes is not new. In fact, this field of study is fairly mature. Most methods were originally developed for stress analysis in the late 1980s but have been subsequently refined to cover the more general structural dynamics problem. The following lines will briefly describe some of the most common methods.

The problem of connecting shells to shells and solids to solids has been tackled by many authors since the 1970s. Some of the most relevant are Atluri [50], Aminpour *et al* [51], Park *et al* [52] [53] and Puso *et al* [54].

When it comes to joining shells to solids the problem becomes more complex. The stiffness and mass properties of shell elements are specified in 6 DOFs for each node, 3 translational and 3 rotational. On the contrary, the nodes in solid elements are only

characterized by 3 translational DOFs. In the early 1990s Liao *et al* [55] and Davila [56] proposed transitional elements that would tie the angular rotations of shells to the translational displacements of solids while ensuring stress continuity across the joint. Nonetheless, the applicability of these methods is restricted to very specific element types.

At the beginning of this decade Dohrman *et al* [57] and McCune *et al* [58] proposed general methods for coupling any type of dissimilar meshes, including shell to solid connections. Both methods are based on energy equilibrium principles. According to these approaches, a correct coupling between dissimilar meshes can be achieved when the total virtual work generated by the internal forces on both sides of the interface is zero. This restriction will generate multi-point constraint equations that will link all DOFs on both sides of the interface. Examples of the multi-point constraint equations that result of the application of this principle to different element types can be found in references [59], [60], [61] and [62].

These days, most commercial FEM packages incorporate methods for hybrid meshing. Due to their generality, the work equilibrium methods are proving the most popular at the moment.

3.5 Case Study - Component Design Model Validation

According to the component prioritisation method described in the previous chapter, all three component design models in the Case Study assembly model require validation. Figure 3.7 shows the supermodels of the three components in the assembly. The creation of these supermodels followed the supermodelling guidelines developed during the VIVACE project [41] by Baker [63] and Loyer [64]. Each of the supermodels was created using the corresponding manufacturing CAD drawings with no geometry simplification. Nominal dimensions and material properties were used. Table 3.1 illustrates some of the characteristics of the supermodels.

The hybrid assembly models in Figure 3.8 (a), (b) and (c) will be used as the reference to validate the COC, HPTIPTC and LPTC component design models respectively.

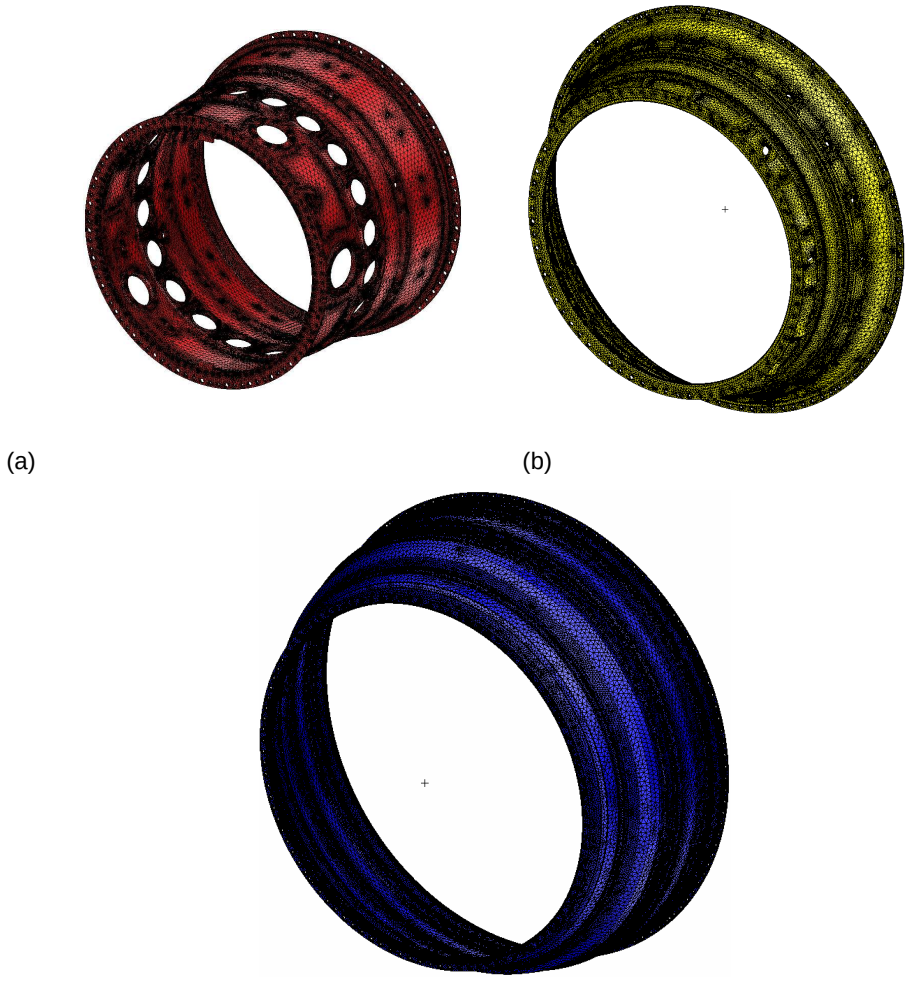

(a) (b)

(c)

Figure 3.7. Case Study supermodels. (a) COC, (b) HPTIPTC and (c) LPTC.

	COC	HPTIPTC	LPTC
Total Number of DOFs	4,978,149	3,670,335	4,047,313
Total Number of Elements	989,469	674,453	834,903
Element Types	TET 10	TET 10	TET 10

Table 3.1. Case Study supermodels.

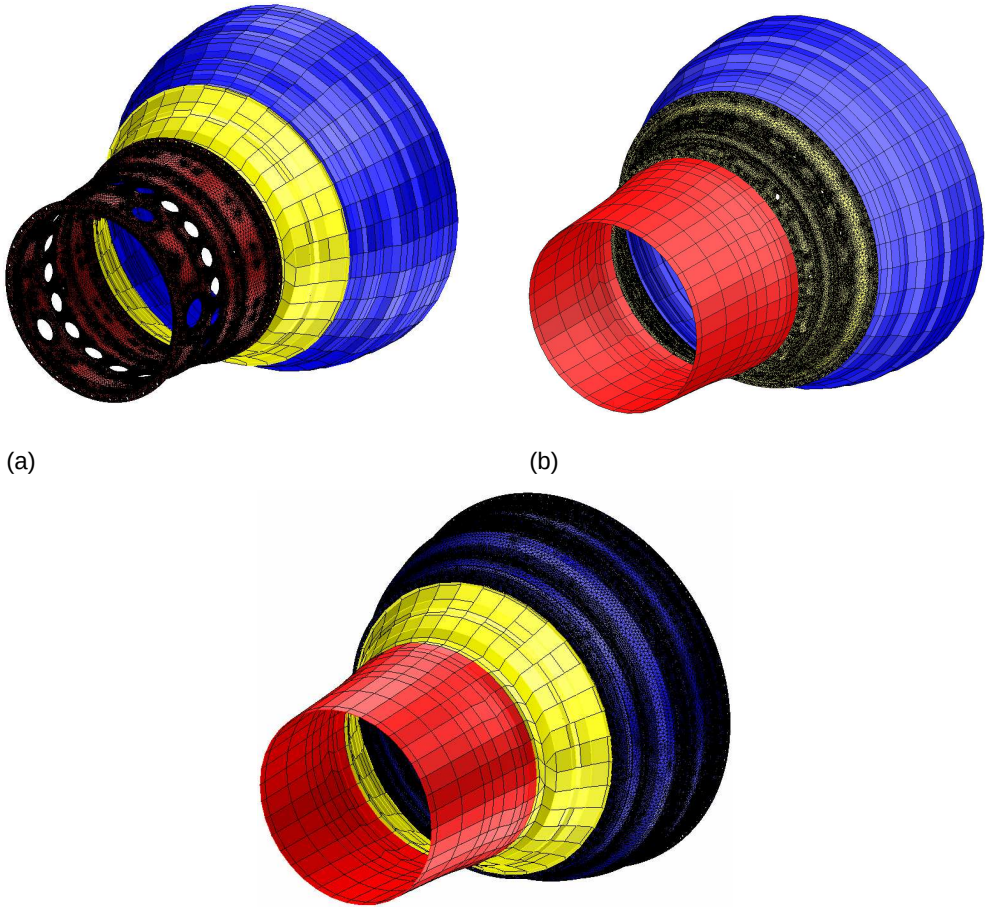

(a) (b)

(c)

Figure 3.8. Case Study hybrid assembly models. (a) COC supermodel; (b) HPTIPTC supermodel and (c) LPTC supermodel.

3.5.1 Validation of the Combustor Outer Casing (COC) Design Model

The original assembly design model predictions were compared against the predictions from the hybrid assembly model in Figure 3.8 (a). The results from the correlation are presented in Figure 3.9.

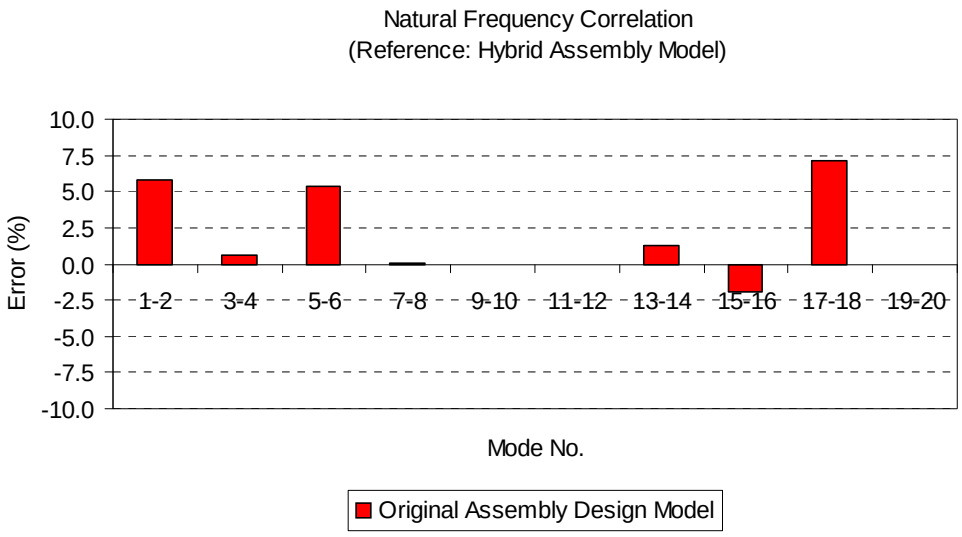

(a)

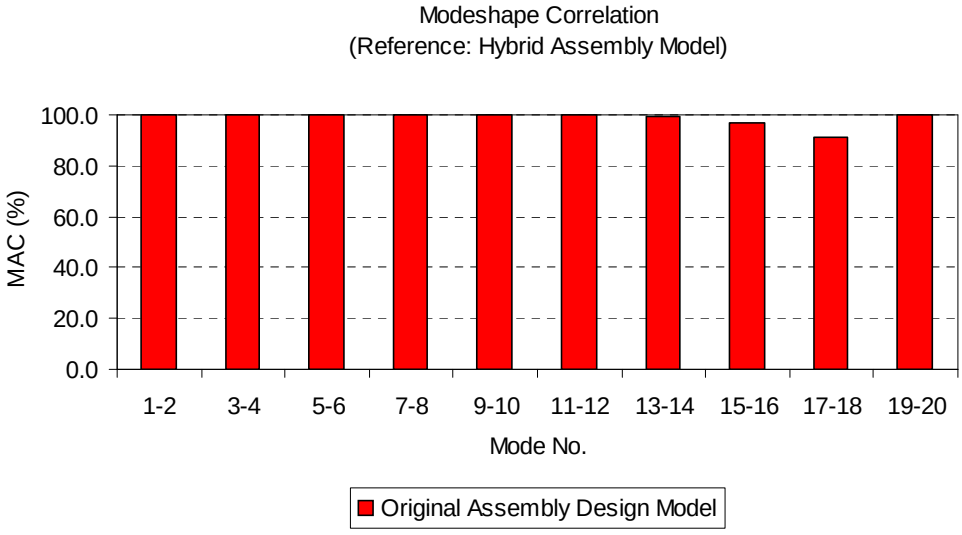

(b)

Figure 3.9. Correlation of Case Study assembly model vs. hybrid assembly model with COC supermodel. (a) Natural frequency and (b) modeshape.

Please note that the assembly design model is axis-symmetric while the hybrid model is not. There are small holes, brackets, bosses, etc. in the COC supermodel which are not equally positioned around the engine axis. As a result, the orthogonally paired modes in

the hybrid assembly model appear rotated with respect to those from the assembly design model. The method proposed by Chan [65] was used to rotate the modeshapes predicted by the assembly design model before the MAC was calculated. Alternative methods such as that proposed by Chen [66] would have also been suitable.

The natural frequency deviation for some mode pairs is significant, for instance the deviation of mode pair 17-18 is around 7.5%. The modeshape correlation is very good for all mode pairs with MAC values close to 100%.

The discrepancies in the correlation can only be attributed to the differences in between the COC design model and the corresponding supermodel. The rest of the component design models are the same in both assemblies.

As a reminder from the previous chapter, the whole assembly design model (three casings joined together) will only be considered valid if the natural frequencies lie within a 5% error when ultimately compared against physical test data. The COC design model on its own is already accountable for errors in the region of 7.5% when compared against the corresponding supermodel. Considering that the other two component design models will potentially add their fair share of errors, the COC design model must be updated to better reflect the reference data provided by the supermodel.

Both the natural frequencies and modeshapes were selected as target responses during the Model Updating. The Young's modulus for each ring of elements in the COC design model, 12 in total, was selected as a potential parameter for updating. This type of selection is common in practice since design models have a carefully tuned mass distribution which will not be modified by changes to the Young's modulus.

The weighted method according to equation (3.20) was selected for Model Updating. All parameters and responses were given the same weighting of 1. Figure 3.10 shows the updating progress. The X-axis corresponds to the iteration number while the Y-axis represents the average natural frequency error of the updated design model when compared to the reference from the supermodel. The iteration process was stopped when the improvement from two consecutive analyses was less than 0.001%. The convergence is smooth with a low error asymptote.

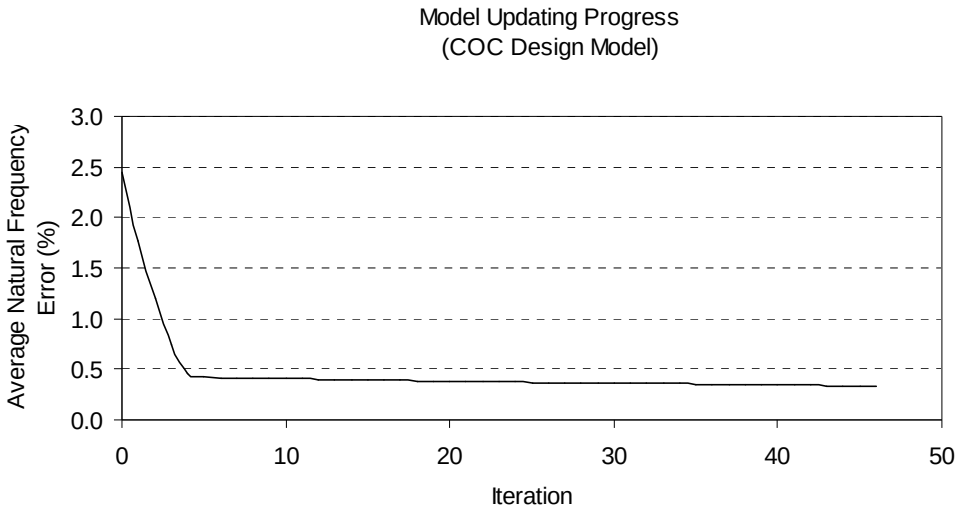

Figure 3.10. COC Model Updating progress.

Figure 3.11 shows the correlation improvements after the Model Update. All natural frequency correlations lie within a 2% error. The MAC correlations remain close to 100%.

Figure 3.12 shows the parameter changes introduced as a result of the Model Updating process. It is always good practice to analyse the parameter changes to make sure that they obey to physical reasons. This avoids producing mathematical models that have no basis in reality. The big changes introduced to the original COC design model are all centred on the third ring of shells starting from the front. An increase in the Young's modulus of around 200% is suggested. Under normal circumstances this could look excessive. Nevertheless, the actual geometry of the region modelled by this continuous ring shells is very complex, see Figure 3.13. The thickness of the ring of shells in the original COC design model is selected to match the mass of this section, however the resultant stiffness is no match for the real behaviour. Subsequently a considerable increase in the Young's modulus is considered to be acceptable.

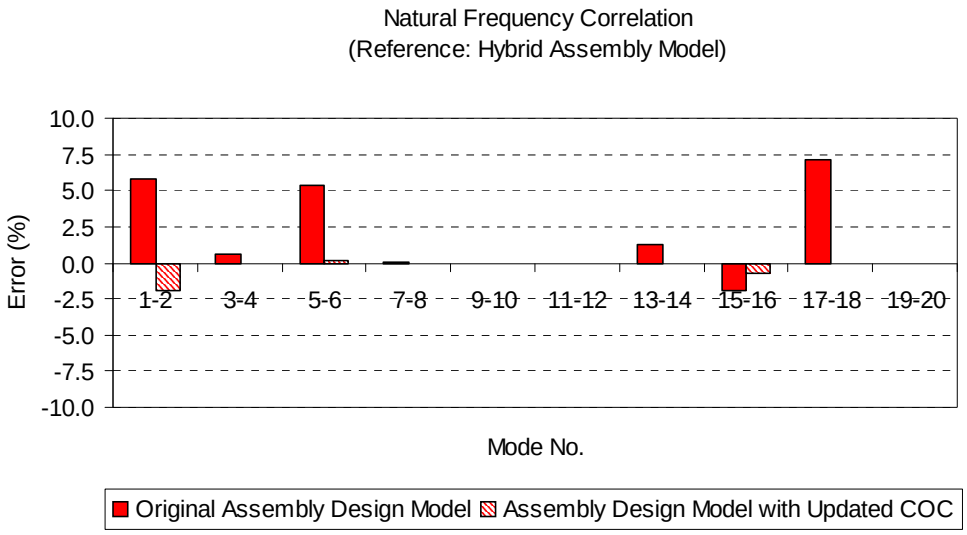

(a)

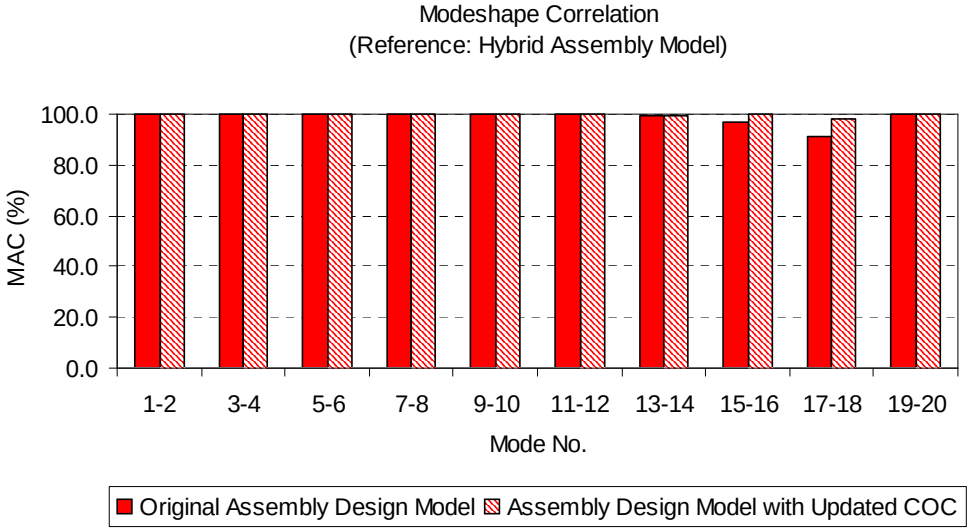

(b)

Figure 3.11. Correlation before and after COC Model Update. (a) Natural frequency and (b) modeshape.

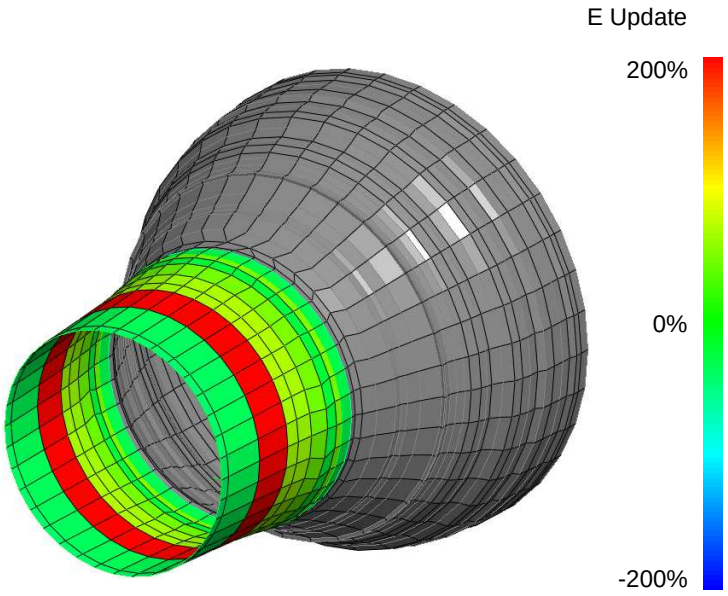

Figure 3.12. COC design model parameter updates.

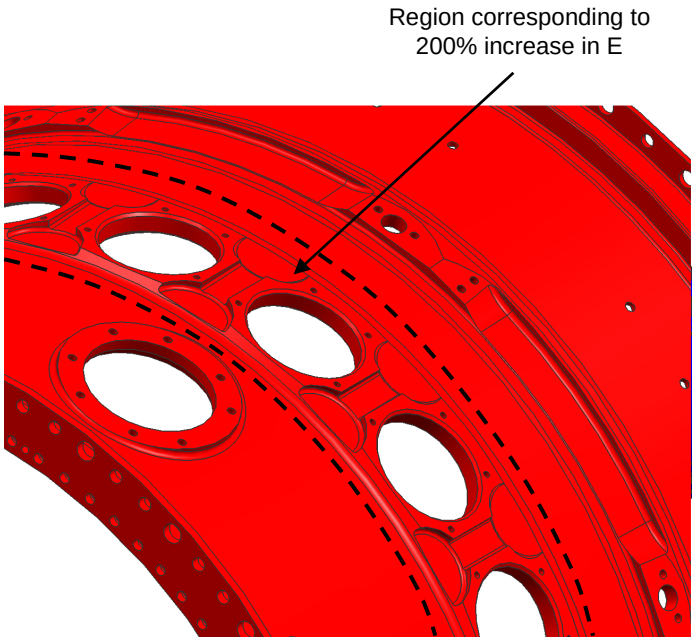

Figure 3.13. COC geometry detail.

3.5.2 Validation of the High Pressure Turbine Intermediate Pressure Turbine Casing (HPTIPTC) Design Model

The validation of the HPTIPTC design follows the same principles explained above for the COC design model. The original assembly design model predictions were compared against the predictions from the hybrid assembly model in Figure 3.8 (b). The results from the correlation are presented in Figure 3.14.

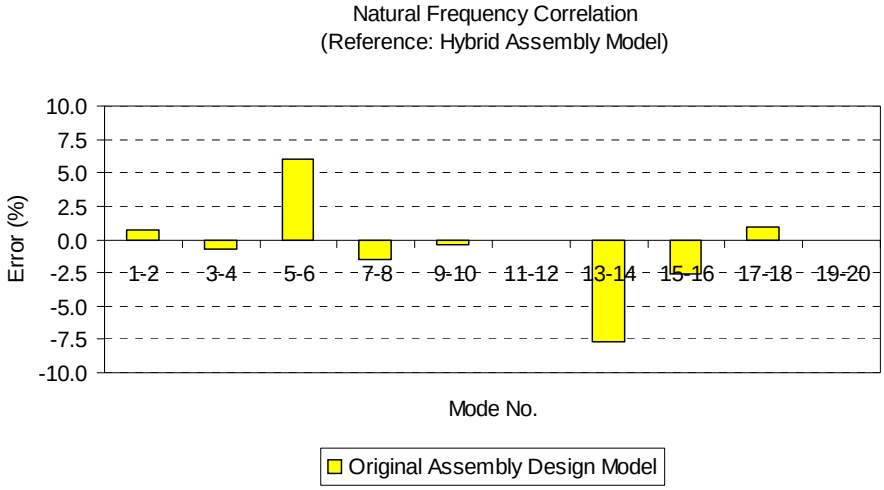

(a)

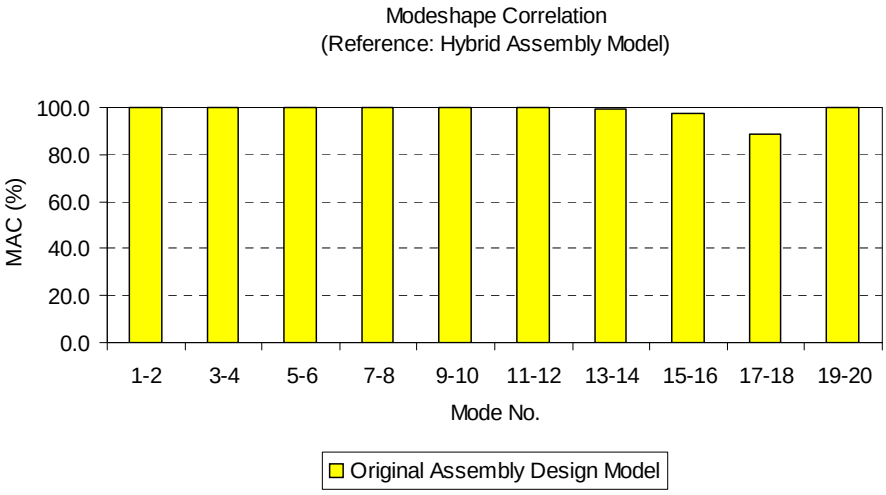

(b)

Figure 3.14. Correlation of Case Study assembly model vs. hybrid assembly model with HPTIPTC supermodel. (a) Natural frequency and (b) modeshape.

Even though the modeshape correlation is very good for all mode pairs, the natural frequency deviation of around 8% for mode pair 13-14 is significant and requires correction.

Again, both the natural frequencies and modeshapes were selected as target responses during the Model Updating. The Young's modulus for each ring of elements in the HPTIPTC design model, 19 in total, was selected as a potential parameter for updating. Figure 3.15 shows the updating progress. In this case the updating diverges in the beginning to then smoothly converge to a low level of error. The original divergence behaviour is likely to be caused by a local minimum of the updating penalty function.

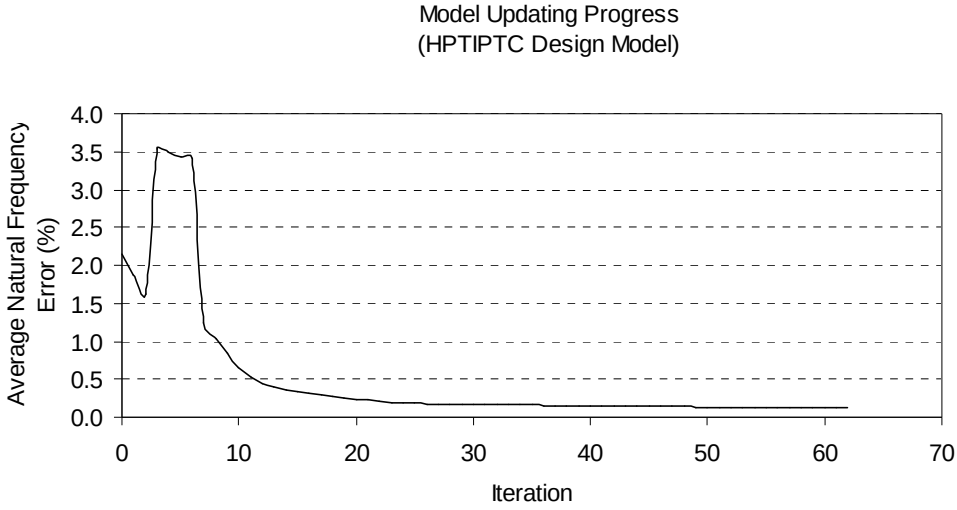

Figure 3.15. HPTIPTC Model Updating progress.

Figure 3.16 shows the correlation improvements after the Model Update. All natural frequency correlations lie within a 0.5% error. The MAC correlations remain close to 100%. Figure 3.17 shows the parameter changes introduced as a result of the Model Updating process.

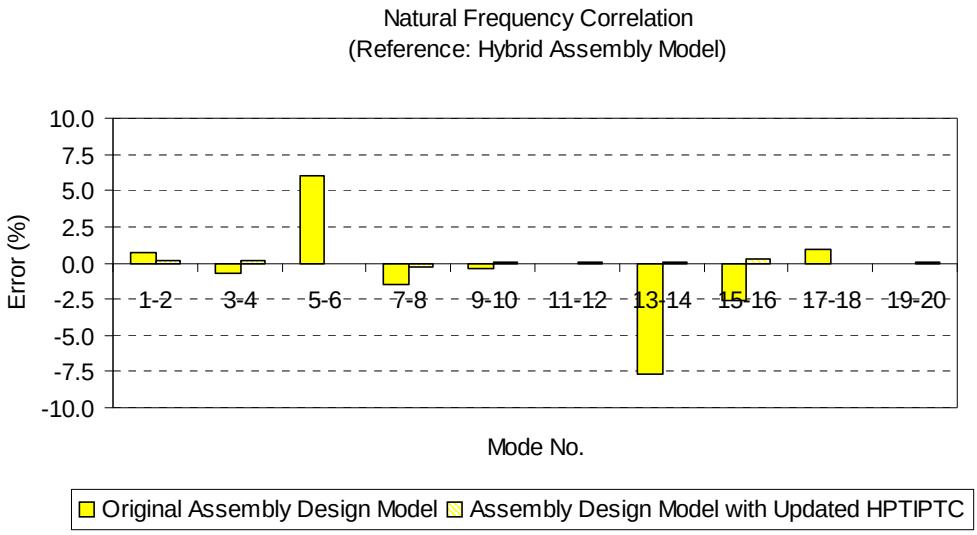

(a)

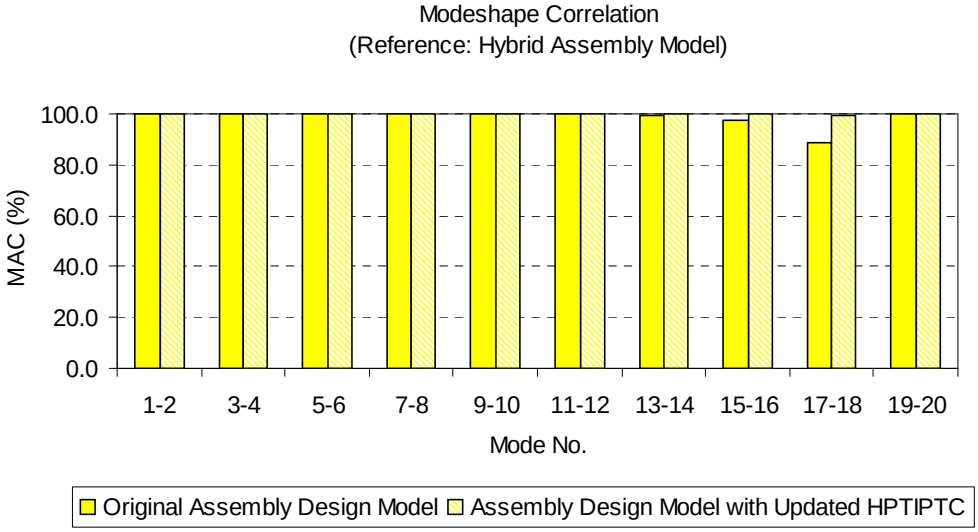

(b)

Figure 3.16. Correlation before and after HPTIPTC Model Update. (a) Natural frequency and (b) modeshape.

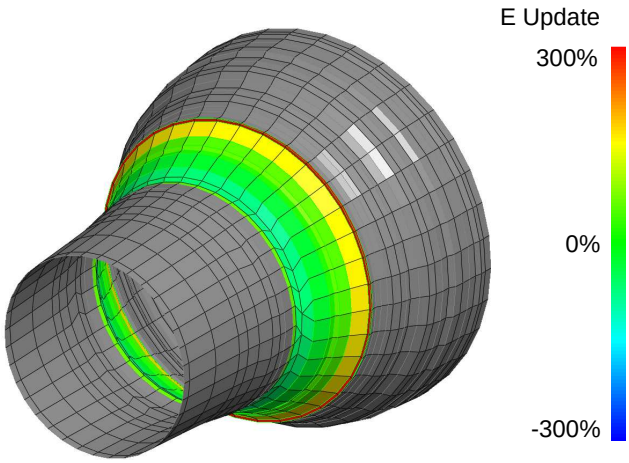

Figure 3.17. HPTIPTC design model parameter updates.

The most significant changes are centred on the back end of the component. Figure 3.18 (a) shows a cross-section detail of the geometry in this area. This step-shape region is modelled by three rings of shells at almost 90°, see Figure 3.18 (b). Shell elements do not have in-plane rotational stiffness. Hence, the vertical ring of shells will have a much reduced radial stiffness. Model Updating compensates for this lack of stiffness by greatly increasing the Young's modulus in this area. There are diverse views over whether this is an acceptable practice or not. In the context of this work, this modelling approach will be considered to be valid.

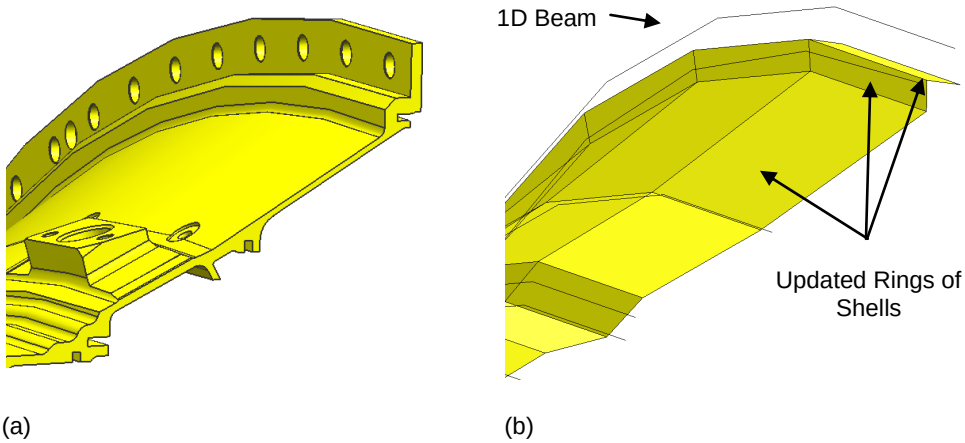

Figure 3.18. HPTIPTC. (a) Cross-section geometry detail and (b) corresponding design model.

3.5.3 Validation of the Low Pressure Turbine Casing (LPTC) Design Model

The original assembly design model predictions were compared against the predictions from the hybrid assembly model in Figure 3.8 (c). The results from the correlation are presented in Figure 3.19.

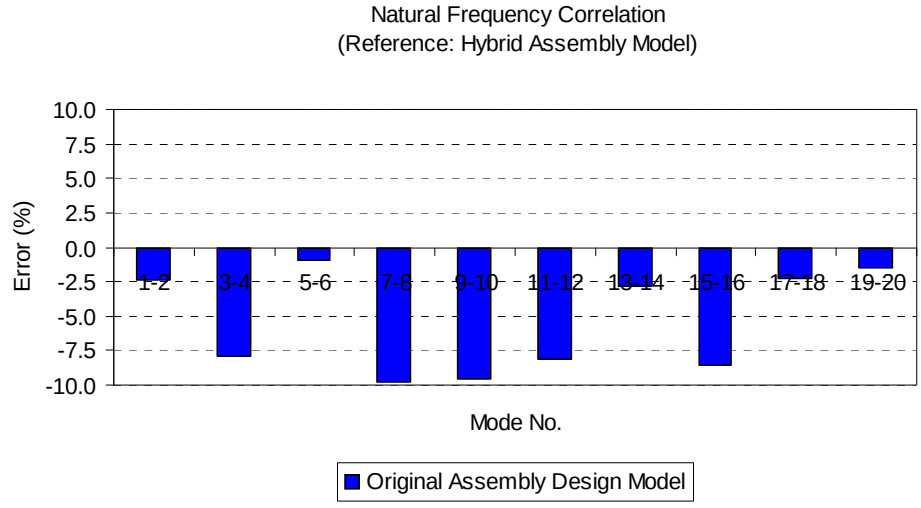

(a)

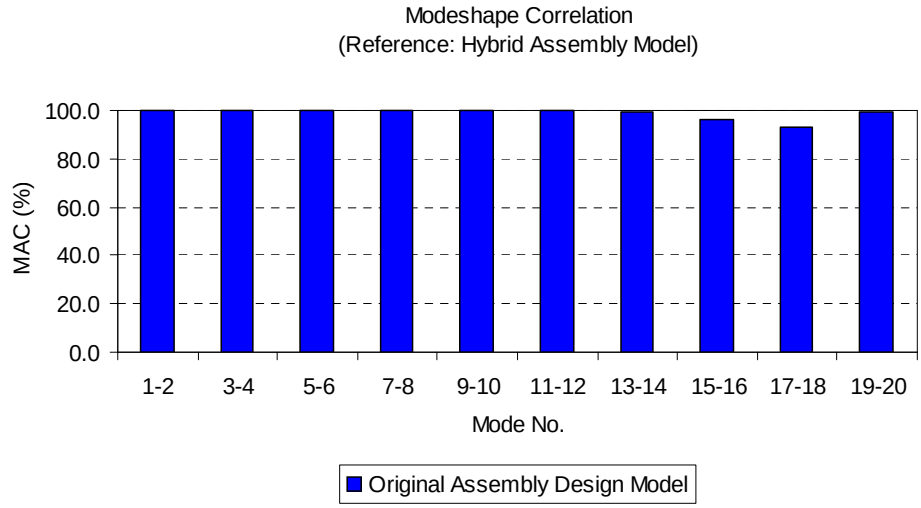

(b)

Figure 3.19. Correlation of Case Study assembly model vs. hybrid assembly model with LPTC supermodel. (a) Natural frequency and (b) modeshape.

Even though the modeshape correlation is very good for all mode pairs, the natural frequency deviation of some mode pairs is significant (10% error for mode pairs 7-8 and 9-10). As a result the LPTC design model needs to be updated.

Again, both the natural frequencies and modeshapes were selected as target responses during the Model Updating. The Young's modulus for each ring of elements in the LPTC design model, 29 in total, was selected as a potential parameter for updating. Figure 3.20 shows the updating progress. The convergence is smooth with a low error asymptote.

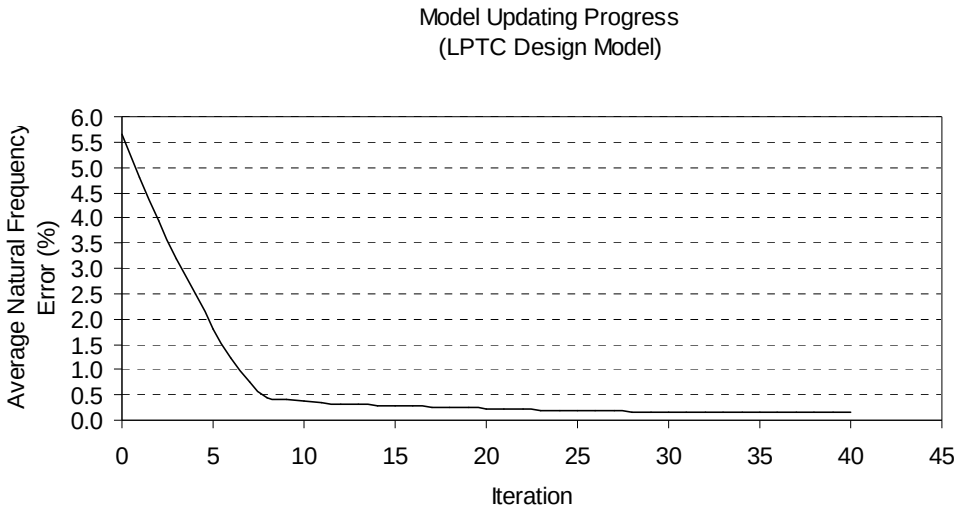

Figure 3.20. LPTC Model Updating progress.

Figure 3.21 shows the correlation improvements after the Model Update. All natural frequency correlations lie within a 0.5% error. The MAC correlations remain close to 100%. Figure 3.22 shows the parameter changes introduced as a result of the Model Updating process.

The most significant changes are centred on the middle section of the component. Figure 3.23 (a) shows a cross-section detail of the geometry in this area. There is a stiffening ring which is not captured in the original design model, see Figure 3.23 (b),

and which effect has been compensated during the Model Update by increasing the Young's modulus of the adjacent shells. Again, this would be considered an acceptable modification as it has real physical meaning.

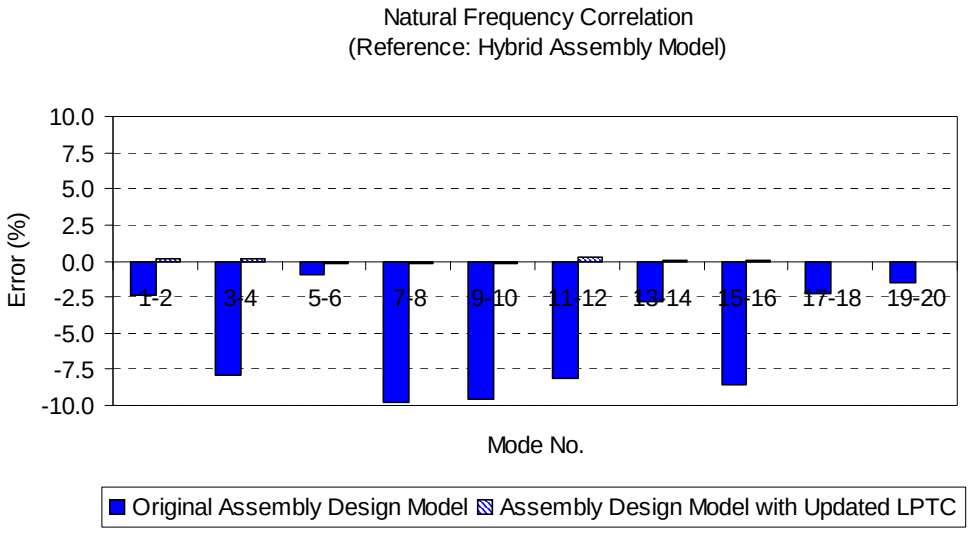

(a)

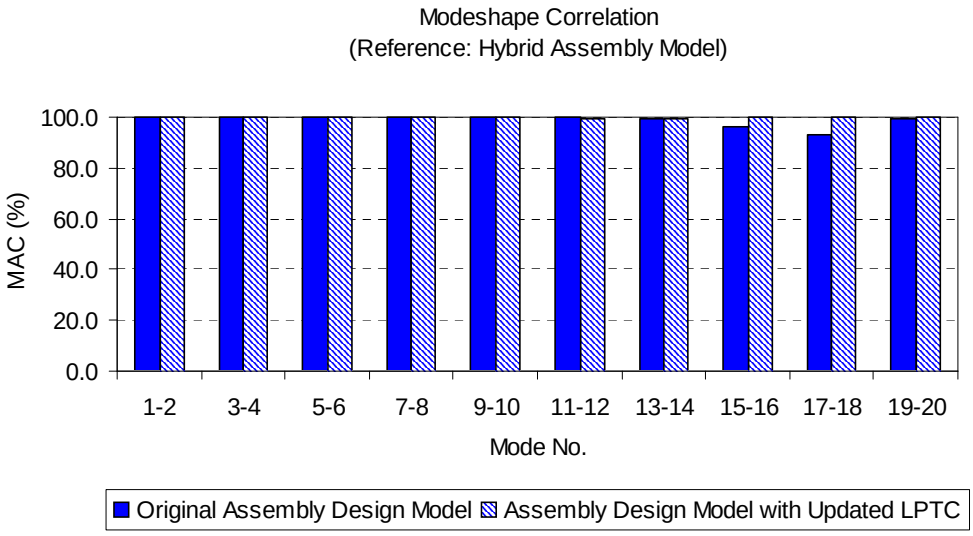

(b)

Figure 3.21. Correlation before and after LPTC Model Update. (a) Natural frequency and (b) modeshape.

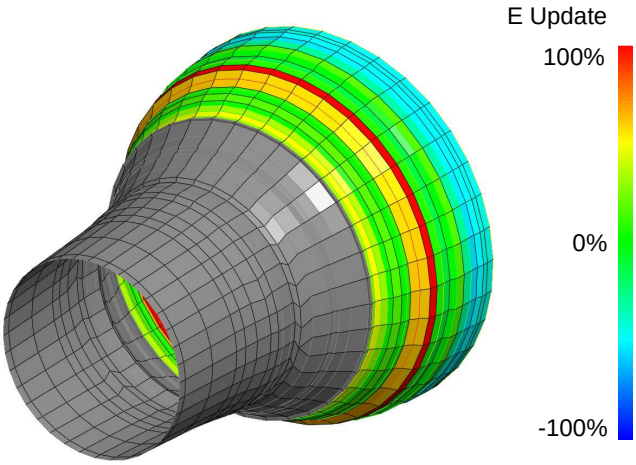

Figure 3.22. LPTC design model parameter updates.

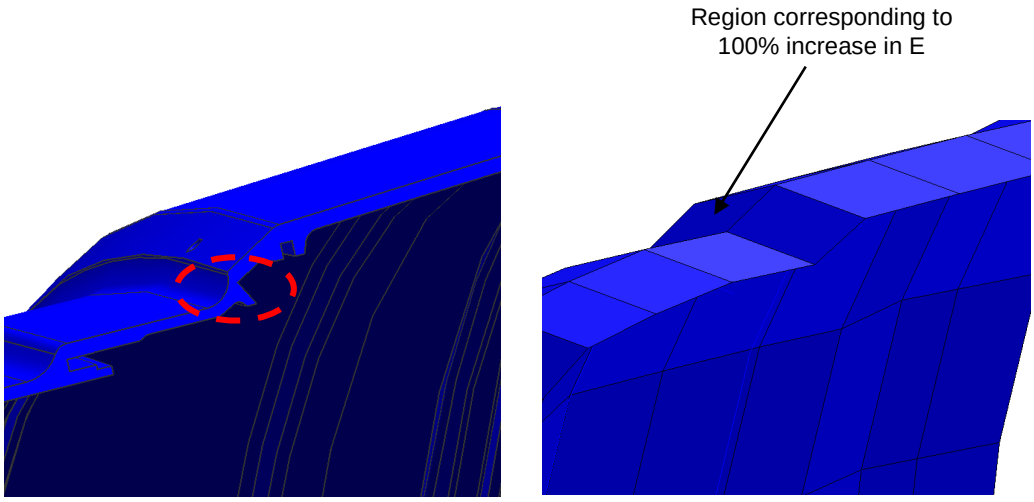

(a) (b)

Figure 3.23. LPTC. (a) Cross-section geometry detail and (b) corresponding design model.

3.6 Case Study - Certification

In order to demonstrate the suitability of the assembly model validation strategy proposed in this work, the predictions from the assembly model containing the validated

component design models will now be compared against the results from a Modal Test. For clarity, this step is highlighted in Figure 3.24.

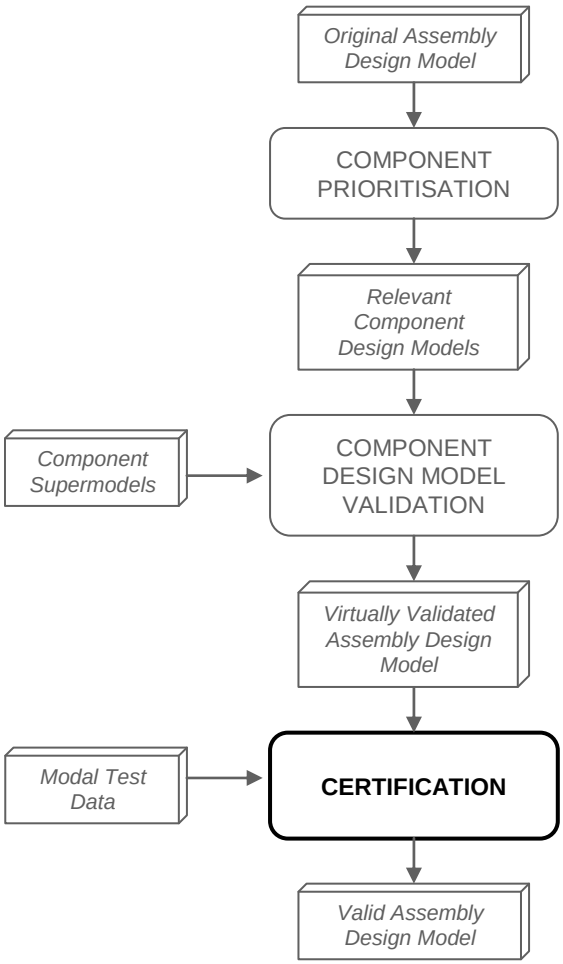

Figure 3.24. Final certification.

The Modal Test was performed on a manufactured prototype of the assembly as part of the VIVACE [41] programme. Figure 3.25 shows the manufactured assembly suspended from very soft elastic ropes that mimic free-free boundary conditions. A multi-reference SIMO (Single Input Multiple Output) Modal Test was selected as the most appropriate technique due to the close proximity of some of the modes of interest. The test made use of a calibrated hammer to excite the structure and a set of

accelerometers to measure the response. The accelerometers remained at the same place throughout the whole test while the hammer moved around the structure.

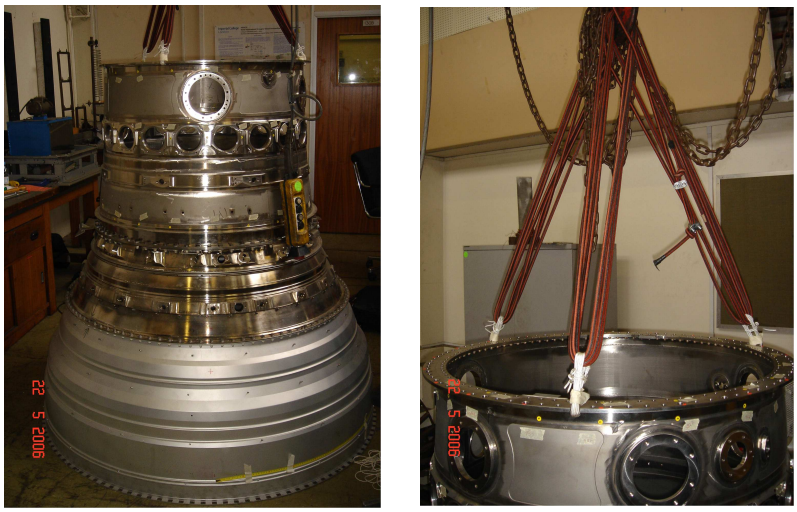

Figure 3.25. Case Study physical test.

The number of impact locations (180 in total) and responses (8 in total) as well as their positions were optimised using the predictions from the "virtually" validated assembly model. This process is commonly referred to as Test Planning [31]. Figure 3.26 shows the Measurement wireframe. A detailed description of this test can be found in reference [67].

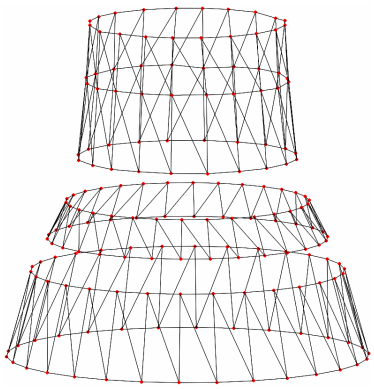

Figure 3.26. Case Study Measurement wireframe.

Figure 3.27 shows the correlation against test data of the original assembly model and the validated one. The improvement in the natural frequency correlation is significant. For instance, the correlation of the mode pair (i.e. 5-6) has been reduced from around 15% to a mere 3%. In fact, all mode pairs but two (i.e. 13-14 and 15-6) have seen a significant improvement in their frequency correlation which has brought them well within the 5% threshold. The modeshape correlation of all mode pairs remains very good with all MAC values above the requirement of 80%.

These improvements are significant and very encouraging. Nonetheless they are somehow overshadowed by the natural frequency correlation of the updated mode pairs 13-14 and 15-16 with values of around 6% and 6.5% respectively. One could argue that the design models were validated using nominal supermodels as reference while the tested structure is subject to manufacturing tolerances. Moreover, measurement errors and other test uncertainties might contribute to deviations in the correlation. However, it is unlikely that the combination of these factors can explain such big differences. It is more likely that there is a physical explanation behind these poor correlations.

A closer analysis of the correlation values reveals some interesting findings. For instance, the original design model was not either consistently stiffer or softer when compared to the measured modes. Mode pair 5-6 was predicted to be 15% stiffer than that of the real structure while mode pair 7-8 was 8.5% softer. On the contrary, the validated model seems to be consistently stiffer for all modes. The only exceptions are mode pairs 1-2 and 17-18, but in both cases the correlation is very close to 0.

It is now time to revisit some the assumptions taken during the validation process, particularly the hypothesis that the joints between components do not play any significant part in the behaviour of the assembly. Throughout the whole validation process using supermodels, the interfaces between components have been assumed to be perfectly rigid. This can potentially explain why the validated assembly model seems to be overstiff.

The following sections take a look at the influence that joints might have on the assembly behaviour and discusses how to incorporate their effect during the validation process.

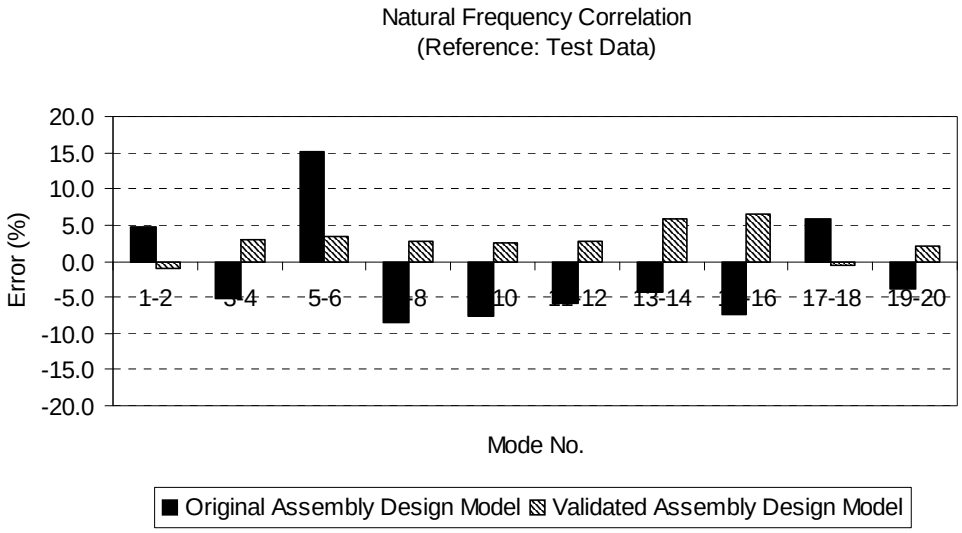

(a)

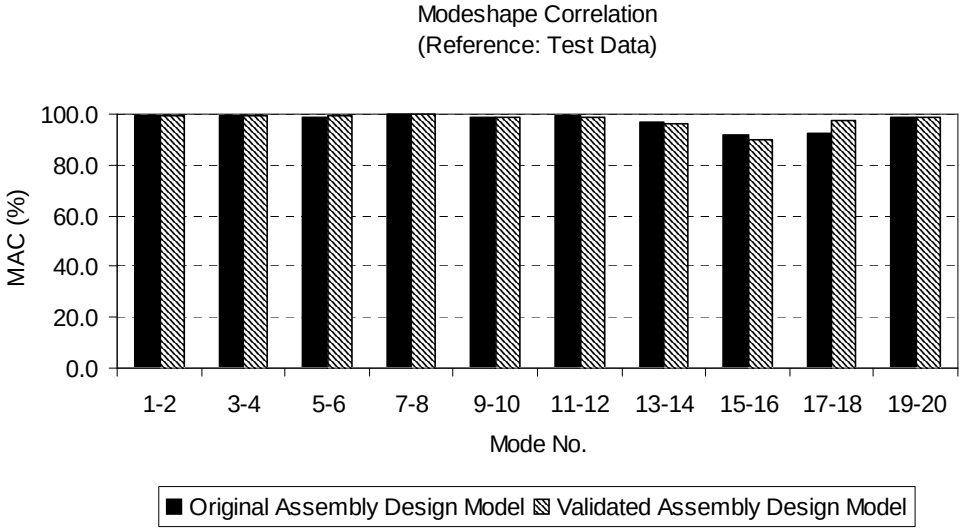

(b)

Figure 3.27. Correlation of Case Study assembly model vs. physical test data. (a) Natural frequency and (b) modeshape.

3.7 Case Study - Influence of Joints

In order to assess the effect of joints on the dynamic behaviour of assemblies, a simple exercise is devised. The rigid links between components in the validated assembly model are replaced by springs to make the joints flexible, see Figure 3.28.

The stiffness of those springs will be modified to assess the effect of the flexibility of the joints on the behaviour of the assembly.

The design models of the Case Study are made up of shells and beams. In practical terms this means that each of the nodes is defined by 6 DOFs, 3 translational and 3 rotational. As a result, the stiffness of the spring between two nodes must be defined in six directions:

- K_z is the translational spring stiffness between two nodes in the engine's axial direction;
- K_r and K_θ are the radial and tangential translational stiffness respectively;
- R_z is the angular spring stiffness between two nodes in the engine's axial direction and;
- R_r and R_θ are the radial and tangential angular stiffness respectively.

In order to simplify the analysis, the following constraints are considered:

- all stiffness components change uniformly across all node pairs in a given joint. This is fairly representative of the actual joints where the connecting bolts are usually equally spaced and with the same torque value applied. Also;
- the value of the translational axial stiffness K_z is an order of magnitude higher than that of the radial and tangential components, K_r and K_θ respectively. This accounts for the fact that the radial and tangential stiffness are mostly driven by friction forces across the flange. Also;
- the value of the angular axial stiffness R_z is an order of magnitude lower than that of the radial and tangential components, R_r and R_θ respectively. Similarly to the translational case, this accounts for the fact that the angular axial stiffness is mostly driven by friction forces. Finally;

- K_r is equal to K_θ and R_r is equal to R_θ. This assumes equal stiffness in the radial and tangential direction.

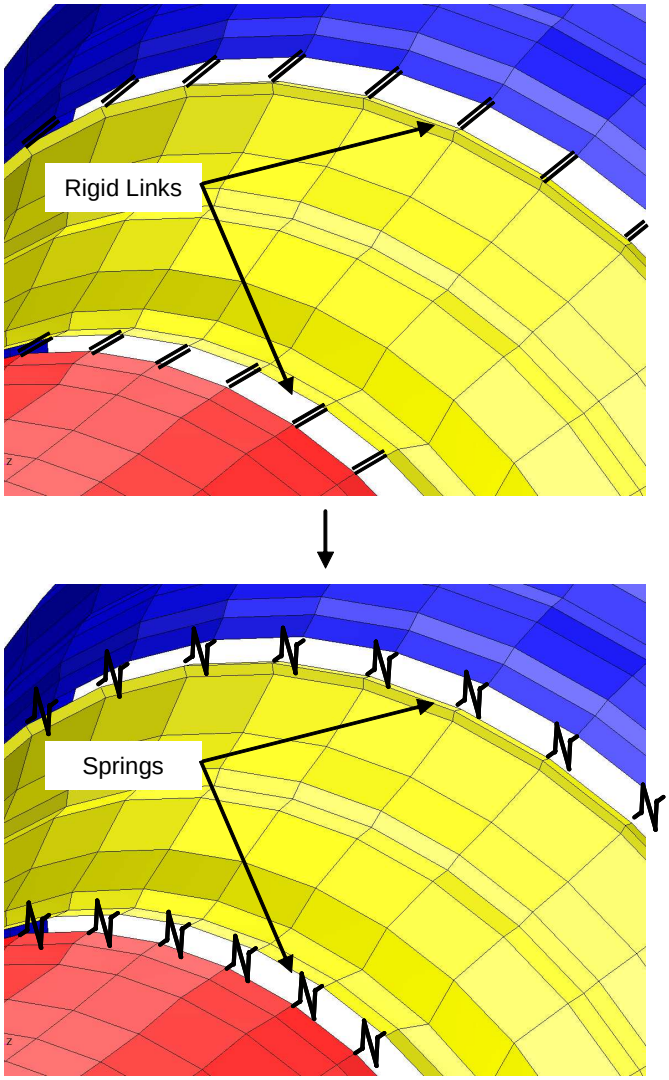

Figure 3.28. Rigid to flexible joints.

As a result, there are four parameters that fully define the stiffness of the two joints in the assembly:

- $K_{z\,1}$ defines the translational stiffness between two nodes of the front joint ($K_{r\,1}$ = $K_{\theta\,1}$ = 0.1 $K_{z\,1}$);
- $R_{z\,1}$ defines the angular stiffness between two nodes of the front joint ($R_{r\,1}$ = $R_{\theta\,1}$ = 10 $R_{z\,1}$);
- $K_{z\,2}$ defines the translational stiffness between two nodes of the rear joint ($K_{r\,2}$ = $K_{\theta\,2}$ = 0.1 $K_{z\,2}$) and;
- $R_{z\,2}$ defines the angular stiffness between two nodes of the rear joint ($R_{r\,2}$ = $R_{\theta\,2}$ = 10 $R_{z\,2}$).

In order to assess the effect of each parameter individually the following methodology is followed. One parameter is selected and its stiffness is modified to span across different levels of flexibilities. In the meantime the rest of the joint parameters are considered to be perfectly rigid.

For instance, the graphs in Figure 3.29 (a) represent the effect of the translational stiffness of the front joint on the natural frequency predictions for the first 10 mode pairs of the assembly. The X-axis corresponds to the translational stiffness of the front joint represented by the value of $K_{z\,1}$ (in logarithmic scale). The Y-axis corresponds to the natural frequency deviation with respect to perfectly rigid connections. Obviously, the softer the joint, the lower the natural frequency predicted for all modes. However the effect on each individual mode pair is noticeably different. For instance, the natural frequency of mode pair 13-14 is noticeably the most affected by the translational stiffness of the front joint. The graphs in Figure 3.29 (b) describe the influence of the angular stiffness of the front joint while those in Figure 3.30 correspond to the influence of both the translational and angular stiffness of the rear joint.

The analysis of these graphs reveals that there are three mode pairs which are particularly affected by the stiffness of the joints. These are the mode pairs 13-14 and 15-16 and to a smaller scale the mode pair 5-6.

Now let us come back to the correlation of the validated assembly model against the data from physical testing in Figure 3.27. The model overpredicts the natural frequency of mode pairs 15-16, 13-14 and to a smaller scale 5-6. Interestingly these are exactly the same modes that are most affected by the flexibility of the joints. This hardly seems

like a coincidence and strongly suggests that the effect of joints cannot be ignored anymore if accurate predictions from assembly models are required. This in turn raises the question of how to deal with the joints during the validation process.

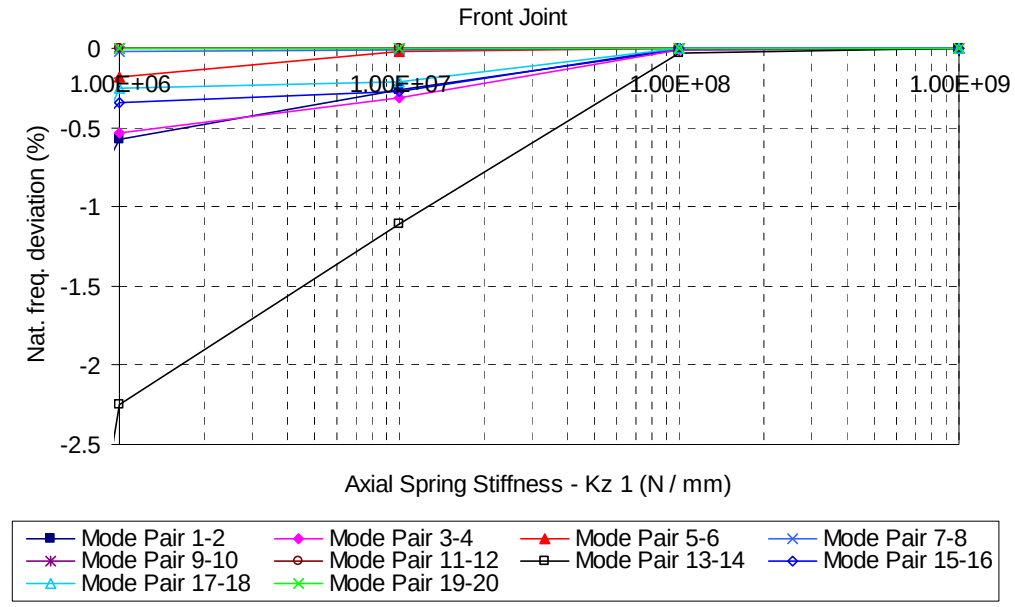

(a)

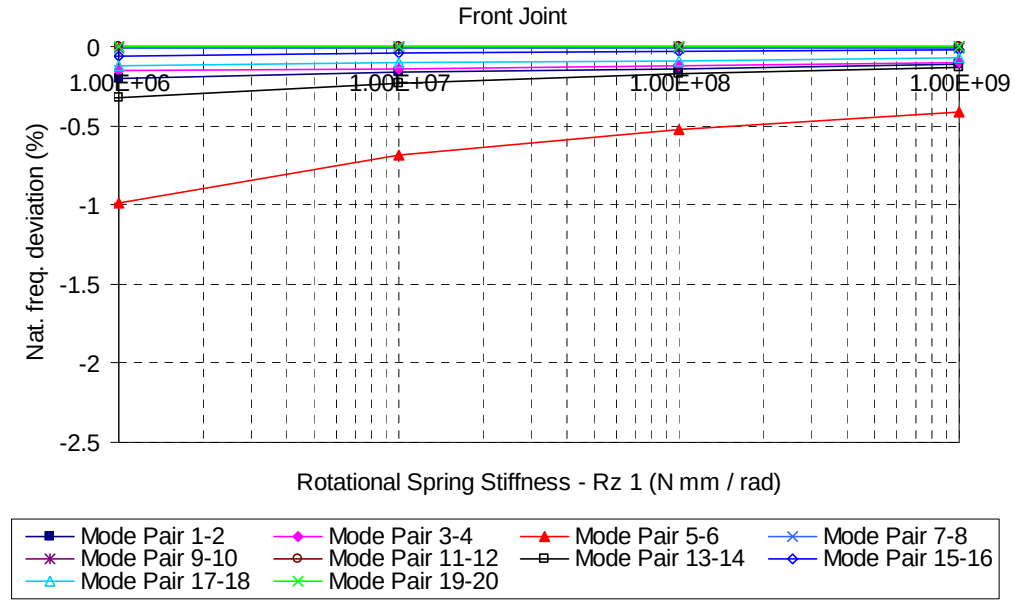

(b)

Figure 3.29. Front joint COC-HPTIPTC. (a) Effect of translational stiffness and (b) effect of rotational stiffness.

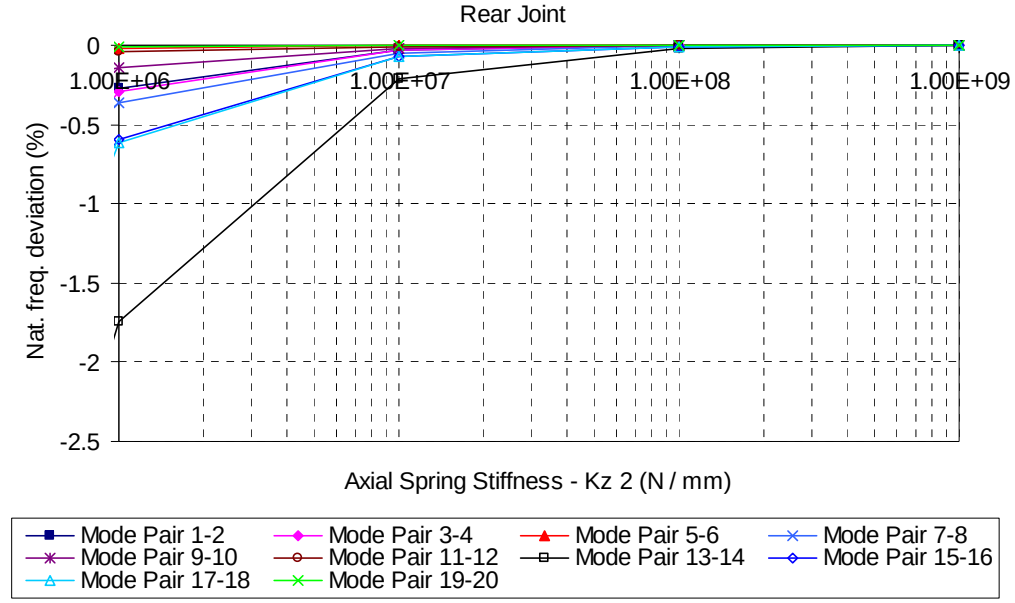

(a)

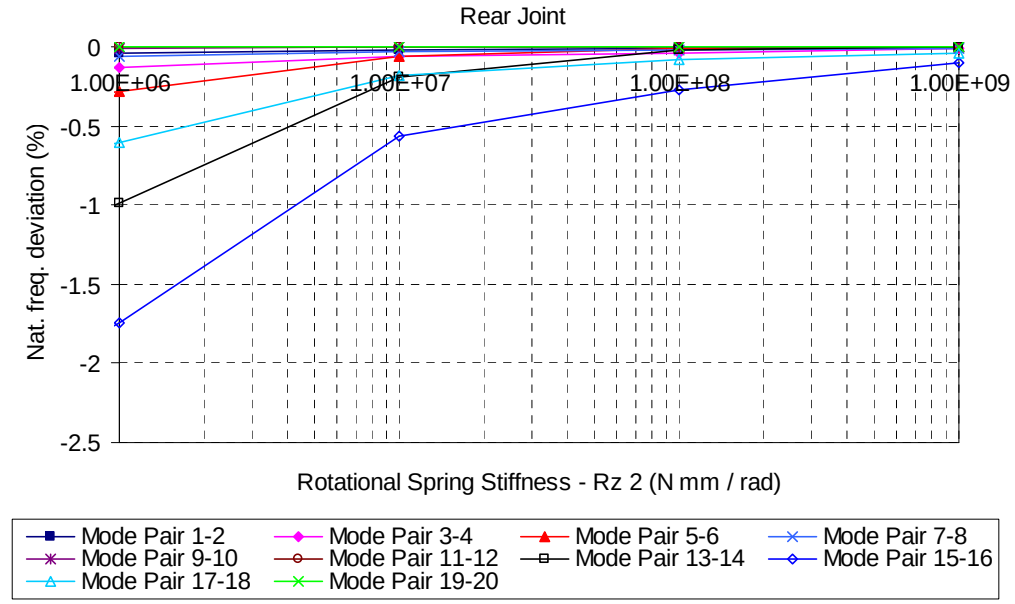

(b)

Figure 3.30. Rear joint HPTIPTC-LPTC. (a) Effect of translational stiffness and (b) effect of rotational stiffness.

3.8 How to Deal with Joints

The methodology presented in this chapter facilitates the robust validation of component design models. Nevertheless, it looks like an assembly made up of validated component models might still not yield sufficiently accurate predictions if the effect of joints is ignored.

This does not necessarily mean that the validation approach proposed here is flawed. The separation of an assembly into components and joints is completely artificial. A joint is in itself another component in the assembly. It might not have mass but it definitely has stiffness and damping. If joints were modelled and treated like any other component, the validation approach proposed in this work would still be applicable. Similarly to any other component, the supermodel of a joint would be used to validate its corresponding, and less refined, design model.

Unlike continuous components made of isotropic materials, it is most likely that the behaviour of joints can only be understood at a microscopic level. The effects of surface finish and other complex tribology phenomena are likely to have a significant effect on the properties of the joints. Current computing technology does not allow model refinements at a microscopic level and joint models must rely on gross assumptions which usually lead to poor predictions. Nonetheless, the rapid developments in computing technology are quickly changing this scenario. It is most likely that models at a microscopic level will be a reality in a few years. This will facilitate a better understanding of the joint's properties and the creation of accurate supermodels in the near future. It is also important to understand that a thorough experimental programme will be required to support the development of these supermodelling techniques.

Understandably, industry cannot wait until joint supermodels are a feasible option to validate assembly design models using the methodology presented above. A short term solution is required to bridge the problem of the joints. Figure 3.31 shows a proposal to validate complex assembly models which takes into account the effects of joints.

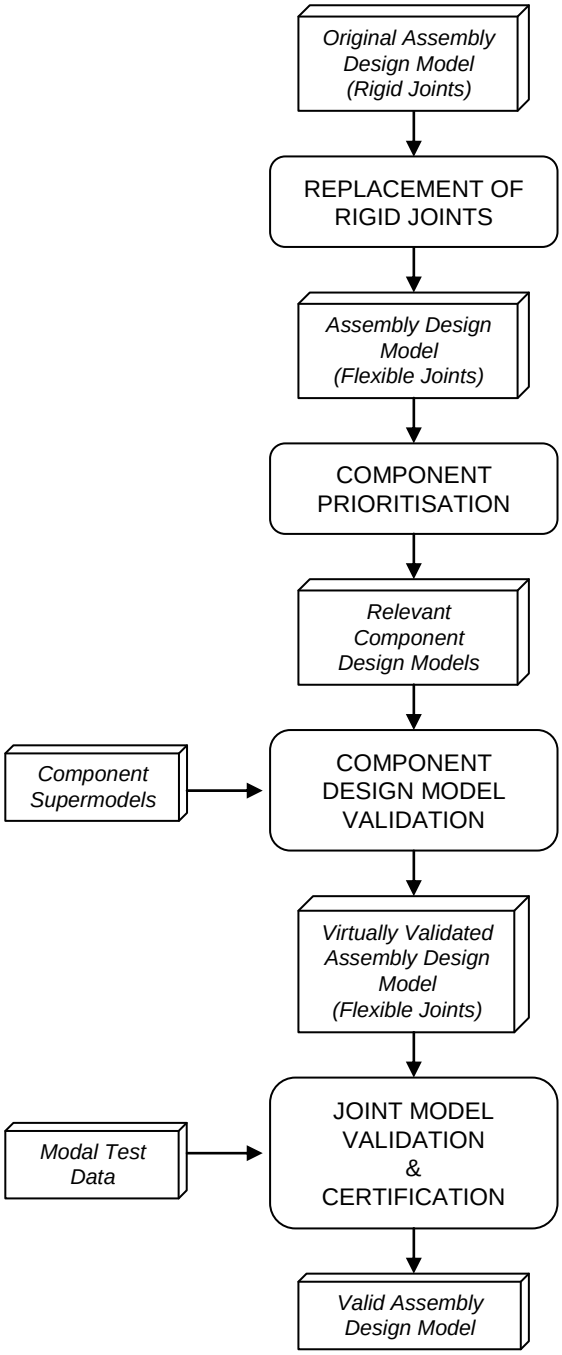

Figure 3.31. Proposed validation strategy to account for the influence of joints.

In the first stage of the process, the rigid links between components are substituted by simplified joint models. These models will usually consist of springs with high values of stiffness associated. Preferably, the stiffness parameters would be selected according to the best existing joint modelling practice, nevertheless, it is most likely that in many cases an “informed guess” will be used. The next stage is to validate the component design models using their corresponding supermodels as the reference. This can be done at the very early stages of the engine programme and well ahead of manufacture.

It is important to understand that the validation of a component model at this stage is not compromised by the influence of the joints as long as both the original assembly model and the corresponding hybrid assembly model share the same models for the joints. In other words, the only difference between the assembly design model and the hybrid assembly must only be the model of the component being validated. Keeping the same model of the joints in the hybrid assembly model is quite simple in practice. Figure 3.32 illustrates the methodology that must be followed. The picture at the top corresponds to two design models linked together using springs. In the picture at the bottom, one of the component design models has been substituted by a supermodel. In order to maintain the same model of the joints, an extra set of nodes is created at the same positions where the original interface nodes of the substituted component were. These extra nodes are then linked on one side to the supermodel and on the other to the adjacent component using the original model of the joints.

Once the component design models have been “virtually” validated the next step is to validate the models of the joints. As supermodels for joints do not exist yet, the validation of the joint models in the assembly must make use of physical test data. The results from a test on a prototype of the assembly will be compared against the assembly model predictions. Any discrepancy at this stage can only be attributed to the joints since all the component models are already validated. If necessary, these discrepancies can be reduced by updating the parameters in the joint models to better match the test results. The final certification of the model will take place once the assembly model is deemed valid.

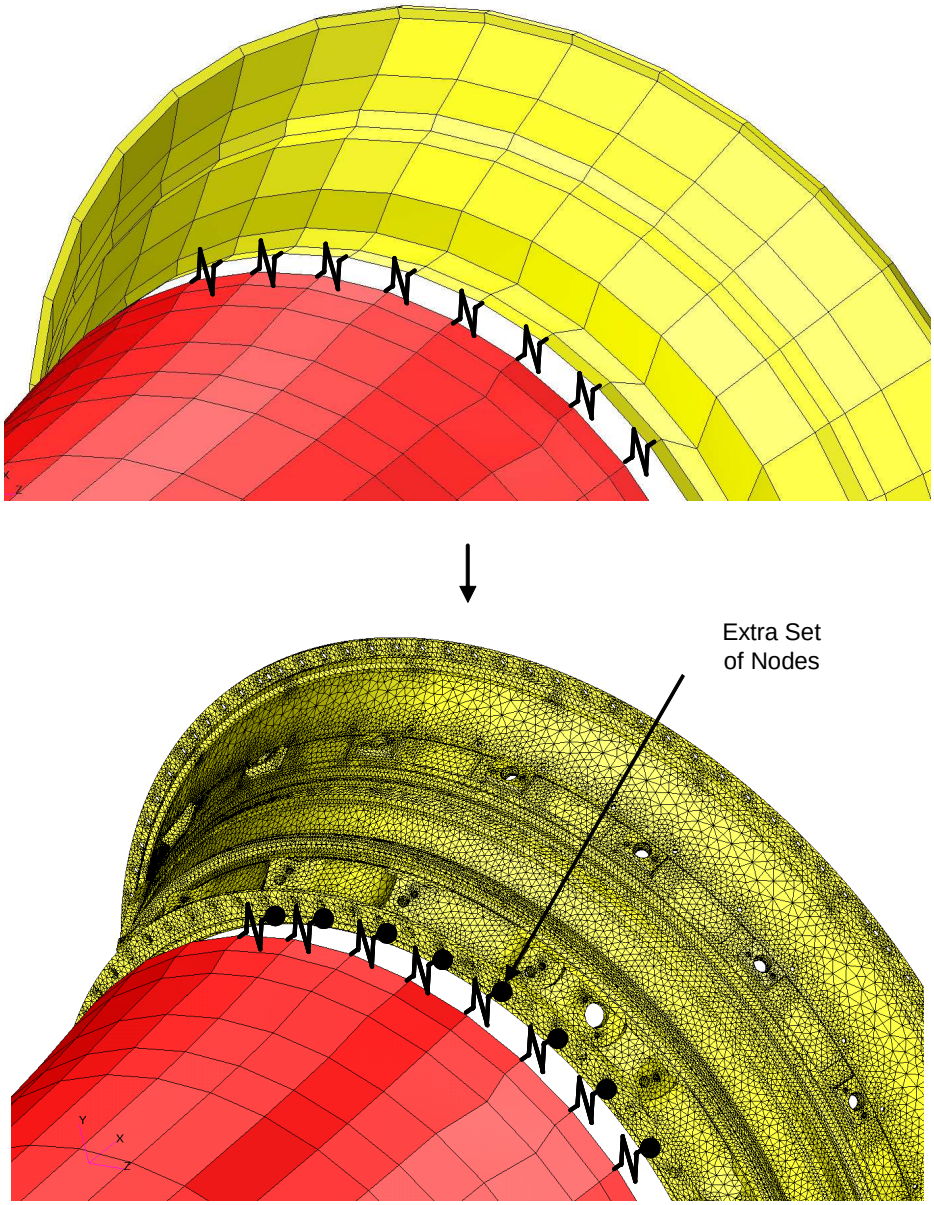

Figure 3.32. Joint modelling in hybrid assembly models.

This approach is a short term compromise where most of the assembly validation takes place before manufacture. Only the validation of the joints must wait until physical test data is available.

The proposed approach will now be demonstrated using the Case Study. The original rigid links between the component design models are substituted by springs. Each pair of connecting nodes between components is linked by 6 springs similarly to the exercise in the previous section.

For any of the j-th joints in the assembly, the value of the translational axial stiffness $K_{z\,j}$ can be estimated using the axial stiffness of the bolts that connect the casing flanges. The axial stiffness of a single bolt is given by:

$$K_{bolt} = \frac{EA}{L} \tag{3.33}$$

where E is the Young's modulus, A the section area and L the length of the bolt. As the nodes in the flanges of the assembly model are equally spaced, the value of $K_{z\,j}$ for the j-th joint is given by:

$$K_{z\,j} = K_{bolt\,j} \frac{n_{bolts\,j}}{n_{nodes\,j}} \tag{3.34}$$

where $n_{bolts\,j}$ is the number of bolts in the j-th joint and $n_{nodes\,j}$ is the number of node pairs in the connecting flange.

The radial and tangential stiffness, $K_{r\,j}$ and $K_{\theta\,j}$ respectively, are usually driven by friction forces and will be considered to be an order of magnitude lower than the axial stiffness $K_{z\,j}$.

$$K_{r\,j} = K_{\theta\,j} = \frac{K_{z\,j}}{10} \tag{3.35}$$

The estimation of the values for the angular stiffness parameters ($R_{r\,j}$, $R_{\theta\,j}$ and $R_{z\,j}$) is much more difficult and would require very complex calculations. For this test case, realistic values were used. Table 3.2 shows the initial estimates for the longitudinal and angular joint stiffness parameters corresponding to the front (COC-HPTIPTC) and rear (HPTIPTC-LPTC) joints.

Joint	Parameter	Initial Estimate
1 (COC – HPTIPTC)	$K_{z\,1}$	$K_{bolt\,1}\frac{n_{bolts\,1}}{n_{nodes\,1}}$
	$K_{r\,1}$, $K_{\theta\,1}$	$\frac{K_{z\,1}}{10}$
	$R_{z\,1}$	1.0E+06 N mm/rad
	$R_{r\,1}$, $R_{\theta\,1}$	1.0E+07 N mm/rad
2 (HPTIPTC – LPTC)	$K_{z\,2}$	$K_{bolt\,2}\frac{n_{bolts\,2}}{n_{nodes\,2}}$
	$K_{r\,2}$, $K_{\theta\,2}$	$\frac{K_{z\,2}}{10}$
	$R_{z\,2}$	1.0E+06 N mm/rad
	$R_{r\,2}$, $R_{\theta\,2}$	1.0E+07 N mm/rad

Table 3.2. Estimated values for joint stiffness parameters.

Once the simplified models for the joints are in place, the next step in the process according to Figure 3.31 is the validation of the component design models using the supermodels as reference. This process has been thoroughly explained in this chapter and will not be repeated here. It is just important to point out that now the hybrid assembly models contain the same simplified models of the joints as those used to join the component design models.

Figure 3.33 show the correlation against test data of:

- the original assembly model with rigid links and;
- the assembly model with validated components using supermodels as reference and simplified joint models.

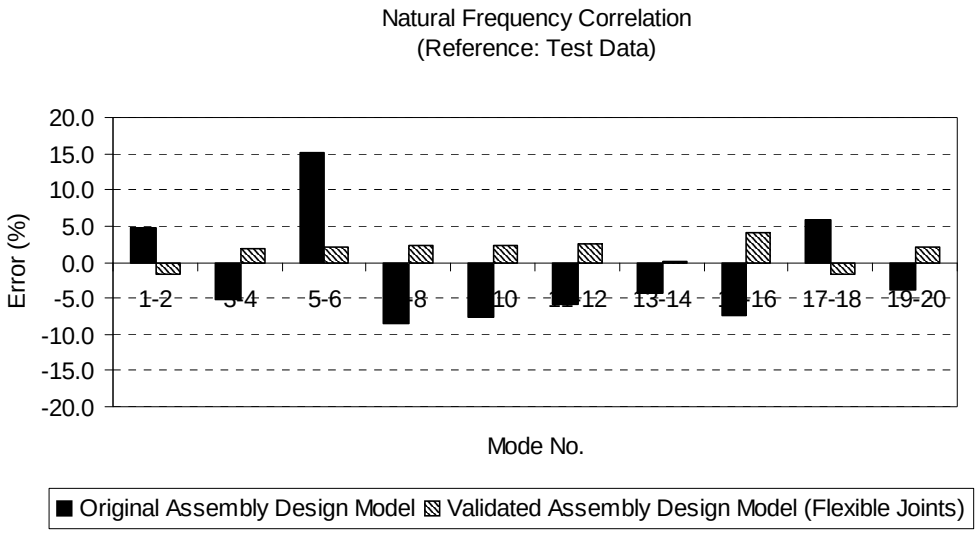

(a)

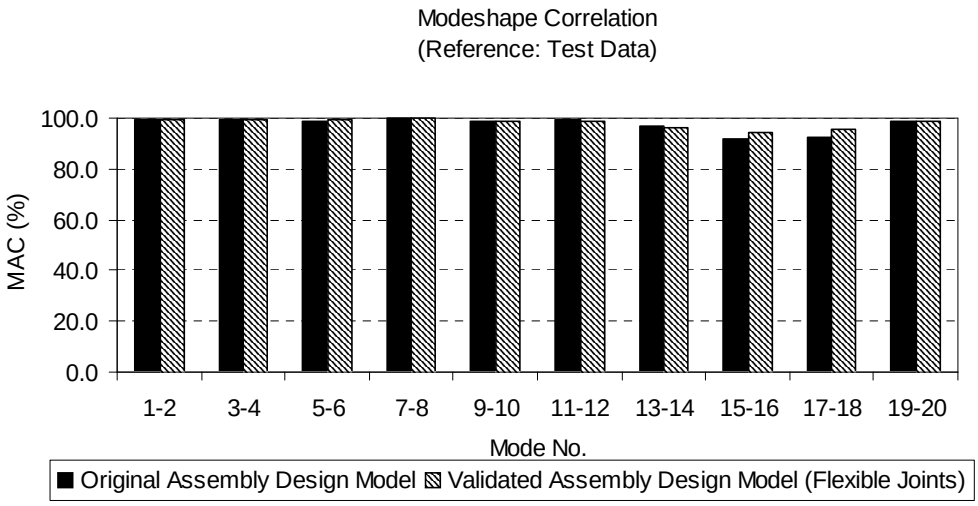

(b)

Figure 3.33. Influence of joints. Correlation of Case Study assembly model vs. physical test data. (a) Natural frequency and (b) modeshape.

The assembly model with validated component models and an initial estimate of the stiffness of the joints already fulfils the accuracy requirements of 5% natural frequency error and 80% in MAC correlation. As a reminder, when the effects of joints were

ignored, the virtually validated assembly model was not capable of fulfilling the accuracy requirements.

As the certification requirements have already been met, there is no need for further refinement of the joint models. Nonetheless there is still some interest in finding out the parameter values in the joint models that would give the most accurate predictions. This will help engineers in building up much needed experience in joint modelling.

The same automated Model Updating procedure used during the validation of component models was used here to refine the parameter values of the joints. Figure 3.34 shows the updating progress.

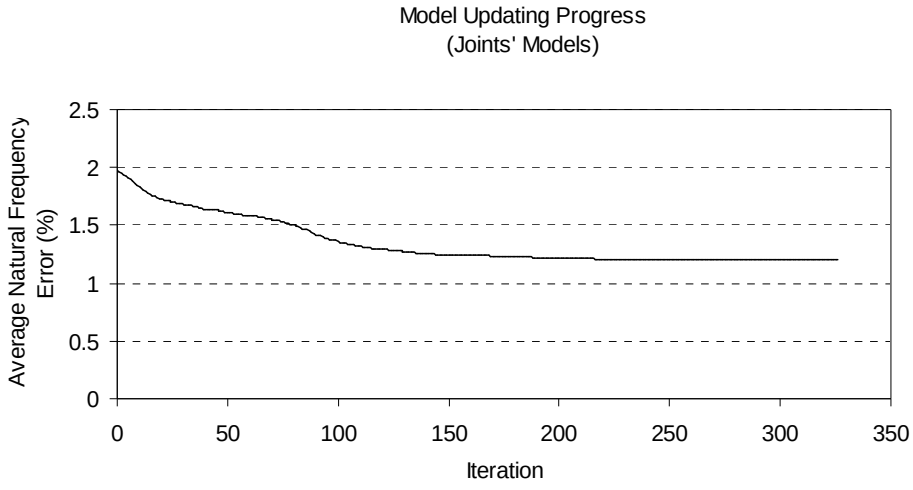

Figure 3.34. Joints Model Updating progress.

Figure 3.35 extends the results presented Figure 3.33 to cover the correlation of the assembly model with validated components and updated joint models. The worst natural frequency error is now around 2.5% (mode pair 17-18), a slight improvement with respect to the validated assembly model with the initial estimate of the joint stiffness (4% error in mode pair 15-16). Table 3.3 shows the change in the stiffness parameters of the joint models as a result of the Model Updating process. The large variation in some of the parameters highlights the lack of accuracy of the initial estimates and the need for improved methods to better model the stiffness of joints.

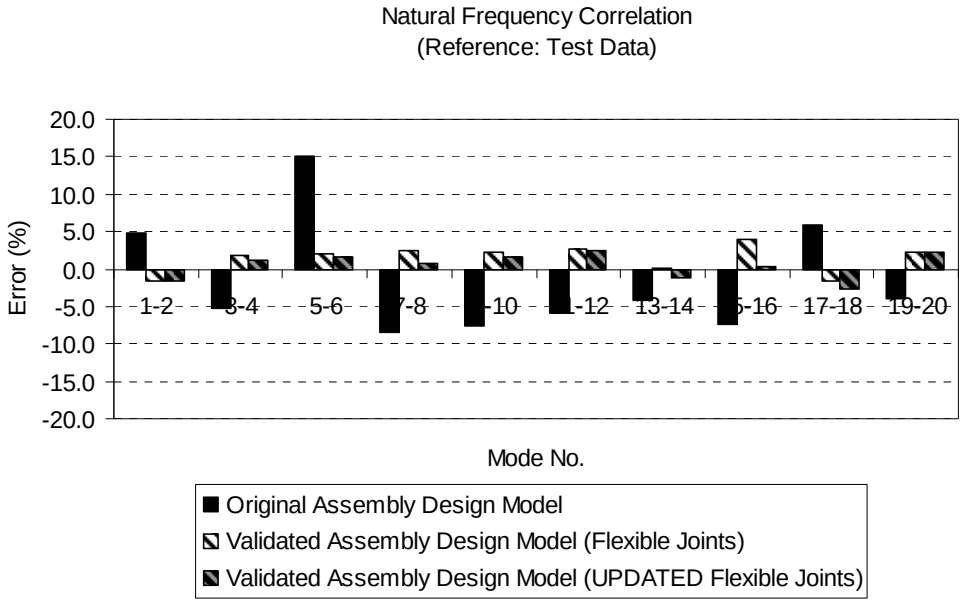

(a)

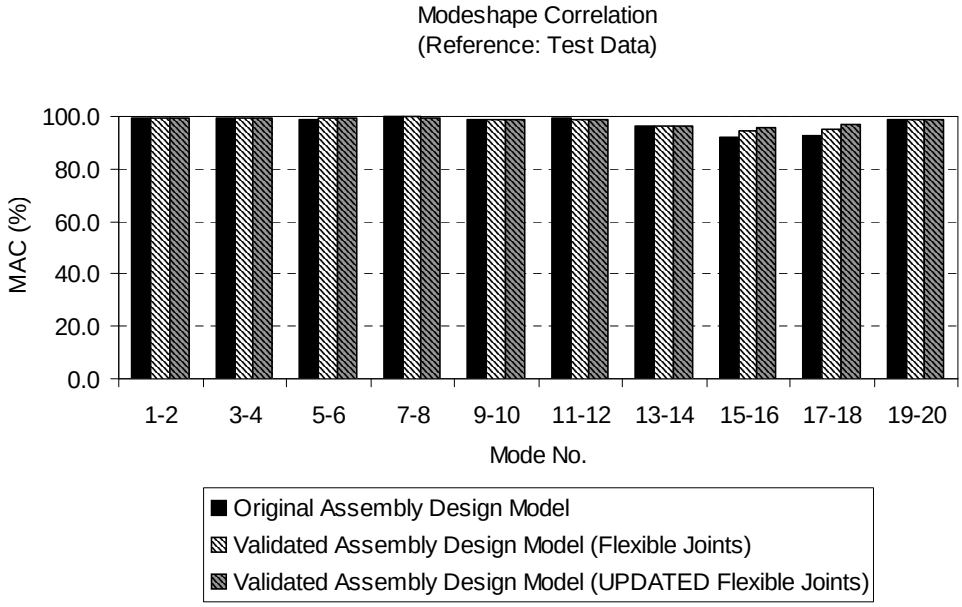

(b)

Figure 3.35. Joints Model Updating. Correlation of Case Study assembly model vs. physical test data. (a) Natural frequency and (b) modeshape.

Joint	Parameter	$\frac{\text{Updated Value}}{\text{Initial Value}}$
1 (COC – HPTIPTC)	$K_{z\,1}$	27.8
	$K_{r\,1}$, $K_{\theta\,1}$	15.1
	$R_{z\,1}$	1.0
	$R_{r\,1}$, $R_{\theta\,1}$	0.1
2 (HPTIPTC – LPTC)	$K_{z\,2}$	2.5
	$K_{r\,2}$, $K_{\theta\,2}$	0.1
	$R_{z\,2}$	0.8
	$R_{r\,2}$, $R_{\theta\,2}$	1.2

Table 3.3. Joints Model Updating. Parameter changes.

3.9 Conclusions

A component design model is only considered to be valid if it is capable of predicting the dynamic behaviour of the component when it is part of the assembly model. The boundary conditions that can be imposed on a component in a laboratory environment usually differ from those that the component will experience when connected to other parts in service. That is why it is not uncommon for a component design model to accurately predict the dynamic behaviour of the component under laboratory conditions but for it to yield inaccurate predictions when it is part of the assembly.

The objective of Test Strategy methods is to design test configurations in which to validate the component design models. However, as reviewed in this chapter, the application of these methods usually results in the need for complex test fixtures which can add a great deal of uncertainty to the test measurements.

The development of supermodels has transformed the approach to model validation. The application of boundary conditions to a supermodel is simply a mathematical

exercise which is not constrained by the traditional limitations of physical testing. A new method has been presented in this chapter which extracts the component design model under validation from the original assembly model and replaces it with the corresponding supermodel to create a so-called “hybrid assembly model”. The predictions from the supermodel as part of the hybrid assembly model correspond to the behaviour of the component when it is part of the assembly. This is the behaviour that the component design model should accurately predict if it is to be considered valid and hence it represents the ideal reference data for validation.

The proposed validation methodology was demonstrated using a representative Case Study where the individual components in an assembly model were validated using the virtual reference provided by hybrid assembly models. The assembly model made up of virtually validated components showed a worst natural frequency error of 6.5% when compared against the measurements from a Modal Test. This is a significant improvement with respect to the worst correlation of 15% that would have been achieved by the original assembly model had it not been validated. Even though this improvement was significant, the worst discrepancies between the predictions from the virtually validated assembly model and the data from the Modal Test (i.e. 6.5% error in natural frequency) were difficult to explain in view of the low manufacturing variability expected from the tested hardware and the low uncertainty associated with the Model Test (i.e. free-free configuration and state-of-the-art measurement equipment and data processing tools).

A comprehensive study carried out in this chapter highlighted that the most likely cause of the discrepancies was due to the influence of the joints which had been neglected when validating the assembly model. It has been shown that the original validation strategy (using supermodels as the reference) can easily accommodate the presence of joints. It simply requires considering each joint as any other component in the assembly and, as for any component, design models of the joints should be included in the assembly model and validated using the corresponding supermodels as the reference.

Unfortunately, supermodel techniques for joints are almost non-existent. As a result, physical testing remains the only reference for the validation of joint models. A modification to the original validation strategy has been presented in this chapter to cope with the presence of joints until reliable joint supermodels become a reality. The

approach consists of first validating the component design models using supermodels as the reference and then using the measurements from a Modal Test to fine tune the models of the joints. The bulk of the validation work is still carried out in a virtual environment well ahead of manufacture; however, physical testing still remains necessary to complete the validation.

The application of the revised validation strategy to the Case Study resulted in a worst natural frequency error of only 2.5% between the predictions from the validated assembly model and the results from the Modal Test. This level of correlation is well within expectations considering the inevitable uncertainties associated with the measurements and the expected deviations of the manufactured components with respect to nominal. Moreover, this level of correlation represents a remarkable improvement with respect to the frequency error of 15% associated with the original assembly model and the 6.5% error achieved when the assembly model was validated neglecting the influence of joints.

Chapter 4 - Technology Demonstration on an Industrial Application

4.1 Introduction

The validation strategy proposed in the previous chapters promises to reduce the cost and timescales currently associated with the validation of complex assembly models. In fact, the virtual nature of this approach facilitates the validation of complex assembly models during the early stages of the product development cycle at almost no financial cost and with few time penalties.

The previous two chapters made use of a simple Case Study to illustrate the proposed methodology. This Case Study consisted of the validation of an assembly model comprising three simple casings. Even though the results from the validation proved very successful, this example could be considered too simple to draw firm conclusions for applications to more complex structures. At the end of the day, the three casing were quasi-cylindrical and the modes validated were not particularly challenging.

This chapter will now consider the validation of a sub-assembly model containing some of the most complex components in an engine. The modes selected for validation have also historically been difficult to predict accurately.

This work was carried out as part of an actual engine certification programme. The strict deadlines and the tight cost limitations associated with these types of programme represent an ideal scenario to demonstrate the maturity of the proposed methodology and its suitability for full-scale deployment into industry.

4.2 Assembly Model Description and Requirements

The Front Structure sub-assembly illustrated in Figure 4.1 (a) is one of the key structural elements in an aeroengine. This sub-assembly is responsible for:

- holding in place the front bearings that support the engine's shafts and;
- directing the airflow from the fan towards the engine bypass and the inner core.

The design of the Front Structure sub-assembly must be robust enough to withstand the loading from the shafts due to normal (e.g. rotor unbalance) and abnormal (e.g. fan bade off) loading, it must also be aerodynamically efficient and very importantly, it must be light. This difficult balance results in one of the most complex designs in the engine.

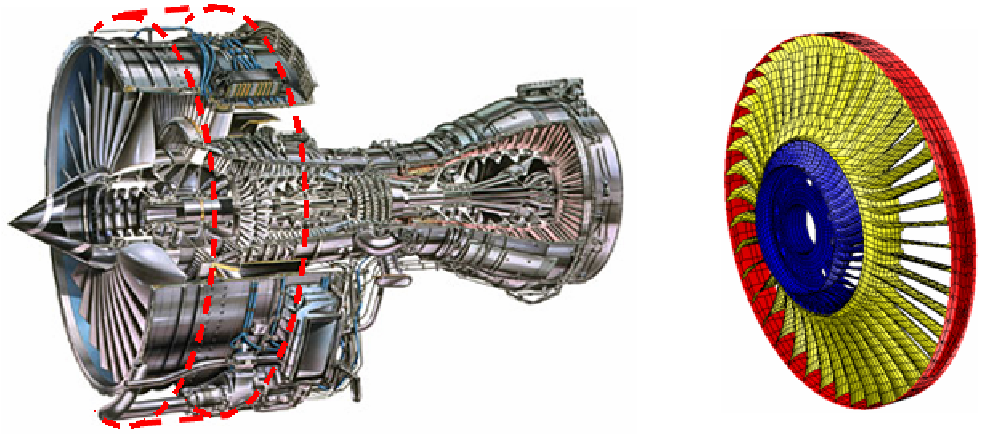

(a) (b)

Figure 4.1. Front Structure. (a) Location in the aeroengine and (b) design model.

The criticality of the Front Structure coupled with its complex design means that the corresponding structural design model must be validated as part of the engine certification programme. Figure 4.1 (b) shows the Front Structure design model that will be validated in this chapter. This model is constructed using shell and beam elements.

The Front Structure sub-assembly is made up of three components, the Mount Ring (MR), the Fan Outlet Guided Vanes (FOGV) and the Front Bearing Housing (FBH), see Figure 4.2. Table 4.1 illustrates some of the characteristics of the different models. All three components are connected together using bolted joints.

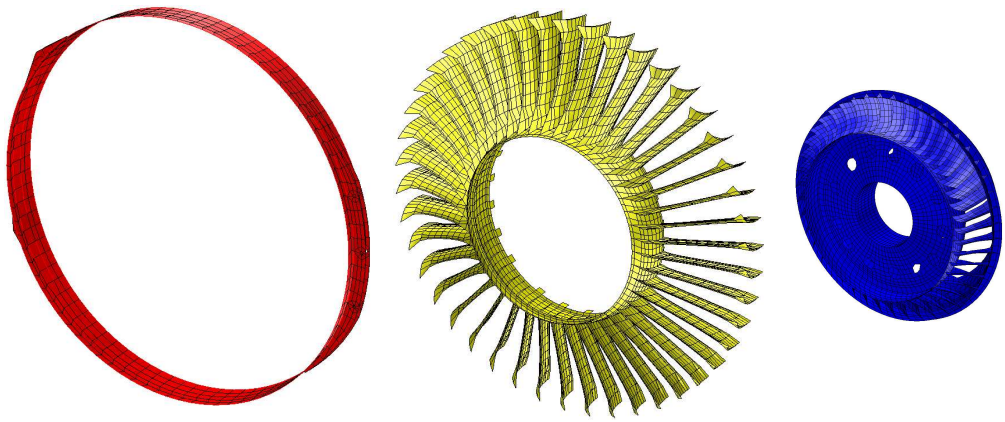

(a) (b) (c)

Figure 4.2. Front Structure component design models. (a) MR, (b) FOGV and (c) FBH.

	MR	FOGV	FBH	TOTAL
Total Number of DOFs	5,052	45,912	37,842	88,806
Total Number of Elements	916	9,456	8,220	18,592
Element Types	SHELL & BEAM	SHELL & BEAM	SHELL & BEAM	SHELL & BEAM

Table 4.1. Case Study assembly model.

In order to achieve certification, it must be demonstrated that the Front Structure model is capable of accurately predicting a clearly specified set of modes. Physical test data must be used as the final reference data for the assessment of the predictions.

The modes that must be accurately predicted by the sub-assembly model are (i) the torsion mode, (ii) the 2D axial mode and (iii) the 1D pitch mode when the structure is tested in a free-free configuration. The model of the sub-assembly is quasi axis-symmetric. That is why the two modeshapes with diametral nodal lines (i.e. 2D axial and 1D pitch) appear in orthogonal pairs. For simplicity, from now on only one of the axial modes and one of the pitch modes will be considered.

Figures 4.3 and 4.4 show the modeshapes and natural frequency distribution* of these modes as predicted by the original design model of the sub-assembly. These modes are the first 5 modes of the structure when tested in a free-free configuration.

The selection of these specific modes by the certification authorities is not random. When this sub-assembly is part of the whole engine the main dynamic loads applied to it are the axial loads from the shafts, the rotor out of balance forces and the axial load when the reverse thrust is engaged. The modeshapes targeted for validation closely resemble the deflections patterns of the sub-assembly when it is subject to those loads:

- the axial loading from the shafts is directly applied to the hub of the FBH through the bearings. Due to the stagger angle of the aerofoils this forces the whole structure to untwist. This deformed shape closely resembles the torsion mode;
- the rotor out of balance forces are always applied in the radial direction. This forces the Front Structure to tilt. This deformed shape closely resembles the 1D pitch mode. Finally;
- when the reverse thrust is engaged during the landing operations a significant axial load is applied to the rear flange of the MR. This axial loading is usually not uniform across the whole circumference, see Figure 4.5. The resultant deformed shape of the Front Structure under this load closely resembles the 2D axial modeshape.

* The actual natural frequencies cannot be shown for commercial reasons.

In order to consider the model valid all natural frequencies must be fall within a ±5% error band when compared against physical test data. The MAC correlation must be higher than 80%.

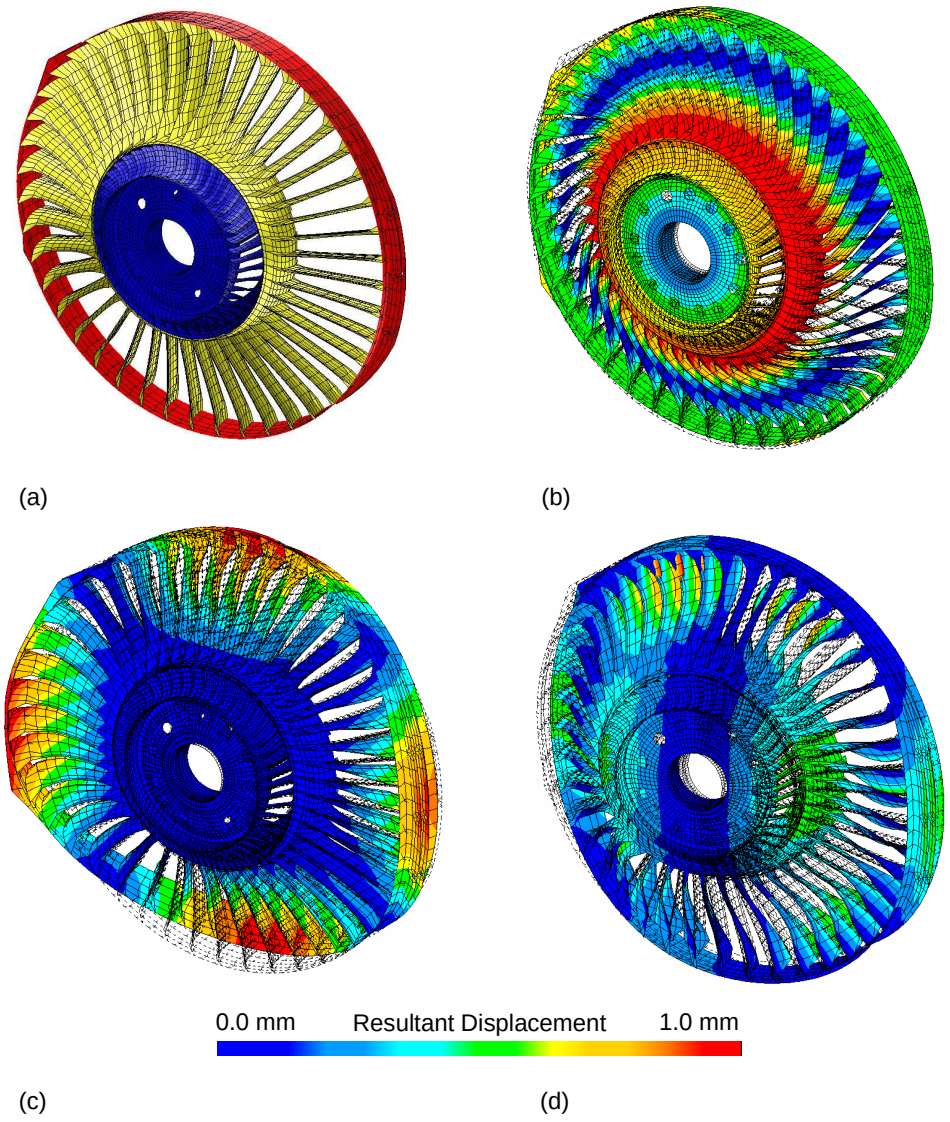

Figure 4.3. Predicted modeshapes. (a) Undeformed model, (b) torsion mode, (c) 2D axial mode and (d) 1D pitch mode.

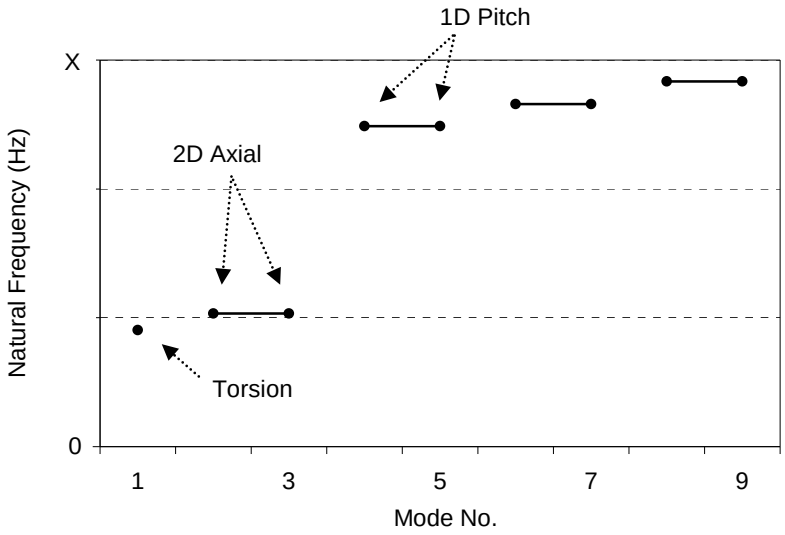

Figure 4.4. Predicted natural frequency distribution.

Figure 4.5. Reverse thrust engaged during a landing operation.

4.3 Validation Strategy

The validation strategy proposed in the previous chapters will be used here to validate the design model of the Front Structure sub-assembly. For clarity this process is illustrated again in Figure 4.6.

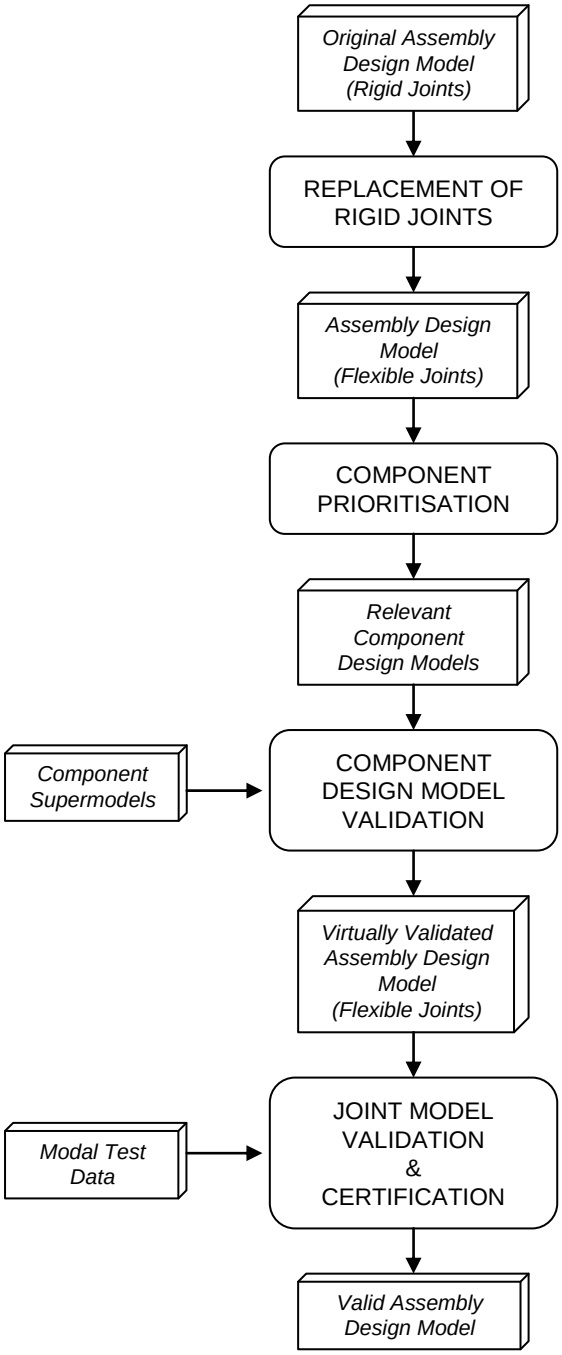

Figure 4.6. Validation Strategy.

The first step is to replace the rigid connections between components in the original assembly design model by flexible joints. The next step is to select the individual components in the assembly that require validation (i.e. component prioritisation). These components will be validated using their corresponding supermodels as the reference. Please remember that a supermodel must be embedded into the original assembly design model (hybrid assembly model) so that it can provide an accurate estimation of the component's behaviour when it is part of the assembly.

Once all the high-priority component models have been validated the next step is to validate the models of the joints. This validation still requires physical testing. This test data will also be used to ultimately certify that the model predictions fulfil the accuracy requirements.

Most of the model validation takes place in a virtual environment and can start well ahead of the test data being available. In fact the test data is simply used at the very late stages to validate the joint models and to certify that the final predictions meet the accuracy requirements. This is quite handy since there is usually only a few weeks margin between the test data being available and the deadline for the certification report.

4.4 Flexible Joints

Figure 4.7 highlights this step in the validation strategy.

The rigid connections between components in the original assembly model must be replaced by flexible joints to account for the actual flexibilities of the interfaces. There are two joints in the sub-assembly, that between the MR and the FOGV and that between the FOGV and the FBH.

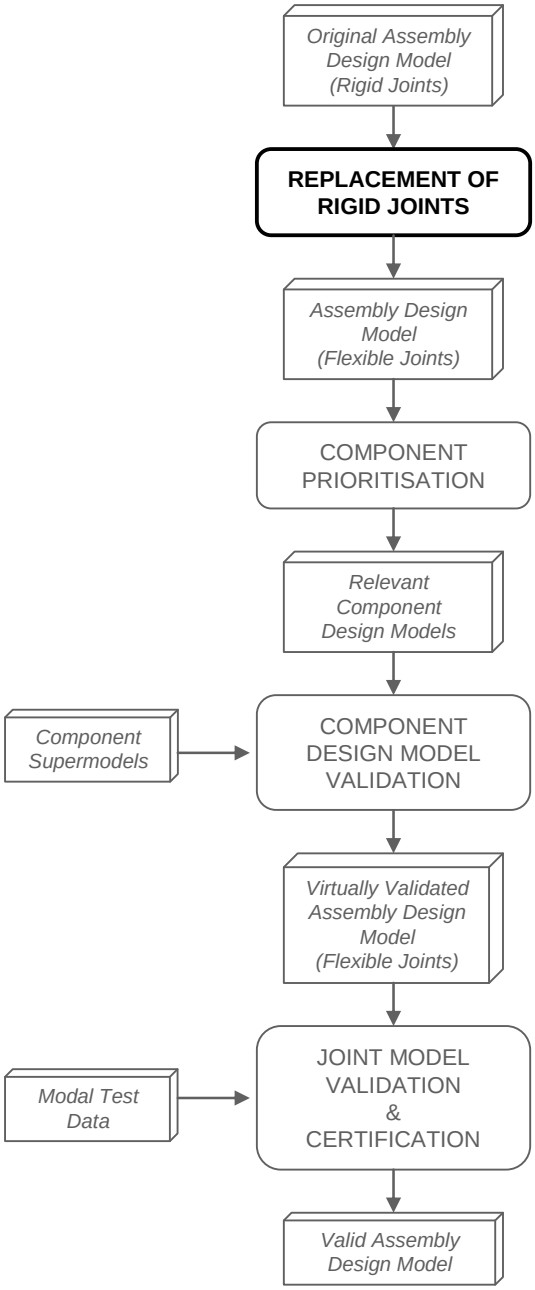

Figure 4.7. Validation Strategy. Flexible joints.

4.4.1 Mount Ring (MR) - Fan Outlet Guided Vanes (FOGV) Joint

Each of the vanes in the FOGV is connected to the MR using two bolts, one close to the leading edge tip and the other one close to the trailing edge tip. Figure 4.8 shows the manufacturing CAD drawings corresponding to this connection.

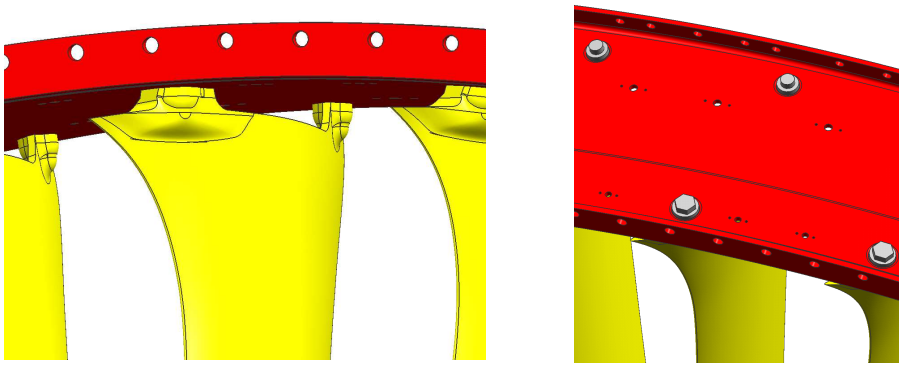

Figure 4.8. MR to FOGV joint details.

There are two nodes in each of the vanes of the FOGV model placed at the same position as the two connecting bolts, see Figure 4.9 (a). In the original assembly model these two nodes are rigidly connected to a matching pair of nodes placed on the MR model, see Figure 4.9 (b).

In order to represent the flexibility of the joint, the rigid links between the FOGV and MR nodes are replaced by springs in the 6 DOFs. It is best if the values associated with the stiffness of the sprigs are fairly representative. Nonetheless their accurate definition is not that important at this stage. They simply represent an initial estimation which will be updated as soon as the test data becomes available.

For each of the bolted connections, the value of the spring stiffness in the direction normal to the joint (radial direction) is assumed to be the same as the longitudinal stiffness of the connecting bolt according to equation (3.33). The stiffness in the two directions parallel to the contact surface is mainly driven by friction forces, hence the stiffness values in these two directions are assumed to be an order of magnitude lower than the normal stiffness according to equation (3.35). The values of the spring stiffness

associated with the rotational DOFs were selected based on engineering judgement. Table 4.2 shows the spring values initially associated with each of the leading and trailing edge bolted joints.

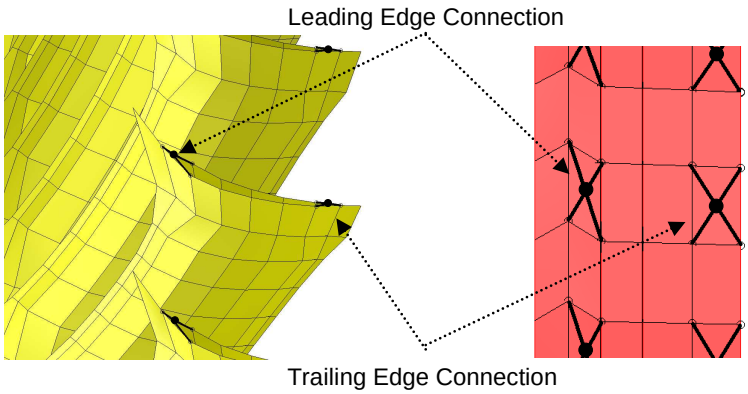

(a) (b)

Figure 4.9. MR – FOGV joint. (a) FOGV model detail and (b) MR model detail.

Joint	Parameter	Initial Estimate
1 (MR – FOGV Leading Edge)	$K_{r\,1}$	$K_{bolt\,1}$
	$K_{\theta\,1}$, $K_{z\,1}$	$\frac{K_{r\,1}}{10}$
	$R_{r\,1}$	1.0E+06 N mm/rad
	$R_{\theta\,1}$, $R_{z\,1}$	1.0E+07 N mm/rad
2 (MR – FOGV Trailing Edge)	$K_{r\,2}$	$K_{bolt\,2}$
	$K_{\theta\,2}$, $K_{z\,2}$	$\frac{K_{r\,2}}{10}$
	$R_{r\,2}$	1.0E+06 N mm/rad
	$R_{\theta\,2}$, $R_{z\,2}$	1.0E+07 N mm/rad

Table 4.2. MR – FOGV joint spring stiffness.

4.4.2 Front Bearing Housing (FBH) - Fan Outlet Guided Vanes (FOGV) Joint

The FOGV is bolted to the FBH across a more conventional flange, see Figure 4.10.

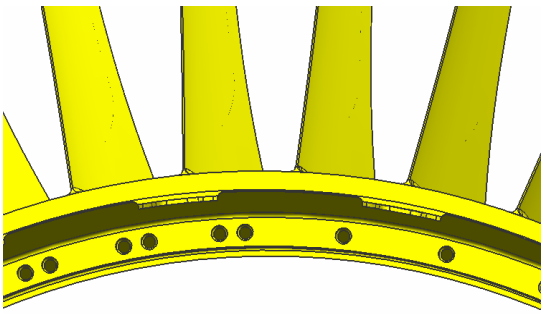

Figure 4.10. FOGV to FBH joint detail.

The design models corresponding to both components have a ring of nodes where the two components meet, see Figure 4.11. In the original assembly model the nodes on both sides of the joint are rigidly connected.

Again, the rigid links between each of the node pairs must be replaced by springs to simulate the flexibility of the joint. The values associated with the springs in each node pair are shown in Table 4.3. These values are an initial estimate which takes into account the stiffness of the connecting bolts according to equations (3.33), (3.34) and (3.35).

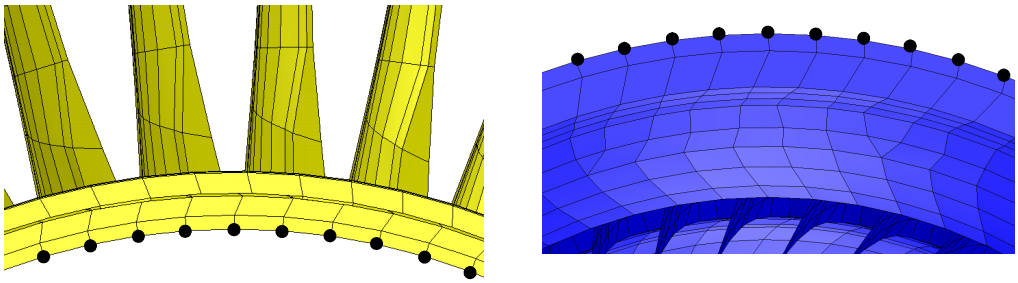

(a) (b)

Figure 4.11. FBH - FOGV joint. (a) FOGV model detail and (b) FBH model detail.

Joint	Parameter	Initial Estimate
3 (FBH – FOGV)	$K_{z\,3}$	$K_{bolt\,3}\frac{n_{bolts\,3}}{n_{nodes\,3}}$
	$K_{r\,3}$, $K_{\theta\,3}$	$\frac{K_{z\,3}}{10}$
	$R_{z\,3}$	1.0E+06 N mm/rad
	$R_{r\,3}$, $R_{\theta\,3}$	1.0E+07 N mm/rad

Table 4.3. FBH – FOGV joint spring stiffness.

4.5 Component Prioritisation

Figure 4.12 highlights this step in the validation strategy.

The sensitivity density contour plots in Figure 4.13 give an indication of the regions in the assembly model where an incorrect modelling will have a bigger effect in the predictions of the natural frequencies and modeshapes. A look at these plots indicates that the highly sensitive areas are all concentrated in the MR and the FOGV. It seems that the accurate definition of the FBH design model is not as important since changes to its stiffness have little effect on the assembly predictions.

Figure 4.14 show the quantitative assessment of the importance of each of the components to the accuracy of the assembly predictions according to equation (2.62). These values reinforce our initial estimation that the validation of the models corresponding to the MR and the FOGV should be given the highest priority. In fact the validation of the FBH design model can be spared altogether since its contribution is negligible for all the modes of interest.

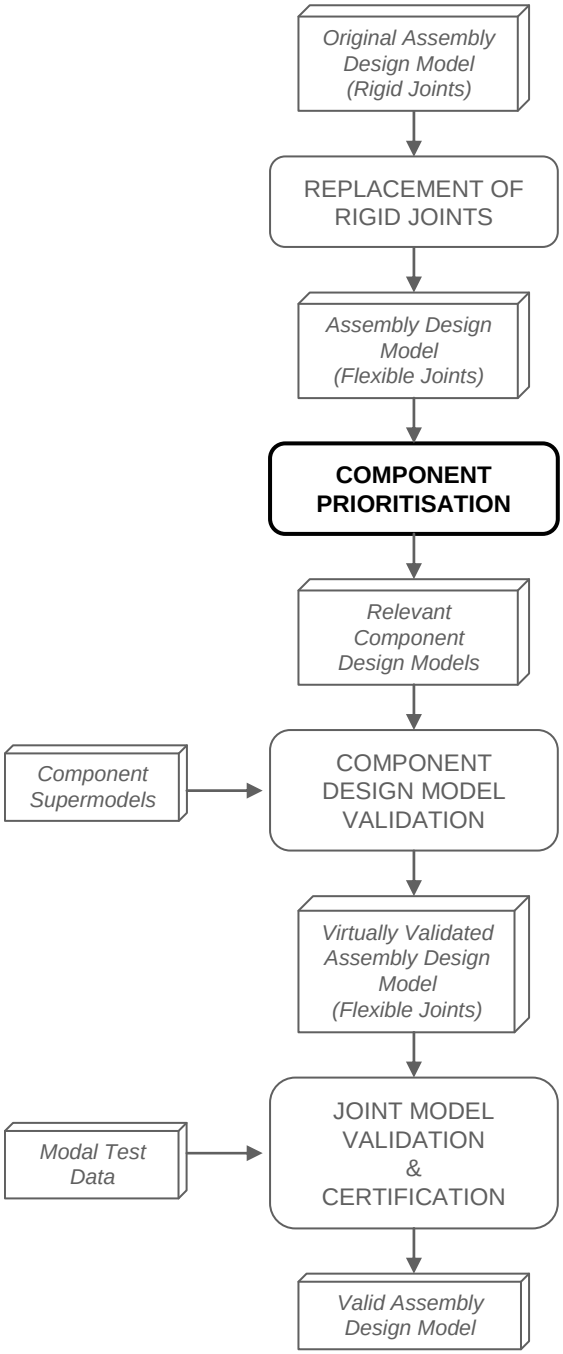

Figure 4.12. Validation Strategy. Component prioritisation.

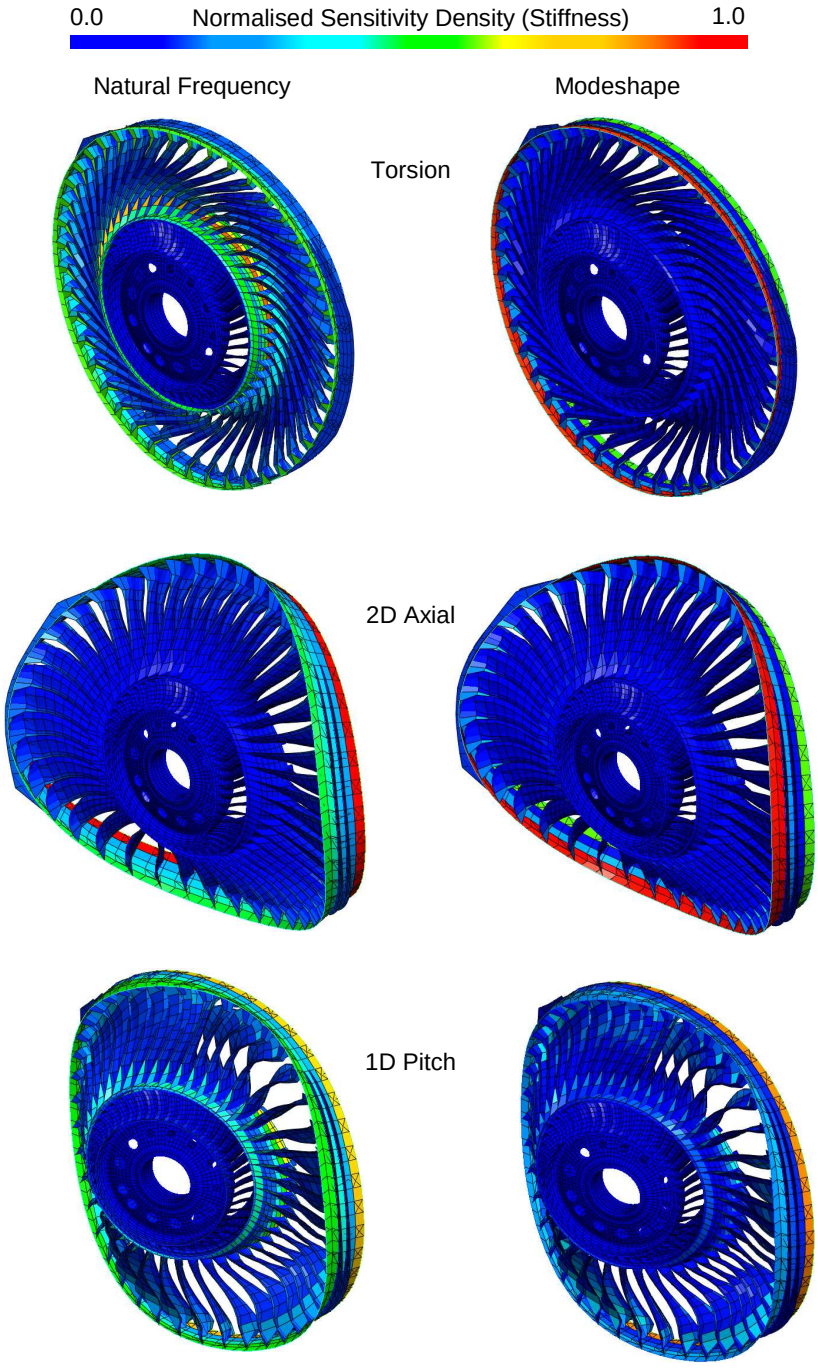

Figure 4.13. Sensitivity density to changes in stiffness.

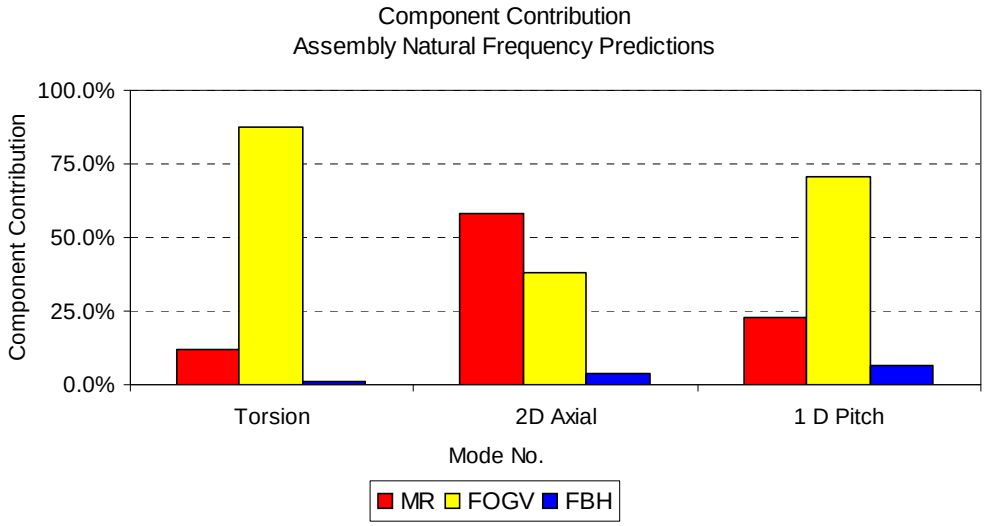

(a)

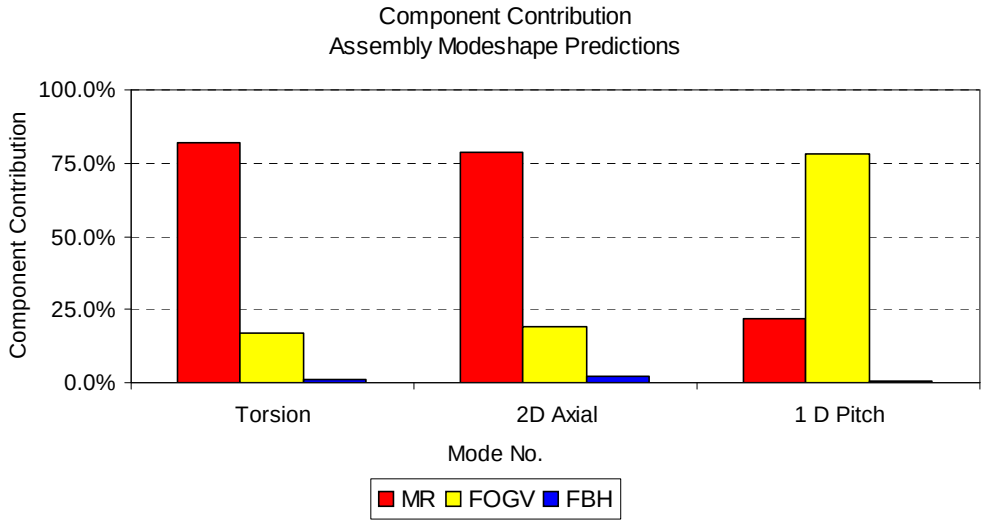

(b)

Figure 4.14. Component prioritisation. Individual contribution to (a) natural frequency and (b) modeshape.

4.6 Component Design Model Validation

Figure 4.15 highlights this step in the validation strategy.

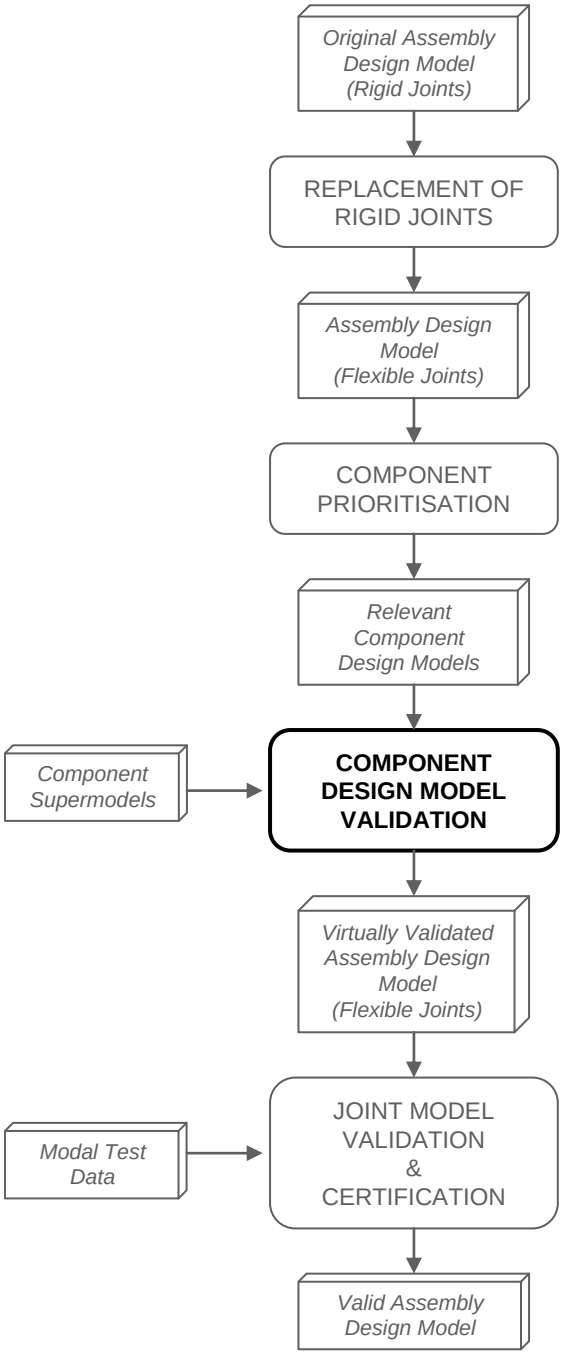

Figure 4.15. Validation Strategy. Component design model validation.

4.6.1 Component Supermodels

The creation of the supermodels made use of the supermodelling guidelines proposed by Baker [63] and Loyer [64]. The geometry CAD models used for the creation of the MR and FOGV supermodels did not contain any simplification and fully reflected the manufactured geometry of a nominal component. Figures 4.16 and 4.17 show some of the details of the MR and FOGV supermodels respectively. Table 4.4 gives an insight into their size.

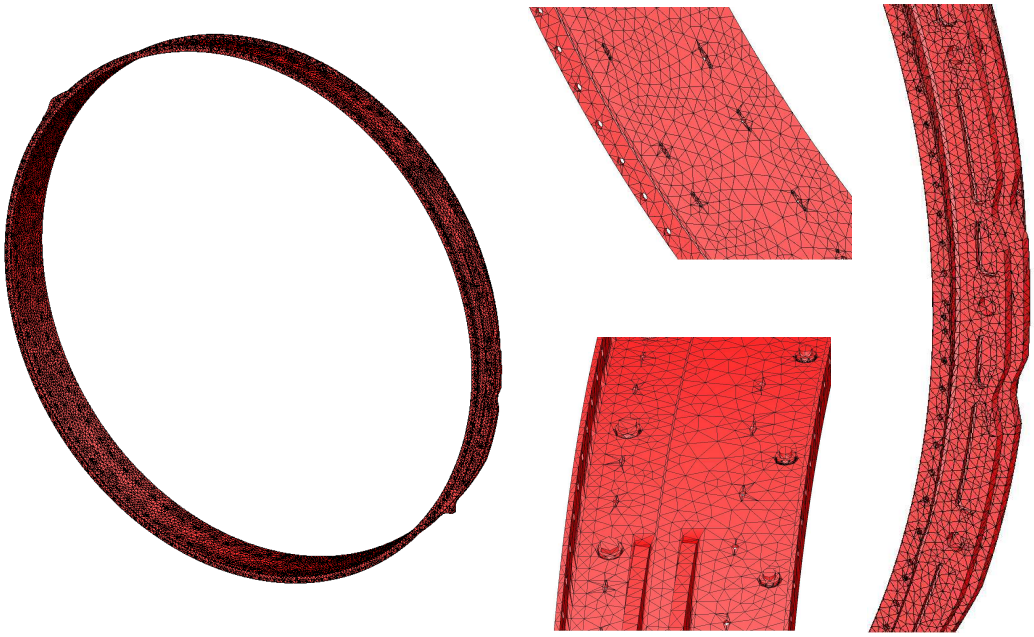

Figure 4.16. MR supermodel.

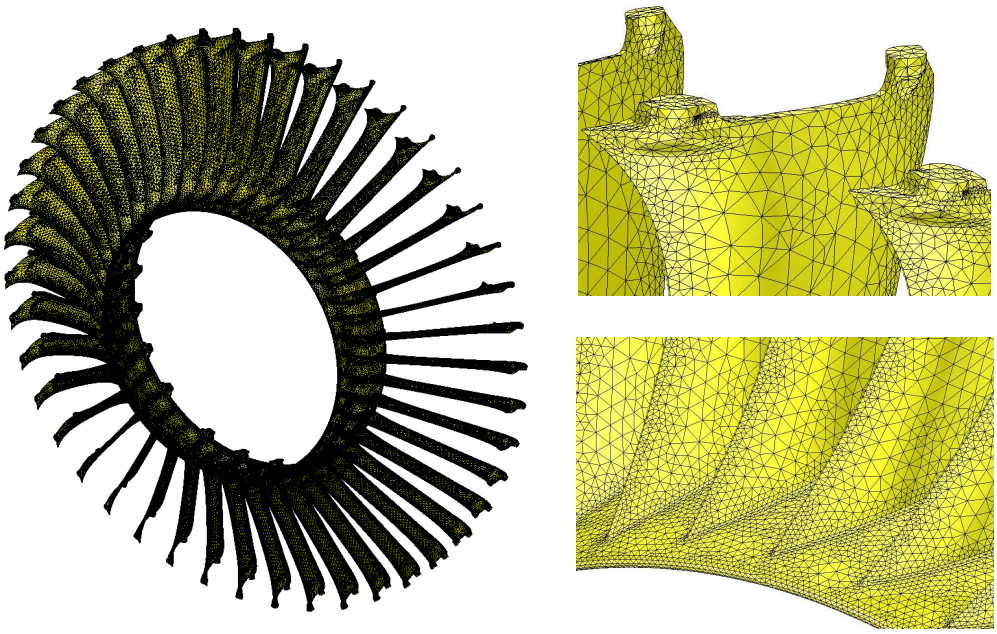

Figure 4.17. FOGV supermodel.

	MR	FOGV
Total Number of DOFs	1,166,934	6,619,596
Total Number of Elements	204,564	1,161,632
Element Types	TET 10	TET 10

Table 4.4. Component supermodels.

4.6.2 Validation of the Mount Ring (MR) Design Model

Figure 4.18 (a) shows the assembly design model containing the original component design models linked together using flexible joints. In Figure 4.18 (b) the design model of the MR has been substituted by the corresponding supermodel. The models corresponding to the rest of the components, including the joints, remain exactly the same. This means that any discrepancies between the predictions from both assembly

models can only be attributed to the differences between the MR design model and the corresponding supermodel.

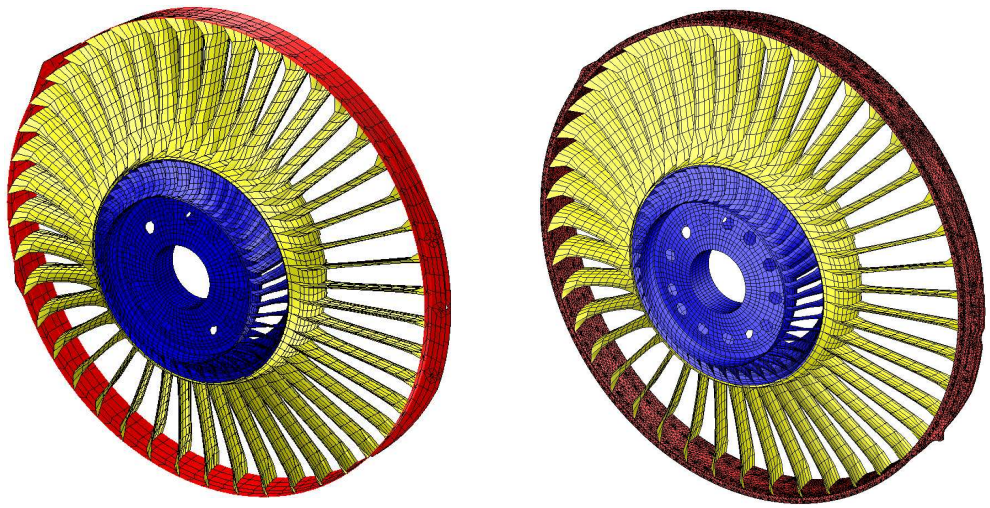

(a) (b)

Figure 4.18. (a) Assembly design model and (b) hybrid assembly model containing the MR supermodel.

Figure 4.19 shows the correlation between the assembly design model predictions and those from the hybrid assembly model. The discrepancies are significant, particularly the natural frequency error corresponding to the axial mode. These discrepancies must be reduced if we want to achieve the level of accuracy required for certification.

Parameter sensitivity based Model Updating was used to update the original MR design model to better match the predictions from the supermodel. The Young's modulus for each ring of elements in the MR design model was selected as a potential parameter for updating. The selection of the Young's modulus as the updating parameter is very convenient since it does not affect the carefully tuned mass distribution of the original component design model.

Both the natural frequencies and modeshapes were selected as target responses during the Model Updating. The weighted method according to equation (3.20) was selected for Model Updating. All parameters and responses were given the same weighting of 1.

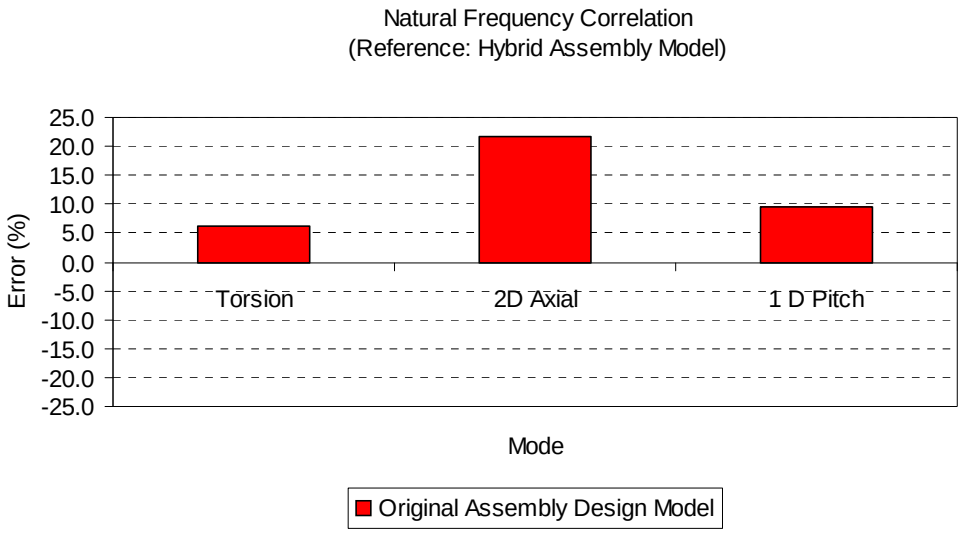

(a)

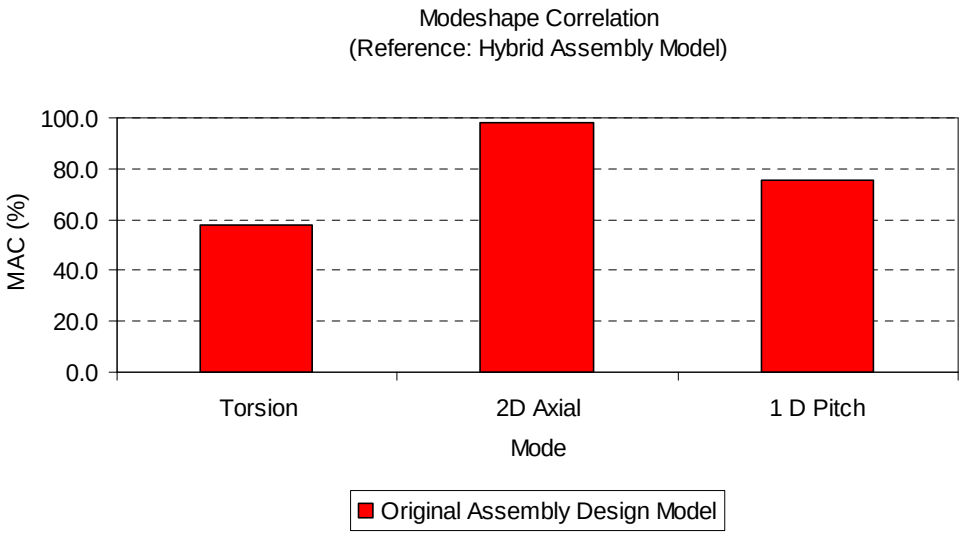

(b)

Figure 4.19. Correlation of assembly design model vs. hybrid assembly model with the MR supermodel. (a) Natural frequency and (b) modeshape.

Figure 4.20 shows the updating progress. The X-axis corresponds to the iteration number while the Y-axis represents the average natural frequency error of the updated

design model when compared to the reference from the supermodel. The iteration process was stopped when the improvement from two consecutive analyses was less than 0.001%. The convergence is smooth with a low error asymptote.

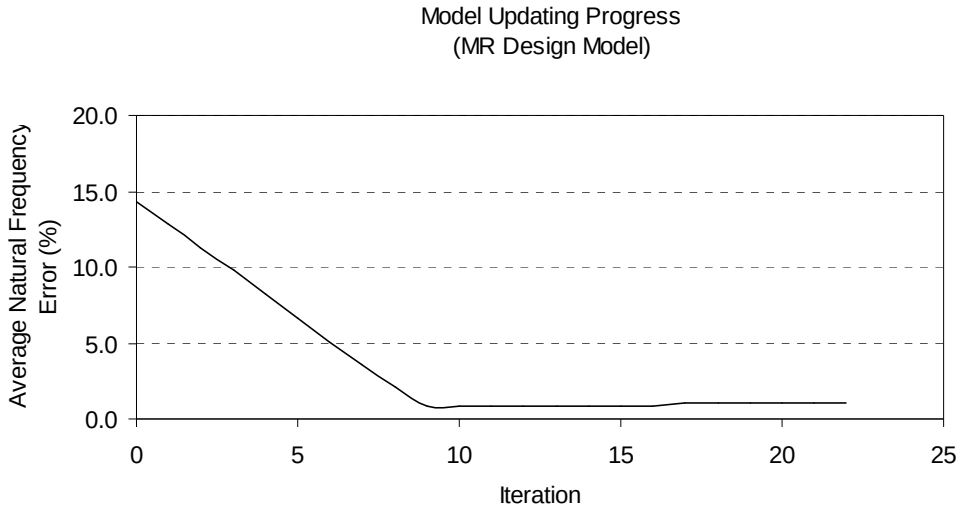

Figure 4.20. MR Model Updating progress.

Figure 4.21 shows the correlation after the Model Update. The levels of correlation are very satisfactory with all natural frequency errors close to 0% and all modeshape correlations close to 100%

As usual, it is important to make sure that the parameter changes obey to physical reasons. Figure 4.22 shows the parameter changes introduced as a result of the Model Update. The biggest changes are introduced in the two regions highlighted in Figure 4.23. These regions do not contain any particularly challenging feature to model. Nonetheless, the changes introduced to the original MR design model are surprisingly high (Young's modulus reduction of around 50%). This is usually an indication that there is something fundamentally wrong in the original model which has been mathematically compensated in the updated model. The use of mathematical models with little resemblance of the actual physics is dangerous and should be avoided wherever possible.

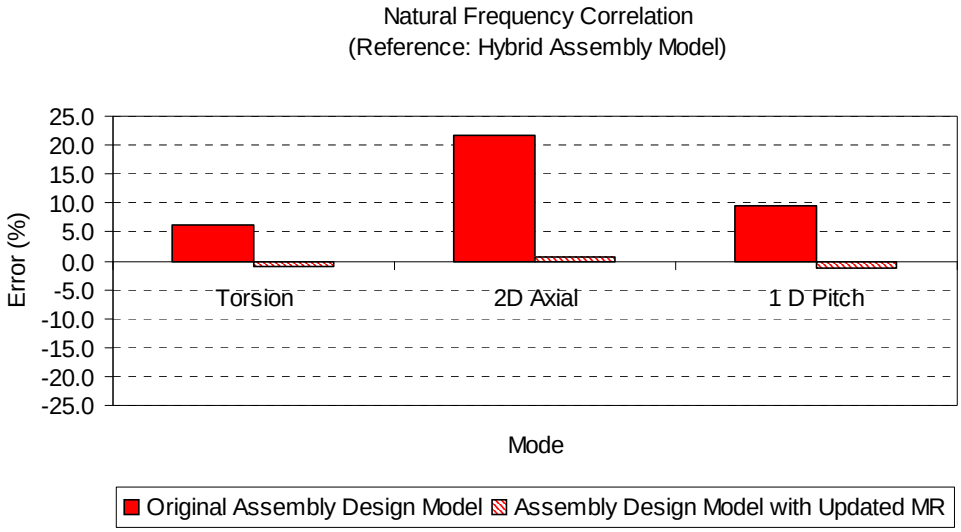

(a)

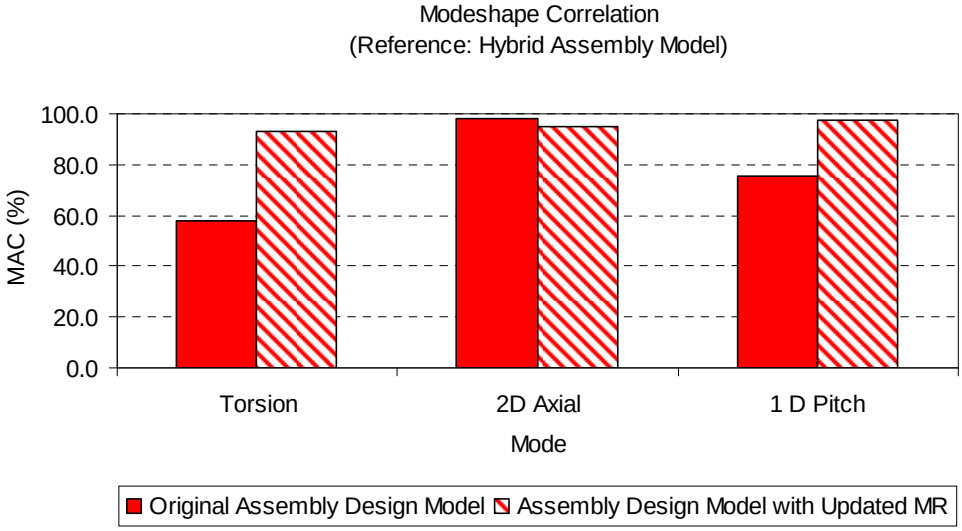

(b)

Figure 4.21. Correlation before and after the MR Model Update. (a) Natural frequency and (b) modeshape.

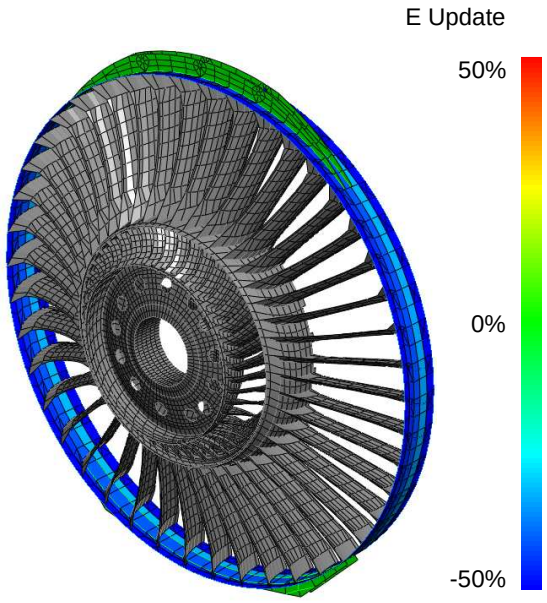

Figure 4.22. MR design model parameter updates.

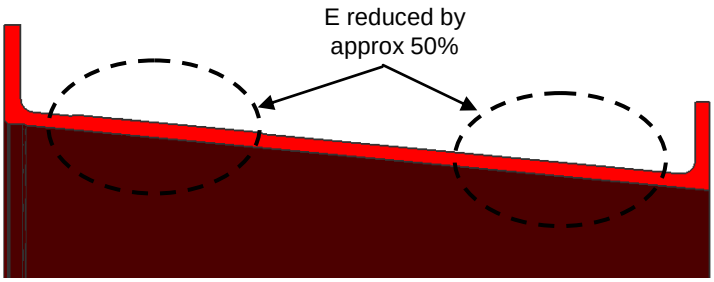

Figure 4.23. Regions of the MR where the biggest parameter changes were suggested.

The results from the Model Updating give us an indication of what is wrong with the original model. According to Figure 4.22 the biggest parameter changes take place in the regions where the MR is connected to the FOGV vanes. Figure 4.24 shows the modelling practice in these regions. For each of the FOGV vanes there are two nodes in the MR model, each of them located at the position where the vane is bolted to the MR. These are the nodes that are connected to the FOGV through flexible springs.

In the original MR model, each of the nodes placed at a bolt location is rigidly connected to the four nodes on the closest shell. This in turn makes some of the shells perfectly stiff. The Model Updating compensates for this over prediction of the stiffness by reducing the Young's modulus of the elements close to those regions.

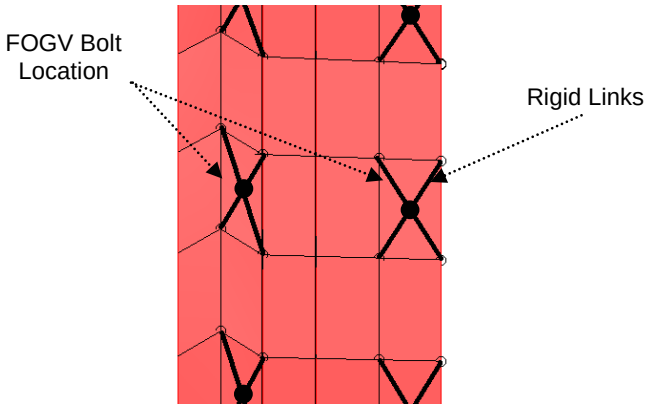

Figure 4.24. Modelling practice for the regions where the MR is connected to the FOGV vanes.

This modelling error can be easily removed by calculating the displacement of the nodes at the bolt locations as the average displacement of the four nodes in the closest shell. Model Updating could have never removed this modelling error simply because there was not any parameter to update in the original model which would have removed the presence of the rigid shells. This type of modelling error is usually referred to as configuration error [32].

It is very important that all configuration errors are removed from the original model before Model Updating is used. Otherwise it is most likely that the updated model will have very little physical sense. This phenomenon was recently studied in detail by Chen [32] who suggested that all models should be subject to a Verification process before they are updated.

Figure 4.25 shows the correlation achieved using an updated model of the MR where the configuration errors had been corrected before the start of the Model Updating process. The correlation of the updated model is remarkable with all natural frequency errors close to 0% and all MAC correlations close to 100%. Figure 4.26 shows the

parameter changes that resulted of the Model Updating. The changes are all quite small and can be easily explained from a physical point of view.

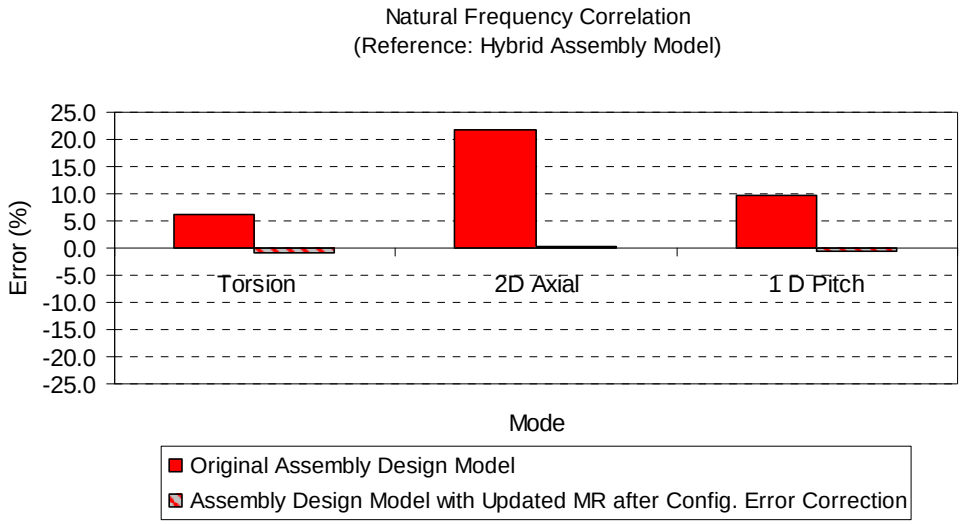

(a)

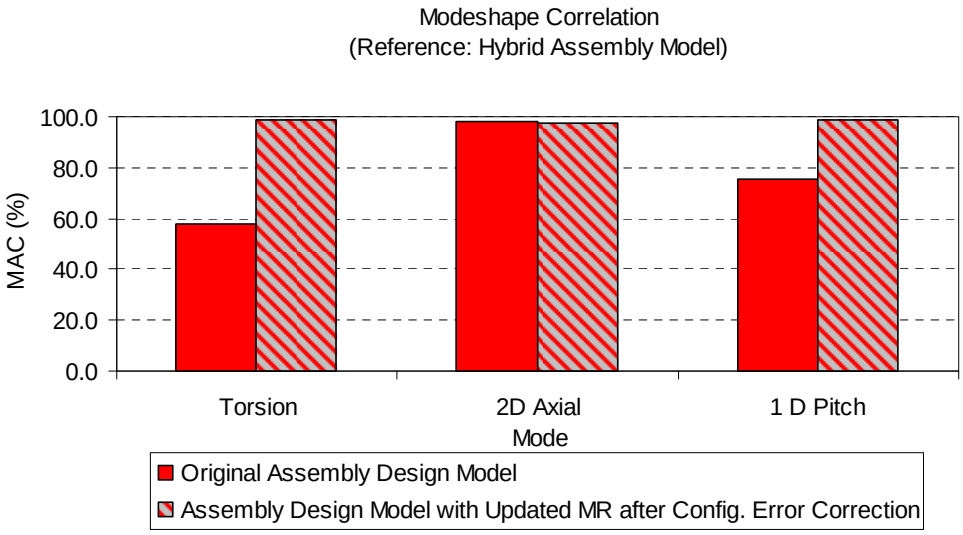

(b)

Figure 4.25. Correlation before and after MR configuration error correction and Model Update. (a) Natural frequency and (b) modeshape.

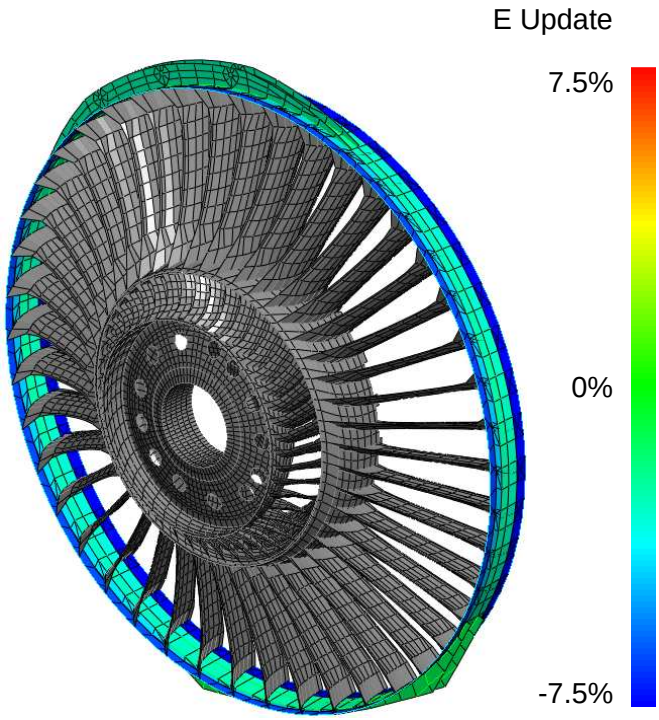

Figure 4.26. MR design model parameter updates where configuration errors were removed before Model Updating.

4.6.3 Validation of the Fan Outlet Guided Vanes (FOGV) Design Model

Figure 4.27 (a) shows the assembly design model containing the original component design models linked together using flexible joints. In Figure 4.27 (b) the design model of the FOGV has been substituted by the corresponding supermodel. The design models corresponding to the rest of the components, including the joints, remain exactly the same. This means that any discrepancies between the predictions from both assembly models can only be attributed to the differences between the FOGV design model and the corresponding supermodel.

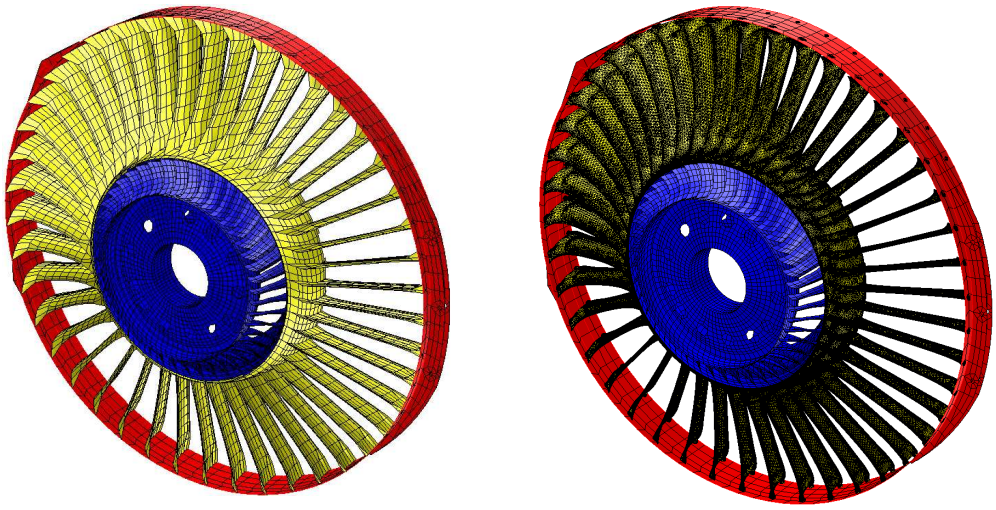

(a) (b)

Figure 4.27. (a) Assembly design model and (b) hybrid assembly model containing the FOGV supermodel.

Figure 4.28 shows the correlation between the assembly design model predictions and those from the hybrid assembly model. The discrepancies are not as big as in the case of the MR, nevertheless it is always worth reducing the differences to a minimum in order to increase our chances of meeting the certification requirements

Parameter sensitivity based Model Updating was used to update the original FOGV design model to better match the predictions from the supermodel. The Young's modulus for each ring of elements in the FOGV design model was selected as a potential parameter for updating. Both the natural frequencies and modeshapes were selected as target responses during the Model Updating. The weighted method according to equation (3.20) was selected for Model Updating. All parameters and responses were given the same weighting of 1. Figure 4.29 shows the updating progress. The iteration process was stopped when the improvement from two consecutive analyses was less than 0.001%. The convergence is smooth with a low error asymptote.

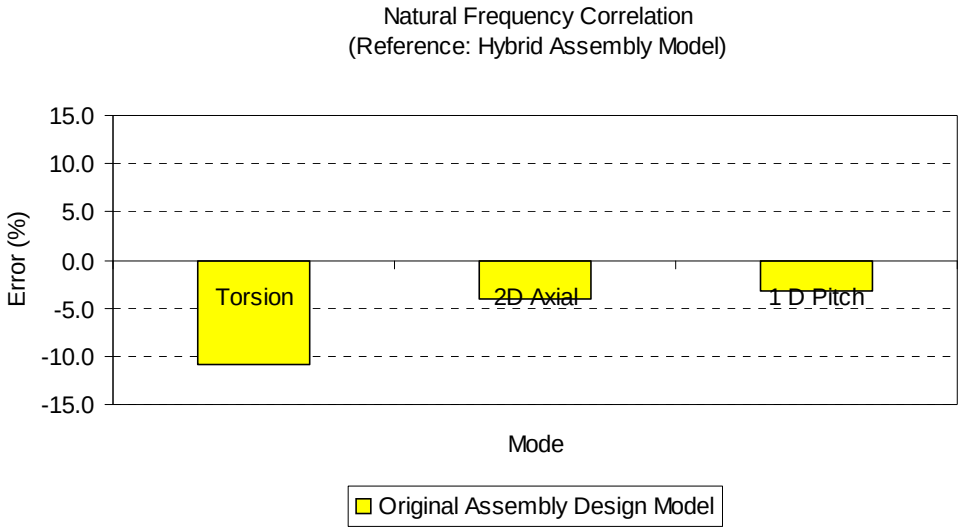

(a)

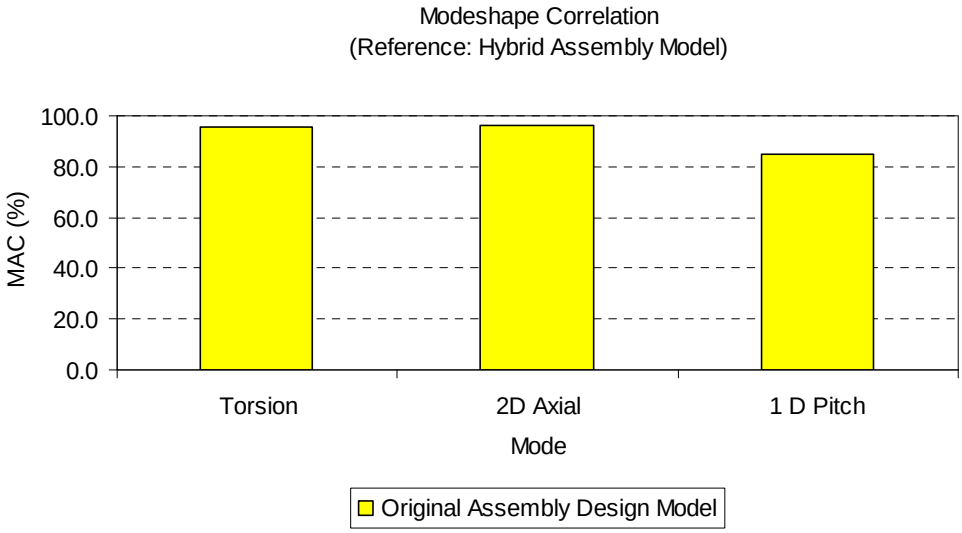

(b)

Figure 4.28. Correlation of assembly design model vs. hybrid assembly model with the FOGV supermodel. (a) Natural frequency and (b) modeshape.

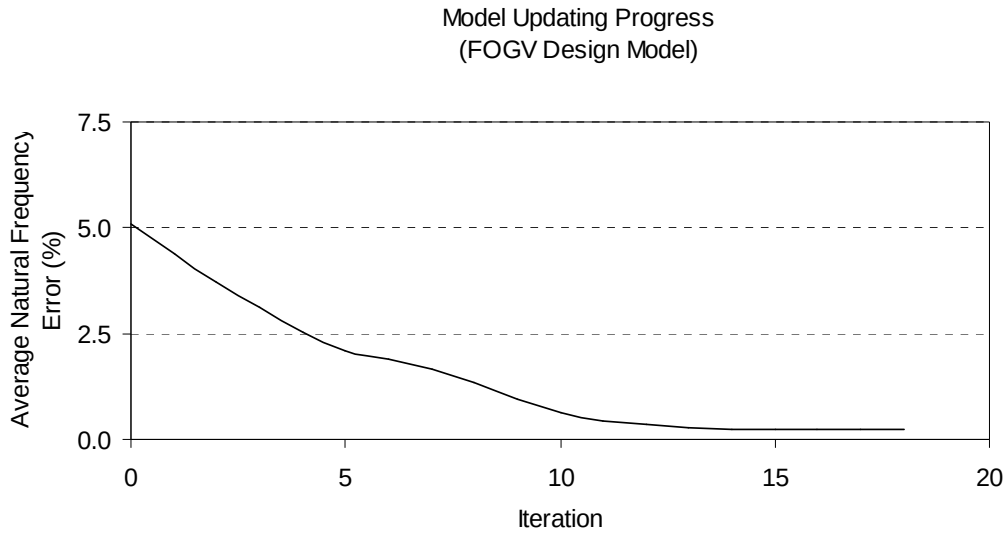

Figure 4.29. FOGV Model Updating progress.

Figure 4.30 shows the correlation after the Model Update. The levels of correlation are very satisfactory with all natural frequency errors close to 0% and all modeshape correlations close to 100%

As usual, it is important to make sure that the parameter changes that result from the Model Update have some physical meaning. Figure 4.31 shows the parameter changes introduced as a result of the Model Update. The biggest parameter changes take place in the inner rim with an increase in the Young's modulus of around 125%. Figure 4.32 shows the actual geometry of this region. The cross-section of this area is clearly thicker than the adjacent regions. Nevertheless, the original model did not capture this local increase of stiffness. As a result, it is perfectly justifiable to increase the value of the Young's modulus in this area.

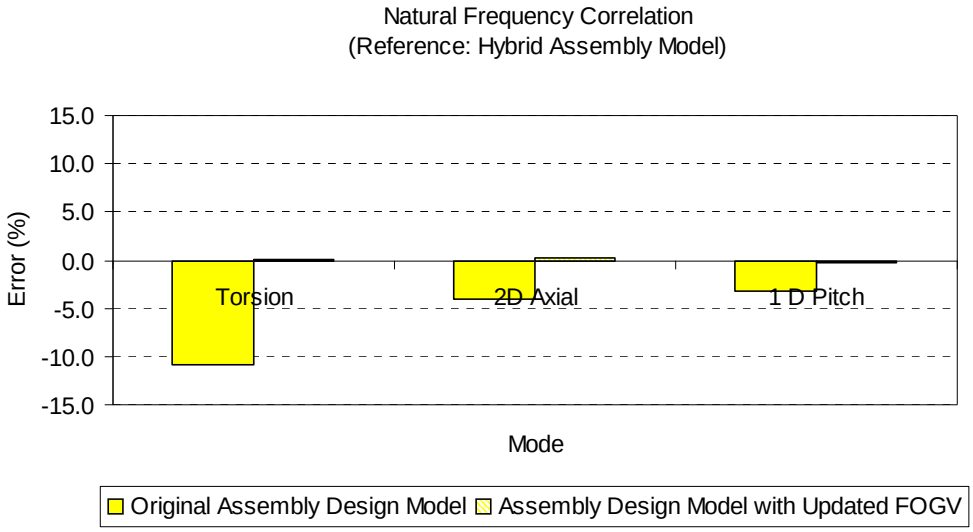

(a)

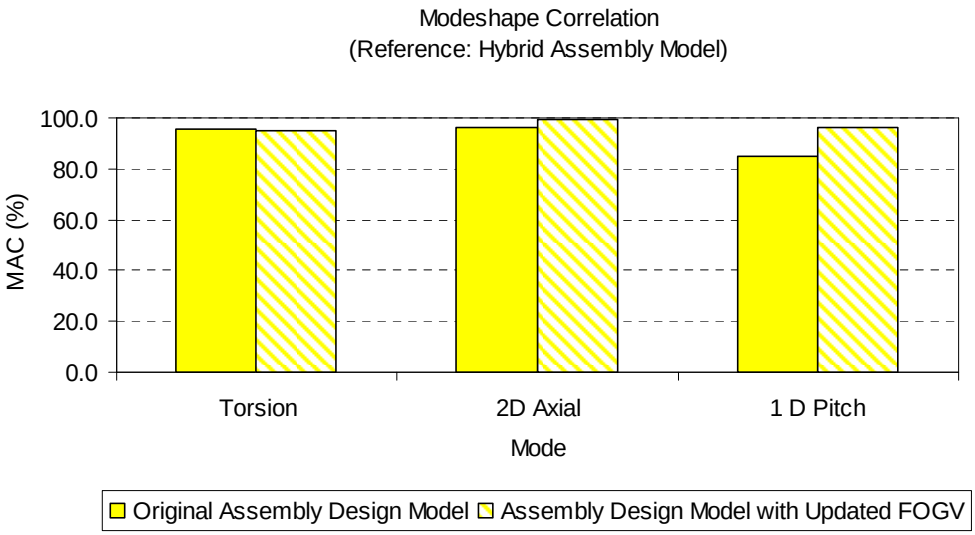

(b)

Figure 4.30. Correlation before and after the FOGV Model Update. (a) Natural frequency and (b) modeshape.

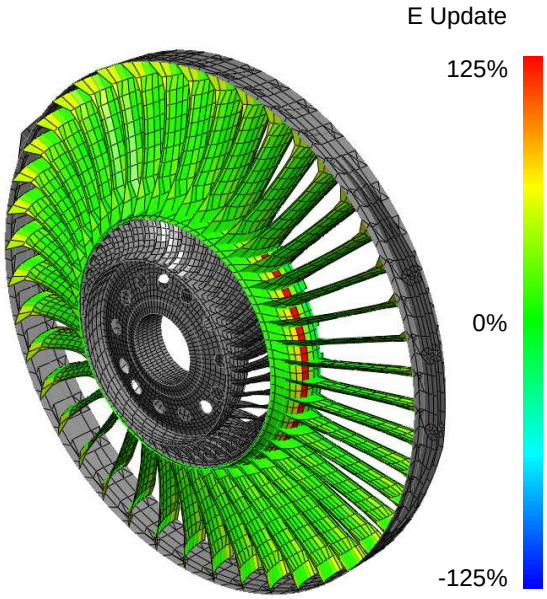

Figure 4.31. FOGV design model parameter updates.

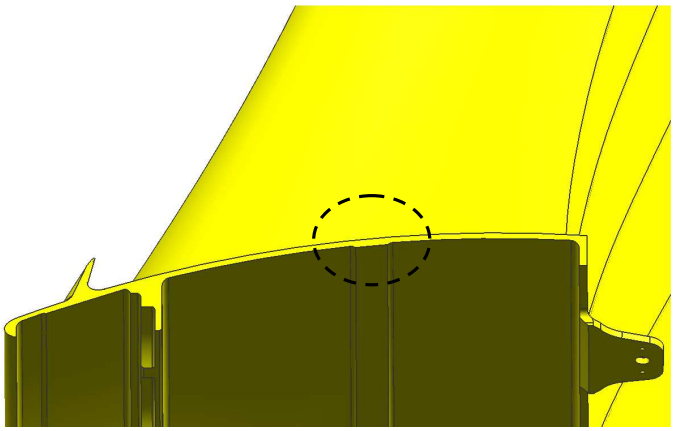

Figure 4.32. FOGV inner rim cross-section geometry.

4.7 Joints Model Validation and Final Certification

Figure 4.33 highlights these two steps in the validation strategy.

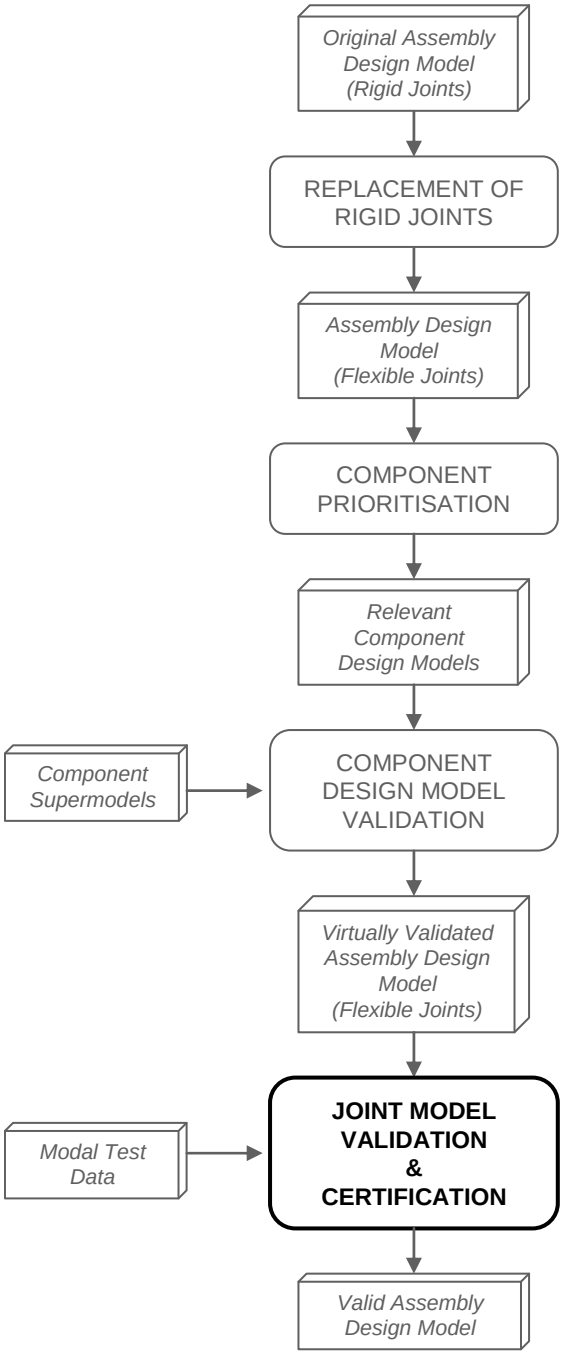

Figure 4.33. Validation Strategy. Joints validation and certification.

The picture in Figure 4.34 illustrates the test configuration used during the Modal Testing of the Front Structure sub-assembly. In order to simulate the free-free conditions the structure was lifted off a trolley using elastic ropes connected to three cranes.

Figure 4.34. Modal Test.

Some of the modes of interest were predicted to appear at very close frequencies. A traditional SISO (Single Input Single Output) Modal Test is not well suited to differentiate closely coupled modes. A multi-reference SIMO (Single Input Multiple Output) Modal Test was selected as the most appropriate technique in this case. The test made use of a calibrated hammer to excite the structure and a set of accelerometers to measure the response. The accelerometers remained at the same place throughout the whole test while the hammer moved around the structure.

The number of impact locations (386 in total) and responses (12 in total) as well as their positions were optimised using the predictions from the “virtually” validated assembly

model. This process is commonly referred to as Test Planning [31]. Figure 4.35 shows the Measurement wireframe.

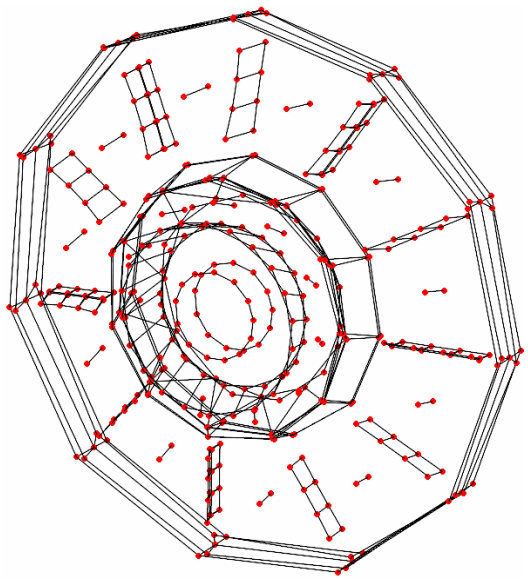

Figure 4.35. Measurement wireframe.

The availability of test data means that we can now validate the models of the joints. Please remember that the “virtually validated” assembly contains valid models for the components but rough estimates of the flexibilities of the joints.

Figure 4.36 shows the correlation between the “virtually validated” assembly model and the test results. The correlation corresponding to the original assembly model with non-validated component models and rigid joints is also included for comparison purposes.

The “virtually validated” assembly model represents a remarkable improvement with respect to the original model. In fact, the predictions from the “virtually validated” model, which contains a coarse model of the joints, are already well within the certification requirements. This reinforces the claim that the bulk of the validation can take place in a virtual environment well ahead of any test data being available.

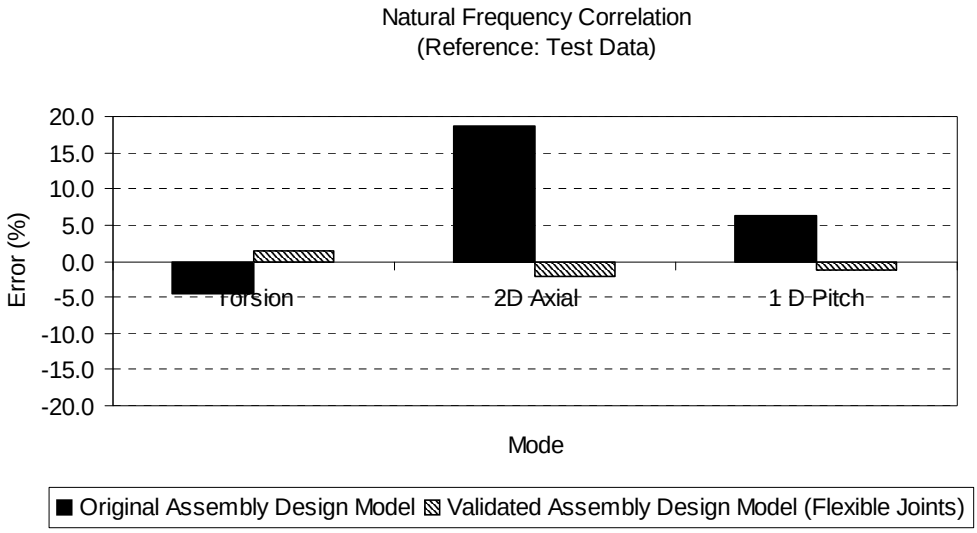

(a)

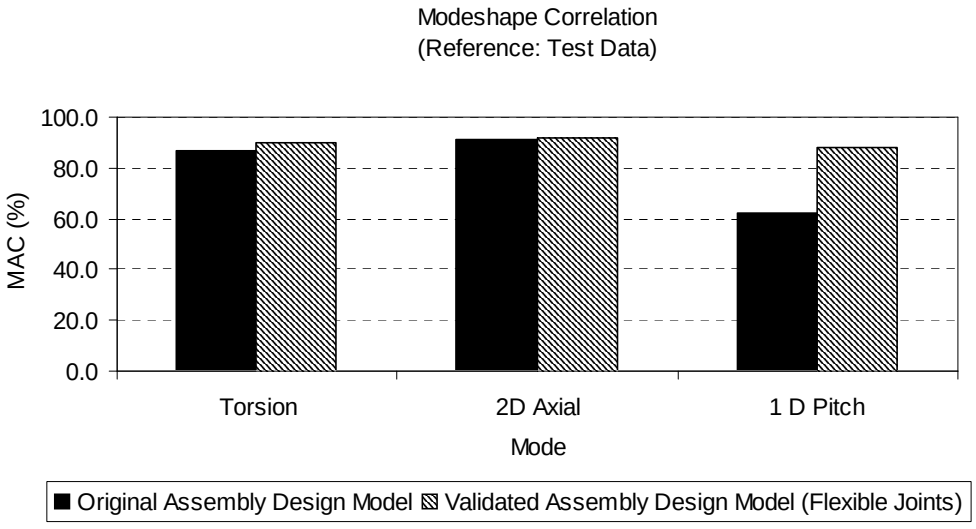

(b)

Figure 4.36. Correlation between “virtually validated” assembly model and the test data. (a) Natural frequency and (b) modeshape.

As the certification requirements are already met we could stop the validation process at this stage and leave the models of the joints as they are. Nevertheless, it is good practice to carry out an update of these models to get a better understanding of the actual flexibility of the joints. This is important to support the development of better modelling techniques. The same automated Model Updating procedure used during the validation of component models was used here to refine the parameter values of the joints. Figure 4.37 shows the updating progress.

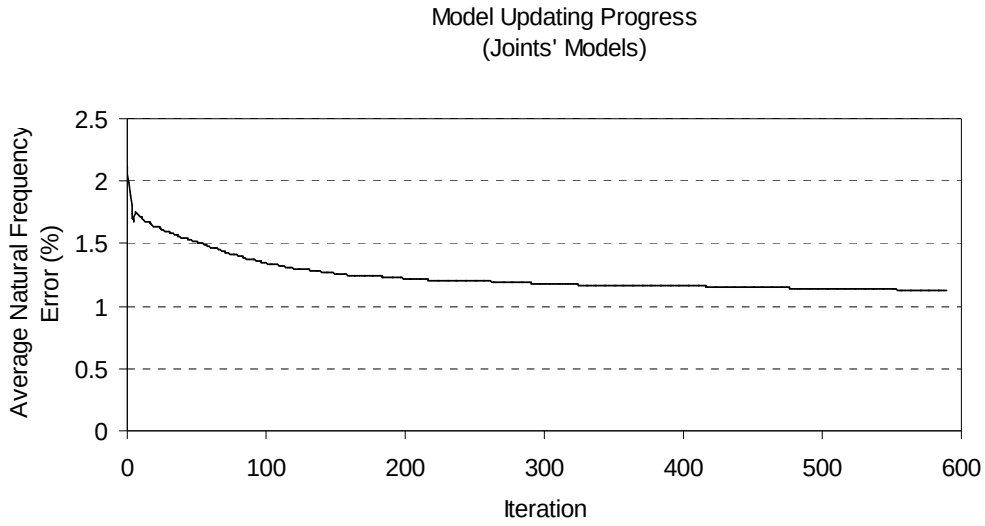

Figure 4.37. Joints Model Updating progress.

Figure 4.38 shows the correlation before and after a sensitivity-based updating of the joint models. Even though the correlation is slightly better, the remarkable correlation already achieved before the updating means that there was not much room for improvement. Nonetheless the main purpose of this exercise is to get a better understanding of the actual stiffness of the joints, which is shown in Table 4.5. Again, the updated values are significantly different from the original estimates.

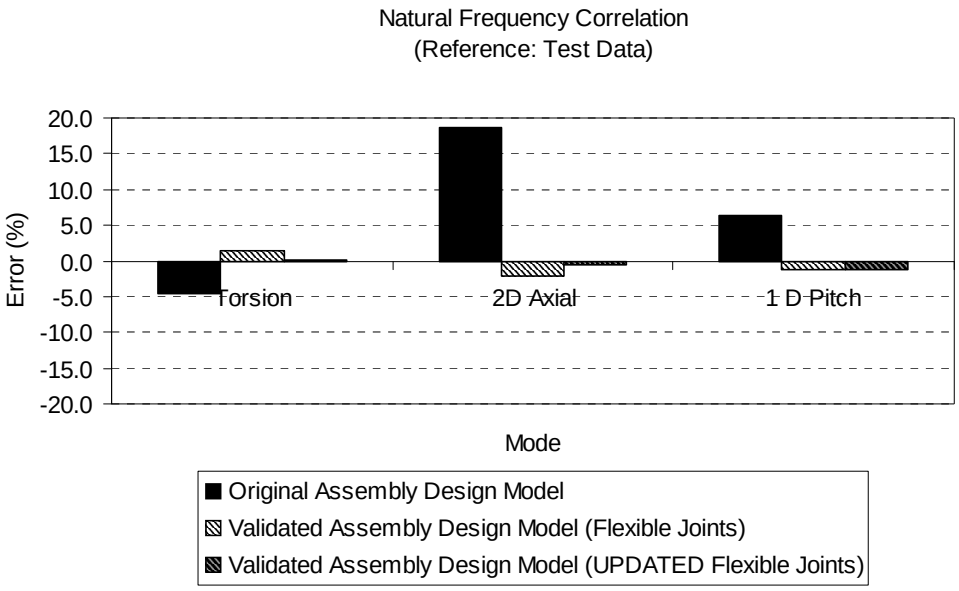

(a)

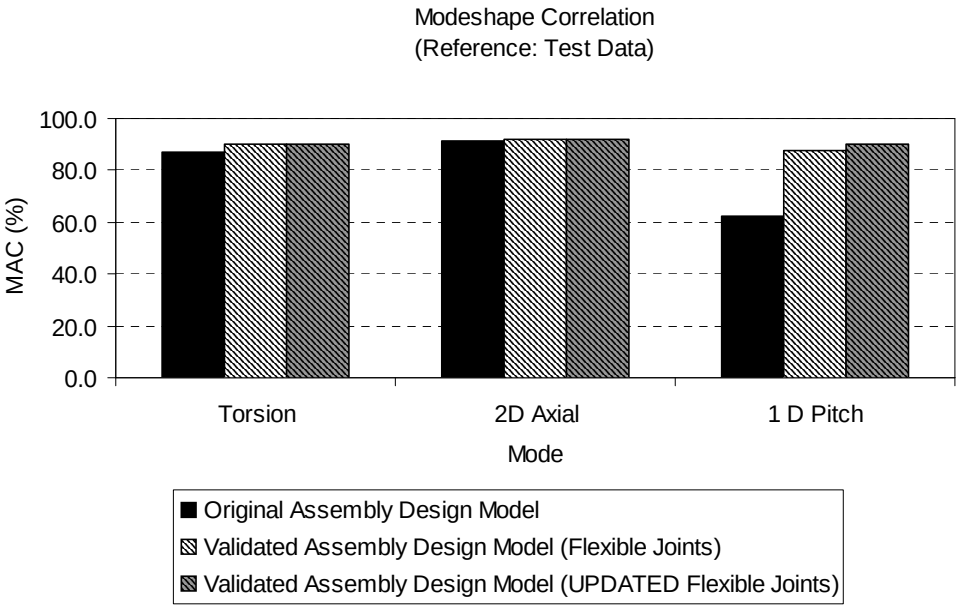

(b)

Figure 4.38. Joints Model Updating. (a) Natural frequency and (b) modeshape.

Joint	Direction	$\frac{\text{Updated Value}}{\text{Initial Value}}$
1 (MR – FOGV Leading Edge)	$K_{r\,1}$	8.0
	$K_{\theta\,1}$, $K_{z\,1}$	0.9
	$R_{r\,1}$	6.9
	$R_{\theta\,1}$, $R_{z\,1}$	0.2
2 (MR – FOGV Trailing Edge)	$K_{r\,2}$	23.0
	$K_{\theta\,2}$, $K_{z\,2}$	14.5
	$R_{r\,2}$	1.6
	$R_{\theta\,2}$, $R_{z\,2}$	3.3
3 (FBH – FOGV)	$K_{z\,3}$	1.6
	$K_{r\,3}$, $K_{\theta\,3}$	11.5
	$R_{z\,3}$	1.0
	$R_{r\,3}$, $R_{\theta\,3}$	1.2

Table 4.5. Joints Model Updating. Parameter changes.

4.8 Conclusions

The proposed strategy for the validation of assembly models has been used in this chapter to validate the model of a complex aeroengine sub-assembly. The most relevant component design models in the assembly were first identified using the sensitivity methods proposed in Chapter 2 and then validated using highly refined supermodels as the reference following the methodology outlined in Chapter 3. All this work took place in a virtual environment well ahead of the test data being available. However, as supermodels of joints remain unreliable, the design models corresponding to the

component interfaces (i.e. joints) could only be validated once the Modal Test data became available.

The final validated assembly model resulted in a remarkable worst natural frequency correlation of less than 2% when compared against the results from the Modal Test. This level of correlation falls within what would be expected due to the manufacturing variability and the inevitable uncertainties associated with testing. Moreover, the validated assembly model represents a significant improvement with respect to the original model whose worst natural frequency error would have been around 20%, had it not gone through the validation process.

During the course of this validation exercise it was necessary to correct some of the component design models to better match the reference data provided by the supermodels. This highlighted the importance of correcting the configuration errors in any model before attempting Model Updating. When this is ignored, the changes introduced to the parameters in the model can be unrealistic, resulting in a mathematical model having little or no physical meaning. The use of such “mathematical models” is not advisable as the actual cause of the original discrepancies will remain hidden and could surface again when the conditions under which the model operates are changed.

The example presented in this chapter was part of a real engine certification programme. A model validation exercise where the bulk of the work can take place in a virtual environment well ahead of manufacture is particularly advantageous for this kind of programme where there is usually very little time between the test data being available and the certification deadline. Also, this is a particularly demanding industrial scenario in which to demonstrate any new technology. The successful outcome achieved reinforces the confidence in the maturity of the proposed validation strategy for its staged release into industry.

Chapter 5 - Validation of Supermodels

5.1 Introduction

The use of supermodels is central to the validation strategy proposed in this work. Predictions from supermodels are used to validate the less refined component design models during the early stages of the product development cycle, even before manufacture. This “virtual” validation strategy can potentially reduce the need for physical testing by an order of magnitude when compared with more traditional validation approaches. Nevertheless, the successful outcome of this approach relies on the capability of supermodels to predict accurately the dynamic properties of the components that they represent.

The concept of a supermodel was introduced in the first years of this century by Fotsch [1]. Even though there has been significant progress in the development of supermodelling techniques [63] [64], there is still further work required before reliable supermodels can be generated for all cases.

The development of valid supermodelling techniques invariably requires some physical testing but it is important to highlight here the difference in the role of physical testing when compared to a more traditional validation exercise. Traditionally, physical testing is used to validate a specific model so that it accurately predicts the dynamic properties of a given structure. Here, physical testing will be used to validate the supermodelling technique and not the models themselves. The supermodels selected for validation must contain features that current supermodelling techniques find challenging to model properly. The validation of such supermodels will, in turn, serve to validate the techniques employed during their creation. Importantly, this validation can take place off the critical path of the design.

The whole idea of using a supermodel to validate its less refined design model counterpart revolves around the concept that the supermodel predictions are highly

accurate in much the same way that experimental data from a physical test are considered to be the “true” values. Subsequently, a supermodel can only be considered valid if its predictions can be shown to closely resemble test measurement. But, how close do they need to be?

It is important to consider that during a validation exercise, the model usually represents the nominal geometry and material properties. The actual dimensions and material properties of the manufactured component(s) are usually uncertain and are only known to be within manufacturing tolerances of the nominal design values. Moreover, in a laboratory environment measurements will invariably be affected by noise and other uncertainties such as those arising from transducer calibration. As a result, even perfectly valid supermodels will never match the test measurements with a 0% error.

Traditionally, model validation exercises have taken a deterministic approach to deal with uncertainty. A model (e.g. supermodel) is considered to be valid if the distance between the predictions and the measurements is within a specified threshold. This threshold is typically selected based on “what looks reasonable” taking account of the manufacturing tolerances of the test specimens, the estimated measurement errors and, most importantly, the modelling error allowance. This validation approach is well suited for validating coarse models where the modelling error allowance is typically much higher than the potential effects of the manufacturing variability or the measurement errors. However, supermodels are expected to provide predictions so accurate that they rival the accuracy of physical testing.

The accuracy expected from supermodels calls for a more robust validation criterion where the differences between the predictions and the measurements are judged in relation to the uncertainties present during the validation process. Those uncertainties are usually defined using probabilistic terms. This means that the model validation strategy must shift its focus from a deterministic to a stochastic approach.

This chapter will present efficient ways of quantifying the uncertainties associated with the predictions from a supermodel (e.g. due to manufacturing variability) and those associated with the test. The characterisation of the uncertainty associated with the supermodel predictions can become computationally prohibitive at times, that is why reduced models of the supermodel (i.e. metamodels) may be used instead for such purpose. This chapter will review some of the most common types of metamodels (e.g.

sensitivity-based, “neural nets”, etc.) highlighting their benefits and shortfalls. An efficient method will also be presented to quantitatively establish the maximum difference allowed between the predictions and the measurements when considering whether a supermodel is valid. The application of these methods will be illustrated by using the validation of the COC supermodel used in Chapters 2 and 3 as a Case Study.

5.2 Different Approaches to Probabilistic Model Validation

The traditional approach to probabilistic model validation is to compare the predictions from a nominal model against the results from a number of tests. These tests must be representative of the different uncertainties present during the model validation process. For instance, a number of manufactured components must be tested to account for the expected manufacturing variability, different transducers should also be used to account for potential measurement error, different practitioners should also be employed to account for human errors, and so on.

If the number of tests is sufficiently high, the measured responses can be characterised in probabilistic terms. Different metrics have been proposed over the years to estimate the validity of a model based on the correlation between the nominal predictions and the probabilistic characteristics of test results.

One of the most basic validation metrics, which is still very common, is the distance between the nominal predictions and the mean of the responses. The principle behind this metric is simple. If none of the uncertain factors in the validation process is biased (high and low values are equally possible) and the nominal model is valid, one should expect a close match between the predictions and the mean values of the test results.

Brownlee [68] in the 1960s and Miller and Freund [69] in the 1980s proposed to use the median of the test results instead of the mean to calculate the distance between the predictions and the measurements. Other authors such as Beck and Arnold [70] in the late 1970s or Reckhow *et al* [71] in the early 1990s went further and considered a model valid if the predictions fell within the limits specified by a percentage (e.g. 95%) of the test results.

All these techniques rely on the availability of extensive test data to characterise the uncertainties associated with the model validation process. However, the use of extensive test programmes for the validation of models is simply not realistic in a modern industrial environment. Time and cost are certainly some of the main reasons but there are others. For instance, during the development phase of a modern aeroengine there will be typically less than a dozen engine prototypes ever built. This means that, at best, a much reduced number of manufactured components will be available for testing. This number will usually not be enough to fully explore, for instance, the effect of manufacturing variability.

A realistic model validation approach must take into account the fact that very limited test data might be available. In fact, it is not unusual for only a single test to be ever performed. In the absence of comprehensive test data, there is no other option but to characterise the uncertainty in the validation process analytically. The model will be considered to be valid if the differences between the predictions and the measurements are consistent with the anticipated uncertainty. An important benefit of this approach is the fact that it compels the test engineers to fully understand the mechanisms that drive the uncertainty in the validation process so that they can improve the design of the tests.

The two main sources of uncertainty present in the validation process have their origins in the model and the measurements, respectively. The following sections describe how to characterise analytically the uncertainty associated with both the model predictions and the test measurements.

5.3 Model Uncertainty

In the context of this work, a supermodel is a comprehensive mathematical representation of the physics that fully govern the dynamic behaviour of a component. The predictions from a supermodel depend mainly on two factors:

- the mathematical description of the problem. In other words, the modelling technique, and;
- the model input parameters comprising the geometrical dimensions, the material properties and the boundary conditions.

One could argue that there is a third factor which has an effect on the predictions, namely, the numerical method used to resolve the mathematical equations. However, the significant advances in this area over the past decades have relegated the importance of this factor to a secondary role.

When validating a supermodel, the objective is to make sure that the modelling techniques are appropriate. Nevertheless, even in the absence of measurement errors and using perfect modelling techniques, the supermodel predictions will not match the test results if the dimensions, material properties and boundary conditions used in the model are different to those of the manufactured component(s). This does not mean that the model is wrong, just that the supermodel simply represents a different test.

Ideally, one would create a supermodel using the exact geometrical dimensions, material properties and boundary conditions of the real test. This would focus the attention on the validation of the modelling techniques and not on the right definition of the model input parameters. However, the only data usually available are the tolerances over which the geometrical dimensions, the material properties and, to some extent, the boundary conditions might vary. Subsequently, even when the modelling techniques used for the creation of a supermodel are accurate, uncertainty still remains that the test modelled might not correspond exactly to the one that takes place in reality.

5.4 Characterisation of Model Input Parameter Uncertainty

The characterisation of uncertainty is usually done in statistical terms. For instance, the uncertainty associated with the definition of the Young's modulus in a supermodel can be characterised using a Probability Density Function (PDF) such as that in Figure 5.1. The data used to construct this curve typically comes from a series of tensile tests performed on specimens made of the material of interest.

The shape of most PDFs can be approximated using standard functions. Examples of such functions are: Normal distribution, Lognormal distribution, Weibull distribution, Gumbel distribution, Uniform distribution, Triangular distribution, etc. A comprehensive description of these distributions can be found in any statistics textbook, e.g. [72].

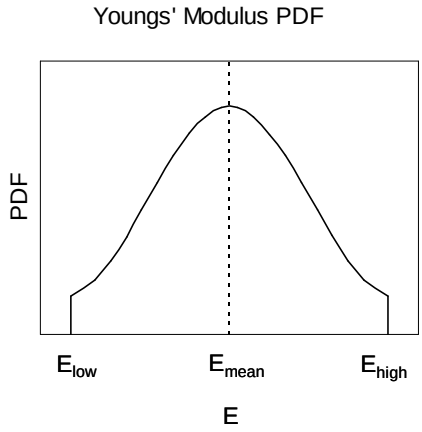

Figure 5.1. Typical PDF of a material's Young's modulus.

The shape of the PDF in Figure 5.1 resembles a Normal distribution, although the tails have been truncated. This means that the Young's modulus of the material will always lie within a specified set of bounds. This characteristic is typical of parameters which are tightly controlled during the manufacturing processes. For instance, the strict quality checks in the aeroengine industry will prevent the use of any material whose Young's modulus falls outside a given error band with respect to the nominal value.

The estimation of the PDFs for some model input parameters is relatively easy. For instance, the Materials Laboratory will usually provide a good estimation of the PDFs for the basic material properties, Young's modulus, Poisson's ratio, density, etc.

In the case of the geometrical dimensions, the upper and lower bounds are usually well defined and strictly controlled during manufacturing. However, the shape of the PDF is less clear and it is usually estimated based on a detailed understanding of the manufacturing processes.

The characterisation of uncertainty associated with the value of the parameters used to describe the test boundary conditions is most difficult in practice. For instance, it is very difficult to characterise the uncertainty associated with the values of the parameters used to describe the contact stiffness between the component and a test fixture. The usual approach in these cases is to consider that the values of the parameters can change over a wide range (i.e. high uncertainty). The shapes of the PDFs are then typically determined based on "engineering judgement".

The free-free configuration is a particular case where the component is tested in the absence of boundary conditions. This eliminates the complex task of characterising the uncertainty associated with the modelling of the boundary conditions. Moreover, the lack of uncertainty in their definition will result in a much reduced uncertainty in the free-free model predictions when compared with more complex test configurations.

5.5 Model Uncertainty Propagation

The uncertainties in the input parameters will be invariably propagated through the model and will manifest themselves as uncertainties in the predictions. For instance, let us consider that the material density of a model is defined by a Normal distribution such as that shown in Figure 5.2 (a). The total mass, M, of a solid homogenous model is predicted using:

$$M = \rho V \tag{5.1}$$

where ρ is the material density and V is the total volume.

Let us also assume that there is no uncertainty over the dimensions of the component and therefore the volume remains constant. Under these circumstances, it can be easily demonstrated that the total mass predicted by the model will also follow a normal distribution, see Figure 5.2 (b), where the mean and standard deviation σ are given by:

$$M_{mean} = \rho_{mean} V \tag{5.2}$$

$$\sigma(M) = \sigma(\rho) V \tag{5.3}$$

This is one of the simplest examples of uncertainty propagation. There is only one uncertain parameter in the model and the mathematical function that relates the input parameter to the prediction of interest (i.e. total mass) is linear.

In a general case, the uncertainty in the model predictions will be the result of more than one input parameter. Moreover, the mathematical relationship between the input parameters and the predictions might not be explicit, let alone linear.

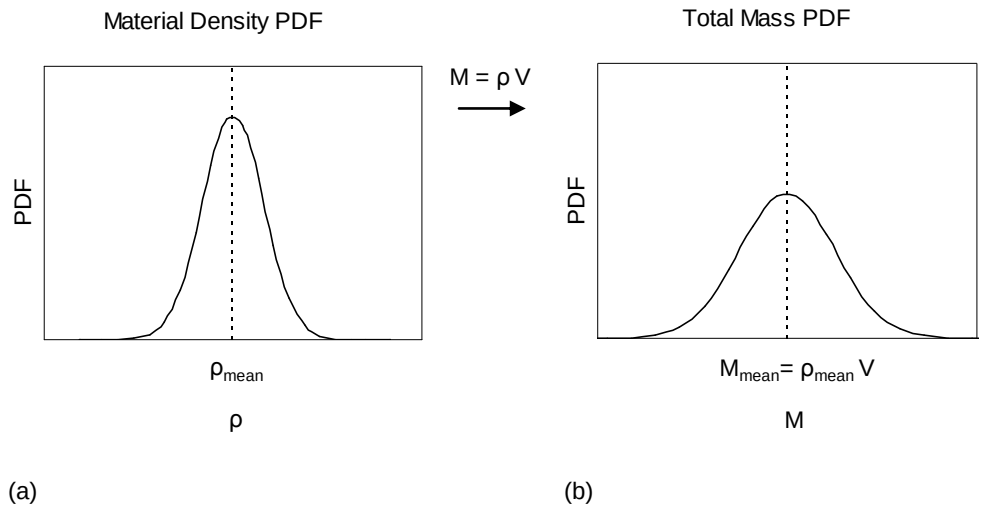

Figure 5.2. (a) Material density PDF and (b) mass prediction PDF.

5.5.1 Parametric CAD Models

In order to calculate the propagation of uncertainty through a model it is necessary to establish a mathematical relationship between its input parameters and the output predictions. In other words, the predictions must be expressed as a function of the input parameters.

As explained above, when validating a supermodel (and subsequently the modelling techniques) the biggest uncertainty in the predictions comes from an inability to exactly match the geometrical dimensions, material properties and boundary conditions of the test components. In practice, it is very difficult to mathematically determine the relationship between the model predictions and some of those parameters. For instance, assume that we want to establish the uncertainty in the natural frequency predictions of a casing supermodel due to the variation of the front flange thickness. It can prove very challenging to construct the stiffness and mass matrices of the supermodel as a function of this parameter. Moreover, the natural frequencies cannot be predicted from the stiffness and mass matrices explicitly, requiring the solution of an eigen problem instead.

The relationship between a set of input parameters in the supermodel and its predictions can be resolved more easily taking the indirect approach shown in Figure 5.3.

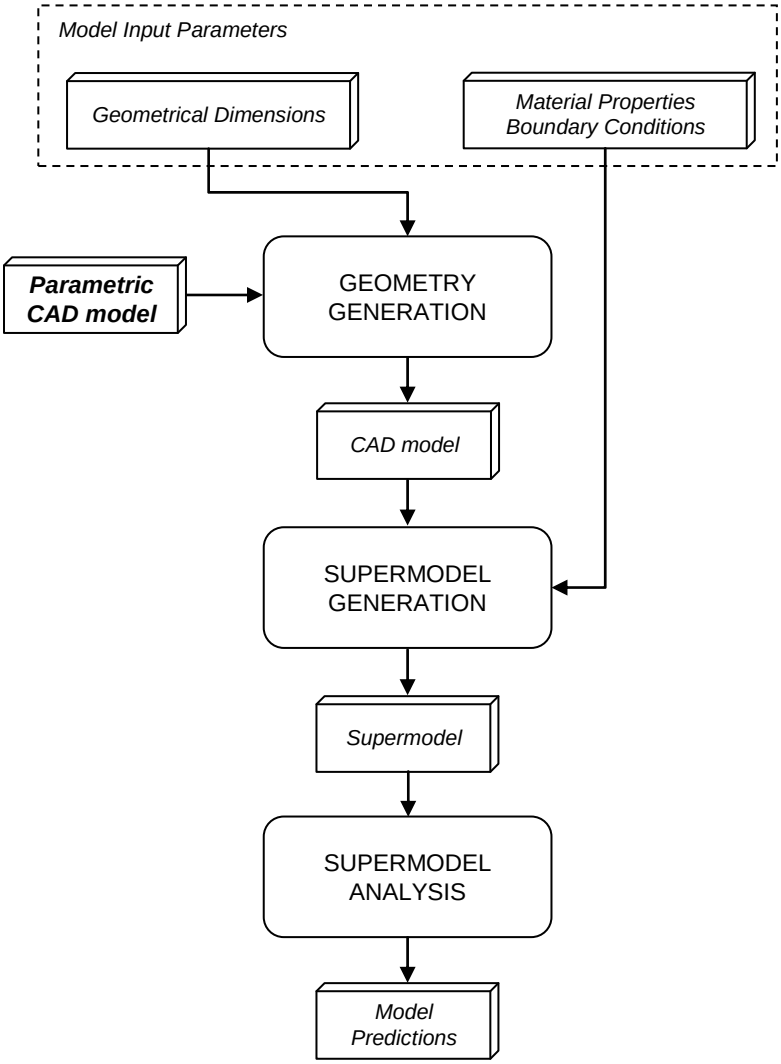

Figure 5.3. Indirect approach for the calculation of the relationship between the input parameters and the model predictions.

The first step in the process is to create a CAD model of the component with the right dimensions. This is usually done by inputting the specified set of dimensions into a parametric CAD model. A supermodel is then generated using the appropriate supermodelling techniques. A set of material properties and boundary conditions are added to the model at this stage. The predictions from the supermodel will correspond to the geometrical dimensions specified in the CAD model and the material properties and boundary conditions subsequently added to the supermodel. This in effect

establishes the correspondence between the model input parameters and the predictions. Even though this correspondence is not described in the strictest mathematical sense, it is a pragmatic way of calculating the values of the supermodel predictions for a given set of input parameters.

One could argue that different supermodels are used for each set of input parameters. Nonetheless, each of those supermodels is created using the same modelling techniques and will not differ much from each other. Moreover, as explained before, the actual objective of the validation exercise is to validate the supermodelling techniques and not the supermodels themselves.

5.5.2 Monte Carlo Simulation

Monte Carlo Simulation is probably the most extended method for the calculation of uncertainty propagation through models where the relationship between the input parameters and the predictions cannot be formulated explicitly. According to this method, the probabilistic data of the model responses (e.g. mean, standard deviation, distribution type) can be characterised using the predictions from a model evaluated a great number of times, each time for a different set of input parameter values selected randomly according to their PDFs.

Figure 5.4 illustrates this method when applied to the characterisation of the uncertainty in the predictions from a supermodel. At each iteration the values of the model input parameters are selected randomly according to their PDFs. A CAD model of the component is first created using randomly selected values of the geometrical dimensions. The CAD model is then meshed using supermodelling techniques. The values corresponding to the material properties and boundary conditions are applied to the supermodel at this stage. The model is then analysed to evaluate the values of the predictions corresponding to the input parameters which were selected randomly. Finally the uncertainty in the response predictions is characterised statistically.

One of the main advantages of this method is its accuracy. The predictions from the model at each sample are exact. This means that if the number of samples is sufficiently high, the probabilistic characterisation of the model responses will be very accurate. In

fact, Monte Carlo Simulations are typically used as the accuracy benchmark for other approximate methods used in uncertainty propagation analysis.

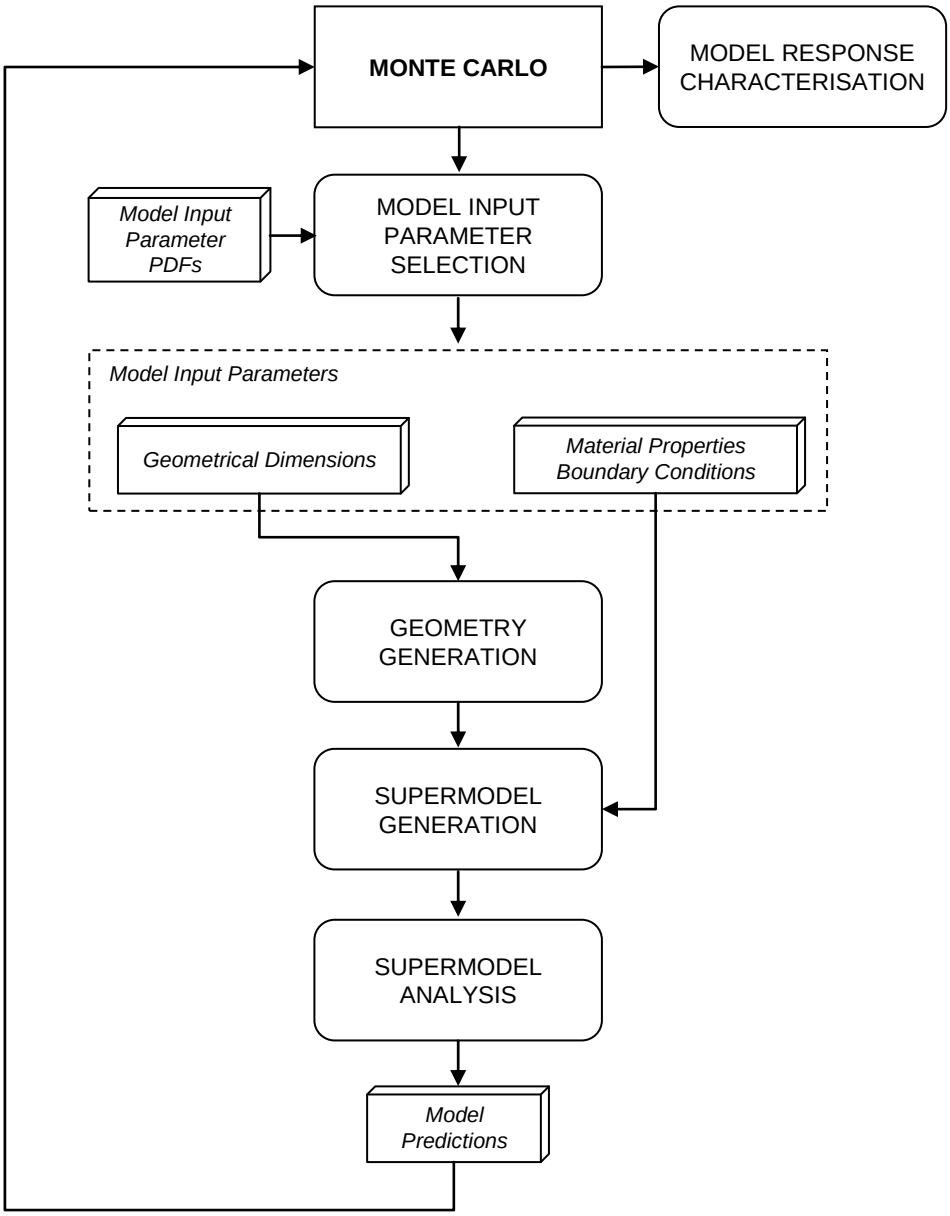

Figure 5.4. Monte Carlo Simulation.

The number of samples usually required by Monte Carlo Simulations can be in the order of tens of thousands. This number might increase if an accurate characterisation of the tails of the response PDFs is required. This is the biggest downside of this method when applied to complex models. For instance, a single analysis of a supermodel for the computation of its modal properties takes a considerable amount of time even with the aid of High Performance Computing (HPC) Capabilities. The analysis of this model tens of thousands of times is simply unrealistic.

A number of variations of the Monte Carlo Simulation method have been proposed over the years to reduce the number of samples required for an accurate estimation of the model response PDFs. The most relevant are those from Halton [73], Hammersley [74], and Hammersley and Handscomb [75] in the 1960s, and those from Owen [76], Hurtado and Barbat [77], Ziha [78] and Saliby [79] in the 1990s. Even though these techniques facilitate an important reduction in the number of samples required, this number is still very high.

5.5.3 Sensitivity-based Metamodels

Sensitivity analysis can be used as an efficient tool to overcome some of the limitations associated with the Monte Carlo Simulation. If z represents a supermodel prediction (e.g. natural frequency) whose value depends on a set input parameters, $p_1,p_2,p_3,\ldots$, then $z(p_1,p_2,p_3,\ldots)$ can be approximated using the first-order terms of the Taylor series:

$$z(p_1,p_2,p_3,...) \cong z_{mean} + \frac{\partial z}{\partial p_1}\left(p_1 - p_{1\,mean}\right) + \frac{\partial z}{\partial p_2}\left(p_2 - p_{2\,mean}\right) + \frac{\partial z}{\partial p_3}\left(p_3 - p_{3\,mean}\right) + ... \tag{5.4}$$

where:

- $p_1,p_2,p_3,\ldots$ are the uncertain input parameters in the supermodel;
- z_{mean} is the value of the supermodel prediction when evaluated using the mean values of the input parameters $p_{1\,mean}$, $p_{2\,mean}$, $p_{3\,mean}$, ..., and;
- $\frac{\partial z}{\partial p_j}$ is the first-order derivative of supermodel prediction z with respect to the input parameter p_j when evaluated at $p_{1\,mean}$, $p_{2\,mean}$, $p_{3\,mean}$, ...

Equation (5.4) is in effect a much reduced approximate model of the original supermodel's response z. These models-from-models are usually referred to as metamodels. The creation of a metamodel according to equation (5.4) requires only the calculation of the mean response z_{mean} and the first-order sensitivity terms $\frac{\partial z}{\partial p_j}$. In general, these sensitivities cannot be calculated explicitly and finite difference methods such as that in equation (2.19) must be applied. This in turn means that the original supermodel needs to be evaluated as many times as the number of input parameters. Nevertheless, this is typically a much reduced number of supermodel analyses than those required by a standard Monte Carlo Simulation. The process of creating a metamodel from a supermodel is graphically illustrated in Figure 5.5.

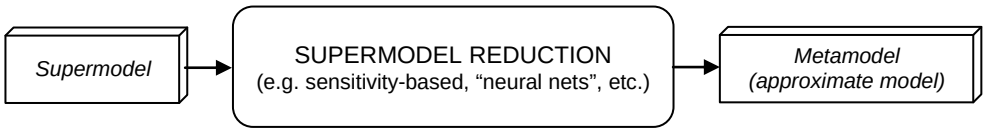

Figure 5.5. Creation of metamodels.

The analysis of model uncertainty propagation is much easier when using a reduced metamodel, such as that described in equation (5.4), instead of the original supermodel. For instance, the Monte Carlo Simulation described in Figure 5.6 is computationally inexpensive even when using millions of iterations to characterise the statistical properties of the response.

Moreover, the linearity of equation (5.4) means that in many cases where the uncertainty of the input parameters is described by standard PDF functions, the uncertainty of the response can be characterised explicitly without the need of a Monte Carlo Simulation. For instance, if all input parameters in equation (5.4) are defined by Normal distributions, the response z will also follow a Normal distribution where the mean value is z_{mean} and the variance (squared of the standard deviation σ) is given by:

$$\sigma^2(z) = \left\{ \frac{\partial z}{\partial p_1} \frac{\partial z}{\partial p_2} \frac{\partial z}{\partial p_3} \ldots \right\} \begin{bmatrix} \sigma^2(p_1) & \mathrm{cov}(p_1,p_2) & \mathrm{cov}(p_1,p_3) & \ldots \\ \mathrm{cov}(p_2,p_1) & \sigma^2(p_2) & \mathrm{cov}(p_2,p_3) & \ldots \\ \mathrm{cov}(p_3,p_1) & \mathrm{cov}(p_3,p_2) & \sigma^2(p_3) & \ldots \\ \ldots & \ldots & \ldots & \ldots \end{bmatrix} \begin{Bmatrix} \frac{\partial z}{\partial p_1} \\ \frac{\partial z}{\partial p_2} \\ \frac{\partial z}{\partial p_3} \\ \ldots \end{Bmatrix} \tag{5.5}$$

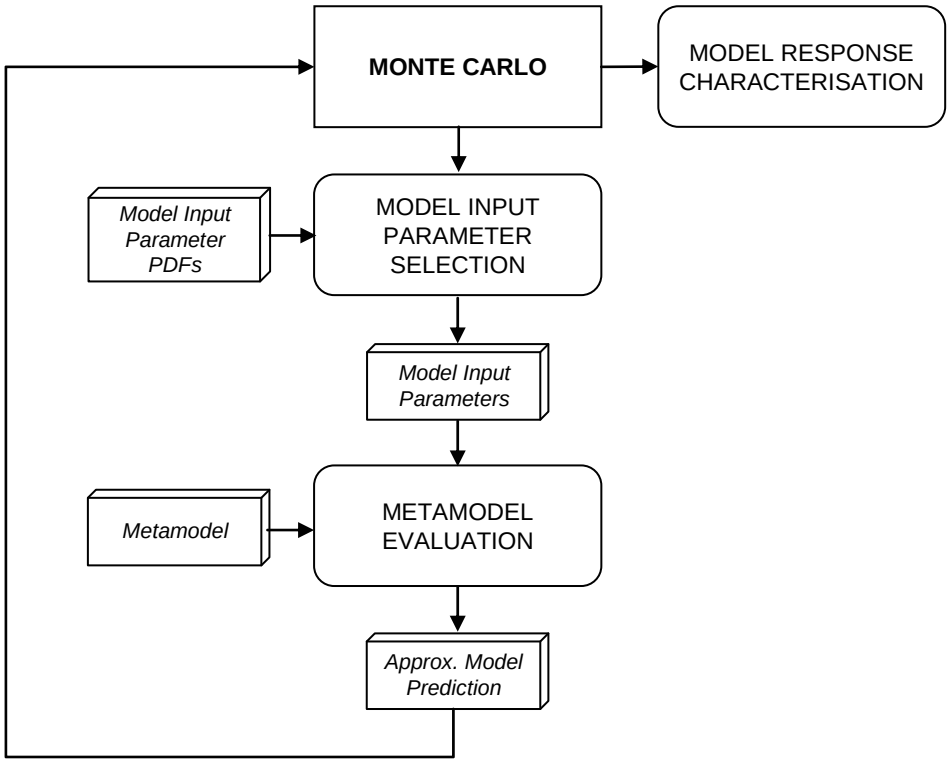

Figure 5.6. Monte Carlo Simulation using a metamodel.

The benefits of the sensitivity-based metamodels are sometimes obscured by their poor accuracy. The first-order Taylor approximation in equation (5.4) is only exact for linear models. Reasonably good accuracy can still be achieved for moderately non-linear models when the input parameters only change over a reduced range. However, for a general non-linear model where the parameters might change considerably, the use of a linear approximation is usually too coarse.

The inclusion of higher order terms to the Taylor series would improve the accuracy of sensitivity-based metamodels. Nonetheless, the computational effort required to estimate those terms is usually significant.

5.5.4 Design of Experiments - Response Surface Model

The use of metamodels can simplify the analysis of model uncertainty propagation. Sensitivity-based methods are capable of generating simple metamodels, however, their lack of accuracy hinder their application in practice. The use of Design of Experiment (DoE) techniques coupled with Response Surface Models (RSM) offer the possibility of creating accurate metamodels which can be confidently used for uncertainty propagation analysis of general non-linear models where the input parameters might vary significantly.

The illustration of this approach is easier when using a practical example. For instance, let us consider that we want to characterise the uncertainty of a model response z which depends on two model input parameters, p_1 and p_2, according to:

$$z = z(p_1, p_2) \tag{5.6}$$

where the values for the parameters p_1 and p_2 are defined using the general PDFs in Figure 5.7. These PDFs are both bounded by upper and lower limits.

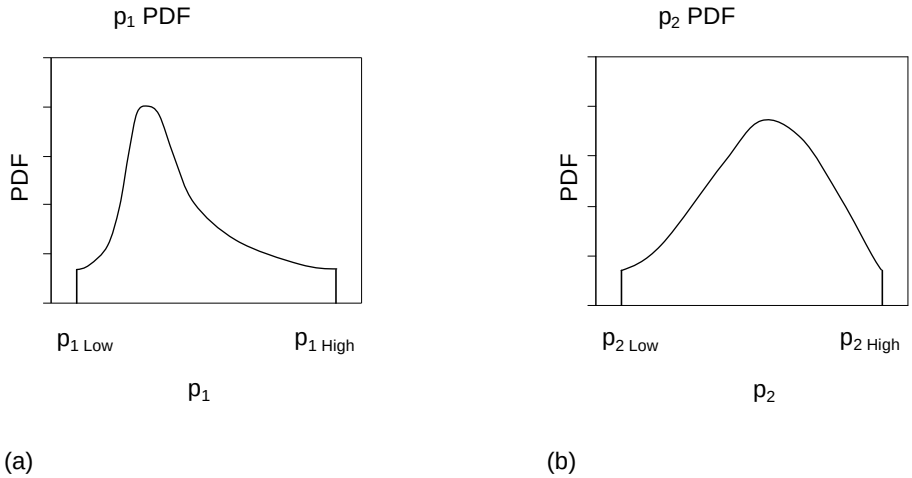

Figure 5.7. PDFs corresponding to (a) parameter p_1 and (b) parameter p_2.

In a general case, the model represented by equation (5.6) will be non-linear and implicit. As explained above, the use of Monte Carlo Simulations to characterise the uncertainty propagation of these models is usually prohibitive.

Let us consider now that the model prediction z is evaluated at a number of combinations of the parameters p_1 and p_2 as illustrated in Figure 5.8. Please note that every combination (sample) lies within the input parameter bounds (e.g. p_{Low} to p_{High}). The response z for a combination of parameters p_1 and p_2 different from those used during the sampling can be approximated by interpolating the responses from the closest samples. The interpolation functions create a surface contour such as that in Figure 5.9. This contour is usually referred to as Response Surface Model (RSM).

The RSM is a metamodel of the original response function in equation (5.6) where the value of the model response for any combination of input parameters can be easily calculated using simple interpolation functions. This metamodel can now be used instead of the original model to easily calculate the model uncertainty propagation (e.g. using a Monte Carlo Simulation).

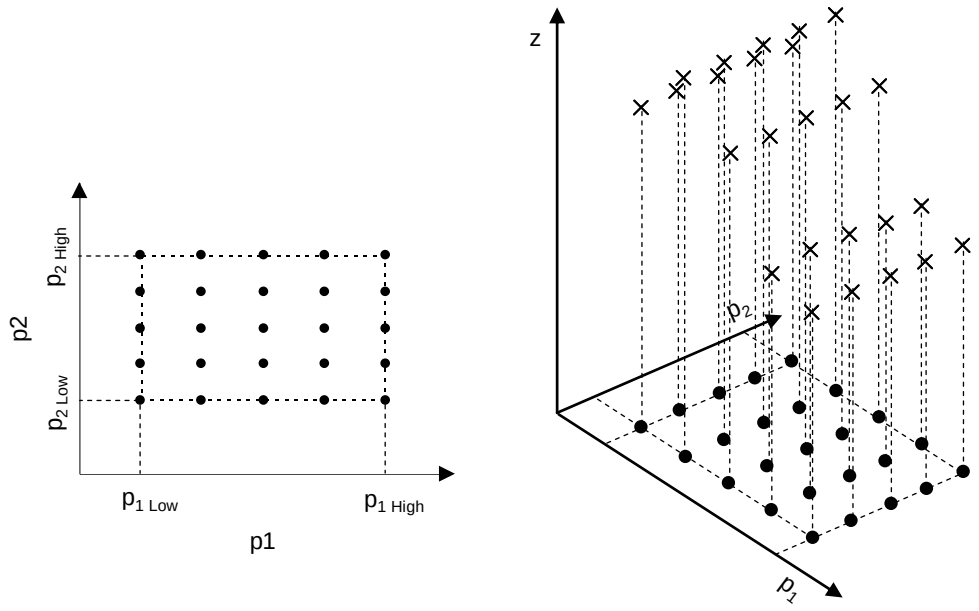

(a) (b)

Figure 5.8. (a) Parameter sampling and (b) model response.

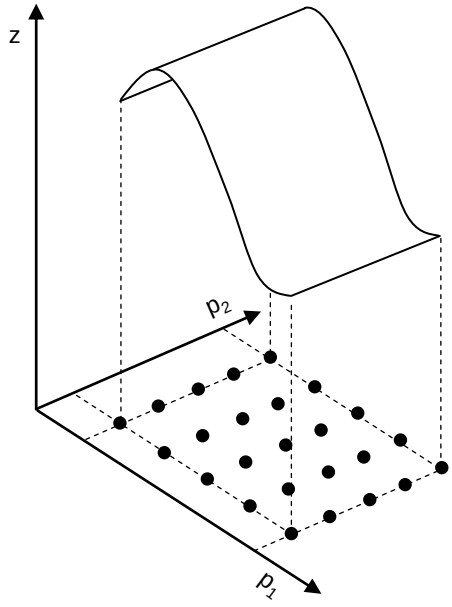

Figure 5.9. Model prediction at each sample.

The extension of this methodology to account for the existence of more than two uncertain model input parameters is straight-forward. However, the RSM then becomes a multi-dimensional function which cannot easily be illustrated graphically.

The number of samples chosen plays a significant role on in the accuracy of the RSM. As a general rule, the more samples the better approximations from the metamodel. Nonetheless, there is another factor which has a great effect on the metamodel's accuracy, this is, the distribution of the samples. In order to illustrate this point, let us consider again the simple model in equation (5.6). Figure 5.10 (a) and (b) show two different sampling options for the input parameters. Both options make use of the same number of points. The interpolation functions are more likely to give a better estimate of the model's response (for any input parameter combination within the uncertainty range) when using the evenly spaced sampling corresponding to Option 2.

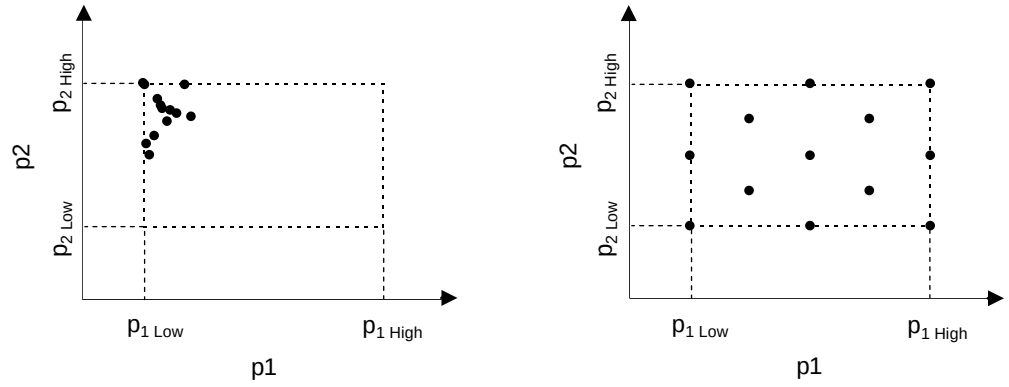

(a) (b)

Figure 5.10. Sample distribution. (a) Option 1 and (b) Option 2.

DoE techniques are typically used to optimise the sampling distribution. The concept of DoE was first formulated by Fisher [80] in the 1930s and has been an active area of research since then. The Full Factorial technique is one of the earliest and most basic DoE methods which is still in use today. According to this technique, the continuous uncertainty range for each of the p model input parameters is first reduced to a finite number of L equally spaced values. The sampling takes place at all L^p possible parameter combinations. Figure 5.11 shows an example of a Full Factorial sampling for a model such as that in equation (5.6) with 2 input parameters and 4 point discretisation (4^2 possible combinations).

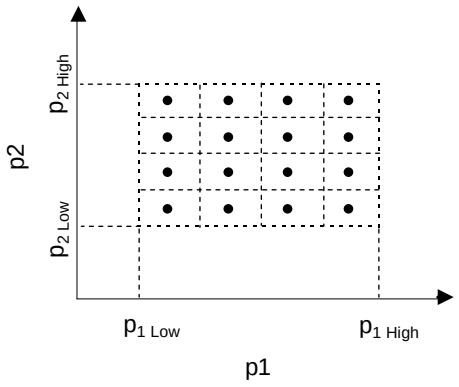

Figure 5.11. Full Factorial sampling.

The number of samples used can only be controlled to a certain extent by the number of L divisions used to discretise the continuous parameters. Nevertheless, for models with a considerable number of input parameters p, even a small number of L divisions will lead to a vast number of samples, L^p. In fact, the number can be so big that it may become prohibitive to sample the original model at so many points.

Different authors have proposed variations of the Full Factorial method to reduce the number of samples required. Some of the most important contributions are attributed to Plackett and Burman [81] in the 1940s and their Orthogonal Arrays method and Ross [82] in the 1980s, who used a modified Full Factorial approach.

The Latin Hypercube method is another popular DoE technique which takes a different approach with respect to Full Factorial methods. This methodology was first proposed by McKay *et al* [83] in the late 1970s and more recently refined by Iman *et al* [84]. The basics of this methodology are simple. Again, the continuous uncertainty range for each of the p model input parameters is first reduced to a finite number of L equally spaced values. The user then specifies the number of samples required, n_s. The parameter combination for each of the samples is selected randomly. Figure 5.12 shows an example of a Latin Hypercube sampling for a model such as that in equation (5.6) with 2 input parameters, 4 point discretisation and a total of 10 samples.

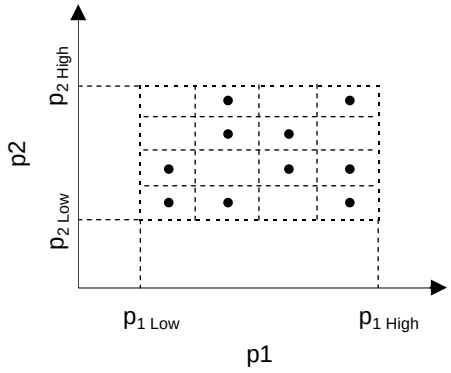

Figure 5.12. Latin Hypercube sampling.

The user has now full control over the number of samples used. The random nature of this techniques means that a sufficiently high number of samples is usually required in order to achieve a good sampling distribution. Otherwise the distribution of the samples might not evenly cover the uncertainty range of the input parameters.

A very interesting modification to the Latin Hypercube method was recently proposed by Jin *et al* [85] and is called Optimal Latin Hypercube Method. In this method, an initial sampling is created using the standard Latin Hypercube technique. The samples are then rearranged according to an optimisation procedure to achieve a more even distribution across the uncertainty range of the input parameters. This allows a reduction in the number of samples required by the standard Latin Hypercube method. Figure 5.13 shows an example of a Optimal Latin Hypercube sampling for a model such as that in equation (5.6) with 2 input parameters, 4 point discretisation and a total of 6 samples.

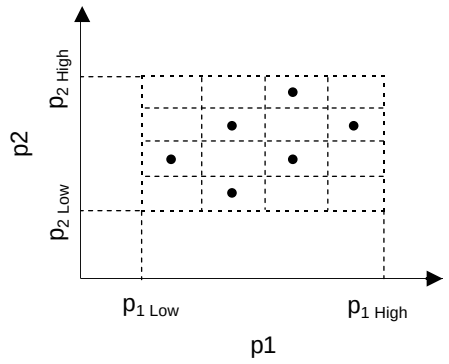

Figure 5.13. Optimal Latin Hypercube sampling.

There are no general rules for an optimum selection of the number of sample points required to produce an accurate RSM. This selection depends on the nature of the model response and the DoE technique used for the sampling. For instance, highly non-linear model responses will require many more samples than those required for linear or quasi-linear models. Moreover, a larger number of samples is required if a standard Latin Hypercube sampling method is used instead of its optimised version.

There is however an absolute minimum of samples required to create an RSM and this number depends on the type of interpolation functions used. For instance, if a

polynomial interpolation function is used to approximate the model response, at least as many samples as polynomial coefficients are required. The number of coefficients for a linear polynomial function is p+1 where p is the number of input parameters. If the function is quadratic the number of coefficients becomes (p+1)(p+2)/2. This number increases to (p+1)(p+2)/2+p for cubic functions and to (p+1)(p+2)/2+2p for fourth-order polynomials.

It is common practice to use more samples than the absolute minimum required, in which case, the polynomial coefficients will be calculated to provide the best fit. Under these circumstances it is possible that the interpolation function might not exactly match the original response at the sample points.

The use of polynomial functions for the creation of RSMs must be carried out with great care. For instance, the use of a linear interpolation will be completely inappropriate to represent highly non-linear responses. Moreover, high-order polynomials can introduce local instabilities that can compromise the accuracy of the approximation.

Radial Basis Functions (RBF), also referred to as “neural nets”, provide a reliable alternative to polynomial functions for the creation of RSMs. These functions were initially introduced by Weissinger [86] in the 1940s and have been subsequently refined by other authors such as Hardy [87] in the 1970s and Broomhead and Lowe [88] in the 1980s. In very simple terms, RBFs are spline functions that connect the response values from all samples. The use of splines removes the instabilities associated with high-order polynomial functions. These functions are particularly well suited for highly non-linear models.

The mathematical formulation of these functions is complex and will not be reproduced here. The interested reader is directed to the authors referred above. It is however important to mention here that the minimum number of samples required to fully characterise a RSM using RBFs is 2p+1.

Unlike polynomial functions, RBFs always match the original response values at the sample points even when the number of samples is higher than the minimum required.

5.5.5 Metamodel Error Uncertainty

A metamodel is an approximation of the original model response which greatly simplifies the calculation of uncertainty propagation. The downside is that the response values from the metamodel are approximate and therefore carry some level of error. As discussed above, the more samples used, the better the approximation. Nonetheless for highly complex models the approximation errors cannot be fully eliminated.

The approximation error will be in general different for each parameter combination. Moreover, it is almost impossible to anticipate what the error will be for a given combination. For that reason the approximation error can be considered an uncertainty in itself.

The uncertainty in the approximation error can easily be characterised by comparing the response from both the original model and the metamodel at a sufficient number of samples other than those used to create the metamodel. Those samples, usually referred to as “check samples”, can be selected randomly or using an appropriate DoE technique.

When calculating the uncertainty propagation using metamodels, the approximation error uncertainty must be added to the uncertainty in the predictions which result from the uncertainty in the model input parameters. This process is illustrated in Figure 5.14 for the case where the uncertainty propagation is calculated using a Monte Carlo Simulation. On each iteration, an error selected randomly according to the approximation error PDF is added to the prediction from the metamodel.

The clear benefits of using a metamodel for the calculation of the uncertainty propagation usually outweighs the extra uncertainty introduced. Moreover a careful sampling when creating the metamodel can greatly reduce this uncertainty.

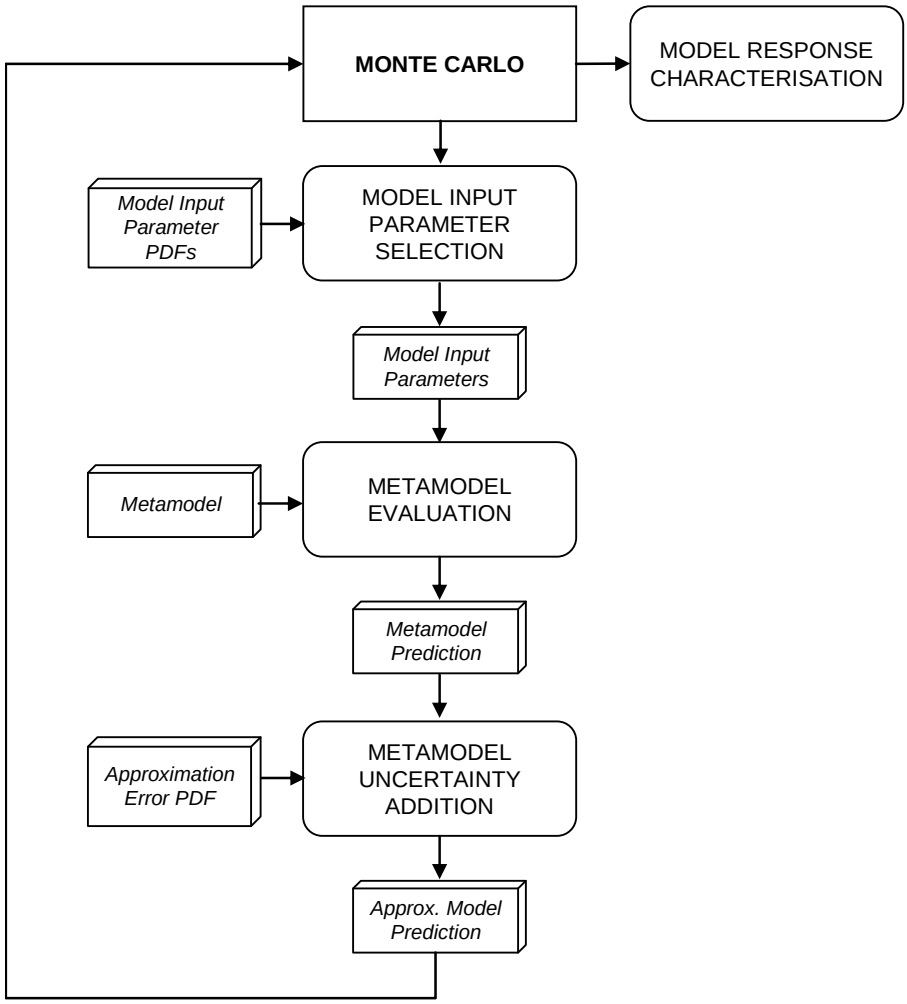

Figure 5.14. Metamodel uncertainty.

5.6 Measurement Uncertainty

The other major source of uncertainty present during the validation process is that associated with the test measurements. In order to illustrate the main sources of measurement uncertainty we will follow the sequence of events that usually take place during a typical Modal Test.

Once the manufactured component has been delivered to the laboratory and set-up for testing, the first step is to mark the excitation and response locations on the component. Those locations are usually specified beforehand using Test Planning methods [31]. The

test practitioner will always try to closely match those locations on the structure. This is particularly important to ensure a consistent correlation between the measurements and the predictions. For certain components, such as those containing aerofoil shapes, the accurate positioning of measurement points can be very challenging. Unless accurate measurement devices are available in the laboratory, the uncertainty over the positioning of the excitation/measurement points can be significant. This will have a negative effect when correlating the measured and the predicted modeshapes.

Moreover, the measurement direction of transducers is also important. For instance, it is a common requirement to measure the vibration response only in a direction normal to the surface. If we are using a hammer to excite the structure it might be difficult to accurately hit the component perpendicular to its surface, hence increasing the measurement uncertainty.

Transducers are themselves subject to manufacturing tolerances. The transducer calibration is usually only known to lie within a tolerance. This tolerance is usually supplied by either the manufacturer or a certified calibration laboratory.

The transfer of the signal from the transducer to the data acquisition box makes use of electrical wiring. Electrical noise from adjacent equipment usually introduces undesired effects on the signal and distorts the actual measurements. Also, mechanical vibration from adjacent machinery might be transmitted to the component being tested, thus corrupting the quality of the measured response. A good practitioner will always try to reduce the noise in the signal by insulating the electrical equipment and by isolating as much as possible the test from external mechanical vibration. Moreover, measurements are usually repeated a number of times to average out the influence of noise. These procedures will reduce the uncertainty in the measurements due to noise, nonetheless the noise will never be totally removed.

These days, the analogue signal from a transducer is usually digitised for further processing. This is, in effect, a conversion from a continuous signal to one defined by a discrete number of points. Most of the time, the digitised data will also be transformed from the time domain to the frequency domain using Fourier analysis. All these conversions will inevitably introduce errors in the final results.

The end result from the signal conditioning process is a set of Frequency Response Functions (FRF). The extraction of natural frequencies and modeshapes from these data requires a further step usually referred to as Modal Analysis. In very simple terms, Modal Analysis methods try to find a mathematical model (i.e. Modal Model) that best fits the measured data. The modal properties of the Modal Model are assumed to be those of the component tested.

The user must make a few decisions over the type of mathematical model that will be used to fit the test data. For instance, damping is typically assumed to be either hysteretic or viscous. In reality it might be neither. For the same set of data, different types of mathematical models will provide different answers. Furthermore, for a given mathematical model there is a great variety of techniques that can be used to fit the test data. Again, different fitting algorithms will in general provide slightly different answers.

The uncertainty associated with Modal Analysis is particularly high when the modes of the tested structure have very close natural frequencies. In these cases, the fitting errors are usually significant leading to extracted modal properties that barely resemble those of the test component. In fact, it is not uncommon for the Modal Analysis to wrongly identify some of the modes or introduce extra “mathematical modes” which have no physical meaning.

Last but not least, the environmental conditions, particularly temperature, can have an important effect on the modal properties. Most modern test facilities can provide environmental control to a certain extent. Nonetheless, it is not uncommon to see shifts in the measured natural frequencies throughout the test due to temperature changes. Modern Modal Analysis methods are very sensitive to frequency shifts in the measurements and even slight deviations can seriously compromise the results.

5.7 Characterisation of Measurement Uncertainty

The measurement uncertainty is the resultant of the propagation of all the uncertainties in the measurement chain. This uncertainty must be characterised statistically to be included in the model validation process.

One could argue that the same principle used for the calculation of the model uncertainty propagation could be applied here to characterise the measurement

uncertainty. According to this approach, all the uncertainties in the measurement chain would be characterised individually and then propagated through a mathematical model that reflects the interaction between the different factors. This can be very difficult in practice though. First of all, it can be very difficult to individually characterise the uncertainty of some factors in the measurement chain. But most importantly, the interaction between the different factors (e.g. transducer calibration, curve-fitting errors) is highly complex and difficult to determine mathematically.

An alternative approach is to characterise the measurement uncertainty with the use of extensive test programmes. This approach is conceptually simple: for a given manufactured component under laboratory conditions (e.g. free-free) the same Modal Test is repeated by different practitioners, each of them using different transducers, different data acquisition hardware, different analogue-to-digital converters, different Modal Analysis software, different curve fitting methods, etc.

If the component and the boundary conditions remain the same during all tests, deviations in the measurements can only be attributed to the test uncertainty. If the number of tests is sufficiently high, this uncertainty can be characterised statistically.

The experimental approach, even though possible in theory, is not viable in an industrial environment. A proper statistical characterisation of the measurement uncertainty would require so many test variations that the cost would rapidly escalate to unacceptable levels.

In practice, the characterisation of the measurement uncertainty will usually take a much more pragmatic approach. In fact, it is common to estimate this uncertainty based on “engineering judgement”. For instance, the uncertainty associated with the measurement of natural frequencies is known to be low. The measurement errors are not likely to be outside a ±1% band when using modern equipment. A PDF such as that in Figure 5.15 is probably not a bad estimation of the uncertainty in the natural frequency measurement error. This PDF follows a Normal distribution with the mean at 0% error, and standard deviation of 0.1% and upper and lower limits at ±1%.

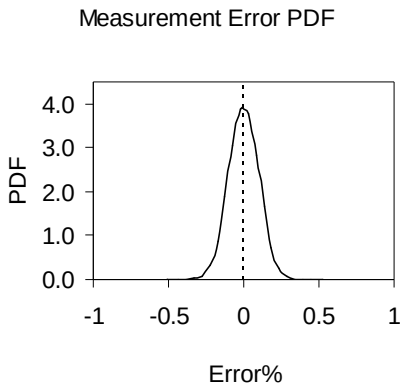

Figure 5.15. Typical natural frequency measurement error uncertainty.

5.8 Probabilistic Model Validation

Let us assume that the PDF in Figure 5.16 describes the uncertainty associated with the prediction of the first natural frequency of a component when using a supermodel. Let us also assume that the vertical red line in Figure 5.16 corresponds to a single test measurement.

As described in the previous section, the measurement is also subject to uncertainty. The measurement uncertainty is plotted in Figure 5.17 alongside the model uncertainty.

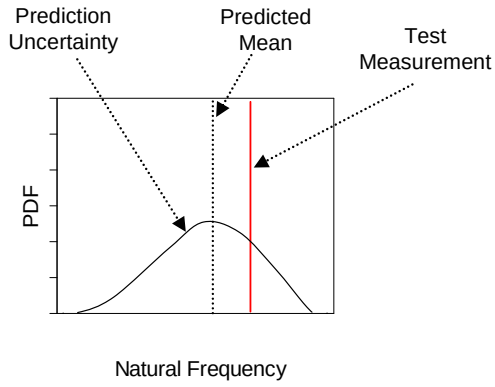

Figure 5.16. Typical prediction uncertainty and test result.

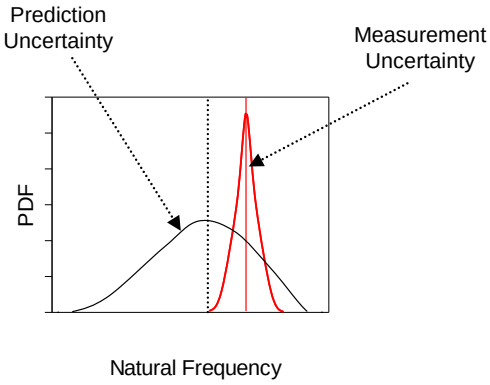

Figure 5.17. Typical prediction and measurement uncertainty.

An overlap of the two PDFs indicates that the model prediction is consistent with the test result. At first one would be tempted to use the area where the two PDFs overlap as a numerical estimation of the confidence in the model. Nevertheless, this approach is misleading. For instance, let us consider the two cases in Figure 5.18. In Case I the measurement exactly matches the mean of the predictions while in Case II these two values differ. Moreover, the low uncertainty associated with the measurement in Case I reinforces the confidence in the test data. Under these circumstances the test result in Case I should provide a higher confidence in the model than the measurement in Case II. Nonetheless, the small uncertainty in the measurement in Case I reduces the total area where the two PDFs overlap. In fact, this area is bigger in Case II where the test measurement does not match the mean value of the predictions and the uncertainty in the measurements is higher.

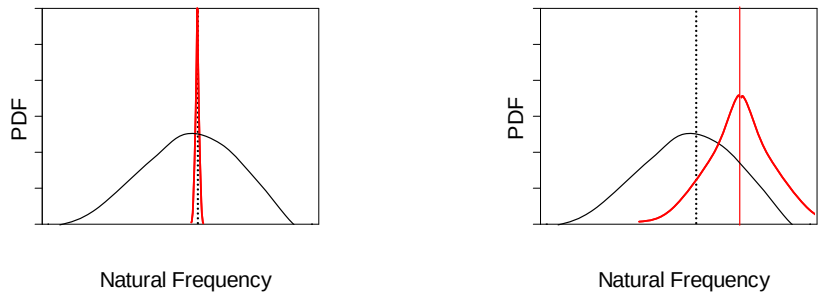

(a) (b)

Figure 5.18. Overlap of prediction and measurement PDFs. (a) Case I and (b) Case II.

In recent years, Hills and Trucano [89] [90] [91] presented an elegant solution to accept or reject a model as valid in view of the actual measurements. The first step in their approach is to incorporate the measurement uncertainty to the prediction uncertainty as illustrated in Figure 5.19. Conceptually, the combined uncertainty represents the uncertainty associated with the predictions from a model of the whole test. This model includes not only the finite element model but also the model of the measurement chain.

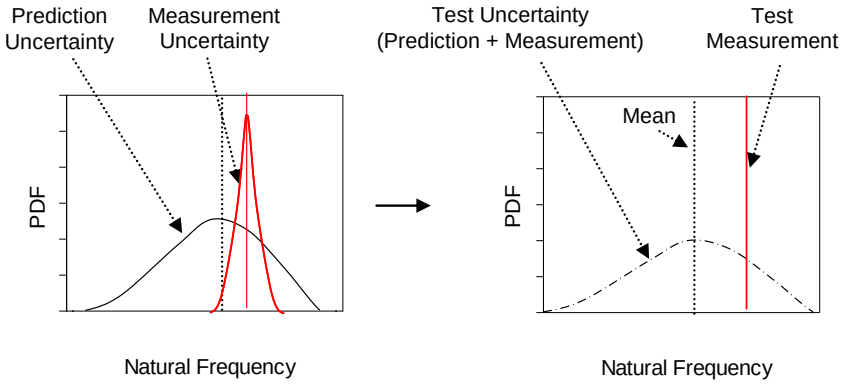

Figure 5.19. Test uncertainty (prediction + measurement).

The characterisation of the uncertainty associated with a model of the whole test is not difficult in practice. For instance, the process in Figure 5.20 illustrates how to calculate this uncertainty using a Monte Carlo Simulation. A random measurement error is introduced to the predictions from the metamodel to simulate what happens during a real test. The statistical characterisation of the "measured" response uncertainty contains the combined effect of the uncertainties in the model input parameters and measurement errors expected during the test.

According to Hills and Trucano [89] the model of the whole test is considered valid if all the measurements fall within certain bounds of the uncertainty in the predictions. For instance, let us consider that the PDF in Figure 5.21 corresponds to the uncertainty associated with one of the predicted natural frequencies from the model of the test. The left and the right dashed lines determine the range over which 95% of the predictions lie. If an actual measurement falls within those bounds it will be consistent with 95% of the predictions. This gives us a good confidence in the model. On the contrary, if the measurement falls outside the predicted bounds, there is only a 5% chance that the

measurement is consistent with the model predictions. This certainly reduces our confidence in the model. According to Hills and Trucano, all measurements must fall within a specified confidence limit (95% in this case) to consider the model valid.

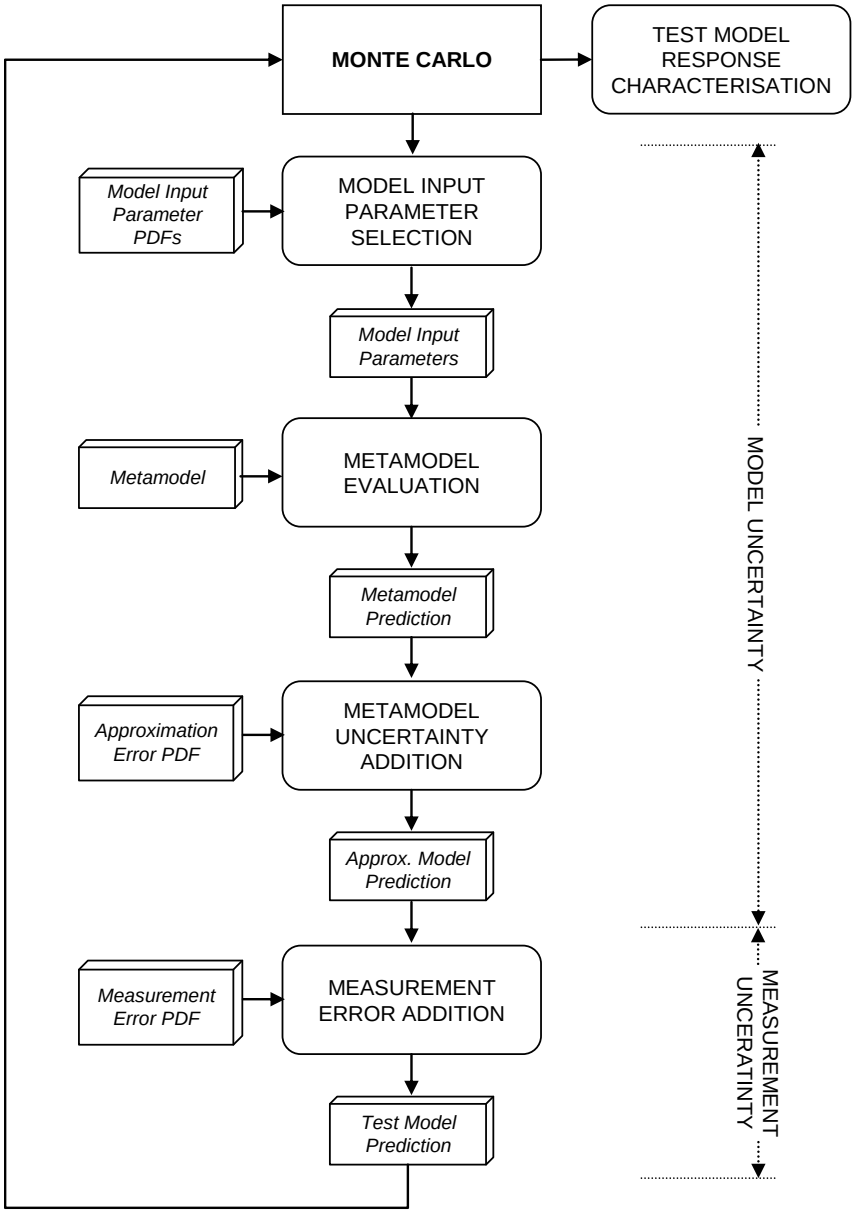

Figure 5.20. Test uncertainty characterisation.

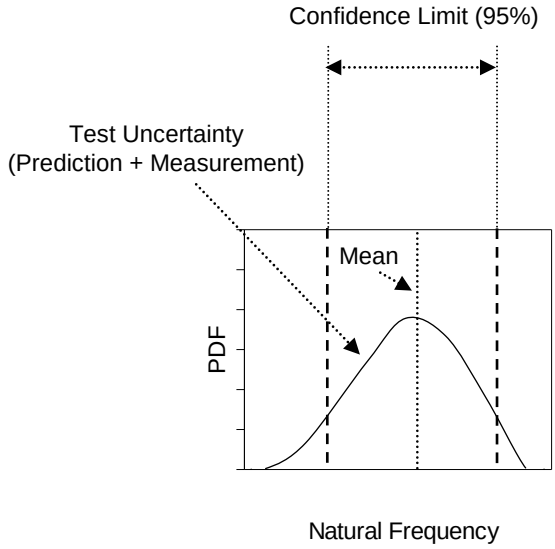

Figure 5.21. Confidence limit.

One could rightly argue that according to this method, there is a 5% chance of rejecting a valid model. This is in fact true and it is usually referred to as Type I error [68] (i.e. rejection of a valid model).

Why do not we eliminate the Type I error by increasing the confidence limit to 100%? In this case, if any measurement falls outside the predicted bounds we can categorically consider the model invalid. There is a problem though. A higher confidence limit increases the range over which the measurements are considered to be consistent with the test model predictions. This in turn increases the chances of accepting an invalid model. This is usually referred to as Type II error [68] (i.e. acceptance of an invalid model).

The chances of committing a Type I error (i.e. rejection of a valid model) are fixed by the value of the confidence limit. For instance, if the confidence limit is 95% the chances of a Type I error are invariably 5%. On the contrary, for any given confidence limit, the chances of a Type II error (i.e. acceptance of an invalid model) can be minimised. For instance, the more test results the less chances of all measurements falling within the confidence bounds if the model is invalid. A reduction in the uncertainty associated with

some of the model input parameters (e.g. dimensions of the test components) will also result in a reduction of the uncertainty associated with the test model predictions. This will minimise the chances of the measurements falling within the predicted test uncertainty unless the model is valid.

The selection of the confidence limit must take these factors into account. For instance, when there are many test measurement available and the uncertainty associated with the test model predictions is low it is justifiable to use a high confidence limit to minimise the chances of Type I error (i.e. rejection of a valid model). Nonetheless, when there is only a single measurement or the uncertainty in the test model predictions is significant, a high confidence limit will increase the chances of a Type II error (i.e. acceptance of an invalid model), therefore a lower limit should be selected.

In practice, it is usually recommended that a limit of 99% is used when there are a reasonable number of test measurements and the uncertainty in the test model predictions is low. When the number of tests is reduced (e.g. only one) and/or the uncertainty is significant, a 95% confidence limit is suggested. These numbers are not selected randomly. For a Normal distribution, a confidence limit of 95% covers all points within a distance with respect to the mean value of approximately ±2 times the standard deviation. In the case of 99%, the distance increases to ±3 times the standard deviation.

5.8.1 Multiple Response Validation

In general, the validation of a model requires the accurate prediction of more than one response. For instance, it is common when a model is only considered to be valid if it is capable of accurately predicting all natural frequencies within a specified frequency range.

The simplest way of approaching this problem is to consider the validation of each response independently. For instance, Figure 5.22 shows the uncertainty associated with the predictions of four responses (e.g. natural frequencies). According to this approach, the model is considered valid if all the measured responses fall within the confidence limit bounds.

In general, the responses from a model are not independent from each other though. For instance, an increase of the Young's modulus in the model will consistently affect to

all the predicted natural frequencies. The same is applicable to the measured responses. If two manufactured components have very similar dimensions but the Young's modulus of one of them is slightly higher, all the measured natural frequencies will in general be consistently higher for this component. As a result, it makes good sense to validate all the predicted responses at once.

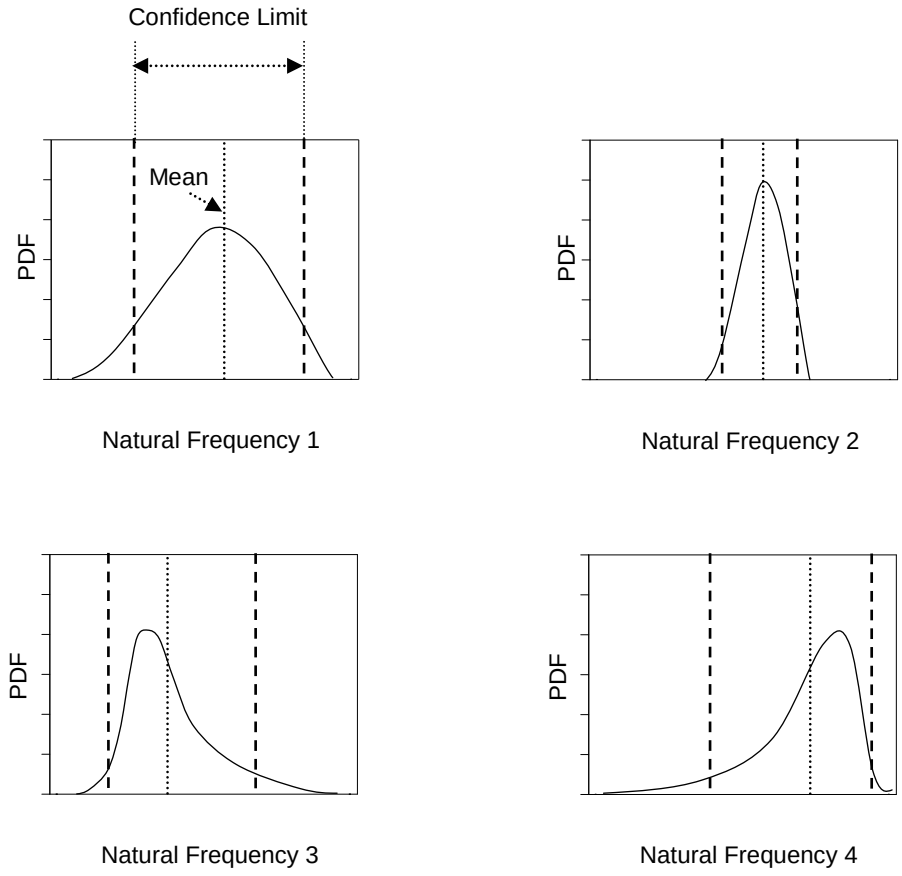

Figure 5.22. Multiple responses. Individual validation.

Figure 5.23 shows the uncertainty associated with the prediction of two responses (e.g. natural frequencies) when considered together. The measurement point represents the measured responses for a given test. The characterisation of the bi-dimensional uncertainty follows a similar principle to that used when considering a single response, see Figure 5.20. The only difference is that now the two responses from the test model

are evaluated at the same time during each Monte Carlo iteration and instead of creating a PDF for each response individually, the combined uncertainty is computed. The concentric lines represent iso-lines of equal probability density.

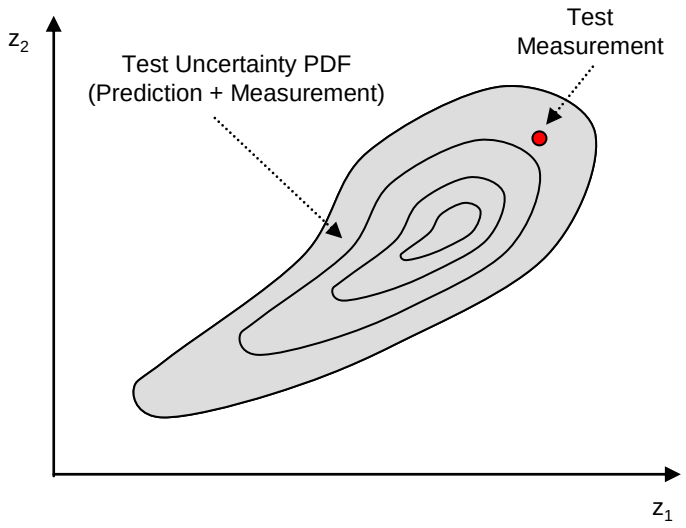

Figure 5.23. Combined uncertainty of multiple responses.

The model validation approach introduced for a single response can be easily extended to a multiple response scenario. Considering the two-response example above, the dashed line in Figure 5.24 defines the boundary where 95% (confidence limit) of the test measurements should fall to consider the model valid.

The extension to more than two responses is straight-forward, however, the combined variability is a multi-dimensional PDF which is difficult to plot graphically.

It can sometimes be difficult to calculate whether the responses measured during a test fall within the confidence limit bounds of a multi-dimensional PDF. Hills and Trucano [89] proposed a mathematical solution to this problem which is applicable to the case where the individual PDFs of all the model responses follow a Normal distribution.

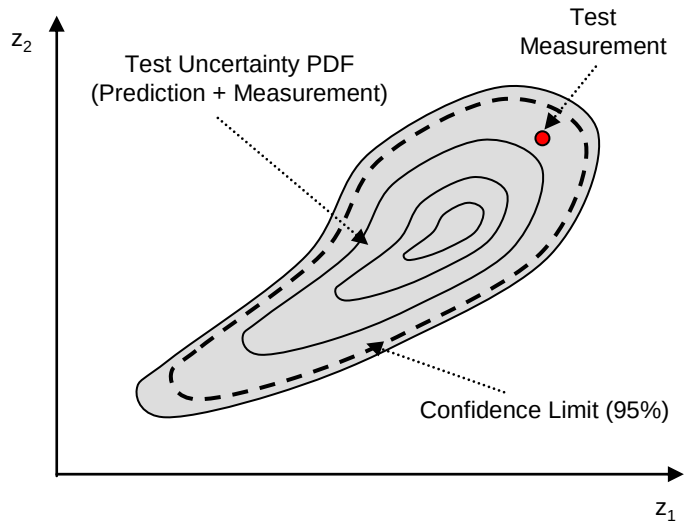

Figure 5.24. Combined uncertainty of multiple responses showing confidence limit.

According to Hills and Trucano, if r^2 is defined according to:

$$r^2 = \begin{pmatrix} z_{X\,1} - z_{Pred\,1\,mean} & z_{X\,2} - z_{Pred\,2\,mean} & \cdots & z_{X\,q} - z_{Pred\,q\,mean} \end{pmatrix} V^{-1} \begin{pmatrix} z_{X\,1} - z_{Pred\,1\,mean} \\ z_{X\,2} - z_{Pred\,2\,mean} \\ \cdots \\ z_{X\,q} - z_{Pred\,q\,mean} \end{pmatrix} \tag{5.7}$$

where $z_{X\,q}$ represents the test's q-th measured response, $z_{Pred\,q\,mean}$ is the corresponding predicted mean value and the matrix V contains the predicted response variances:

$$V = \begin{bmatrix} \sigma^2(z_{Pred\,1}) & \mathrm{cov}(z_{Pred\,1}, z_{Pred\,2}) & \cdots & \mathrm{cov}(z_{Pred\,1}, z_{Pred\,q}) \\ \mathrm{cov}(z_{Pred\,2}, z_{Pred\,1}) & \sigma^2(z_{Pred\,2}) & \cdots & \mathrm{cov}(z_{Pred\,2}, z_{Pred\,q}) \\ \cdots & \cdots & \cdots & \\ \mathrm{cov}(z_{Pred\,q}, z_{Pred\,1}) & \mathrm{cov}(z_{Pred\,q}, z_{Pred\,2}) & \cdots & \sigma^2(z_{Pred\,q}) \end{bmatrix} \tag{5.8}$$

then the test measurement containing the response vector ($z_{X\,1}$, $z_{X\,2}$, …, $z_{X\,q}$) is within the bounds defined by a γ % confidence limit if:

$$r^2 \leq I_\gamma^2(q) \tag{5.9}$$

where $I_\gamma^2(q)$ is the value for which the cumulative distribution function of the chi-square distribution function $\chi^2(q)$ is equal to γ.

Quite recently, Chen *et al* [92] extended the method by Hills and Trucano to consider the case where the response PDFs might take a general form.

5.9 Reduction of the Test Model Prediction Uncertainty

According to the probabilistic model validation method described above, a model is considered to be valid if the measurements fall within certain bounds of the uncertainty associated with the predictions from a model of the test. When the uncertainty is high, a measurement might deviate significantly from the predicted mean value but still fall within the acceptance bounds. Under these circumstances one starts to question whether the model is in fact valid or whether the range over which the measurements are allowed to vary is too forgiving.

In order to reduce the risk of accepting an invalid model as valid (Type II error) it is important to reduce the uncertainty associated with the test model predictions as much as possible. This will tighten the margins over which the measurements are considered to be consistent with the model predictions, hence reducing the chances of a measurement falling within the acceptance bounds when the model is invalid.

There are many ways in which the uncertainty associated with the test model predictions can be reduced. For instance, modern techniques such as Computed Tomography (CT) scanning allow the accurate measurement of the geometrical dimensions of the component being tested. This can substantially reduce the uncertainty associated with the definition of the geometrical dimensions in the model and subsequently reduce the uncertainty in the test model predictions.

Nevertheless, the main contributor to the uncertainty in the test model predictions is usually the uncertainty associated with the modelling of the boundary conditions. There is an exception though. The uncertainty associated with the modelling of a free-free

configuration is almost none. In fact this configuration represents a total lack of boundary conditions. For this reason the free-free test configuration should always be the preferred option when validating a supermodel.

One could argue that a component supermodel is ultimately used to provide accurate predictions of the component's behaviour when it is part of a bigger assembly (using hybrid assembly models). According to this argument, it is those predictions that should be validated and not the modal properties of the component in free-free configuration. Nevertheless, it is important to remind ourselves that the real objective when validating a supermodel is to validate the supermodelling techniques and not the model itself. The ultimate use of the component represented by the supermodel is irrelevant.

Also, the natural frequencies should always be used as the preferred responses when validating a model. The measurement uncertainty associated with them is much reduced when compared to the measurement of modeshapes. Again, this minimises the chances of a Type II error (i.e. acceptance of an invalid model).

5.10 Validation Frequency Range

We have established that the free-free configuration is the preferred option to validate a supermodel. Also, the validation of the natural frequency predictions should be given the highest priority due to the small measurement uncertainty they have. Nonetheless we have not established yet the frequency range over which the predictions and the measurements must be consistent with each other to consider the supermodel validated.

The predictions from any model will inevitably deteriorate as the frequency increases. This is mainly due to the non-continuous nature of Finite Element Models. As the natural frequency increases, the modeshapes become more complex and the model's interpolation functions find it increasingly difficult to accurately predict the deformation patterns.

The more refined the model the higher the frequency at which the predictions remain accurate. In the case of a supermodel, its refinement should guarantee accurate predictions even for high-order modes.

Ideally one would like to validate a supermodel up to high frequencies. Nonetheless practical limitations present during testing will inevitably restrict the maximum frequency of the measurements. For instance, when a hammer is used to excite a component during a Modal Test, the energy input will always decay with frequency. Figure 5.25 shows a typical hammer input force auto-spectrum. The input force is reasonably constant up to a certain frequency and then starts to drop quickly.

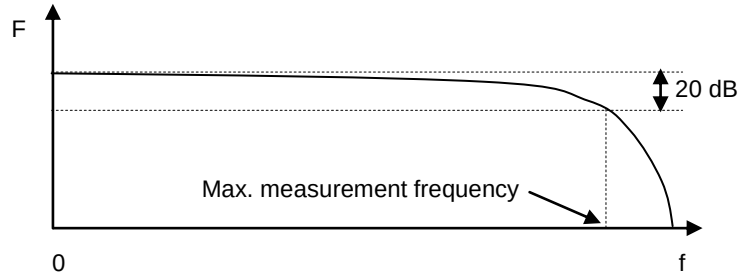

Figure 5.25. Typical hammer input force auto-spectrum.

The lower the input force, the lower the response. At high frequencies, the low signal to noise ratio for both the force and response measurements will result in unacceptably poor measurements. It is common practice to only accept measurements up to a frequency where the input force has decayed 20 dB with respect to the level recorded at low frequencies.

There are ways of increasing the measurement frequency range. For instance, when using a hammer as the excitation method, the lighter the hammer the higher the frequency range. Also, hard tips (e.g. steel) will introduce forces in the structure at higher frequencies when compared to soft tips (e.g. rubber).

The best available measurement equipment should be used in order to validate the supermodel to the highest possible frequency with confidence.

5.11 Case Study - Probabilistic Model Validation

We will now illustrate the probabilistic model validation methods presented in this chapter using an industrial Case Study. The COC supermodel in Figure 5.26 (a), used in

Chapters 2 and 3, will now be validated using physical test data as the reference. Due to time and cost limitations only a single manufactured component was made available for testing, see Figure 5.26 (b).

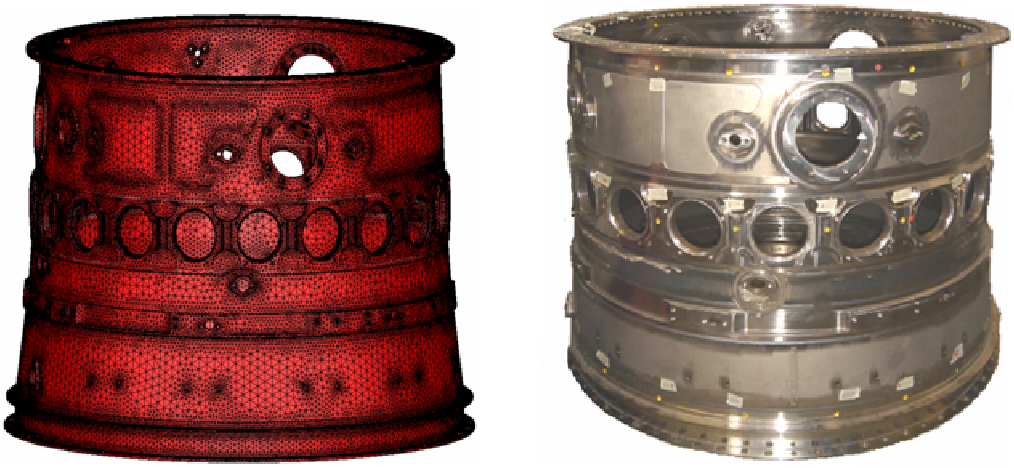

(a) (b)

Figure 5.26. Case Study COC. (a) Supermodel and (b) manufactured component.

5.11.1 Modal Test

A detailed description of the Modal Test and Modal Analysis carried out can be found in reference [67]. We will only highlight here the most important characteristics of the test.

A free-free configuration was the preferred option to reduce the uncertainty in the predictions. This configuration was easily achieved by suspending the component using flexible bungees, see Figure 5.27.

The component was excited at 60 different locations (normal to the surface) using a calibrated hammer. For each excitation, the response was measured (normal to the surface) at six different positions using uniaxial accelerometers. This Modal Test technique is usually referred to as Single Input Multiple Output (SIMO) and is particularly useful to average out noise and accurately measure ‘close’ modes. Figure 5.28 shows the measurement wireframe used.

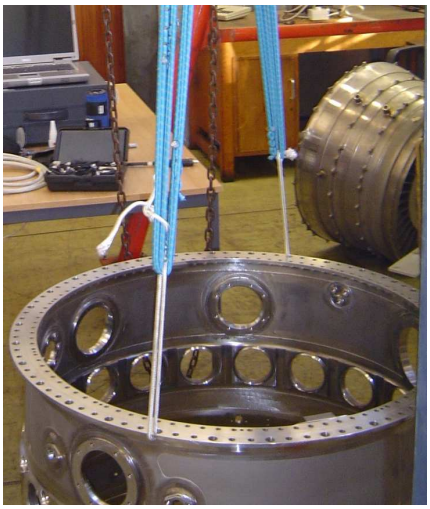

Figure 5.27. Case Study COC. Free-free test configuration.

The smallest hammer available in the test facility was used to maximise the frequency range of the measurements*. After the Modal Analysis, the number of modes measured in the measurement frequency range was 42. Figure 5.29 shows the natural frequency distribution of the measured modes.

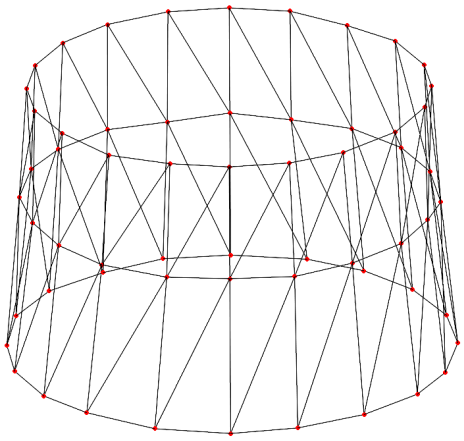

Figure 5.28. Case Study COC. Measurement wireframe.

* The actual measurement frequency range cannot be shared for commercial reasons.

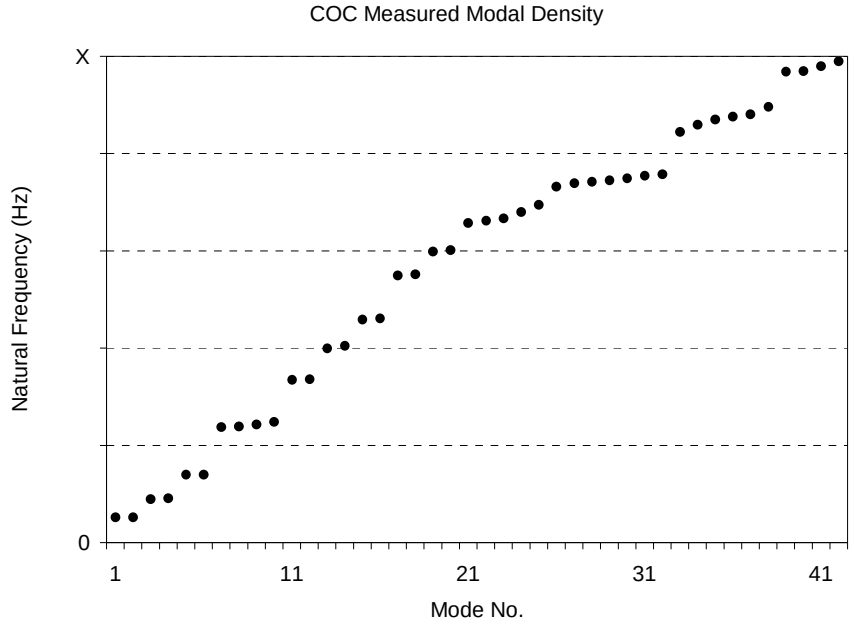

Figure 5.29. Case Study COC. Natural frequency distribution of the measured modes.

Close examination of Figure 5.29 reveals that the low frequency modes come in pairs. At higher frequencies, this pattern is broken and the modes do not appear in pairs anymore. This is typical behaviour of quasi axis-symmetric components like the COC. In these components, the most basic low-frequency modes appear in orthogonal pairs with the two modes at very close frequencies. Figure 5.30 shows the modeshapes corresponding to the first two modes. As the frequency increases, the modes become more localised and are increasingly influenced by the non axis-symmetric features in the component (e.g. holes, bosses, etc.). Figure 5.31 shows the modeshapes corresponding to the modes 41 and 42.

It is also important to point out that the modeshapes associated with the high frequency modes are very intricate, see Figure 5.31. Only highly refined models (e.g. supermodel) have the potential to accurately predict these modes. This gives us confidence that the frequency range covered by the Modal Test is sufficient to validate the supermodel.

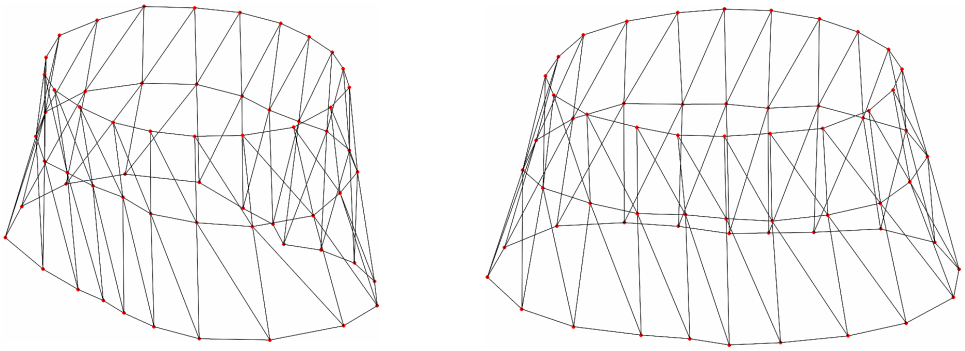

(a) (b)

Figure 5.30. Case Study COC measured modeshapes. (a) Mode 1 and (b) mode 2.

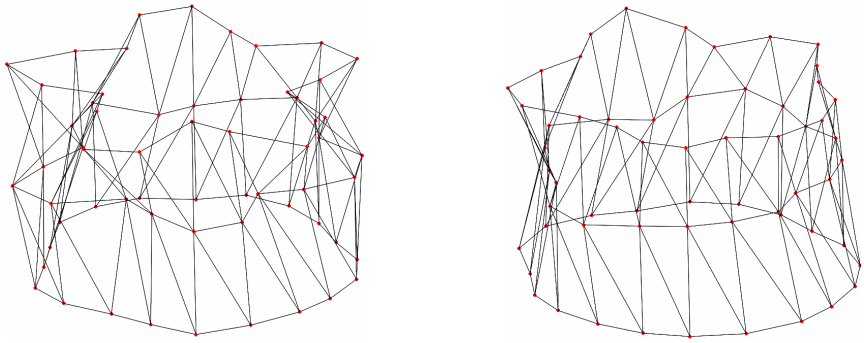

(a) (b)

Figure 5.31. Case Study COC measured modeshapes. (a) Mode 41 and (b) mode 42.

5.11.2 Nominal Model Correlation

Before embarking in the probabilistic validation of the COC supermodel it is interesting to analyse the correlation between the predictions from a nominal model and the Modal test results. This will give us a good first impression of the accuracy of the supermodel.

Figure 5.32 illustrates the natural frequencies predicted from the nominal model. There are a total of 42 modes predicted in the measurement frequency range.

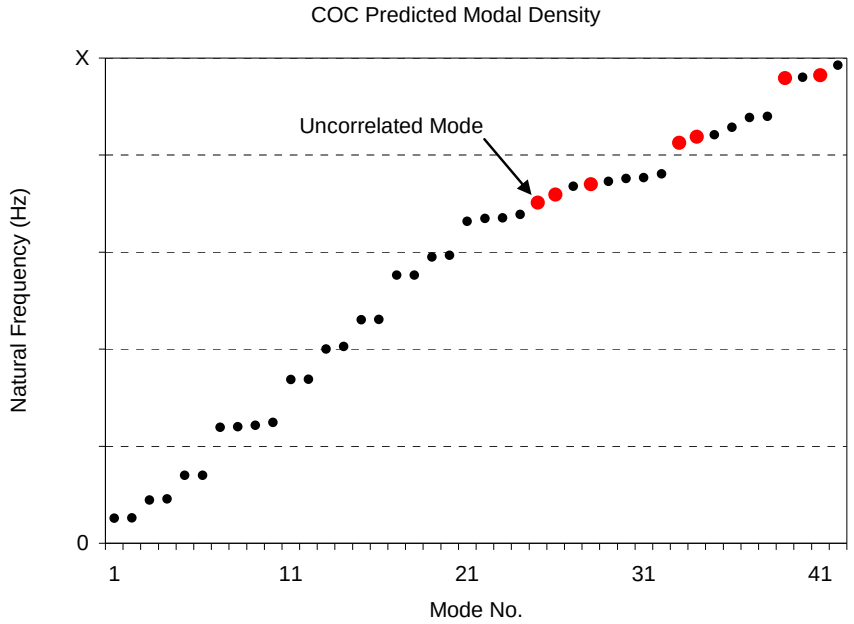

Figure 5.32. Case Study COC. Natural frequency distribution predicted by a nominal model.

This is the same number of modes measured during the test. Moreover, the graph in Figure 5.32 is very similar to that in Figure 5.29 corresponding to the measured modes. This would be considered an encouraging indication that the supermodel is accurate. Nevertheless, when performing a MAC correlation between the predicted and the measured modeshapes, 7 of the predicted modes could not be matched with any of the measured modes (MAC value below a threshold of 30%). Even though there were modes measured at frequencies close to prediction, the predicted and measured modeshapes were different. The red spots in Figure 5.32 identify these uncorrelated modes.

The unmatched modes appear in areas of high modal density. At first one could attribute the lack of correlation to the fact that Modal Analysis can sometimes struggle to provide an accurate estimation of the measured modeshapes when the modes appear in areas of high modal density. Even though this can certainly be a contributing factor to the lack of correlation, we will demonstrate later that it is not in fact the only reason in this case.

Figure 5.33 shows the natural frequency correlation between the nominal predictions and the measurements. Obviously, no correlation is possible for the unmatched modes.

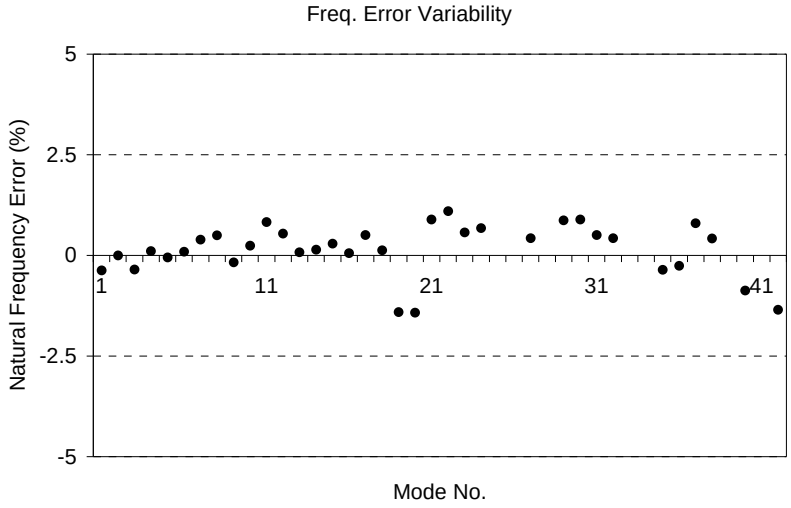

Figure 5.33. Case Study COC. Nominal model, natural frequency correlation.

Again, the remarkable level of correlation (within ±2%) gives us a good first impression of the accuracy of the supermodel.

5.11.3 Model Uncertainty

One would always like to create a supermodel that represents faithfully the actual dimensions, material properties and boundary conditions of the component being tested. These are the so-called model input parameters. A reduction in the uncertainty of these parameters would reduce the uncertainty associated with the predictions. The use of a free-free configuration is a step in the right direction and eliminates the uncertainty due to the boundary conditions. Nonetheless, the actual dimensions and material properties of the test components are only known to vary within certain, well defined, limits (i.e. manufacturing tolerances).

The calculation of the effects that the uncertainty in the input parameters might have on the supermodel predictions (i.e. uncertainty propagation) requires that the supermodel can be modified to reflect different dimensions and material properties. As described in

Section 5.5.1, the creation of a supermodel to reflect a set of model input parameter values is done indirectly. The specified geometrical dimensions are first input into a parametric CAD model to create a geometry model with the right dimensions. This CAD model is then meshed using the appropriate supermodelling techniques. The values for the material properties are added at this stage and the model is ready to be analysed.

In the case of the COC, the parametric CAD model contains 177 of the most important geometrical dimensions that describe this casing. The dimensions were selected based on the manufacturing drawings for this component. The manufacturing drawings also specify the tolerances over which the dimensions will lie. Those are the bounds of the PDFs that characterise the dimensional uncertainties. It is important to highlight that the tolerances in the geometrical dimensions are very tight, in fact, the maximum deviation from nominal allowed is only 0.3 mm and 1° for the longitudinal and angular dimens ions respectively. This means that the bounds in the PDFs are very close indeed.

The actual shapes of the PDFs are not known precisely. Normal distributions are usually considered to provide a good estimation though. The nominal dimensions are selected as the mean values of the distributions. Standard deviations of 0.1 mm and 0.1° were assumed to be appropriate for the longitudinal and angular dimensions respectively. These engineering estimates are believed to be fairly representative of the accuracy of the processes used during the manufacturing of this casing.

The material properties that can vary in the COC supermodel are the Young's modulus, Poisson's ratio and mass density. The limits for their values are specified as a ±2% deviation from the nominal value for Young's modulus and Poisson's ratio and ±1% for density. Again, these tolerances are very tight. The PDFs follow Normal distributions with the mean value corresponding to the material's nominal properties. The standard deviations are 1% of the nominal values. This probabilistic data is usually provided by the Materials Laboratory or Vendor.

In total there are 180 uncertain input parameters in the supermodel, 177 geometrical dimensions and 3 material properties.

5.11.4 Response Metamodels

In general, the calculation of the uncertainty in the predictions from the model of the whole test requires a Monte Carlo Simulation. Unless we are prepared to analyse thousands of supermodels it is best to create a much reduced metamodel for each of the supermodel responses that we plan to validate (i.e. all natural frequencies in the measurement frequency range).

The creation of a metamodel for a given response was described in Section 5.5.4. In very simple terms, the response of interest (e.g. first natural frequency) is predicted for a carefully selected number of combinations of the supermodel's input parameters. The response for any parameter combination is then interpolated using a Response Surface Model (RSM).

The relationship between most of the input parameters in the supermodel and the predicted natural frequencies is highly non-linear. Radial Basis Functions (RBF) are the best suited for the creation of non-linear RSMs (i.e. metamodels). The minimum number of input parameter combinations required to create a RSM using these interpolation functions is 2p+1, where p is the total number of input parameters (i.e. 180 for the COC supermodel).

The nominal COC supermodel predicts 42 modes in the measurement frequency range. The creation of a metamodel corresponding to the natural frequency of a given mode requires a minimum of 361 (i.e. 2x180+1) supermodel predictions. The same combinations of model input parameters can be used for the creation of all 42 RSMs. This means that a minimum of 361 supermodels need to be analysed to provide accurate RSMs for all of the natural frequencies in the measurement frequency range.

In order to improve the accuracy of the metamodels it was decided that an extra 100 combinations would be added to the minimum required, bringing the total number of parameter input combinations to 461.

The 461 input parameter combinations were optimised using the Optimal Latin Hypercube technique [85]. This technique should ensure an even distribution of the combinations across the uncertainty range of the input parameters.

It is important to keep in mind that the order in which the modes appear might be altered when the model input parameters change. This is very common when the modes appear at very close frequencies as it is the case for the COC supermodel. In order to be consistent, all the natural frequency predictions used to create a given frequency response metamodel must correspond to the same mode.

In the case of the COC, the order in which the modes appear for a nominal model was considered to be the datum. For each of the 461 supermodels created, a MAC correlation was performed between the predicted modeshapes and those corresponding to a nominal model. This allowed a match to be made between the modes corresponding to a given parameter combination and those corresponding to the nominal model.

All 461 COC supermodels predicted 42 modes in the measurement frequency range, the same number as in the nominal model. This was not unexpected as the input parameters are only allowed to change over a very small range. Nonetheless, something remarkable was observed for some input parameter combinations. Some of the 42 nominal modeshapes could not be matched to any of the modes predicted by some of the supermodels (MAC value below a threshold of 30%). The blue dots in Figure 5.34 highlight the 13 nominal modes which, at one point or another, could not be matched to any of predicted modes.

Why would some of those 13 modes disappear for some parameter combinations? The answer is simple. All of the 13 “unstable modes” are in areas of high modal density. When two or more modes have very close frequencies the small frequency shifts caused by the parameter changes can result in very big changes to the modeshapes. The nominal modes disappear in favour of new ones. Remember that the total number of modes remained the same (i.e. 42) for all parameter combinations.

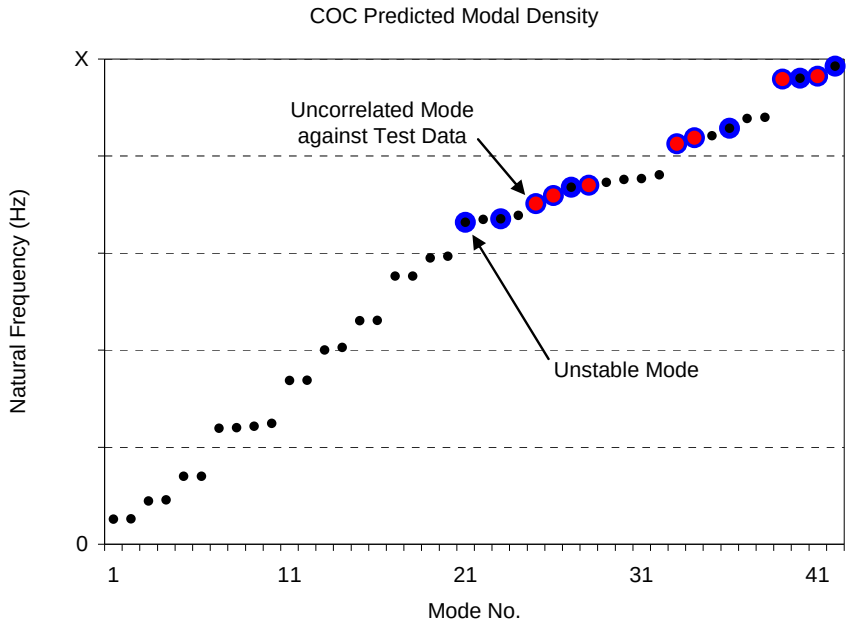

Figure 5.34. Case Study COC. Unstable modes.

The red dots in Figure 5.34 highlight the 7 modes predicted by the nominal supermodel that could not be matched to any of the measured modes. It can be seen that these modes coincide with some of the “unstable” modes. Initially we discussed the possibility that the reason behind the mismatch could be found in the difficulty of Modal Analysis to characterise close modes. Nonetheless, in view of the results above it is far more likely that the 7 modes could not be matched because the actual combination of the dimensions and material properties of the manufactured component tested results in a set of modes of which 7 have a different shape when compared to the nominal component. Unfortunately this can only be demonstrated if a supermodel was created using the exact dimensions and material properties of the component used during the test.

The “unstable modes” cannot be used during the validation of the supermodel. These modes disappear for certain parameter combinations and new ones appear instead. As a result, the natural frequency of an “unstable mode” cannot be evaluated consistently across the whole uncertainty range of the input parameters.

A total of 29 (42-13) metamodels corresponding to the natural frequency predictions of the "stable modes" were created. The supermodel will be considered valid if the natural frequency measurements for the 29 "stable modes" are consistent with the uncertainty associated with the prediction of these modes.

5.11.5 Metamodel Error Uncertainty

The probabilistic characterisation of the approximation error corresponding to a metamodel requires the comparison between the supermodel and the metamodel predictions for a number of input parameter combinations.

Ideally one would like to use many "check samples", however, each of them requires the generation and analysis of a supermodel. In the case of the COC, 100 supermodels were used to estimate the approximation errors of the 29 metamodels. The 100 input parameter combinations were selected using the Optimal Latin Hypercube technique [85].

The reduced number of samples means that it is difficult to characterise the shape of the PDF corresponding to the error introduced by each metamodel. This error will be assumed to follow a normal distribution with a mean of 0% error. The values for the standard deviations are considered to be the same as those calculated for the 100 "check samples", see Table 5.1. It is clear from these figures that the approximation errors are extremely low (within 0.07%). This is a good indication that the metamodels represent accurate approximations of the supermodel predictions.

5.11.6 Measurement Uncertainty

There are too many factors that can influence the measurement errors, these rank from electrical noise to transducer calibration. As explained in Section 5.7, the accurate characterisation of the measurement uncertainty is very difficult in practice.

State-of-the-art equipment was used during the Modal Test of the COC component, and the latest Modal Analysis packages were used to post-process the measured data [67]. Subsequently, one would expect to see only small errors associated with the measurement of the natural frequencies.

The measurement error uncertainty was assumed to be the same for all modes. A Normal distribution with the mean at 0% error, and standard deviation of 0.1% and upper and lower limits at ±1% was considered to provide a realistic estimation of the uncertainty associated with the measurement error.

Mode No.	Metamodel Uncert. σ (%error)	Mode No.	Metamodel Uncert. σ (%error)	Mode No.	Metamodel Uncert. σ (%error)
1	0.053	11	0.050	22	0.053
2	0.052	12	0.052	24	0.062
3	0.058	13	0.055	29	0.050
4	0.058	14	0.054	30	0.066
5	0.051	15	0.047	31	0.069
6	0.051	16	0.056	32	0.070
7	0.055	17	0.054	35	0.057
8	0.051	18	0.057	37	0.058
9	0.060	19	0.051	38	0.052
10	0.059	20	0.065		

Table 5.1. Case Study COC. Metamodel error uncertainty.

5.11.7 Individual Response Validation

The calculation of the uncertainty associated with the 29 natural frequency predictions used for validation followed the process described in Figure 5.20. Each of the responses was considered individually. A total of 5000 Monte Carlo iterations were carried out to characterise the PDFs. These PDFs are shown in Figure 5.35. The natural frequency

deviations with respect to the nominal model predictions are plotted instead of the actual natural frequencies in order to more easily assess the level of variation that could be expected during the test.

All PDFs have well defined upper and lower bounds. It is important to remember that all the geometrical dimensions, material properties and measurement errors considered in the model of the test have upper and lower limits. That is why the predictions only change over a limited range.

The vertical dotted lines represent the upper and lower limits corresponding to a confidence limit of 95%. The vertical red line in each PDF corresponds to the actual measurement recorded during the Modal Test.

All measured natural frequencies sit comfortably within the confidence limits. If we were to validate the supermodel by validating its predictions individually then we could certainly say that the model is valid.

5.11.8 Multiple Response Validation

The shapes of all PDFs in Figure 5.35 are similar to Normal distributions. This means that equations (5.7), (5.8) and (5.9) can be used to calculate whether the measurements fall within the confidence limit when all the responses are considered together.

The process described in Figure 5.20 was followed to calculate the statistical parameters required in equations (5.7) and (5.8). A total of 5000 Monte Carlo iterations were carried out. It is important to keep in mind that during each Monte Carlo iteration all responses must be evaluated together.

The value of r^2 according to equations (5.7) and (5.8) is 22.6. The value of $l^2_{0.95}(29)$ corresponding to 29 responses and a 95% confidence limit is 42.6. The value of r^2 is clearly lower than the value of $l^2_{0.95}(29)$:

$$r^2 = 22.6 < l^2_{0.95}(29) = 42.6 \tag{5.10}$$

According to equation (5.9) this means that the measurements fall within the 95% confidence limit when all responses are considered together. Subsequently the model can be considered valid.

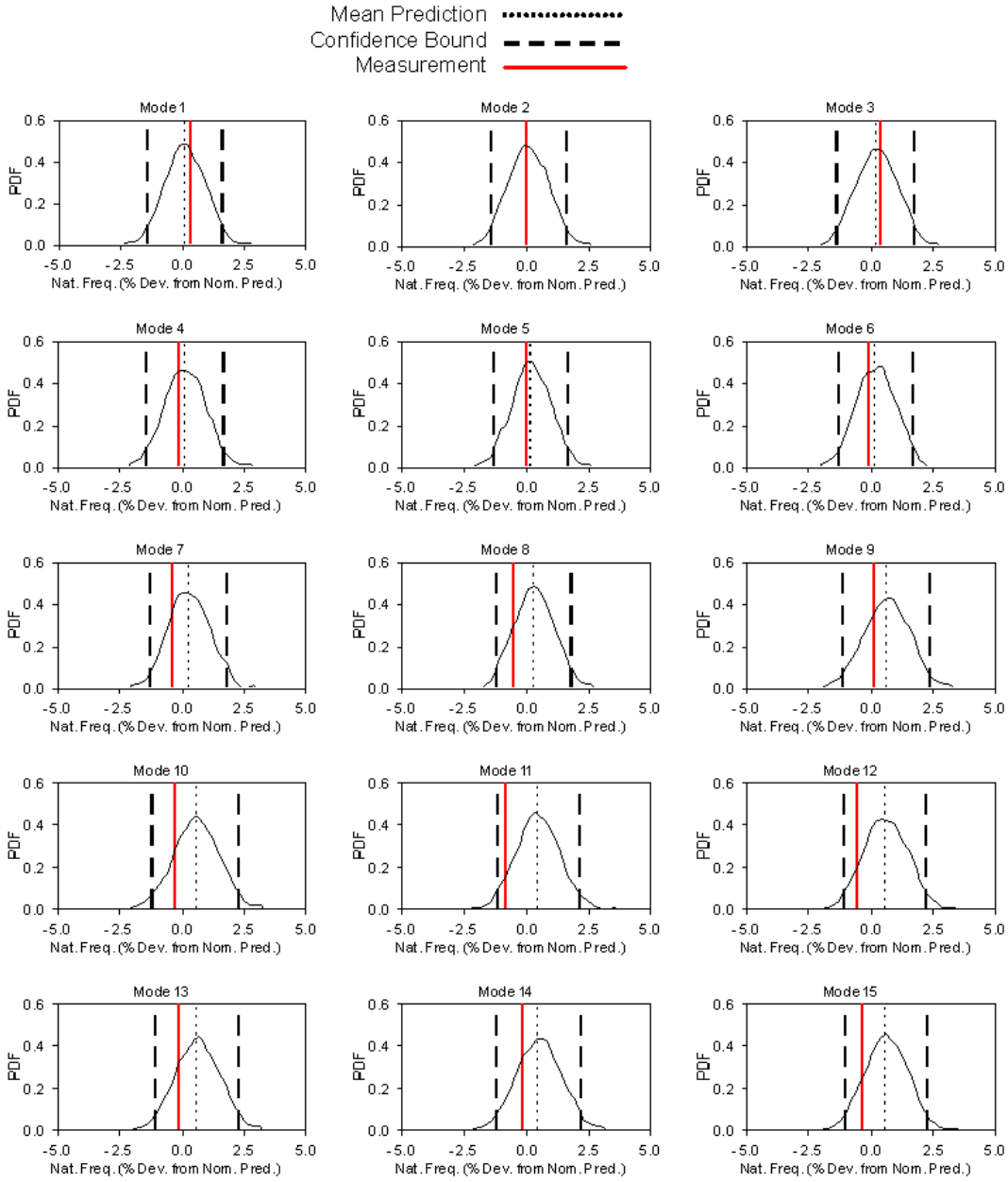
Mean Prediction
Confidence Bound
Measurement
Mode 1
Mode 2
Mode 3
Mode 4
Mode 5
Mode 6
Mode 7
Mode 8
Mode 9
Mode 10
Mode 11
Mode 12
Mode 13
Mode 14
Mode 15
PDF
0.0
0.2
0.4
0.6
-5.0
-2.5
0.0
2.5
5.0
Nat. Freq. (% Dev. from Nom. Pred.)

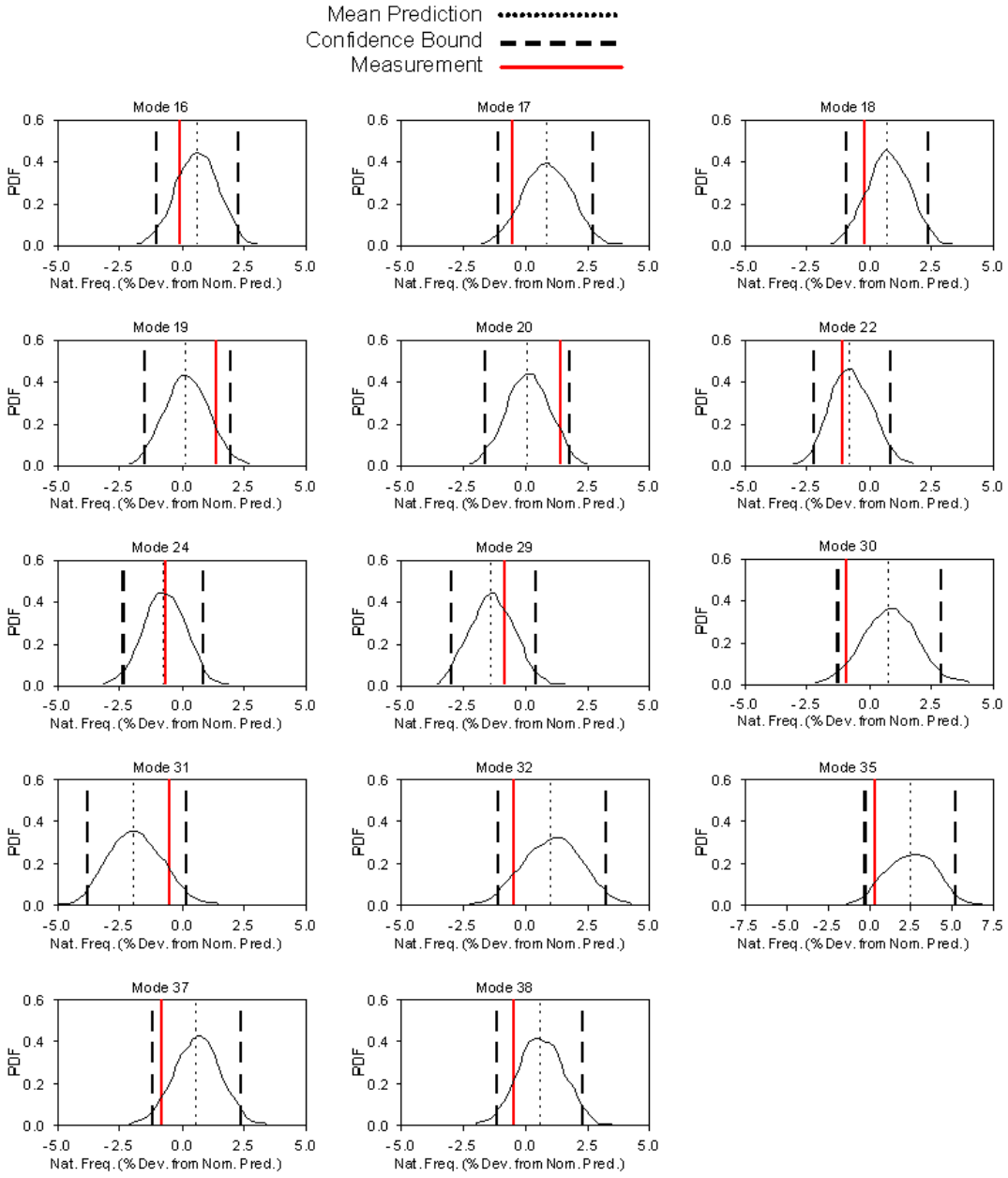

Figure 5.35. Case Study COC. Uncertainty associated with the natural frequency predictions.

5.12 Conclusions

Supermodelling techniques are still in their infancy and further developments will inevitably require physical testing so that the predictions from supermodels can be validated against a reliable reference.

It is important to keep in mind that supermodels are expected to provide predictions whose accuracy can rival that from physical testing, which traditionally has been considered the “true” reference for the validation of design models. As a result, the predictions from a supermodel should be very close to the test measurements before the supermodel can be considered as valid. However, even when a supermodel is flawless, the distance between the predictions and the measurements is unlikely to be zero as the tested components will be subject to manufacturing variability and the measurements will be inevitably corrupted by noise. Under these circumstances, the maximum difference allowed between the measurements and the predictions must be defined in view of the uncertainties associated with both the definition of the supermodel (e.g. geometrical dimensions, material properties, etc.) and those associated with the measurements.

The statistical estimation of the uncertainties associated with the supermodel predictions requires the use of uncertainty propagation techniques capable of analytically determining the uncertainty in the model output predictions (e.g. natural frequencies) from the uncertainties in the model input parameters (e.g. geometrical dimensions and material properties). However, the traditional methods for calculating the propagation of the uncertainty (e.g. Monte Carlo simulation) can be computationally prohibitive when using supermodels. A solution to make use of the Monte Carlo method at a much reduced cost has been proposed in this chapter. This solution is based on creating a computationally efficient, and yet accurate, model of the supermodel (i.e. metamodel) susceptible of being evaluated thousands of times in a matter of seconds.

Hills and Trucano [89] [90] [91] recently presented an efficient method for determining, to a given level of statistical confidence (e.g. 95%), the bounds within which all measurements must fall to consider a supermodel as valid. These bounds are calculated using the probabilistic definition of the uncertainties associated with the model predictions and the test. This method has been illustrated in this chapter by

validating the supermodel of the COC previously used in Chapters 2 and 3. The measured data from a Modal Test invariably fell within the bounds specified by a confidence limit of 95% (i.e. confidence limit commonly used when there is only data from a single test). As a result, the supermodel was deemed valid with a 95% confidence.

Chapter 6 - Conclusions and Future Work

6.1 Overall Conclusions

The role of simulation tools during the design cycle of new products has rapidly increased over the years. In the aeroengine industry, the bulk of any new engine design takes place in a virtual environment where simulation tools are used in the pursuit of an optimised solution. Traditionally, the validation of the models used to drive the design has had to wait until physical prototypes become available for testing. This usually happens late in the development cycle when any redesign would incur serious time and cost penalties to the project.

This thesis has presented a novel methodology that facilitates the validation of complex assembly models (e.g. WEM) used for structural dynamic analysis early in the design cycle, even before manufactured prototypes become available for testing. The new methodology starts with a prioritisation of the most important components in the assembly using a novel approach which makes use of sensitivity analysis methods. Each of the most relevant component design models (typically less than one tenth of the total number of components in an aeroengine) is then validated using the corresponding supermodel as the reference according to a new technique which ensures that the predictions from the supermodel correspond to the component as part of the assembly and not when it is in isolation. This is achieved by replacing the component design model in the original assembly by its corresponding supermodel to create a so-called “hybrid assembly model”.

This new validation approach overcomes current technology limitations which restrict the use of supermodels to components modelled in isolation and reduces the validation of complex assembly models to the validation of only a few of its constituent

components. Moreover, the virtual nature of this approach means that complex assembly models can be validated at almost no financial cost and with few time penalties, hence satisfying the original target specified in Section 1.4 of reducing by an order of magnitude the cost and timescales currently associated with the validation of complex assembly models used in the aeroengine industry, which historically have required extensive test programmes.

The concept of a supermodel was introduced only a few years ago [1] and, as a result, supermodelling techniques are still in their infancy. The development of these techniques inevitably requires physical testing as the reference and appropriate model validation methods. A robust method for the validation of supermodels has been outlined in this thesis. This method makes use of probabilistic techniques to specify the bounds within which all measurements must fall to consider a supermodel valid.

This chapter will review some of the specific conclusions drawn in this thesis, some of which come from the application of the proposed techniques to industrial Case Studies. This will be followed by a summary of contributions, suggestions for future work and some closing remarks from the author.

6.2 Specific Conclusions

Detailed individual conclusions for each of the topics covered in this thesis have already been presented throughout the previous chapters. The following sections highlight some of the most important conclusions drawn from this work in line with the original objectives described in Section 1.4.

6.2.1 Component Prioritisation

Currently-available computing power restricts the use of supermodels to components modelled in isolation. This means that complex assembly design models (e.g. WEM) cannot be validated against full-scale assembly supermodels. An alternative is to validate the assembly model by validating each of its constituent components individually. However, a complex assembly can comprise hundreds of components which means that hundreds of supermodels would be required. For some time to come, supermodels will run on the limits of the available computing power and the creation and

analysis of hundreds of supermodels will take a considerable amount of time and computing resources, thereby limiting the potential advantages of supermodels over physical testing.

A new approach has been presented in this thesis to reduce the validation of complex assembly models to the validation of just a few of its constituent components. Sensitivity contour plots are used to identify the regions in the assembly model where modelling errors could have the biggest effect in the accuracy of the predictions. The design models of the components describing those regions are given the highest priority for validation. The new method is also capable of quantitatively assessing the contribution of each of the components to the accuracy of the assembly predictions, hence reducing the subjectivity traditionally associated with the selection of the target components for validation.

It is estimated that, for the case of an aeroengine, the application of the proposed method could reduce the validation of the corresponding WEM to the validation of less than a tenth of its constituent components.

6.2.2 Validation of Individual Components

When validating a component design model which is part of a bigger assembly it is important that the model performs well when it is part of the assembly and not just when it is considered in isolation. Over the years a few methods have been proposed to design test configurations in which to validate component design models. All these methods are constrained by the fact that they only consider using physical testing as the reference data for model validation. This usually results in complex test configurations which are either very expensive, very difficult to achieve in practice, or both.

The virtual platform provided by supermodels means that the traditional constraints of physical testing do not apply any more when validating a component design model. A new method has been proposed to validate a component design model using its corresponding supermodel as the reference while ensuring that the validated model performs well when it is part of the assembly model.

The method consists of substituting the original component design model in the assembly by its corresponding supermodel. This results in a so-called “hybrid assembly

model" where the supermodel is linked to the rest of the components in the assembly. The predictions from the supermodel under these conditions correspond to the behaviour expected from the component when it is part of the assembly. This is the behaviour that the component design model must predict accurately to be considered valid and hence it represents the ideal reference data for validation.

This method was demonstrated using a Case Study consisting of three quasi-cylindrical aeroengine casings bolted together. The assembly model comprised of "virtually" validated component design models showed a worst natural frequency error of around 6.5% when compared against the measurements from a Modal Test. The original assembly model would have shown a 15% natural frequency error when compared against the measurements, had it not been validated using supermodels as the reference. Even though the "virtually" validated assembly model represents a significant improvement with respect to the original model, it is difficult to attribute a natural frequency error of 6.5% to deviations of the manufactured hardware with respect to nominal or to measurement errors.

A detailed study concluded that the source of discrepancy between the predictions from the "virtually" validated assembly model and the measurements from the Modal Test were attributable to the fact that the effects of component interfaces (i.e. joints) had been neglected during the validation process.

6.2.3 Influence of Joints

An assessment of the effects of joints in the dynamic behaviour of assemblies concluded that the modelling of the interfaces between components using rigid links is not appropriate for the general case. The flexibility of the joints must be modelled properly if a valid assembly model is sought.

The validation strategy proposed in this thesis can equally cope with the presence of joints. This simply requires considering a joint as any other component in the assembly, and, as for any other component, the design model of a joint should be validated against its corresponding supermodel. However, supermodelling techniques for joints are almost non-existent. This is mainly due to the fact that the underlying physics that drives the behaviour of joints is not completely understood. Unfortunately, this means that physical testing is still the only reliable option to validate the design model of a joint at this time.

A modified version of the original validation strategy has been proposed to cope with the presence of joints until supermodelling of joints becomes a reality. The approach is simple, the design models of the components in the assembly are validated first using their corresponding supermodels as the reference. This is followed by the validation of the design model of the joints when physical test data becomes available. This represents a temporary compromise of the proposed validation strategy where most of the validation work can be done in a virtual environment well ahead of manufacture and the fine tuning of the joint models is carried out once physical test data becomes available.

The implementation of this method to the Case Study consisting of three quasi-cylindrical aeroengine casings resulted in a worst natural frequency correlation of only 2.5% between the predictions from the validated assembly model and the measurements from a Modal Test. This level of correlation is in line with expectations considering that the tested structure will invariably deviate from nominal and that measurements are subject to noise. Moreover, this level of correlation represents a significant improvement with respect to the 6.5% error obtained when validating the assembly model using supermodels as the reference but neglecting the influence of the joints.

6.2.4 Implementation of the Assembly Model Validation Strategy in Industry

The overall validation strategy proposed in this thesis has been demonstrated on a real industrial Case Study consisting of a sub-assembly comprised of some of the most challenging structural components in an aeroengine. This validation exercise was carried out as part of an actual certification programme whose tight cost and time constraints represent the ideal scenario to demonstrate whether any new technology is ready for deployment into industry.

The bulk of the validation took place in a virtual environment where the most relevant components in the assembly were identified using the novel sensitivity-based methods and then validated using hybrid assembly models as the reference. Once manufactured prototypes became available, the results from a Modal Test were used to fine tune the original design models of the joints.

The worst natural frequency error from the validated assembly model was less than 2% when compared against measurements. This remarkable level of correlation was well within the 5% limit required to successfully achieve certification. Interestingly, the original assembly model would have failed the certification requirements, had it not been validated, with a worst natural frequency error of 20%.

6.2.5 Validation of Supermodels

The use of supermodels is central to the methodology proposed in this thesis for the validation of assembly models. However, supermodelling techniques were only introduced a few years ago and their development will inevitably require physical testing and appropriate methods to validate supermodels.

Supermodels are expected to provide predictions whose accuracy can rival that of the measurements from physical tests. As a result, one should expect a very close match between the predictions from a supermodel and the test measurements to consider the supermodel valid. However, even when a supermodel has been created using perfect modelling techniques, the differences between prediction and measurement will never be zero. First and foremost, it is most unlikely that the supermodel and the actual test specimens will have exactly the same dimensions and material properties. That does not mean that the supermodel is wrong, it simply means that what has been modelled differs from what has been tested. Also, physical testing is invariably subject to measurement errors which can be minimised through careful practice but can never be removed completely.

The traditional approach to model validation would be to consider the supermodel as valid if the distance between the predictions and the measurements is below a specified threshold. The selection of this threshold is typically based on “what looks reasonable” considering the manufacturing tolerances of the tested specimens, the estimated measurement errors and, most importantly, the modelling error allowance. This approach might be acceptable for the validation of coarse models where the modelling error allowance is typically high in comparison with the variation expected due to the manufacturing tolerances or the measurement errors. However, supermodels are expected to serve as a reliable substitute of physical testing during the validation of assembly models. For this reason the modelling error allowance is almost none. This

means that the differences between the predictions and the measurements must be fully explained before the model is considered to be valid.

Some of the causes of the discrepancies between the supermodel predictions and the measurements can only be understood in probabilistic terms. As a result, it was concluded that a probabilistic approach would be best suited to validate supermodels. A robust method was presented in the thesis capable of determining the bounds within which all measurements must fall to consider the supermodel valid. Those bounds depend on the uncertainties associated with the model predictions (e.g. due to dimensional and/or material variability), those linked to the test measurements and the statistical confidence required for the validation (e.g. 95%).

This method was illustrated by validating the supermodel of an aeroengine casing using the measurements from a Modal Test as the reference. All measurements fell within the bounds prescribed by the proposed validation method which corresponded to a specified confidence limit of 95% and, as a result, the supermodel was deemed valid.

6.3 Summary of Contributions

- A novel methodology for the validation of complex assembly design models early in the design cycle, even before manufacture, has been presented. This methodology consists of validating the assembly model by validating a reduced number of its constituent component design models using their corresponding supermodels as the reference.
- A new method has been presented for the identification of those component design models in the assembly in most urgent need of validation. This method consists of identifying the regions in the assembly model which are most sensitive to modelling errors. The component design models describing those areas are given the highest priority for validation.
- A new method for the validation of individual component design models using supermodels as the reference has been proposed. This method consists of replacing the original component design in the assembly by its corresponding supermodel. This results in a so-called hybrid assembly model where the

predictions from the supermodel correspond to the component as part of the assembly and, subsequently, the ideal reference for validation.

- It has been shown how an assembly model made up of valid component design models might still yield inaccurate predictions if the joints between components are considered to be rigid. A preliminary study demonstrated how the flexibility of joints can affect the accuracy of the predictions from an assembly model.

  A solution to incorporate the effects of joints into the assembly model validation strategy has been proposed. This method first validates the most relevant component design models using their corresponding supermodels as the reference and then fine tunes the design models of the joints when physical test data becomes available. This is a viable approach to take until reliable supermodels of joints become available.

- It has been demonstrated that the overall strategy for the validation of complex assembly models performs well under the pressures of a highly demanding industrial scenario (i.e. aeroengine certification programme). As a result, the methodology is considered to be well-suited for full-scale deployment into industry.

- An efficient method for the validation of supermodels has been reviewed. This method takes a probabilistic approach to model validation and is able to determine the validity of a supermodel depending on whether the measurements fall within the expected uncertainty associated with the predictions.

6.4 Suggestions for Future Work

6.4.1 Supermodels

The use of supermodels is central to the validation strategy proposed in this work. However, supermodelling techniques are still in their early days and there are still not robust methods for the generation of reliable supermodels for all components.

Moreover, most of the efforts so far have been concentrated on the generation of supermodels for homogeneous isotropic components. Non-isotropic materials such as Carbon Fibre Reinforced Plastics are increasingly being used in industry. Techniques will soon be required for the creation of supermodels of components made from such materials.

6.4.2 Joint Modelling

The modelling of joints remains seriously underdeveloped. This is mainly due to the fact that most of the research work directed at improving the modelling of assemblies has focussed, almost exclusively, on reducing the sources of error associated with the models of components. Now that supermodels are capable of reducing the errors in component models to the same level expected from manufacturing variability, joints have become the weakest link in the modelling of assemblies.

Unfortunately, the physics that drive the dynamic behaviour of joints are not yet well understood and, as a result, joint models are typically quite poor. A significant amount of research will be required to first understand the physics behind the behaviour of joints and then to translate the physics into reliable models.

6.4.3 Probabilistic Model Validation

The reliability of the probabilistic methods for the validation of models largely depends on the ability to identify and characterise the sources of uncertainty present during the validation tests. This can be difficult and imprecise at times.

The main uncertainties associated with a model validation have their origins in the manufacturing variability and the test measurement errors. The correct characterisation of the manufacturing variability will require a better understating of the manufacturing processes and how they influence on the characteristics of the final products. The accurate characterisation of the uncertainty in the measurements will require a much better understanding of the sources of the measurement errors, their statistical properties and how they propagate through the measurement process.

6.4.4 Forced Response Validation

The research work presented in this thesis has focussed on the validation of assembly models so that a set of natural frequencies and modeshapes are accurately predicted. These modal properties only depend on the stiffness and mass matrices of the FEM. The proposed methodology should be extended to facilitate the validation of assembly models so that they are capable of accurately predicting the more general forced response case. This will require methods to accurately validate both the damping factors used in the assembly model and the force vectors used to characterise the loads.

6.4.5 Other Applications

This thesis has focused on the validation of assembly models used in the aeroengine industry. Most of the methodologies presented here can obviously be applied to other engineering fields, most notably Aerospace and Automotive.

A range of representative Case Studies will need to be evaluated using the proposed methods to establish their strengths and weaknesses for the general case.

6.5 Closing Remarks

The overall objective of this research work was to develop a suitable methodology that would facilitate the validation of complex assembly models early in the design cycle when manufactured prototypes are still not available. It is believed that the proposed validation approach represents a viable solution to satisfy this objective.

The virtual nature of the proposed methodology can potentially eliminate a great deal of the physical tests currently required to validate a complex assembly model. In fact, it is estimated that the implementation of this technology in the aeroengine industry could reduce the amount of testing currently required for the validation of assembly models by an order of magnitude. However, it is important to keep in mind that the transition towards a virtual validation scenario must be done gradually. This technology is still in its infancy and the elimination of physical testing should only be attempted when there is sufficient and unequivocal evidence that a virtual validation is reliable. That evidence will typically come from previous projects of similar characteristics where the virtually

validated models consistently fare well when compared against the measurements from physical tests. This highlights the important role that physical testing will play in the implementation of virtual validation methods. Moreover, well-planned physical testing remains essential to further improve supermodelling techniques and expand them into to areas which still remain largely underdeveloped (e.g. joints).

References

[1] Fotsch, D. W. Development of Valid FE Models for Structural Dynamic Design. *PhD Thesis, Imperial College London,* 2001.

[2] Rosenbrock, H. H. Sensitivity of an Eigenvalue to Changes in the Matrix. *Electronics Letters,* vol. 1, pages 278-279, 1965.

[3] Morgan, B. S. Computational Procedure for the Sensitivity of an Eigenvalue. *Electronic Letters,* vol. 2, pages 197-198, 1966.

[4] Reddy, D. C. Sensitivity of an Eigenvalue of a Multivariable Control System. *Electronic Letters,* vol. 2, page 446, 1966.

[5] Nelson, R. Simplified calculations of eigenvector derivatives. *AIAA Journal,* vol. 14, pages 1201-1205, 1976.

[6] Fox, R. and Kapoor, M. Rate of Change of Eigenvalues and Eigenvectors. *AIAA Journal,* vol. 6, pages 2426-2429, 1968.

[7] Ojalvo, I. and Zhang, L. M. Efficient Eigenvector Sensitivities by a New Procedure Based on Lanczos Vectors. *AIAA Journal,* pages 2392-2394, 1996.

[8] Wang, B. Improved Approximate Methods for Computing Eigenvector Derivatives in Structural Dynamics. *AIAA Journal,* vol. 29, no. 6, pages 1018-1020, 1990.

[9] Liu, Z. and Zhao, Y. An Accurate Method for Computing Eigenvector Derivatives of Free-Free Structures. *Computers and Structures,* vol. 52, no. 6, pages 1135-1143, 1994.

[10] Géradin, M. and Rixen, D. Mechanical Vibrations. Theory and Application to Structural Dynamics. *John Wiley & Wiley and Sons,* 1994.

[11] Balmés, E. Parametric Families of Reduced Finite Element Models. Theory and Applications. *Mechanical Systems and Signal Processing,* vol. 10, no. 4, pages 381-394, 1996.

[12] Allemang, R. J. and Brown, D. L. A Correlation Coefficient for Modal Vector Analysis. *Proceedings of the 1st International Modal Analysis Conference, IMAC,* pages 110-116, 1982.

[13] Adelman, H. M. and Haftka, R. T. Sensitivity Analysis of Discrete Structural Systems. *AIAA Journal,* vol. 24, no. 5, pages 823-832, 1986.

[14] Friswell, M. I. The Derivatives of Repeated Eigenvalues and Their Associated Eigenvectors. *Journal of Vibration and Acoustics,* vol. 118, pages 390-397, 1996.

[15] Zhang, D. W. and Wei, F. S. Computation of Eigenvector Derivatives with Repeated Eigenvalues Using a Complete Modal Space. *AIAA Journal,* vol. 33, pages 1749-1753, 1995.

[16] Ojalvo, I. U. Efficient Computation of Mode-Shape Derivatives for Large Dynamic Systems. *AIAA Journal,* vol. 25, no. 10, pages 1386-1390, 1987.

[17] Mills-Curran, W. C. Calculation of Eigenvector Derivatives for Structures with Repeated Eigenvalues. *AIAA Journal,* vol. 26, no. 7, pages 867-871, 1988.

[18] Mills-Curran, W. C. Comment on Eigenvector Derivatives with Repeated Eigenvalues. *AIAA Journal,* vol. 28, no. 10, page 1846, 1990.

[19] Dailey, R. L. Eigenvector Derivatives with Repeated Eigenvalues. *AIAA Journal,* vol. 27, no. 4, pages 486-491, 1989.

[20] Lallement, G. and Kosaneck, J. Parametric Correction of Self Adjoint Finite Element Models in the Presence of Multiple Eigenvalues. *Proceedings of Modern Practice in Stress and Vibration Analysis,* pages 593-603, 1993.

[21] Juang, J. N., Ghaemmaghami, P. and Lim, K. B. Eigenvalue and Eigenvector Derivatives of a Nondefective Matrix. *Journal of Guidance, Control and Dynamics,* vol. 12, no. 4, pages 480-486, 1989.

[22] Bernard, M. L. and Bronowicki, A. J. Modal Expansion Method for Eigensensitivity with Repeated Roots. *AIAA Journal,* vol. 32, no. 7, pages 1500-1506, 1994.

[23] Akgün, M. A. New Family of Modal Methods for Calculating Eigenvector Derivatives. *AIAA Journal,* vol. 32, no. 2, pages 379-386, 1994.

[24] CERES - Cost Effective Rotordynamics Engineering Solutions. *European Union Research Project - Framework V,* Project No. GRD1-1999-10388, 2000-2003

[25] Lenoir, D. and Cogan S. Engine Model Sensitivity Assessment Procedure. *CERES, Project No. GRD1-1999-10338,* Deliverable 2.1.1-1, 2001.

[26] Craig, R. R. and Bampton, M. C. C. Coupling of Substructures for Dynamic Analysis. *AIAA Journal,* vol. 6, pages 1313-1319, 1968.

[27] Doltsinis, I. Stochastic Analysis of Multivariate Systems in Computational Mechanics and Engineering. *International Center for Numerical Methods in Engineering (CIMNE),* 1999.

[28] Rencher, A. C. Methods of Multivariate Analysis. *John Wiley and Sons,* 1995.

[29] Friswell, M. I. and Mottershead J. E. Finite Element Model Updating in Structural Dynamics. *New York: Kluwer Academic Publisher,* 1995.

[30] Berman, A. and Nagy, E. J. Improvement of a Large Analytical Model Using Test Data. *AIAA Journal,* vol. 21, no. 8, pages 1168-1173, 1983.

[31] Ewins, D. J. Modal Testing: Theory, Practice and Application. Second Edition. *Research Studies Press Ltd.,* 2000.

[32] Chen, G. FE Model Validation for Structural Dynamics. *PhD Thesis, Imperial College London,* pages 98-142, 2001.

[33] O'Callahan, J., Avitabile, P. and Riemer, R. System Equivalent \\\reduction Expansion Process. *Proceedings of the 7th International Modal Analysis Conference, IMAC,* pages 29-37, 1989.

[34] He, J. Identification of Structural Dynamics Characteristics. *PhD Thesis, Imperial College London,* 1987.

[35] Lin, R. M. Identification of the Dynamic Characteristics of Non-linear Structures. *PhD Thesis, Imperial College London,* 1991.

[36] Link, M. and Zhang, L. Experience with Different Procedures for Updating Structural Parameters of Analytical Models Using Test Data. *Proceedings of the 10th International Modal Analysis Conference, IMAC*, 1992.

[37] Link, M., Rohrmann, R. G. and Pietrzko, S. Experience with Automated Procedures for Adjusting the Finite Element Model of a Complex Highway Bridge to Experimental Modal Data. *Proceedings of the 13th International Modal Analysis Conference, IMAC,* pages 1063-1070, 1996.

[38] Mottershead, J. E. and Foster, C. D. On the Treatment of Ill-conditioning in Spatial Parameter Estimation from Measured Vibration Data. *Mechanical Systems and Signal Processing,* vol. 5, no. 2, pages 139-154, 1991.

[39] Natke, H. G. On Regularisation Methods Applied to the Error Localisation of Mathematical Models. *Proceedings of the 9th International Modal Analysis Conference, IMAC,* pages 70-73, 1991.

[40] Collins, J., Hart, G., Hasselman, T. and Kennedy, B. Statistical Identification of Structures. *AIAA Journal,* vol. 12, no. 2, pages 185-190, 1974.

[41] VIVACE - Value Improvement through a Virtual Aeronautical Collaborative Enterprise). *European Union Research Project - Framework VI,* Project No. AIP3-CT-2003-502917, 2004-2007.

[42] Neibal, N. Experimental System Identification for Experimental / Analytical Correlation and Modelling. *ASME,* AMD, vol. 67, 1985.

[43] Admire, J. R., Tinker, M. L. and Ivey, E. W. Mass-Additive Modal Test Method for Verification of Constrained Structural Models. *AIAA Journal,* vol. 31, no. 11, pages 2148-2153, 1993.

[44] Karpel, M. and Ricci, S. Experimental Modal Analysis of Large Structure by Substructure. *Mechanical Systems and Signal Processing,* vol. 11, no. 2, pages 245-256, 1997.

[45] Gwinn, K. W., Lauffer, J. P. and Miller, A. K. Component Mode Synthesis Using Experimental Modes Enhanced by Mass Loading. *Proceedings of the 6th International Modal Analysis Conference, IMAC,* pages 1088-1093, 1988.

[46] McGowan, P. E., Edighoffer, H. E. and Wallace, J. W. Development of an Experimental Space Station Model for Structural Dynamics Research. *National Aeronautics and Space Administration, NASA,* Technical Memorandum 102601, 1990.

[47] Ghosh, T., Wilson, J. and Chang, J. Model Validation and Testing of International Space Station Structures Using MSC/NASTRAN. *Proceeding of the MSC Aerospace Users' Conference,* pages 1399-1345, 1999.

[48] Perinpanayagam, S. Modal Test Strategy for Early Model Validation of Practical Engineering Structures. *PhD Thesis, Imperial College London,* 2004.

[49] Garcia, J. V. and Ewins, D. J. Test Strategy for Aero-engine Structural Dynamic Model Validation. *Proceedings of the International Seminar on Modal Analysis, ISMA,* pages 2175-2190, 2006.

[50] Atluri, S. N. On Hybrid Finite-element Models in Solid Mechanics. *Proceedings of the International Symposium: Advances in Computer Methods for Partial Differential Equations,* pages 346-355, 1975.

[51] Aminpour, M. A., Ransom, J. B. and McCleary, S. L. A Coupled Analysis Method for Substructures with Independently Modelled Finite Element Subdomains. *International Journal of Numerical Methods in Engineering,* vol. 38, pages 3695-3718, 1995.

[52] Park, K. C., Felippa, C. A. and Rebel, G. A Simple Algorithm for Localized Construction of Nonmatching Structural Interfaces. *International Journal for Numerical Methods in Engineering,* vol. 53, pages 2117-2142, 2002.

[53] Park, K. C. Partitioned Formulation with localised Lagrange Multipliers and its Applications. *Proceedings of the 6th International Conference on Structural Dynamics, EURODYN,* pages 67-76, 2005.

[54] Puso, M. A. A 3D Mortar Method for Solid Mechanics. *International Journal for Numerical Methods in Engineering,* vol. 59, pages 315-336, 2003.

[55] Liao, C. L., Reddy, J. N. and Engelstad, S. P. A Solid-shell Transition for Geometrically Non-Linear Analysis of Laminated Composite Structures. *International Journal of Numerical Methods in Engineering,* vol. 26, pages 1843-1854, 1988.

[56] Davila, C. G. Solid-to-shell Transition Elements for the computation of Interlaminar Stresses. *Computing Systems in Engineering,* vol. 5, no. 2, pages 193-202, 1994.

[57] Dohrman, C. R., Key, S. W. and Heinstein, M. W. Methods for Connecting Dissimilar Three-dimensional Finite Element Meshes. *International Journal for Numerical Methods in Engineering,* vol. 48, pages 1057-1080, 2000.

[58] McCune, R. W., Armstrong, C. G. and Robinson D. J. Mixed-dimensional coupling in finite element models. *International Journal of Numerical Methods in Engineering,* vol. 49, no. 6, pages 725-750, 2000.

[59] Monoghan, D. J. Automatically Coupling Elements of Dissimilar Dimension in Finite Element Analysis. *PhD Thesis, The Queen's University of Belfast*, 2000.

[60] Monoghan, D. J., Lee, K. Y, Armstrong, C. G and Ou H. Mixed Dimensional Finite Element Analysis of Frame Models. *Proceedings of the 10th International Offshore and Polar Engineering Conference,* vol. 4, pages 263-269, 2000.

[61] Monoghan, D. J. and Armstrong, C. G. Mixed Dimensional Coupling for Efficient Structural Finite Element Analyses. *Proceedings of the 8th Association for Computational Mechanics in Engineering Conference, ACME,* pages 28-31, 2000.

[62] Shim, K. W., Monaghan, D. J. and Armstrong, C. G. Mixed Dimensional Coupling in Finite Element Stress Analysis. *Journal of Engineering with Computers,* vol. 18, no. 3, pages 241-252, 2004.

[63] Baker, P. Finite Element Meshing of the Use Case Intermediate Casing Model in Support of the Creation of Fit-for-purpose Supermodels. *VIVACE, Project No. AIP3-CT-2003-502917,* deliverable D2.3.3.2_4, 2006.

[64] Loyer, J. Fitness-for-purpose Guidelines for the Generation of WEM Supermodels. *VIVACE, Project No. AIP3-CT-2003-502917,* technical report TR2544, 2007.

[65] Chan, D. S. H. Correlation of Aircraft Engine Model Using Experimental Modal Analysis. *In the Proceedings of the 7th ITToMM Conference on Rotor Dynamics,* paper ID 338, 2006.

[66] Chen, G, Fotsch, D., Imamovic, N. and Ewins, D. J. Correlation Methods for Axisymmetric Structures. *Proceedings of the 18th International Modal Analysis Conference, IMAC,* pages 1006-1012, 2000.

[67] Peeters, B., Mosenich, L. and Ghiglione, D. VIVACE Task 2.3.2 Use Case Test Report. *VIVACE, Project No. AIP3-CT-2003-502917,* deliverable D2.3.2.3_2, 2007.

[68] Brownlee, K. A. Statistical Theory and Methodology in Science and Engineering. *John Wiley & Sons Inc.,* 1965.

[69] Miller, I. and Freund, J. E. Probability and Statistics for Engineers. *Prentice-Hall Inc.,* 1985.

[70] Beck, J. V. and Arnold, K. J. Parameter Estimation in Engineering and Science. *John Wiley & Sons Inc.,* 1977.

[71] Reckhow, K. H., Clements, J. T. and Dodd, R. C. Statistical Evaluation of Mechanistic Water Quality Models. *Journal of Environmental Engineering,* vol. 116, no. 2, pages 250-268, 1990.

[72] Dodge, Y. and Marriot, F. H. C. The Oxford Dictionary of Statistical Terms. *Published by Oxford University Press on behalf of the International Statistical Institute,* 2003.

[73] Halton, J. H. On the Efficiency of Certain Quasi-Random Sequences of Points in Evaluating Multi-Dimensional Integrals. *Numerische Mathematik,* no. 2, pages 84-90, 1960.

[74] Hammersley, J. M. Monte Carlo Methods for Solving Multivariate Problems. *Annals of the New York Academy of Sciences,* no. 86, 1960.

[75] Hammersley, J.M. and Handscomb, D.C. Monte Carlo Methods. *Chapman and Hall,* 1964.

[76] Owen, A. B. Latin Hypercube Sampling for Very High Dimensional Simulation. *ACM Transactions on Modelling and Computer Simulation,* vol. 8, no. 1, pages 71-102, 1998.

[77] Hurtado, J. E. and Barbat, A. H. Simulation Methods in Stochastic Mechanics. *Computational Stochastic Mechanics in a Meta-Computing, J. Marczyk ed. CINME,* 1997.

[78] Ziha, K. Descriptive sampling in structural safety. *Structural Safety,* vol. 17, pages 33-41, 1995.

[79] Saliby, E. Descriptive Sampling: A Better Approach to Monte Carlo Simulation. *Journal of the Operational Research Society,* vol. 41, no. 12, pages 1133-1142, 1990.

[80] Fisher, R. Design of Experiments. *Published by Oliver and Boyd, Edinburgh,* 1935.

[81] Plackett, R.L. and Burman, J.P. The Design of Optimum Multifactorial Experiments. *Biometrika*, vol. 33, no. 4, pages 305-25, 1946.

[82] Ross, P.J. Taguchi Techniques for Quality Engineering. *McGraw-Hill Publishing Company,* 1988.

[83] McKay, M.D., Conover, W.J. and Beckman, R.J. A Comparison of Three Methods for Selecting Values of Input Variables in the Analysis of Output from a Computer Code. *Technometrics,* vol. 21, pages 239–245, 1979.

[84] Iman, R.L., Helton, J.C. and Campbell, J.E. An Approach to Sensitivity Analysis of Computer Models, Part 1. Introduction, Input variable Selection and Preliminary Variable Assessment. *Journal of Quality Technology,* vol. 13, no. 3, pages 174–183, 1981.

[85] Jin, R., Chen, W., and Sudjianto, A. An Efficient Algorithm for Constructing Optimal Design of Computer Experiments. *Journal of Statistical Planning and Inference,* vol. 134, no. 1, pages 268-287, 2005.

[86] Weissinger, J. The Lift Distribution of Swept-back Wings. *National Advisory Committee for Aeronautics, NACA,* technical memorandum no. 1120, 1947.

[87] Hardy, R. Multiquadratic Equations of Topography and other Irregular Surfaces. *Journal of Geophysical Research,* vol. 76, no. 8, pages. 1905-1915, 1971.

[88] Broomhead, D. S., and D. Lowe. Multivariable Functional Interpolation and Adaptive Networks. *Complex Systems*, vol. 2, pages. 321-355, 1988.

[89] Hills, G. R. and Trucano, T. G. Statistical Validation of Engineering and Scientific Models: Background. *Sandia National Laboratories,* report no. SAND99-1256, 1999.

[90] Hills, G. R. and Trucano, T. G. Statistical Validation of Engineering and Scientific Models with Application to CTH. *Sandia National Laboratories,* report no. SAND2001-0132, 2001.

[91] Hills, G. R. Model Validation: Model Parameter and Measurement Uncertainty. *Journal of Heat Transfer, ASME,* vol. 128, pages 339-351, 2006.

[92] Chen, W., Baghdasaryan, L., Buranathiti, T. and Cao, J. Model Validation via Uncertainty Propagation and Data Transformations. *AIAA Journal,* vol. 42, no. 7, pages 1406-1415, 2004.

Appendix – Software Tools

The following software tools were used during the research work presented in this thesis.

Software Name	Versions	Vendor	Applications
Unigraphics	NX2, NX4	Siemens PLM Software	CAD Geometry Generation
Patran	2004r2, 2005r2	MSC Software Corporation	FEM Pre-processing FEM Post-processing
Nastran	2004r2, 2005r2	MSC Software Corporation	FEM Processing
SC03	11C0	Rolls-Royce plc.	FEM Post-processing Hybrid Meshing
FEMtools	3.1, 3.2	DDS	Model Correlation Model Updating
i-SIGHT	2.5.5	Engineous Software	Uncertainty Propagation
VIVACEsen	1.1	Rolls-Royce plc.	Sensitivity Analysis Component Prioritisation
LMS Virtual Lab.	6B	LMS International	Test Planning
LMS Test Lab.	8A	LMS International	Modal Analysis

Table. Software tools.